# Fluid Flow, Thermal History, and Diagenesis of the Cambrian-Ordovician Arbuckle Group and Overlying Units in South-Central Kansas

**BY**
**Bradley King**
**B.S., Illinois State University**

**Submitted to the graduate degree program in Geology and the Graduate Faculty of the University of Kansas in partial fulfillment of the requirements for the degree of Master of Science.**

**Advisory Committee:**

**Dr. Robert H. Goldstein** _____
**Committee Chair**

**Dr. Evan K. Franseen** _____

**Dr. David A. Fowle** _____

**Date Defended:** 8/23/2013

The Thesis Committee for Bradley King certifies that this is the approved version of the following thesis:

**Fluid Flow, Thermal History, and Diagenesis of the Cambrian-Ordovician Arbuckle Group and Overlying Units in South-Central Kansas**

**Advisory Committee:**

**Dr. Robert H. Goldstein** _____
**Committee Chair**

**Dr. Evan K. Franseen** _____

**Dr. David A. Fowle** _____

**Date Approved:** **8/23/2013**

# Abstract

Bradley King

Department of Geology, August 2013

University of Kansas

A diagenetic study of the Cambrian-Ordovician Arbuckle Group to the Middle Pennsylvanian Cherokee Group in south-central Kansas produced evidence of regional advective fluid flow and more localized fracture-controlled fluid flow affecting porosity. Late-stage megaquartz, baroque dolomite, and calcite produced high homogenization temperatures (86-144ºC), greater than can be explained by burial, necessitating hydrothermal fluids. Fluid inclusion salinities evolved from connate to those influenced by evaporites. Homogenization temperatures and $\delta^{18}O$ in baroque dolomite suggest warmer fluids stratigraphically shallower. The $^{87}Sr/^{86}Sr$ values indicate a regional advective aquifer during baroque dolomite precipitation, which may have been more locally controlled during calcite precipitation. Ouachita tectonism caused tectonically valved and gravity-driven fluid flow sourced from the Anadarko basin and possibly involved sandstone aquifers or basement. Mechanisms of ancient fluid flow appear to contrast with the modern system, which is separated internally by seal facies. The ancient aquifer system was vertically connected during migration of hydrothermal fluids.

## Acknowledgements

First and foremost, I would like to thank my advisor Dr. Robert Goldstein for taking me on as a student for a project that incorporated techniques I had very little familiarity with; thank you for the challenging and gratifying adventure, and for the confidence to be able to complete such an undertaking. I would also like to thank the Department of Geology at the University of Kansas and the faculty members that make it all possible; I may have never had the chance to take advantage of the same opportunities that eventually led to a promising career if I had never become a Jayhawk. I would also like to thank my family for all of their support during this challenging endeavor; I cannot imagine sweating through all of the trials and tribulations without all of them acting as my biggest fans. As a final point, I would like to thank Dr. David Malone from the Illinois State University; none of this would have been possible without your guidance and unshakeable determination to prepare me for a future as a geologist.

**Material** presented is based upon work supported by the U.S. Department of Energy (DOE) National Energy Technology Laboratory (NETL) under Grant Number DEFE0000002056. This project is managed and administered by the Kansas Geological Survey/KUCR, W. L. Watney, PI, and funded by DOE/NETL and cost-sharing partners.

**Disclaimer:** This report was prepared as an account of work sponsored by an agency of the United States Government. Neither the United States Government nor any agency thereof, nor any of their employees, makes any warranty, express or implied, or assumes any legal liability or responsibility for the accuracy, completeness, or usefulness of any information, apparatus, product, or process disclosed, or represents that its use would not infringe privately owned rights. Reference herein to any specific commercial product, process, or service by trade name, trademark, manufacturer, or otherwise does not necessarily constitute or imply its

endorsement, recommendation, or favoring by the United States Government or any agency thereof. The views and opinions of authors expressed herein do not necessarily state or reflect those of the United States Government or any agency thereof.

# Table of Contents

## List of Figures, Tables, Equations, and Appendices

**List of Figures:**

## List of Tables:



## List of Equations:



## List of Appendices:

# Chapter 1

## 1. Introduction

A complete investigation of the Cambrian-Ordovician Arbuckle Group as a reservoir for $CO_2$ sequestration requires an examination of not only the reservoir itself, but the integrity of potential seals in overlying units as well. Sequestration in the Arbuckle Group saline aquifer in south-central Kansas focuses on seals in the overlying Middle Ordovician Simpson Group, Devonian-Mississippian Chattanooga shale, Lower Mississippian Kinderhookian Stage, and Middle Pennsylvanian Cherokee Group to restrict vertical migration of injected $CO_2$ out of the Arbuckle Group. Analyzing potential for $CO_2$ sequestration in the Arbuckle Group saline aquifer requires a complete diagenetic and geochemical study of the reservoir, subsequently enabling interpretation of the ancient fluid flow affecting the unit. Coupling ancient fluid flow interpretations with studies of modern fluid flow will help establish if ancient and modern fluid flow systems are linked or if different systems have affected the unit in the past. Similar diagenetic and geochemical studies on the Arbuckle Group and its overlying units can be used to evaluate if ancient fluids were able to migrate across potential seals. Conditions and timing of such migration can be used to evaluate the likelihood of such migration in the future, after injection of $CO_2$ into the Arbuckle Group.

Chapter 2 of this study is written as a stand-alone paper on diagenetic, fluid flow, and thermal history of the Arbuckle Group. It focuses on the Wellington 1-32 and Vulcan cores, drilled in south-central Kansas. Data include study of the core in hand sample, transmitted-light, reflected light, cathodoluminescence (CL) and UV epifluorescence petrography, back scattered electron (BSE) microscopy, fluid inclusion analysis, and carbon, oxygen, and strontium isotopes. Results aid in understanding the history and controls on fluid flow in the Arbuckle Group and its

impact on porosity. Placing this history into the context of tectonic and stratigraphic evolution provides insight into the controls on mobility of fluids through the Arbuckle Group. The Ouachita orogeny is hypothesized to have set up a scenario for advective regional flow of hydrothermal fluids out of the Anadarko basin, driven by topography in the adjacent mountains and tectonic valving. A later event of hydrothermal fluid flow was more local in extent and followed different pathways, showing more interaction with basement or siliciclastic sediments, and more localized controls on composition.

Chapter 3 of this study is also written as a stand-alone paper. It focuses on data from the Middle Ordovician Simpson Group, Mississippian strata, and the Middle Pennsylvanian Cherokee Group. These data are used to interpret the ability of ancient fluids to migrate out of the Cambrian-Ordovician Arbuckle Group, across hypothesized seals. The Wellington 1-32 core from south-central Kansas provided the opportunity for hand sample, transmitted light, reflected light, and UV epifluorescence petrography, BSE microscopy, and fluid inclusion analysis. These analyses are merged with carbon, oxygen, and strontium isotopes to aid in understanding the fluid flow and thermal history. This provides a comparison to the history developed for the Arbuckle Group and enables interpretation of the history of seal integrity in the geologic past, as well as predictions in the future. The fluid flow and thermal history experienced by stratigraphic units overlying the Arbuckle Group is similar to the Arbuckle Group. There was a series of events of advective hydrothermal fluid flow likely associated with topography in the adjacent mountains and tectonic valving. This was followed by more localized hydrothermal fluid flow that might have been controlled by later fracturing.

Chapter 4 summarizes conclusions specific to Chapters 2 and 3, as well as conclusions derived from combining and interpreting data from both chapters.

## 2. Methodology

### *2.1. Core observations and sampling strategy*

Core samples were selected in order to: (1) observe cross-cutting relationships between various fractures and cements; (2) observe the succession of cements in various types of porosity; (3) characterize and compare cements in the Arbuckle Group and overlying strata; (4) establish potential fluid migration conduits; and (5) evaluate relationships between diagenetic events and stratigraphically significant surfaces.

### *2.2. Thick section preparation*

Doubly polished, superglue-mounted thick sections were prepared from 141 core samples by Petrographic Services in Montrose, CO and the University of Kansas in Lawrence, KS (Appendix I). Thick sections were prepared for the purpose of fluid inclusion analysis, as well as standard petrography. All thick sections were prepared using techniques specifically aimed at avoiding extensive heating of samples, consequently avoiding alteration of fluid inclusions (Goldstein and Reynolds, 1994).

### *2.3. Sample staining*

Staining of multiple samples was used to identify and distinguish between carbonate minerals present in thick sections. Alizarin red S and Potassium ferricyanide stain (ARS: PF) was used to differentiate calcite from dolomite, calcite from ferroan calcite, and dolomite from ferroan dolomite (Dickson, 1965). Approximately 1/3 of each thick section was stained to preserve the remaining section for fluid inclusion analysis.

### *2.4. Transmitted light, reflected light, and UV epifluorescence petrography*

Following preparation of thick sections, observations were made with transmitted light, reflected light, and UV epifluorescence. An Olympus BX53 research grade microscope was used to describe mineralogy, cross-cutting and superpositional relationships, and fluid inclusions. Reflected light was used to differentiate between sulfides (e.g. galena and pyrite) and to aid in the analysis of fluid inclusions. UV epifluorescence was utilized in initial efforts to recognize and describe multiple dolomite cements and to identify the presence of hydrocarbon stains and hydrocarbon fluid inclusions (e.g. Burruss, 1991).

### *2.5. Cathodoluminescence imaging*

Cathodoluminescence (CL) microscopy was completed at the Kansas Geological Survey using an Olympus BX41 research microscope equipped with a welded stainless steel Reliotron III cathodoluminescence chamber. Thick section images were captured under the general conditions of 50 millitorr, 10 kilovolts, and 0.5 milliamps in a Helium atmosphere; slight variability was noted for each image. Macrophotography was conducted with a Canon EOS Digital Rebel Xti 10.1 Mpx camera with Canon EFS 60 mm f/2.8 Marco USM lens and microphotography was conducted using a Diagnostic Instruments SPOT RT3 Color Slider Camera with high speed Firewire 800 cabling; exposure time ranged from 30 to 150 seconds. Images were captured under transmitted light, reflected light, and CL conditions and then compared and contrasted for cement stratigraphy purposes (e.g. Goldstein, 1991).

### *2.6. Fluid inclusion analysis*

Thick sections prepared from both cores were used for fluid inclusion petrography and microthermometry (Appendix III). A Linkam THMS 600 heating and freezing stage was used for microthermometric analysis of dolomite, megaquartz, and calcite; the Linkam stage is accurate to approximately ± 0.1ºC. The first step involved describing individual fluid inclusions occurring within each mineral occurrence and this was followed by the interpretation of fluid inclusion assemblages (FIA) as primary, secondary, pseudosecondary, or indeterminable (Goldstein and Reynolds, 1994). Samples were then cut into chips using a slow speed diamond-blade saw and then removed from the glass backings via an acetone bath.

Fluid inclusion microthermometry techniques were then used to obtain homogenization temperatures and compositions (Goldstein and Reynolds, 1994). In an effort to avoid modification or reequilibration of fluid inclusions, fluid inclusion analysis was only conducted on samples that were not previously exposed to whole core porosity or permeability tests, CL imaging, SEM analysis, or previously heated in any way (Goldstein and Reynolds, 1994). Microthermometry was only performed on fluid inclusions that had a gas bubble (Goldstein and Reynolds, 1994). Heating of the fluid inclusions was conducted until the gas bubbles present homogenized back into their original state of all-liquid aqueous inclusions; this provided the temperature of homogenization or Th (minimum measurement of entrapment temperature) (Goldstein and Reynolds, 1994). Homogenization temperatures were measured before melting temperatures to avoid potential stretching of inclusions, and fluid inclusions with potentially lower Th values were measured prior to fluid inclusions with higher Th values to avoid thermal reequilibration (Goldstein and Reynolds, 1994). Freezing with subsequent melting was conducted to obtain fluid composition. First melting temperatures (eutectic; $T_e$) were able to be

approximated in some inclusions and the final melting temperature of ice ($Tm_{ice}$) was measured and used to calculate fluid salinities in wt. % NaCl equivalent (Bodnar, 1993).

### *2.7. Scanning electron microscopy*

Scanning electron microscopy (SEM) was conducted at the University of Kansas at the Microscopy and Analytical Imaging lab. Pieces of polished thick sections were cut using a low-speed saw with a diamond blade, and then mounted on stubs. Three samples of baroque dolomite were coated with 15nm of gold prior to sample analysis (Appendix II). Samples were then examined using a four-quadrant back-scattered electron (BSE) detector. The samples were analyzed at 30.0kV with the aperture set at 120μm. A scan speed of 12 (approximately 2 minutes) was used to capture each image.

### *2.8. Stable isotope and strontium isotope analysis*

Stable isotope analysis was conducted at the Keck Paleoenvironmental and Environmental Stable Isotope Laboratory at the University of Kansas (Appendix IV). Sample slabs and thick sections were drilled in the desired location using a Brasseler Dental Rotary Instrument, model DLT50K equipped with carbide drill bits, while peering through a Nikon SMZ800 microscope with support stand. In between samples, drill bits were cleared of residue with an air compressor, dipped in 10% HCl, and rinsed with alcohol to avoid cross contamination. Sixty-two calcite and baroque dolomite samples, ranging from 100 to 200 micrograms, were roasted in a Lindberg/Blue tube furnace at 200ºC under vacuum for 1 hour to ensure that there was no $\delta^{13}C$ interference from organic matter. Samples were then reacted in 100% phosphoric acid and placed in a 25ºC oven for a minimum of 20 hours to allow full

digestion of carbonate powder. Samples are then measured via ThermoFinnigan MAT253 stable isotope ratio mass spectrometer (IRMS) linked via continuous flow Gasbench II front end peripheral to obtain values of $\delta^{18}O$ and $\delta^{13}C$ versus the VPDB scale. For each analytical run, a calibration curve is generated. Typical calibration curves yield an $R^2$ of 0.9998 or better. NIST standards are obtained via the National Institute of Standards

Strontium isotope analysis was conducted at the University of Kansas Isotope Geochemistry Laboratories (Appendix IV). First, nine baroque dolomite and four calcite slabs and thick sections were micro-drilled using a microscope-mounted dental drill with tungsten carbide burs, producing approximately 1,100 to 3,900μg of carbonate powder for each sample. Samples were then dissolved in 3.5 N $HNO_3$ and the strontium eluted through ion-exchange columns filled with strontium-spec resin. High precision $^{87}Sr/^{86}Sr$ ratios were then measured by Thermal Ionization Mass Spectrometer (TIMS), an automated VG Sector54, in the same lab. Isotope ratios were adjusted to correspond to a value of 0.71250 on NBS987 for $^{87}Sr/^{86}Sr$. We also assumed a value of $^{86}Sr/^{88}Sr$ of 0.1194 to correct for fractionation and to apply an exponential fractionation correction. The precision was ±0.000015.

# Chapter 2

## Fluid Flow, Thermal History, and Diagenesis of the Cambrian-Ordovician Arbuckle Group in South-Central Kansas


### Abstract

The Cambrian-Ordovician Arbuckle Group has historically been investigated for prolific oil production and is presently a candidate for carbon dioxide ($CO_2$) sequestration in south-central Kansas. Planning for oil production and $CO_2$ sequestration necessitates an understanding of fluid flow and porosity evolution in the Arbuckle Group and overlying units. Integration of transmitted-light and UV epifluorescence microscopy, cathodoluminescence imaging, fluid inclusion microthermometry, and stable isotope analysis helps to establish a diagenetic history for the Arbuckle Group and to interpret fluid-flow conditions responsible for the reservoir character.

The paragenesis organizes the complex diagenesis of the Arbuckle Group into early- and late-stage sequences of porosity-enhancing and reducing events. Petrographic observations of mineral assemblages suggest multiple hydrothermal fluid migration events through the Arbuckle Group and overlying units via fractures and preferred stratigraphic horizons. The mineral assemblage, comparable to MVT deposits (baroque dolomite, megaquartz, calcite, sphalerite, and galena), supports the migration of hydrothermal fluids in the past. Findings suggest hydrothermal alteration of the extensively dolomitized Arbuckle Group resulted in dissolution and subsequent mineralization. Fluid inclusion homogenization temperatures from late-stage precipitates of the Arbuckle Group yield temperatures ranging from 93-131ºC for baroque dolomite and 87-157ºC for megaquartz, values higher than can be explained by burial conditions or an elevated geothermal gradient. Fluid inclusion ice melting temperatures yield salinities ranging from 16.3-20.4 wt. % NaCl equivalent for baroque dolomite and 3.1-6.0 wt. % NaCl

equivalent for megaquartz, values suggesting multiple fluids, as well as fluid evolution through time. Hydrocarbon fluid inclusions in the late-stage baroque dolomite suggest oil migration concurrent with hydrothermal fluid flow. Depleted $\delta^{13}C$ and $\delta^{18}O$ values provide evidence for a high-temperature basinal fluid source, as well as preferential flow of hot fluids in the upper portion of the Arbuckle Group, where a pore system related to paleokarst is overlain by a less permeable unit. Radiogenic strontium isotopic data, acquired from baroque dolomite (0.70908-0.71019) and calcite (0.71257-0.71716), supports fluid-rock interaction with siliciclastic material or basement rock at some point during the fluid migration history. Highly radiogenic calcite $^{87}Sr/^{86}Sr$ values, compared to those in baroque dolomite, suggest multiple sources of fluids responsible for late-stage cement and a transition from an advective fluid flow system to a vertical fluid flow system. The interpreted dependence of ancient fluid flow systems on major orogenies (Ouachita and Laramide) suggests modern fluids in the reservoir are not related to ancient systems, but are primarily sourced from topographic highs to the west and the east of the study area, as well as northern migration of basinal fluids into southern Kansas due to thermal expansion.

## 1. Introduction and Purpose

The Cambrian-Ordovician Arbuckle Group is a deep saline aquifer, within the Ozark Plateau aquifer system (OPAS) of south-central Kansas (Fig. 2.1A, 2.1B). It is believed to meet requirements for carbon dioxide ($CO_2$) sequestration, including: seal integrity of confining units, brine chemistry, mineralogy, capability for high injectivity, capacity for long isolation from atmosphere, and protection of drinking water (Watney and Bhattacharya, 2009). A system with substantial porosity and permeability greatly enhances the ability of a geologic formation to store

sequestered $CO_2$ (Watney and Bhattacharya, 2009). The Arbuckle Group and age-equivalent units have been noted as having considerable porosity, believed to be modified by dolomitization, karsting, fracturing, and hydrothermal alteration (Fig. 2.2; Franseen et al., 2004; Franseen, 2000; Simo and Smith, 1997; Gao and Land, 1991; Gao et al., 1995; Kerans, 1988; Kupecz and Land, 1991; Montanez and Read, 1992). The porosity evolution and late fluid history of the Arbuckle Group, as well as the integrity of the overlying units (Middle Ordovician Simpson Group to the Lower Pennsylvanian Cherokee Group), is the focus of this study. The Arbuckle Group is overlain by two shale-rich units, including the Devonian-Mississippian Chattanooga Shale and the Pennsylvanian Cherokee Group shales, which serve as potential seals (Fig. 2.3; Merriam, 2005; 1963). Interpreting the complex relationship between diagenesis, fluid flow, and structural deformation enables identification and characterization of fluid migration within the Arbuckle Group, as well as analysis of potential connectivity with overlying units.

Diagenetically late mineral precipitation is the basis for evaluating a potential genetic link between fluids modifying the Arbuckle Group and overlying units. Expulsion of fluids from the Anadarko basin, after extensive fluid-rock interaction, may be the source of hydrothermal brines that are believed to be responsible for late-stage mineral precipitation (Fig. 2.1B; Gao and Land, 1991; Gao, 1990a; Musgrove and Banner, 1993). The mineral assemblage observed in the Arbuckle Group and overlying units are similar to that commonly observed in Mississippi Valley-type (MVT) deposits (Leach and Sangster, 1995; Garven, 1993; Bethke and Marshak, 1990; Sverjensky, 1986; Oliver, 1986). Previous studies that correlated regional MVT deposits with basinal-sourced and orogenically influenced fluid flow models were used to help establish the timing, extent, and control of hydrothermal fluid flow within the Arbuckle Group (Table 2.1; Garven, 1993; Leach and Sangster, 1995; Garven and Freeze, 1984a; 1984b; Leach and Rowan,

1986; Sverjensky, 1986; Oliver, 1986; Sharp, 1978; Cathles and Smith, 1983; Coveney et al. 2000). Previously studied history of tectonic and stratigraphic evolution provides insight into the mobility of Arbuckle Group fluids, including the likelihood of mobility in the future. The tectonic activity associated with the Ouachita (Late Paleozoic) and Laramide (Late Mesozoic-Early Cenozoic) orogenies, as well as the resultant structures, is hypothesized as being responsible for topographic or tectonically controlled fluid flow affecting strata in the study area (Fig. 2.1B).

The Wellington 1-32 and Vulcan cores, drilled in south-central Kansas (Fig. 2.1A, 2.1B), provided the opportunity for core observations and petrographic analysis of the Arbuckle Group and overlying units. Petrographic methods include study of the core in hand sample, transmitted-light, reflected light, cathodoluminescence (CL) and UV epifluorescence petrography, and back scattered electron microscopy (SEM). Petrographic observations have been merged with fluid inclusion analysis and carbon, oxygen, and strontium isotope analyses to aid in understanding the history and controls on fluid flow in the Arbuckle Group and overlying units. Scheffer (2012) conducted a geochemical and microbial study on the Wellington 1-32 core and hypothesized that there is a modern buffer zone that limits fluid connectivity between the upper and middle to lower Arbuckle Group; the results of her study will be incorporated into the interpretation of the fluid flow evolution of this study.

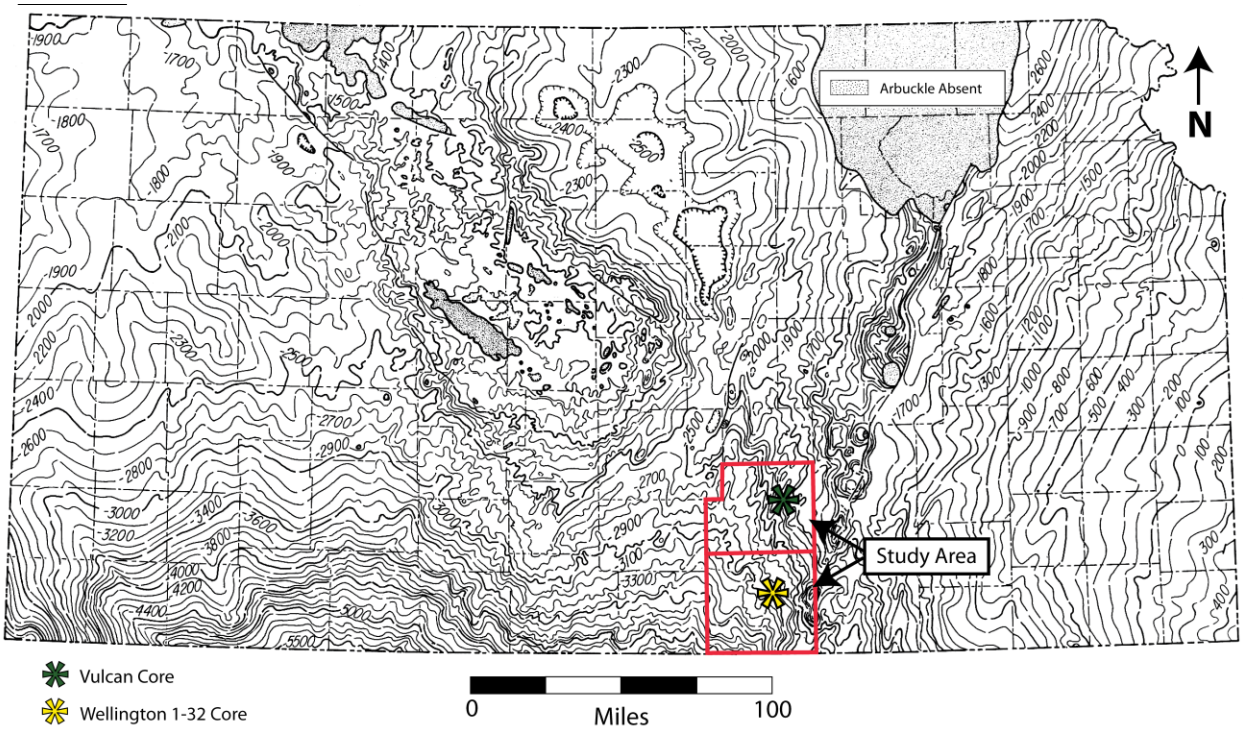


**Figure 2.1A:** Structural contour map on the top of the Arbuckle Group in Kansas with localized Arbuckle Group absences noted, map displays thickening southeastern dip and core locations. Contour interval is 100ft. Image modified from Franseen et al., 2004.

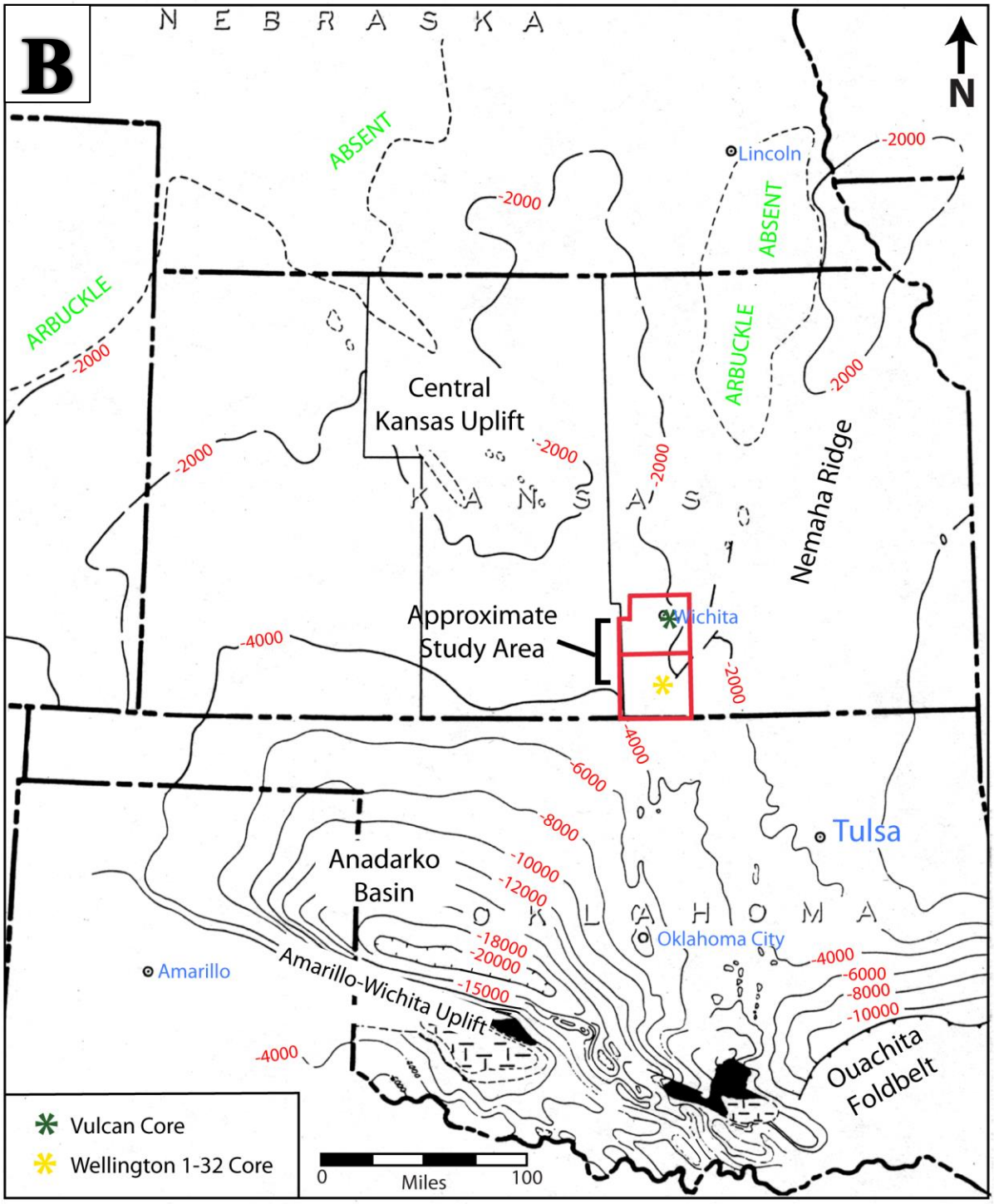


**Figure 2.1B:** Regional structural map on the top of the Arbuckle Group displaying location of Anadarko basin and surrounding structural features relative to the study area. Contour interval is 2,000ft. Image modified from Franseen et al., 2004.

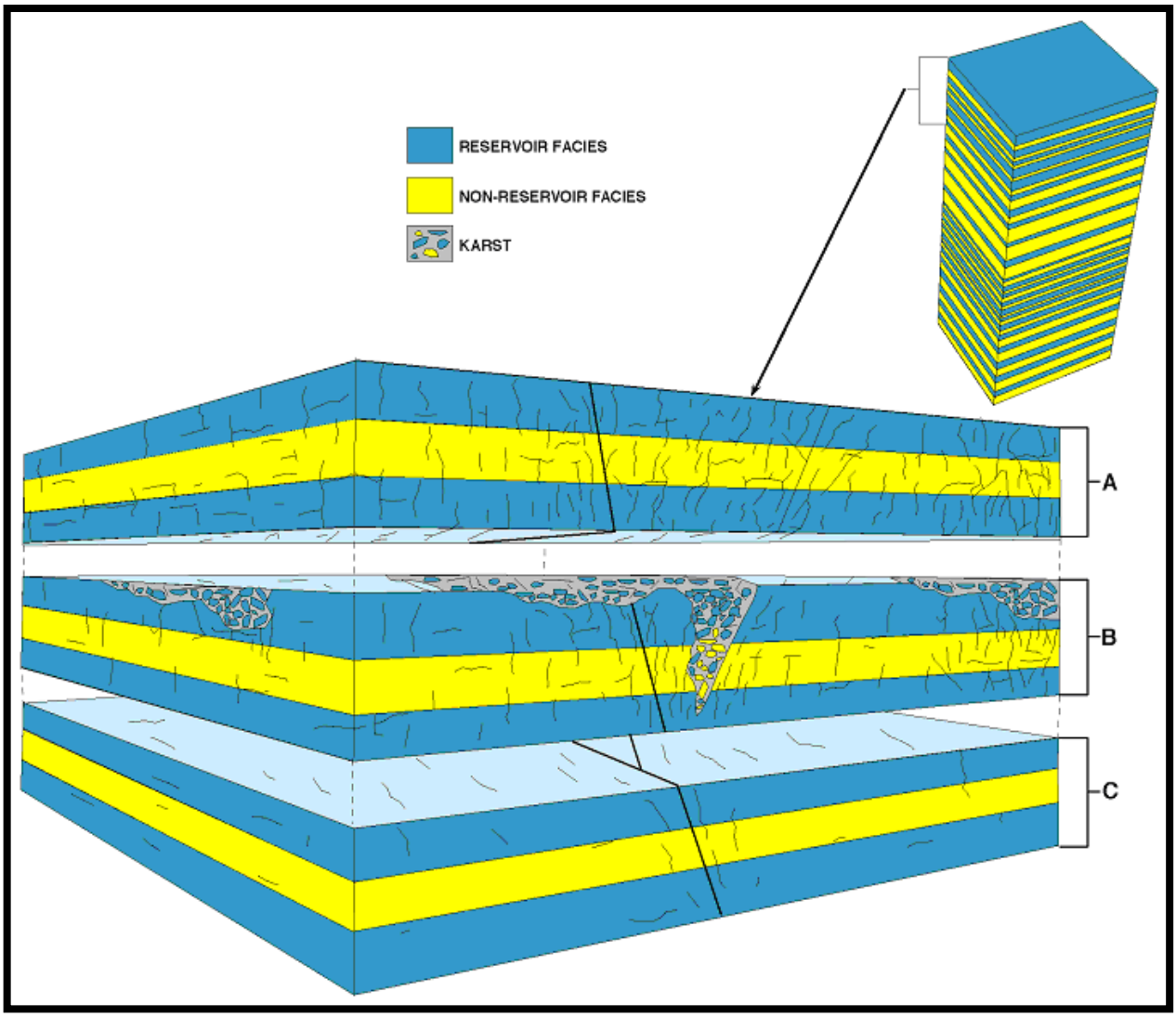


**Figure 2.2:** Illustration of fractures (A), karst (B), and lithology (C) end-members as controls on Arbuckle Group porosity and permeability. If fractures (A) are present, overall permeability may be enhanced and fluid flow may follow fractures Karst overprinting (B) within the Arbuckle typically results in very complex permeability and porosity, varying laterally and possibly enhancing or destroying overall permeability and porosity; there is potential for fluid flow following karst features if permeability and/or porosity were enhanced. If lithofacies (C) are the dominant control on porosity and permeability, then the continuity of strata and potential seals will act as fluid flow constraints (Franseen et al., 2004).

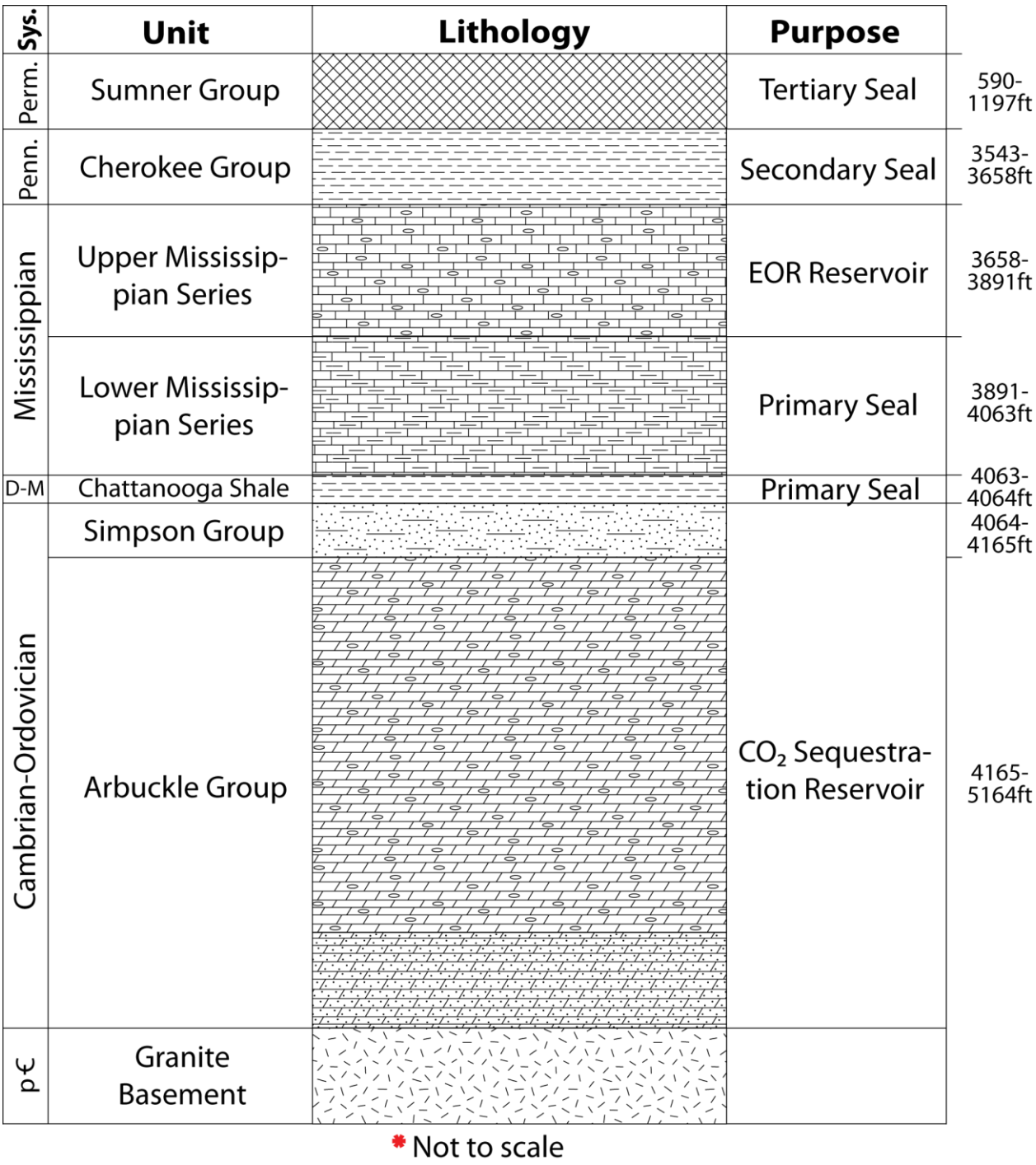


**Figure 2.3:** Stratigraphic section of Precambrian through Permian strata, displaying units of note in this study and the larger scale $CO_2$ sequestration project. Depth markers correlate with depths observed in the Wellington 1-32 core (based on Scheffer, 2012).

| Region of Study | Hydrothermal Fluid Flow Mechanism | Specific Driving Forces | Interpreted Age of Hydrothermal Deposit | Direct Dates | Authors |
|---|---|---|---|---|---|
| SE Kansas | Late-Paleozoic Ouachita orogeny | Progressively deeper thrust faulting | Late Pennsylvanian-Early Permian | N/A | Young, 2010 |
| | Late-Paleozoic Ouachita orogeny | N/A | Late Pennsylvanian | N/A | Wojcik et al., 1992, 1994, 1997 |
| Tri-State | Late-Paleozoic to Late-Mesozoic tectonic activity | Expelled pore fluids or gravity-driven flow | Pennsylvanian-Late Cretaceous | 251±11 Ma; 137±3 Ma; 66±2 Ma | Coveney et al., 2000 |
| | Late Paleozoic Alleghenian-Ouachita orogeny | Gravity-driven flow | Late Permian-Early Triassic | 251±11 Ma | Brannon et al., 1996b |
| | Late-Paleozoic Ouachita orogeny | N/A | >Late Jurassic | >183 Ma | Arne et al., 1992; Leach et al., 2001 |
| SE Missouri | Late-Paleozoic Alleghenian-Ouachita orogeny | N/A | Late Pennsylvanian-Early Permian | 286±20 Ma | Wisniowiecki et al., 1983; Leach et al., 2001 |
| | Late-Paleozoic Alleghenian-Ouachita orogeny | N/A | Early Permian | 273±10 Ma | Symons et al., 1998a; Leach et al., 2001 |
| | N/A | N/A | Late Permian-Eocene | 241±10 Ma; 203±10Ma; 100-50Ma | Arne et al., 1990; Leach et al., 2001 |
| | N/A | N/A | Devonian | 392±21 Ma | Lange et al., 1983; Leach et al., 2001 |
| North Arkansas | Late-Paleozoic Alleghenian-Ouachita orogeny | N/A | Permian | 265±20 | Pan et al., 1990; Leach et al., 2001 |
| Central Missouri | Late-Paleozoic Alleghenian orogeny | N/A | Pennsylvanian | 303±17 Ma | Symons and Sangster, 1991; Leach et al., 2001 |
| Central Tennessee | Late-Paleozoic Alleghenian orogeny | N/A | Late Permian-Early Triassic | 245±10 Ma | Lewchuck and Symons, 1996 |
| | Late-Paleozoic Alleghenian orogeny | Gravity-driven flow | Late Permian | 260±42 Ma | Brannon et al., 1996a |
| East Tennessee | Late-Paleozoic Alleghenian orogeny | N/A | Late Pennsylvanian-Early Permian | 286±20 Ma | Bachtadse et al., 1987; Leach et al., 2001 |
| | Late-Paleozoic Alleghenian orogeny | N/A | Pennsylvanian | 316±8 Ma | Symons and Stratakos, 2000 |
| | Middle-Paleozoic Acadian orogeny | Thrust faulting | Devonian | 377±29 Ma | Nakai et al., 1990; Leach et al., 2001 |
| | Middle-Paleozoic Acadian orogeny | Thrust faulting | Mississippian | 347±20 Ma | Nakai et al., 1990; 1993; Leach et al., 2001 |

**Table 2.1:** Table first lists the studies of overlying units in the study area (S Kansas). The table then lists study areas in the U.S. and the details of the hydrothermal system, including direct dates of late-stage cements.

## 2. Geologic Background

The Cambrian-Ordovician Arbuckle Group is present in the subsurface throughout the majority of Kansas, with the exception of northeastern and northwestern portions of the state that are associated with ancient uplifts (Franseen et al., 2004; Fig. 2.1A, 2.1B). The unit unconformably rests on either Precambrian or Cambrian strata and is topped by a major regional unconformity with either Middle Ordovician, Mississippian, or Pennsylvanian strata overlying (Franseen et al., 2004). In general, the unit gently dips to the south, with a westerly dip on the east side of the Nemaha anticline in the southeast part of the state (Fig. 2.1A, 2.1B; Franseen et al., 2004). The unit thickens to the south, with the thickest portions occurring in southeast Kansas (Franseen et al., 2004).

The Arbuckle Group was deposited as part of the Sauk Sequence and is a major component of the Great American Bank. It is described as shallow-shelf carbonate strata (Franseen et al., 2004). Franseen et al. (2004) described the Arbuckle Group as consisting primarily of coarse-grained skeletal, intraclastic, oolitic, peloidal, dolograinstones/packstones, finer-grained mudstones, thrombolites and stromatolites, intraclastic conglomerate and breccia, and minor shale and siltstone. Following a fall in sea-level in the Early Ordovician, the unit was subaerially exposed allowing for deep weathering and erosion to produce the regionally extensive Arbuckle-Ellenburger-Knox-Prairie du Chien-Beekmantown-St. George karst plain; this extensive karsting generated caves, joint-controlled solution features, and collapse breccias throughout the Arbuckle Group and age-equivalent units (Fig. 2.2; Franseen et al., 2004; Simo and Smith, 1997; Kerans, 1988; Kupecz and Land, 1991; Montanez and Read, 1992). The unit was subsequently buried and later fractured by structural deformation likely associated with the Ouachita orogeny (Late Paleozoic) and possibly the Laramide orogeny (Late Mesozoic-Early

Cenozoic) (Franseen et al., 2004). Previous studies have found evidence for warm, basin-derived brines modifying the Arbuckle Group porosity relatively late in the established paragenesis (Gao et al., 1995). Evidence for regional-scale precipitation of similar mineral assemblages, related to hydrothermal activity and potential basin dewatering, have been observed in areas affected by MVT deposition (Table 2.1; Young, 2010; Leach and Sangster, 1995; Garven, 1993; Wojcik et al., 1992; Bethke and Marshak, 1990; Garven and Freeze, 1984a; 1984b; Leach and Rowan, 1986; Sverjensky, 1986; Oliver, 1986; Cathles and Smith, 1983).

Two four-inch diameter cores (Vulcan and Wellington 1-32), obtained from SE Kansas, were studied and sampled for the purpose of this study (Fig. 2.1A, 2.1B). Only the top 60 feet of the Arbuckle Group was obtained in the Vulcan core and approximately 1,000 feet is present from the top to the bottom of the Arbuckle Group in the Wellington 1-32 core. In both cores, the top of the Arbuckle occurs at roughly 4,000 feet subsurface. The Vulcan core, drilled in Sedgwick County, Kansas, was acquired for analysis as a potential disposal well; this core sampled three unconnected intervals in the subsurface, with only the middle interval sampling the Arbuckle Group from 3961.6-4020.0'. The Wellington core, drilled in Sumner County, Kansas, was acquired specifically for analysis for $CO_2$ sequestration potential; this core sampled the interval from the Lower Pennsylvanian Cherokee Group (3543.5') down to the Precambrian basement (5180.5'). The Arbuckle Group extends from 4165.5-5164.1' in this core, resting on Precambrian basement and capped by the Middle Ordovician Simpson Group. Several portions of the core were not recovered within the Arbuckle Group in the Wellington core, possibly due to extensive karsting and/or fracturing (4655.8-4680.1'; 4818.5-4899.9'; 4997.7-5049.5').

## 3. Paragenesis

The paragenetic sequence of the Arbuckle Group can be separated into 23 major diagenetic events. For the purpose of this study, the events have been divided into an early and late diagenetic stage, relative to the onset of burial. The timing and effect on porosity have been summarized in Figure 2.4. Events 1-13 are grouped into the early diagenetic stage because they occurred prior to burial and compaction. Events 14-23 are grouped into the late diagenetic stage because they formed after burial and compaction. The late diagenetic stage includes evidence for hydrothermal alteration, with mineral assemblages similar to MVT deposits. Pore types are classified using Choquette and Pray (1970). Folk (1965) was used to describe calcite textures and Gregg and Sibley (1984) was used to describe dolomite textures. Core and petrographic observations were combined for the purpose of establishing the Arbuckle Group paragenesis. Any percentages provided are visual estimates from the core and should be viewed with uncertainty.

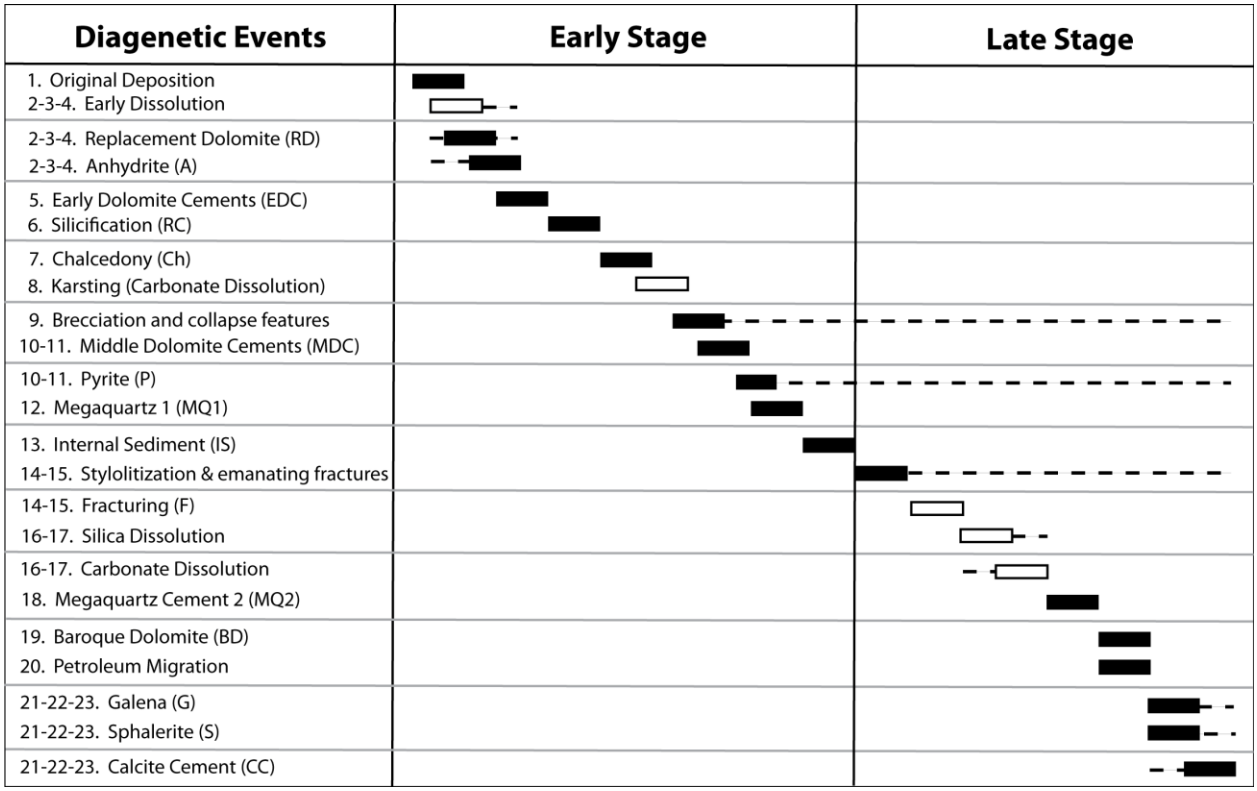

**Figure 2.4:** Paragenesis of the Arbuckle Group with events separated into early and late stages. Porosity evolution is illustrated with solid boxes indicating a decrease in porosity and empty boxes indicating an increase in porosity. Dashed lines indicate a level of uncertainty regarding the duration of some events.

### *3.1. Early diagenetic stage*

*Event 1: Deposition* - Though the unit has been extensively dolomitized, most dolomitization preserved the primary depositional fabric. Lithology and depositional facies of the Wellington 1-32 core were recently described by Lynn Watney of the Kansas Geological Survey (KGS). The current descriptions of the core match well with general descriptions of the Arbuckle Group by Franseen et al. (2004), varying from packstone to wackestone to grainstone with notable occurrences of oolite, microbialite, and mudstone. The dominant environment was a subtidal to intertidal shallow carbonate platform. Significant primary porosity was present prior to secondary diagenetic events, predominantly in the form of interparticle and fenestral porosity (Fig. 2.5A, 2.6A).

*Event 2-3-4: Early dissolution* – Early dissolution of carbonate strata is apparent by the creation of vuggy pores lined with early dolomite cements (event 5) and chalcedony (event 7); these cements do not line vug and cavern porosity created later in the paragenesis (Fig. 2.5B, 2.6B, 6C). Vugs related to this dissolution event contain features occurring as early as early dolomite cements (event 5) and as late as baroque dolomite (event 19) (Fig. 2.5B, 2.6B, 2.6C). Though initial dissolution enhanced porosity, subsequent cementation events have occluded the majority of the porosity created. Early dissolution is likely related to intraformational subaerial exposure events, which can be observed in the core and have been noted as common occurrences in the Arbuckle Group (Franseen et al., 2004). Early minor brecciation occurred as a result, producing fractures that slightly enhanced porosity as well. Secondary porosity created by this

event was mostly destroyed by precipitation of early cements (as early as event 5) and later cements (as late as event 19) (Fig. 2.5B, 2.6B, 2.6C).

*Event 2-3-4: Replacement dolomitization* – Replacement dolomitization (RD) appears to be the most abundant diagenetic event in the Arbuckle Group, affecting >80% of the original depositional fabric and reducing porosity by <10%. It occurs throughout the entire unit and could have potentially occurred as synsedimentary replacement. RD is fine to medium crystalline and displays an idiotopic-S texture with closely packed subhedral to anhedral dolomite crystals (Fig. 2.6B, 2.6D). The original depositional fabric is typically preserved during dolomitization (Fig. 2.5A, 2.6A). RD varies from cloudy brown to cloudy yellow in color under transmitted light, likely due to a high abundance of aqueous fluid inclusions. RD emits mottled yellow to red CL colors with no concentric zoning; the mottling may represent recrystallization of earlier dolomite during later dolomite precipitation events (Fig. 2.13A, 2.13B, 2.13C). RD does not take a stain in ARS:PF solution, indicating it is non-ferroan (Dickson, 1965). RD postdates original deposition because it replaces the original depositional fabric and predates early dolomite cements (event 5) because RD acts as a nucleus for precipitation of early dolomite cements (Fig. 2.6A, 2.6B, 2.6D).

*Event 2-3-4: Anhydrite* – Anhydrite occurs only as solid inclusions within early megaquartz (event 12) and does not appear to be limited to a specific stratigraphic interval (Fig. 2.18B). The exact onset of anhydrite precipitation is poorly constrained. Anhydrite appears to be replaced by early dolomite cements (event 5) in some examples (Fig. 2.7A, 2.7B), indicating precipitation prior to event 5, but the exact relationship is difficult to define. If anhydrite did precipitate prior to early dolomite cements, it may have precipitated simultaneously with replacement dolomite (event 2-3-4). The presence of anhydrite as solid inclusions in megaquartz

1 definitively places anhydrite precipitation prior to event 12 but the timing of its initial precipitation remains poorly defined.

*Event 5: Early dolomite cements (EDC)* – Dolomite cement 1 (DC1) and dolomite cement 2 (DC2) are grouped as early dolomite cements. Early dolomite cements decrease porosity by <5% and do not appear to be restricted to any specific interval in the Arbuckle Group. Both cements display an idiotopic-C texture (Fig. 2.6A, 2.6B) and are present as rhombohedral dolomite crystals, lining vugs and interparticle porosity (Fig. 2.6A, 2.6B). DC1 is non-luminescent under CL and DC2 emits concentrically banded red and dull-red CL colors that appear mottled in some cases; mottling likely represents recrystallization (Fig. 2.13A, 2.13B, 2.13C, 2.13D). Neither of the early dolomite cements take a stain in the ARS:PF solution, indicating they are non-ferroan (Dickson, 1965). The early dolomite cements postdate event 2-3-4 because they partially occlude vugs caused by the early dissolution event and they precipitate on RD (event 2-3-4) (Fig. 2.6B, 2.7C). The early dolomite cements predate replacement chert (event 6) because they partially replace ooids that have been subsequently replaced by chert (Fig. 2.7C).

*Event 6: Silicification* – Replacement chert (RC) is observed commonly throughout the entire unit and does not appear to be restricted to any specific stratigraphic interval within the Arbuckle Group. RC replaces ooids, previously dolomitized material, and undolomitized material, engulfing early dolomite cements (event 5) in some examples (Fig. 2.7C). This microcrystalline quartz is a dull yellow color under transmitted light and is non-luminescent under CL. This event postdates EDC (event 5) because it is found replacing ooids that were already partially replaced by EDC. RC predates chalcedony (event 7) because chalcedony precipitates on chert and into pore space (Fig. 2.7D).

*Event 7: Chalcedony cement* – Chalcedony (Ch) is a minor diagenetic event (decreasing porosity by <1%) that is not noticeably restricted to a stratigraphic interval within the Arbuckle Group. It occurs primarily as a cement in early dissolution features and replaces early dolomite cement (event 5) in some examples. Ch appears light yellow to brown in color under transmitted light and has an undulose, fibrous extinction under crossed polars (Fig. 2.7D). Ch is non-luminescent under CL. Ch postdates RC (event 6) because it can be observed precipitating on RC (Fig. 2.7D). Middle dolomite cements can be observed precipitating after Ch and internal sediment can be observed resting on Ch (Fig. 2.6B, 2.6C). Ch is not observed in porosity believed to be related to events 8 and 9.

*Event 8: Karsting (carbonate dissolution)* – Event 8 was a major diagenetic event, resulting in extensive dissolution of carbonate material and enhancement of porosity by <10%. Enhanced porosity primarily affected the uppermost portion of the Arbuckle Group (~200ft), but similar features can be observed in different locations throughout the unit, including the highly permeable and porous lower Arbuckle Group. Locally, porosity was greatly enhanced, producing large vug and cavern porosity (larger than the width of the core (3 inches) in some examples) (Fig, 2.5C, 2.5D). Porosity related to this event is lined with cements as early as middle dolomite cements (event 10) and as late as calcite and sphalerite (event 21-22-23) (Fig. 2.8A, 2.8B, 2.8C, 2.8D, 2.12D). Dissolution features in the upper Arbuckle Group that are associated with this event were likely a direct cause of the major collapse and brecciation features noted in event 9. The presence of internal sediment (event 13) filling porosity believed to be associated with this event suggests that at least part of this event may be correlated with the stratigraphic surface preserving the regionally extensive post-Sauk subaerial exposure event.

*Event 9: Brecciation and collapse fractures* – Similar to event 8, brecciation and collapse features appear to be most abundant towards the top of the Arbuckle Group (~200), though they can be observed in different locations throughout the unit, including the highly permeable and porous lower Arbuckle Group. Fractures associated with brecciation enhanced porosity by <5%, whereas some collapse features reduced porosity by <1%. Features related to this event are commonly filled with internal sediment (event 13) and lined with middle to late dolomite cements (event 10 to 19) (Fig. 2.5D, 2.12C). Brecciation in the upper Arbuckle Group was likely the direct result of collapse after carbonate dissolution in event 8. Similar to event 8, at least some of this brecciation event can be correlated with the stratigraphic surface that preserves evidence for the post-Sauk subaerial exposure event. Brecciation and collapse features likely continued to occur after the onset of burial.

*Event 10-11: Middle dolomite cements (MDC)* – Dolomite cement 3 (DC3) and dolomite cement 4 (DC4) are grouped as middle dolomite cements. Middle dolomite cements reduced porosity by <1% and they are not noticeably restricted to a specific stratigraphic interval. Both cements display an idiotopic-C texture with DC3 having polyhedral dolomite crystals and DC4 having rhombohedral dolomite crystals (2.13B, 2.13C, 2.13D). The transition from DC3 to DC4 can typically be observed by a thin light brown contact line in transmitted light, differences in UV-epifluorescence, and CL-imaging (Fig. 2.8A, 2.13B, 2.13C, 2.13D, 2.17B). DC3 typically appears mostly clear under transmitted light, with minor presence of fluid inclusions; solid inclusions of pyrite (event 10-11) can be observed in some samples (Fig. 2.17A, 2.17B, 2.17C, 2.17D). DC3 also displays blue, grey, and black banding under UV-epifluorescence and emits dull-yellow, light green, and dead banding under CL (Fig. 2.8A, 2.13B, 2.13C, 2.13D). DC4 appears clear under transmitted light with an overall lack of fluid inclusions (Fig. 2.8B). DC4

displays vague light blue banding under UV-epifluorescence and emits dominantly red luminescence under CL, alternating with dead bands and some yellow bands (Fig. 2.8A, 2.13C, 2.13D). Under CL, DC3 is concentrically zoned and DC4 appears sector zoned (Fig. 2.13B, 2.13C, 2.13D). The middle dolomite cements did not take a stain in the ARS:PF solution, indicating a non-ferroan composition (Dickson, 1965). DC3 and DC4 occur later than early dolomite cements, as evidenced by precipitation after chalcedony (event 7) (Fig. 2.6C). Megaquartz 1 (event 12) can be observed precipitating into pore space after middle dolomite cements (Fig. 2.8C). Internal sediment (event 13) is commonly deposited on top of DC4 (Fig. 2.6C, 2.8B).

*Event 10-11: Pyrite* – Cubic pyrite (Py) can be observed in nearly every sample from both cores and has reduced porosity by <1%. The relative timing of pyrite precipitation is uncertain (Fig. 2.4). Pyrite can be observed as solid inclusions in middle dolomite cements (Fig. 2.17D). The presence of pyrite precipitating in middle dolomite cement growth zones (event 10-11) and appearing to fill pore space after middle dolomite cements (Fig. 2.9B), definitively indicates precipitation during cementation of the middle dolomite cements and for some time after. The possibility for earlier precipitation and continuation of precipitation later in the paragenesis exists, as the relationship with adjacent material is uncertain in many instances.

*Event 12: Megaquartz 1* – Megaquartz 1(MQ1) can be observed in samples spanning the entire length of both cores, decreasing porosity by <5%. MQ1 is present as a cement lining fractures associated with brecciation (event 9) and vug porosity (Fig. 2.7D, 2.8C, 2.8D) and as a replacement feature replacing anhydrite and early dolomite cements (Fig. 2.7A, 2.7B). MQ1 appears clear in transmitted light (Fig. 2.8D). Solid anhydrite and dolomite inclusions, as well as relatively large fluid inclusions, are common (Fig. 2.18A, 2.18B). MQ1 can be observed with

internal sediment (event 13) deposited on the upper surface of crystals (Fig. 2.8D), definitively placing precipitation prior to or at least syn-depositional with event 13.

*Event 13: Internal Sediment* – Internal sediment (IS) can be observed most abundantly in the upper portion of the Arbuckle Group (~200ft), filling open vugs and fractures associated with brecciation, reducing the overall porosity of the Arbuckle Group by <5% (Fig. 2.5B, 2.5C, 2.5D, 2.6C, 2.8B, 2.8D). IS appears light brown in core observations and porous and silty in thick section; it is primarily composed of subangular to rounded silt-sized quartz grains, with some dolomite rhomb fragments. The silty composition of IS is dissolved in some instances. IS can be observed resting on DC4 (event 10-11) and MQ1 (event 12) (Fig. 2.6C, 2.8B, 2.8D). Later megaquartz (event 18) and baroque dolomite (event 19) are observed precipitating into porosity following infiltration of IS (Fig. 2.5C, 2.8B, 2.12A). The infiltrating sediment could be derived from the unconformity on the top of Arbuckle Group during the regional subaerial exposure event or may be the result of infiltration during Simpson Group deposition.

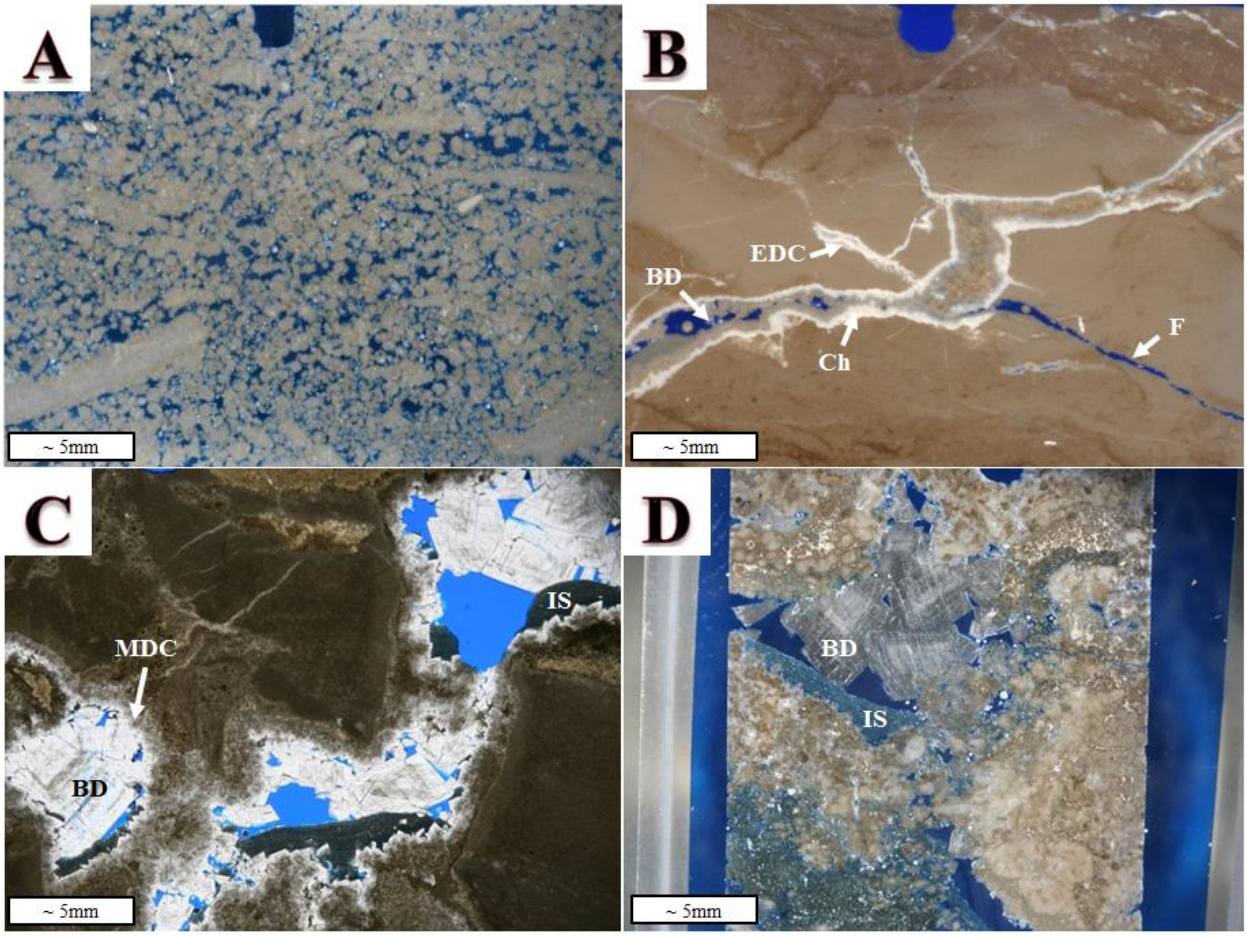


**Figure 2.5:** (A) Reflected light photomicrograph of primary interparticle porosity (sample 3-9 (3987.3ft) from Vulcan); (B) Reflected light photomicrograph displaying brecciation resulting from early dissolution (event 2-3-4), breccia pore is lined with cements as early as early dolomite cements (EDC) and as late as baroque dolomite (BD), also shows fracturing (F) likely associated with event 14-15 (sample 4492.5 from Wellington 1-32); (C) Transmitted light photomicrograph of vug porosity associated with dissolution during event 8, porosity is lined with middle dolomite cements (MDC), internal sediment (IS), and baroque dolomite (BD) (sample 4524.8 from Wellington 1-32); (D) Reflected light photomicrograph of vuggy and brecciated fabric associated with events 8 and 9, porosity is reduced with internal sediment (IS) and baroque dolomite (BD) (sample 4428.7 from Wellington).

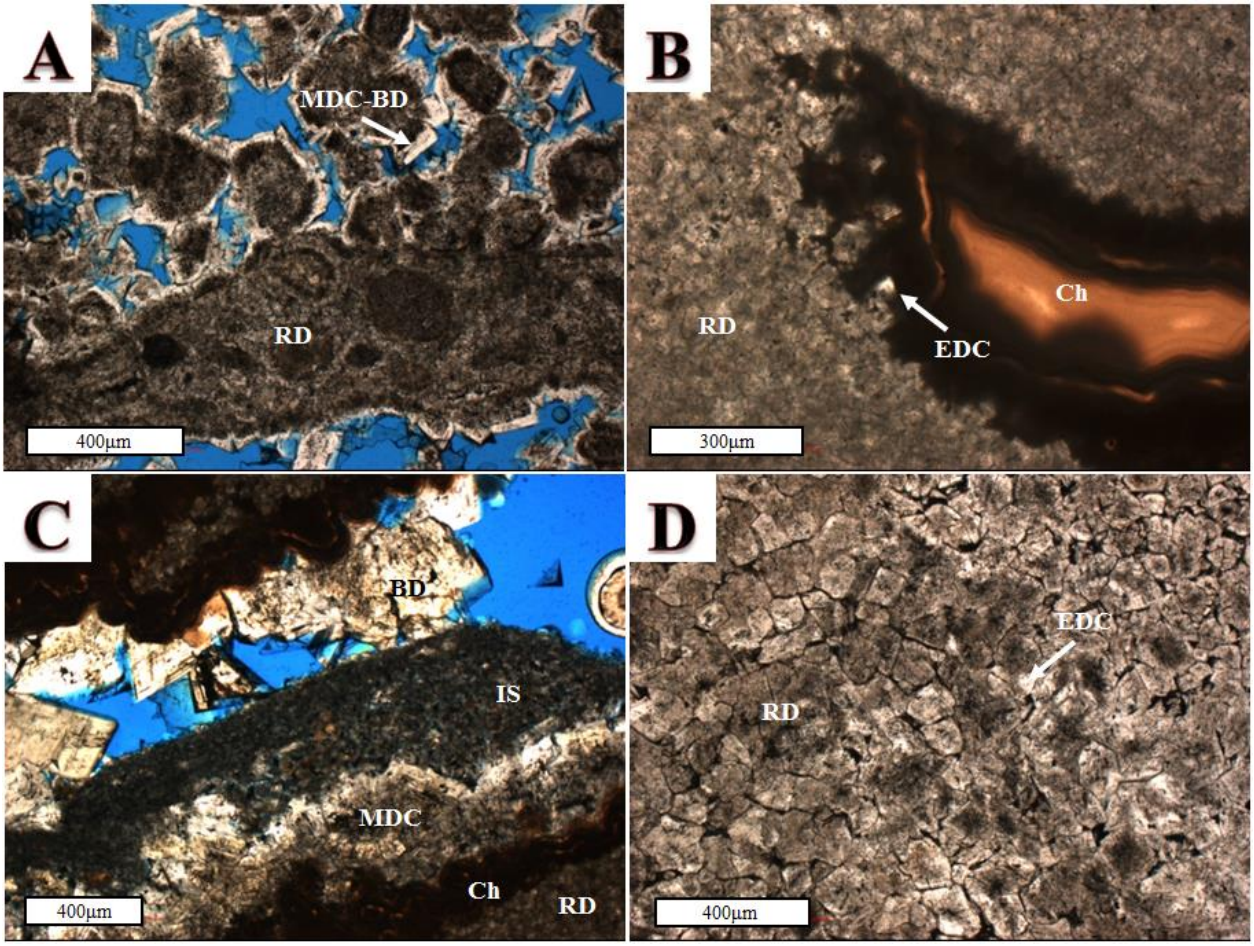


**Figure 2.6:** (A) Transmitted light photomicrograph of a magnified view of Fig. 2.5A, displaying interparticle porosity and middle dolomite cements (MDC) and baroque dolomite (BD) precipitating on material previously replaced by dolomite (RD) (sample 3-9 (3987.3ft) from Vulcan); (B) Transmitted light photomicrograph of a magnified view of Fig. 2.5B, displaying replacement dolomite (RD), and early dolomite cements (EDC) and chalcedony (Ch) lining porosity created during early dissolution (event 2-3-4) (sample 4492.5 from Wellington 1-32); (C) Transmitted light photomicrograph of another magnified view of Fig. 2.5B, shows porosity also lined with middle dolomite cements (MDC), internal sediment (IS), and baroque dolomite (BD) (sample 4492.5 from Wellington 1-32); (D) Transmitted light photomicrograph of idiotopic-S texture of replacement dolomite (RD) and brighter overgrowths of early dolomite cements (EDC) (sample 3-6 (4002.2ft) from Vulcan).

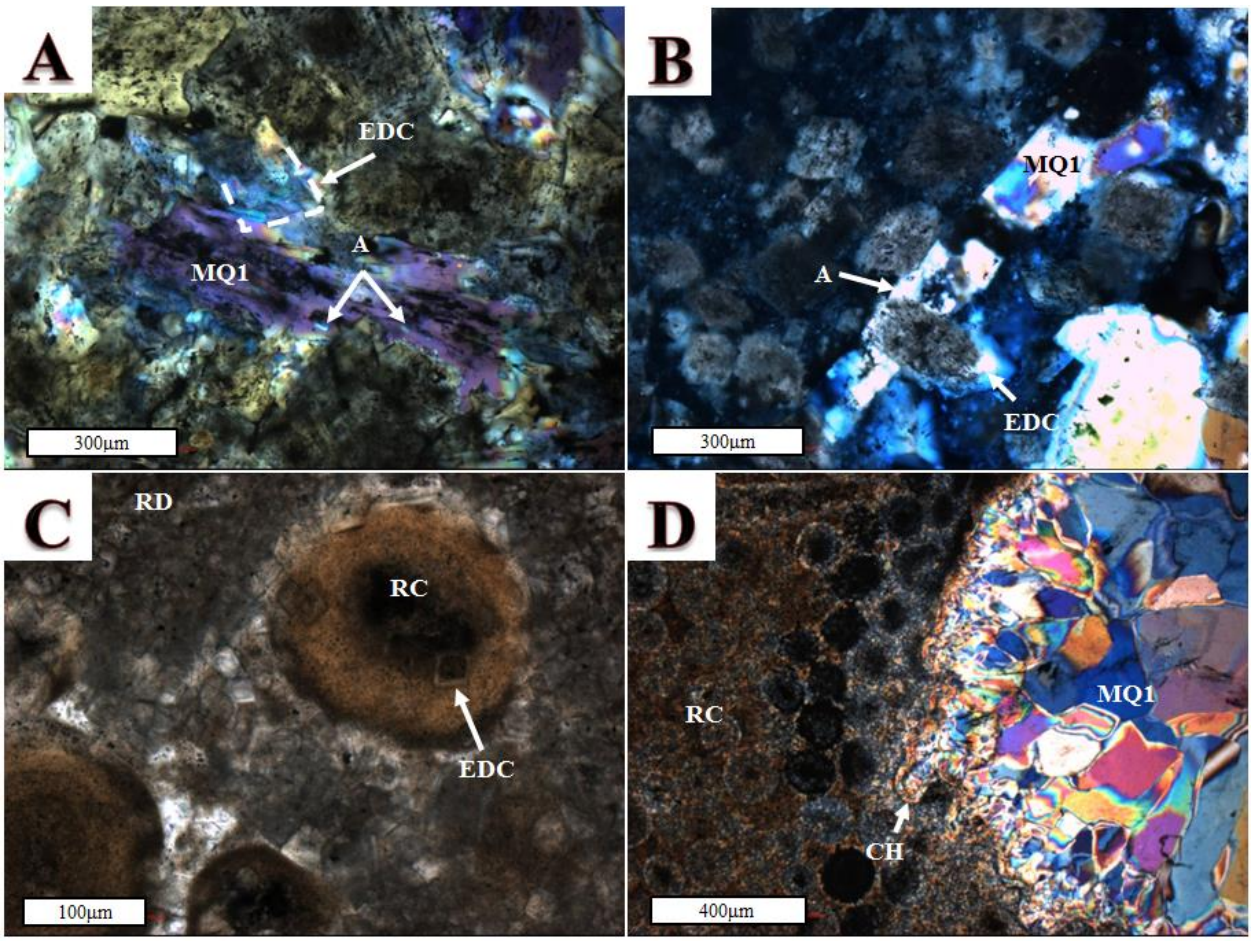


**Figure 2.7:** (A) Crossed-polarized light photomicrograph of early dolomite cements (EDC) and anhydrite (A) precipitating together and appearing to be replaced by megaquartz 1 (MQ1) (sample 4653.9 from Wellington 1-32); (B) Crossed-polarized light photomicrograph of another example of early dolomite cements (EDC) and anhydrite (A) precipitating adjacent to one another and appearing to be replaced by megaquartz 1 (MQ1) (sample 3-19 (3963.5ft) from Vulcan); (C) Transmitted light photomicrograph of ooids that were partially replaced by replacement dolomite (RD) and early dolomite cements (EDC) and then completely silicified by replacement chert (RC) (sample 4314.8 from Wellington 1-32); (D) Crossed-polarized light photomicrograph of silicified (RC) ooids, porosity is likely related to early dissolution (event 2-3-4) because chalcedony (Ch) lines vug prior to megaquartz 1 (MQ1) (sample 4744.0 from Wellington 1-32).

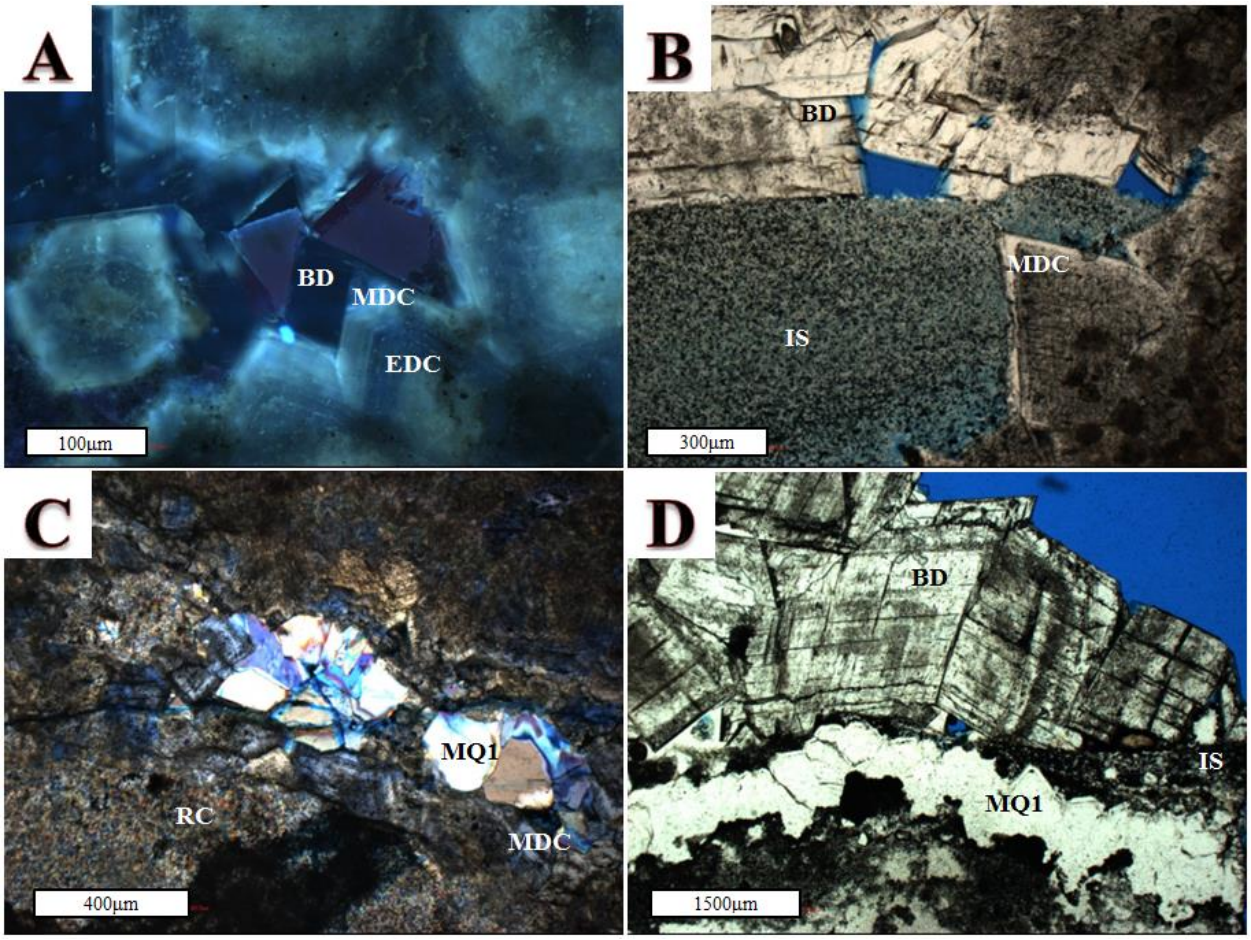


**Figure 2.8:** (A) UV-epifluorescence photomicrograph of porosity likely associated with event 2-3-4 dissolution is successively lined with early dolomite cements (EDC), middle dolomite cements (MDC), and baroque dolomite (BD) (sample 4428.7 from Wellington 1-32); (B) Transmitted light photomicrograph of porosity likely associated with event 8 dissolution is lined with middle dolomite cements (MDC), then reduced by internal sediment (IS), and finally baroque dolomite (BD) (sample 4470.9A from Wellington 1-32); (C) Crossed-polarized light photomicrograph of porosity lined with middle dolomite cements (MDC) and then fully occluded with megaquartz 1 (MQ1) (sample 4984.4A from Wellington 1-32); (D) Transmitted light photomicrograph of porosity lined with megaquartz 1 (MQ1) that is subsequently covered with internal sediment (IS) and finally baroque dolomite (BD) (sample 4966.5 from Wellington 1-32).

### *3.2. Late diagenetic stage*

*Event 14-15: Stylolitization and emanating fractures* – Burial of the Arbuckle Group led to compaction and stylolitization that has continued to develop over time. Stylolites are present throughout the entire unit. Nearly all stylolites observed display fractures emanating from peaks. Fractures and stylolites cross-cut early cements (event 10-11) and can be found occluded by baroque dolomite (event 19) (Fig. 2.9C). Silica dissolution associated with event 16-17 can be observed along fractures emanating from stylolites (Fig. 2.9D). The requirement for burial and presence of late cements filling fractures tentatively places the onset of stylolitization as the first late-stage diagenetic event, with development of pressure solution features as sediment load increased and time progressed (Machel, 1999; Mountjoy et al., 1999; Heimstra, 2003). Stylolitization likely reduced overall porosity, whereas emanating fractures locally enhanced it. Precipitation of late cements in fractures has destroyed the majority of porosity created.

*Event 14-15: Fracturing* – Vertical and sub-vertical fractures (F) can be observed, typically partially to fully occluded with later cements (event 18-23); fractures are solution enhanced in some examples (Fig. 2.10A, 2.10B, 2.10C, 2.10D). Fractures are typically isolated, relatively short, and bedding constrained. Fractures cross-cut middle dolomite cements and megaquartz 1 and are occluded with only late cements, allowing for an approximate placement in the late diagenetic history of the Arbuckle Group (Fig. 2.10A, 2.10B, 2.10C, 2.10D). Fractures associated with this event may correlate with deformation caused by the Late Paleozoic Ouachita orogeny. However, the lack of petrographic observations suggesting a later fracturing event reveals the possibility for a genetic link of at least some of the fractures to the Late Mesozoic-Early Cenozoic Laramide orogeny.

*Event 16-17: Silica dissolution* – Dissolution of silica along fractures, some that appear to be associated with stylolites and some that do not (event 14-15), provides evidence for a dissolution event increasing porosity in chert and chalcedony. The porosity resulting from this event can be observed throughout the core and has enhanced porosity by <5%. Tripolitic chert is seen in both cores and dissolution of chalcedony can be directly observed along fractures emanating from stylolites (Fig. 2.9D, 2.11A, 2.11B). The fact that dissolution is observed propagating from fractures associated with stylolites requires that at least some of the dissolution occurred after burial and compaction, making meteoric diagenesis unlikely for at least some of the dissolution observed. Silica dissolution has been proposed by others as possibly being genetically linked with the onset of hydrothermal activity in the study area (Young, 2010).

*Event 16-17: Carbonate dissolution* – Relatively late dissolution of carbonate material is indicated by large (>10mm) vugs that lack early cements but display partial- to full-occlusion with late cements (event 18-23) (Fig. 2.11C, 2.11D). Porosity resulting from this event can be observed throughout the cores and has enhanced porosity by <1%. The lack of early-stage cements, more specifically cements that are observed in porosity believed to be created by the dissolution associated with the major regional subaerial exposure event (event 8), suggests that this porosity must have occurred after burial and during late-stage diagenesis. The close association of this event with the precipitation of megaquartz cement 2 (event 18) and baroque dolomite (event 19) suggests that carbonate dissolution may be linked to the introduction of hydrothermal fluids.

*Event 18: Megaquartz cement 2* – Megaquartz cement 2 (MQ2) can be observed in samples spanning the entire length of the cores, decreasing porosity by <1%. MQ2 is present as euhedral quartz crystals lining fractures and vugs (Fig. 2.10B, 2.11B, 2.11C, 2.12A). MQ2

appears clear in transmitted light and has small (<5μm) all-liquid and two-phase fluid inclusions that feather out in the direction of crystal growth (Fig. 2.18C, 2.18D). MQ2 is non-luminescent under CL. MQ2 precipitation occurred in porosity associated with event 16-17 and can be observed precipitating into pore space after infiltration of internal sediment (Fig. 2.12A), positioning it late in the paragenesis. The presence of baroque dolomite (event 19) after MQ1 brackets this event between event 16-17 and event 19 (Fig. 2.10B, 2.12B).

*Event 19: Baroque dolomite cement* – Baroque (saddle) dolomite (BD) is the most common late diagenetic cement observed in the Arbuckle Group and can be observed in samples spanning the entire length of the unit in the Wellington 1-32 core and in the upper Arbuckle Group recovered in the Vulcan core. This event reduces porosity by <5%. BD can be found partially to fully occluding fractures and vugs occurring early in the paragenesis and as late as event 16-17 (Fig. 2.5C, 2.6C, 2.10A, 2.10B, 2.10C, 2.10D). Replacement of material not previously dolomitized appears to be common in areas fractured later in the paragenesis (event 14-15). BD displays a xenotopic-C texture with pore- and fracture-lining saddle-shaped crystals characterized by curved crystal terminations and sweeping extinction under crossed polars (Fig. 2.5C, 2.10B, 2.12D). BD appears clear under transmitted light, with cloudy cores and growth bands with a high abundance of fluid inclusions (Fig. 2.18A, 2.18B). BD is the only cement in the Arbuckle Group with recognizable hydrocarbon fluid inclusions (Fig. 2.22C, 2.22D). BD appears dead under UV-epifluorescence and very dully concentrically banded under CL with a thin double band emitting bright orange CL colors in some examples (Fig. 2.8A, 2.13B, 2.14A, 2.14B, 2.14C, 2.14D). When immersed in the ARS:PF solution, BD from the Vulcan core stains blue (ferroan), whereas BD from the Wellington core does not take a stain (non-ferroan). Baroque dolomite can be observed filling pore space following MQ2 (Fig. 2.10B, 2.12B) and

prior to calcite, sphalerite, and galena (Fig. 2.10C, 2.10D, 2.12C, 2.12D). The xenotopic-C texture, saddle morphology, and curved crystal faces of BD are indicators of high temperatures (60-150ºC) at the time of precipitation (Davies and Smith, 2006; Gregg and Sibley, 1984; Radke and Mathis, 1980).

*Event 20: Petroleum migration* – While observing samples under UV-epifluorescence petroleum fluid inclusions were observed within BD (event 19). Staining along fractures associated with event 14-15 also fluoresced under UV-epifluorescence. Petroleum fluid inclusions are present in pseudosecondary or secondary, as well as primary, fluid inclusion assemblages in baroque dolomite from the Arbuckle Group (Fig. 2.22C, 2.22D), suggesting migration during baroque dolomite precipitation and possibly for some time after.

*Event 21-22-23: Galena* – Galena is also a relatively rare precipitate within the Arbuckle Group and was observed in only two samples near the top of the unit (158ft from the top of unit in Wellington 1-32 and 12ft from the top of the unit in Vulcan), decreasing porosity by <0.5%. Galena exists as large cubic crystals that are present in open pore space and fractures (Fig. 2.10C). Galena can be observed precipitating into an open fracture (event 14-15) following precipitation of BD (Fig. 2.10C), but no paragenetic relationships were observed regarding sphalerite and calcite.

*Event 21-22-23: Sphalerite* – Sphalerite is also a relatively rare precipitate within the Arbuckle Group and was only observed in two samples in the upper portion of the Wellington 1-32 core (159ft and 255ft from the top of the unit), decreasing porosity by <0.5%. Sphalerite exists as coarse crystals that appear yellow-brown in core and yellow under transmitted light (Fig. 2.12D). A fine-grained ore with small dolomite rhombs precipitates along with the sphalerite cement (Fig. 2.12D). Sphalerite can be observed precipitating after BD (Fig. 2.10D,

2.12D) into open fractures but no paragenetic relationships were observed regarding galena and calcite. The absence of petroleum fluid inclusions in sphalerite constrains the migration of petroleum as occurring prior to sphalerite precipitation.

*Event 21-22-23: Calcite cement* – Calcite cement (CC) is a minor precipitate in the Arbuckle Group and was only observed in four samples (3 in the Wellington 1-32 core and 1 in the Vulcan core), decreasing porosity by <1%. The samples span from the base to the top of the unit. CC precipitates as very coarsely crystalline equant spar and exists as only isolated large crystals (Fig. 2.12C). CC appears clear in transmitted light with deformation twins and partially healed micro-fractures common. When exposed to CL, CC emits a light yellow color with no zoning or banding (Fig. 2.14C, 2.14D). This cement can be observed filling pore space after BD (Fig. 2.12C) but no relationships were observed regarding galena and sphalerite. Work by other authors has demonstrated that calcite typically occurs as the last stage of cement precipitation in late-stage deposits related to hydrothermal activity (Coveney et al., 2000; Brannon et al., 1996; Garven, 1993; Voss et al., 1989; Hagni and Grawe, 1964), tentatively placing calcite as the last diagenetic event in the paragenesis. The absence of petroleum fluid inclusions in calcite cement also helps to bracket the migration of petroleum as occurring prior to calcite precipitation.

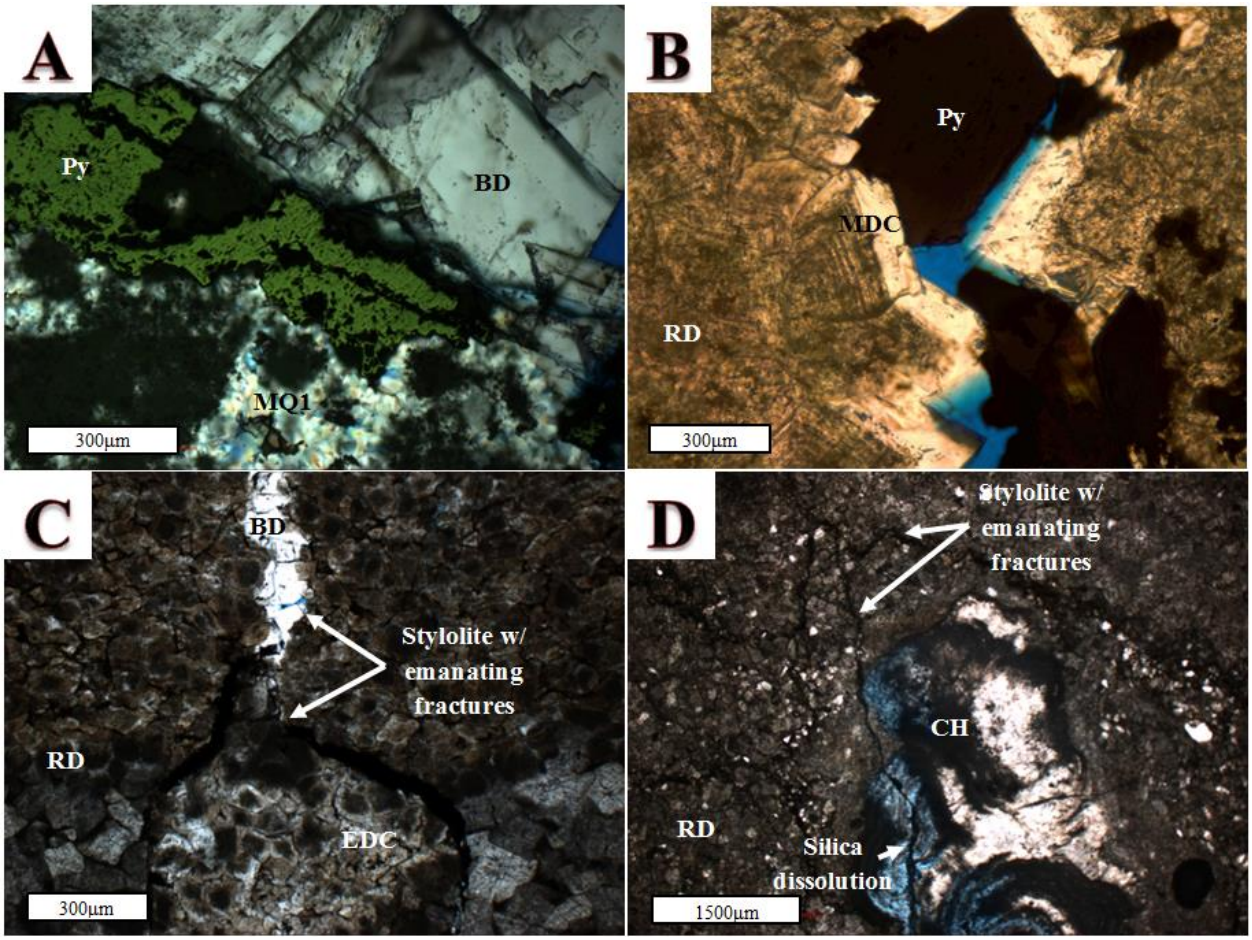


**Figure 2.9:** (A) Combination of bright-field and crossed-polarized light photomicrograph of pyrite (Py) after megaquartz 1 (MQ1), followed by precipitation of baroque dolomite (BD) (sample 4977.7 from Wellington 1-32); (B) Transmitted light photomicrograph of vug likely associated with event 8 dissolution, lined with middle dolomite cements (MDC) and then pyrite (Py) (sample 5070.6 from Wellington 1-32); (C) Transmitted light photomicrograph of replacement dolomite (RD) and early dolomite cements (EDC) truncated by stylolite and emanating fractures (event 14-15), fractures are subsequently filled with baroque dolomite (BD) (sample 4460.7 from Wellington 1-32); (D) Transmitted light photomicrograph of stylolite cross-cutting dolomitized (RD) material, emanating fracture cross-cuts chalcedony (Ch) with silica dissolution (event 16-17) occurring along fracture (sample 5070.6 from Wellington 1-32).

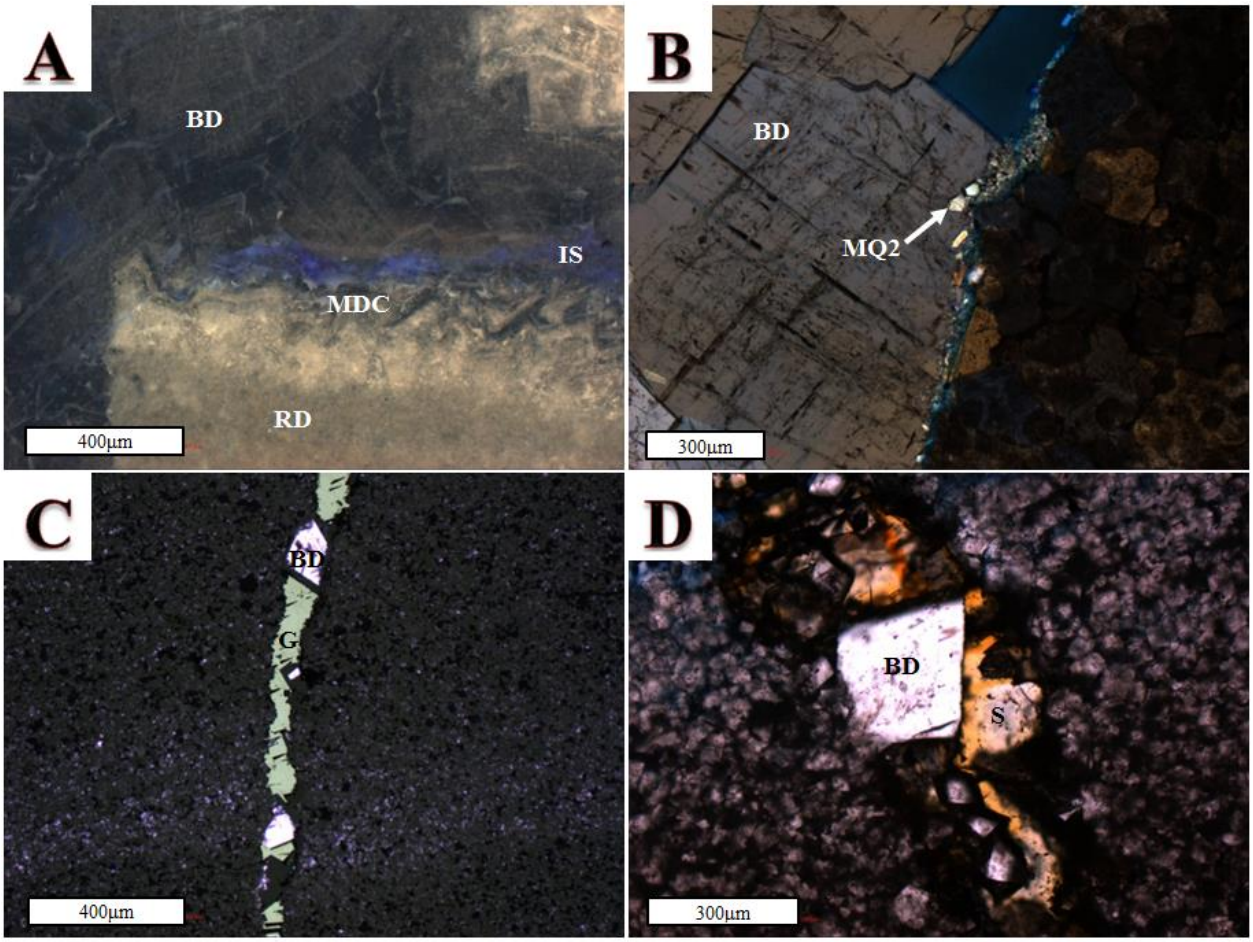


**Figure 2.10:** (A) UV-epifluorescence photomicrograph of early vug lined with middle dolomite cements (MDC) overlain by internal sediment (IS), vug is subsequently fractured (event 14-15) and porosity is occluded with baroque dolomite (BD) (sample 4984.4B from Wellington 1-32); (B) Crossed-polarized light photomicrograph of dolomitized material (RD) fractured (event 14-15) and then lined with megaquartz cement 2 (MQ2) and then baroque dolomite (BD) (sample 4470.9A from Wellington 1-32); (C) Bright-field photomicrograph of carbonate material that had been cut by a fracture (event 14-15), and filled by baroque dolomite (BD) followed by galena (G) (sample 4324.9 from Wellington 1-32); (D) Transmitted light photomicrograph of dolomitized material (RD) fractured (event 14-15) and subsequently filled with baroque dolomite (BD) and then sphalerite (S) (sample 4325.3 from Wellington 1-32).

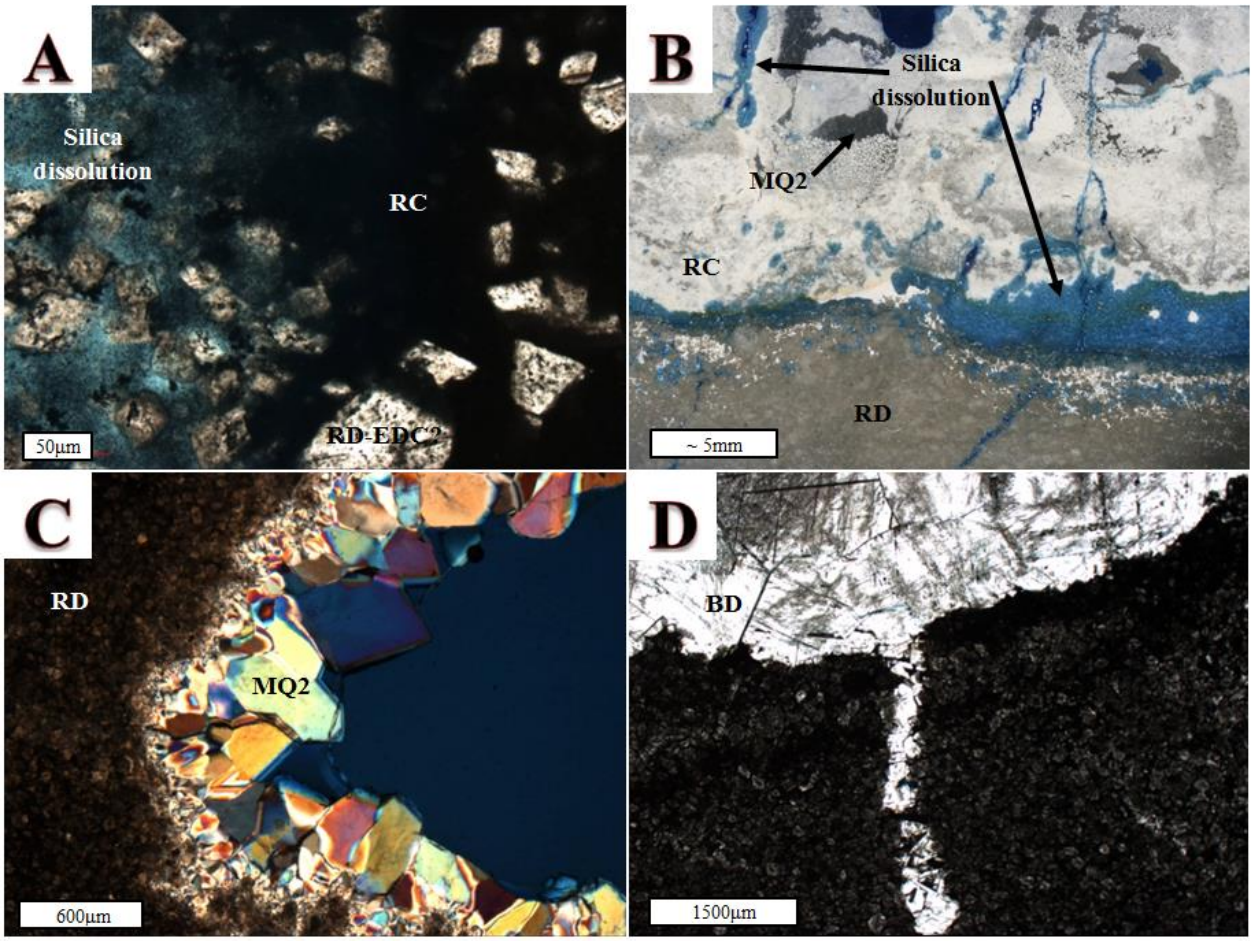


**Figure 2.11:** (A) Transmitted light photomicrograph of carbonate material that appears to have been partially dolomitized (replacement dolomite (RD) or early dolomite cements (EDC)), then silicified (RC), and finally affected by silica dissolution (event 16-17) that produced tripolitic chert (sample 3-17 (3967.3ft) from Vulcan); (B) Reflected light photomicrograph of dolomitized material (RD) that was completely silicified (RC) in the upper portion of photo, subsequent fracturing (event 14-15) allowed for silica dissolution (event 16-17) and then precipitation of megaquartz cement 2 (MQ2) (sample 4401.7 from Wellington 1-32); (C) Crossed-polarized light photomicrograph of dolomitized material (RD) subjected to dissolution likely associated with event 16-17, vug is then lined with megaquartz cement 2 (MQ2) (sample 3-5A (4005.5ft) from Vulcan); (D) Transmitted light photomicrograph of dolomitized material that is fractured (event 14-15), followed by late dissolution likely associated with event 16-17 and subsequently filled with baroque dolomite (BD) (sample 5081.9 from Wellington 1-32).

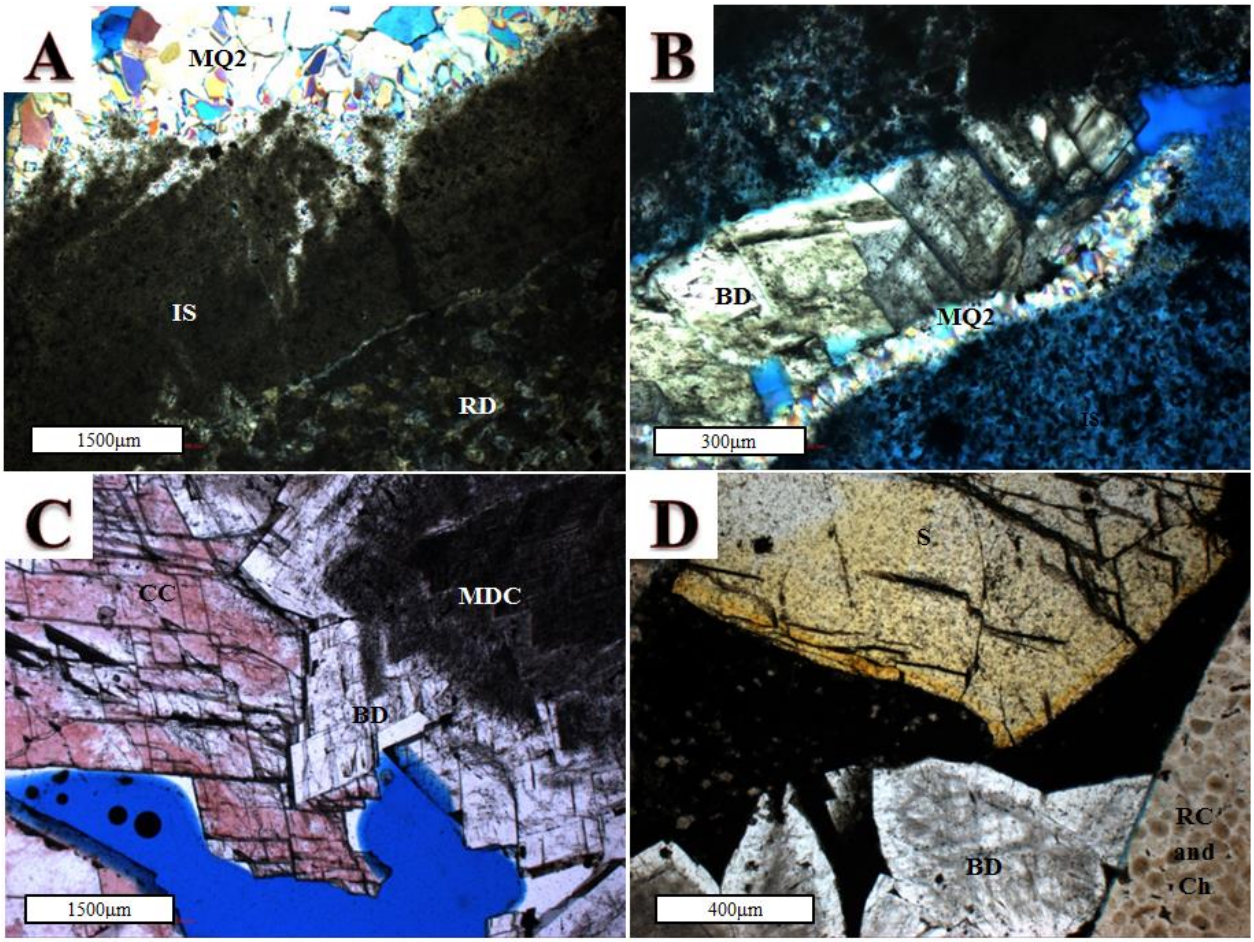


**Figure 2.12:** (A) Crossed-polarized light photomicrograph of dolomitized material (RD) affected by dissolution likely associated with event 8, porosity is subsequently filled with internal sediment (IS) and then precipitation of megaquartz cement 2 (MQ2) (sample 4806.0 from Wellington 1-32); (B) Crossed-polarized light photomicrograph of silica dissolution (event 16-17) enhancing porosity, porosity is occluded with megaquartz cement 2 (MQ2) and then baroque dolomite (BD) (sample 4966.5 from Wellington 1-32); (C) Transmitted light photomicrograph of brecciated material that is lined with middle dolomite cements (MDC) and then baroque dolomite (BD), with calcite cement (CC) that has taken a alizarin red S stain reducing porosity last (sample 5061.5A from Wellington 1-32); (D) Transmitted light photomicrograph of silicified material (replacement chert (RC) and chalcedony (Ch)) is fractured (event 14-15) and then filled with baroque dolomite (BD), sphalerite (S) and fine-grained ore associated with sphalerite appearing to precipitate into fracture following baroque dolomite (sample 4421.1B from Wellington 1-32).

## 4. Cement Stratigraphy

Compositional differences in carbonate cement growth zones are frequently used to correlate the extent of distinctive cements vertically and laterally, allowing for the delineation of a cement stratigraphy (Goldstein, 1991; Meyers, 1991). Cathodoluminescence (CL) imaging has proven to be an effective tool in displaying these distinct compositional differences (Goldstein, 1991; Meyers, 1991; Machel and Burton, 1991) and has been commonly employed in the successful description and correlation of regionally extensive dolomite growth zones in age-equivalent units and MVT deposits (Heimstra, 2003; Smith and Simo, 1997; Montanez and Read, 1992; Kupecz and Land, 1991; Farr, 1989; Voss et al., 1989; Gregg and Hagni, 1987; Gregg, 1985). Dolomite, as a replacement feature or cement, appears to be the most common diagenetic feature affecting the porosity of the Arbuckle Group. CL patterns and spatial distributions of dolomite occurrences and the calcite cement are discussed below and referred to by abbreviations established in the paragenesis (see Paragenesis discussion above or Fig. 2.4).

### *4.1. Dolomite cement stratigraphy discussion*

Dolomite occurrences were separated into one replacement feature (RD) and five cements (EDC - DC1, DC2; MDC - DC3, DC4; and BD), based on petrographic observations and CL characteristics. Regarding overall volume of dolomite occurrences, RD is the most abundant (~75 %), followed by BD cementation (~7%) and then relatively minor occurrences of cements DC1 (~2%), DC2 (~7%), DC3 (~7%), and DC4 (~2%). All dolomite occurrences can be observed throughout the vertical extent of the Arbuckle Group and correlated between the Vulcan and Wellington cores, with little variation in abundance. RD (event 3) displays patchy red and yellow-green CL colors, indicating some spatial variability in composition vertically

(Fig. 2.13A, 2.13B, 2.13C). DC1 (event 5) is consistently non-luminescent under CL with no observed variability (Fig. 2.13A, 2.13B). DC2 (event 5) displays concentric red and non-luminescent bands under CL in some examples, but more commonly appears very patchy with red and non-luminescent mottling (Fig. 2.13A, 2.13B, 2.13C, 2.13D); the contact between DC1 and DC2 can be obscured by extensive mottling. No notable compositional variability was observed in DC2 when progressing up section or between cores. DC3 (event 10) displays concentric banding of thin green-yellow-red and non-luminescent bands that display little variability in CL colors, with potential polyhedral crystal growth and a corrosion surface between DC3 and DC4 (Fig. 2.13B, 2.13C, 2.13D); no variability in composition was observed. DC4 (event 10) displays sector growth zoning of red, non-luminescent, and yellow CL colors (Fig. 2.13C, 2.13D); compositional variability is indicated by the presence of yellow growth bands in some examples as one moves up in section and between cores. BD (event 20) displays concentric banding of non-luminescent, dull orange, and bright orange CL color bands (Fig. 2.13B, 2.14A, 2.14B, 2.14C, 2.14D). The only variability in BD CL pattern is the presence of paired bright orange bands occurring late in cement growth history (always at the outer crystal margin). The paired bands are absent in some samples, but the observation that they only occur late in crystal growth history and are only absent when porosity is fully-occluded implies that porosity was completely occluded prior to the latest stage of fluid migration responsible for BD precipitation in some places, resulting in the local absence of the double bands.

### *4.2. Calcite cement stratigraphy discussion*

CC (event 22-23-24) is the only calcite cement observed in this study and is present in both the Wellington and Vulcan cores as a minor late-stage diagenetic event. Only four samples

contained CC, but the cement was observed at the lower, middle, and upper portion of the Arbuckle Group, spanning the vertical extent of the Arbuckle Group. CC displays a consistent dull yellow-orange color in CL and has no evidence for growth zoning (Fig. 2.14C, 2.14D). There appears to be no variability in color when progressing up section or between cores, indicating the fluid responsible for calcite precipitation was relatively homogeneous in composition throughout the Arbuckle Group.

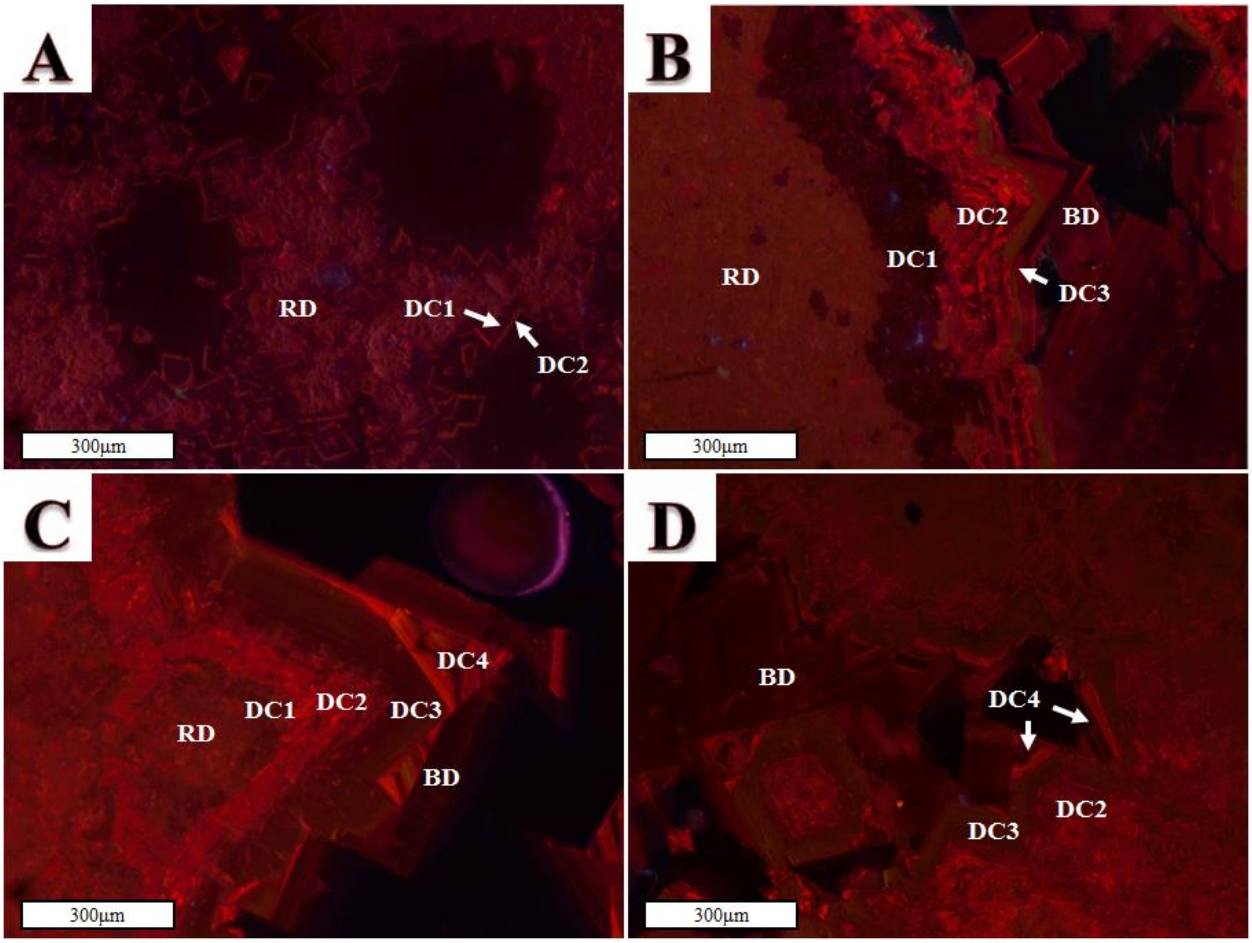

**Figure 2.13:** All images are CL photomicrographs: (A) Replacement dolomite (RD) appears red and mottled, but can have a more yellow-green tint in other samples (Fig. 13B, 13C); Dolomite cement 1 (DC1) is commonly non-luminescent and dolomite cement 2 (DC2) appears as red bands, with both early dolomite cements typically appearing mottled, which is indicative of recrystallization or potentially large empty fluid inclusions (sample 4314.8 from Wellington 1-32); (B) mottled replacement dolomite (RD) appears to have been partially recrystallized by dolomite cement 1 (DC1) which was followed by highly mottled dolomite cement 2 (DC2), Dolomite cement 3 (DC3) displays thin green-yellow-red and non-luminescent bands and possible polyhedral growth; this is followed by precipitation of baroque dolomite (BD) with thick dull-red luminescent bands and the presence of double bright red-orange bands (sample 4271.5 from Wellington 1-32); (C) displays highly mottled replacement dolomite (RD), dolomite cement 1 (DC1), and dolomite cement 2 (DC2), with minor mottling of dolomite cement 3 (DC3), image also shows typical sector zoning of thin red, yellow, and non-luminescent bands in dolomite cement 4 (DC4), with baroque dolomite (BD) precipitation following (sample 4574.4 from Wellington 1-32); (D) displays extensively mottled dolomite cement 2 (DC2), followed by precipitation of dolomite cement 3 (DC3), dolomite cement 4 (DC4) and baroque dolomite (BD) (sample 4428.7 from Wellington 1-32).

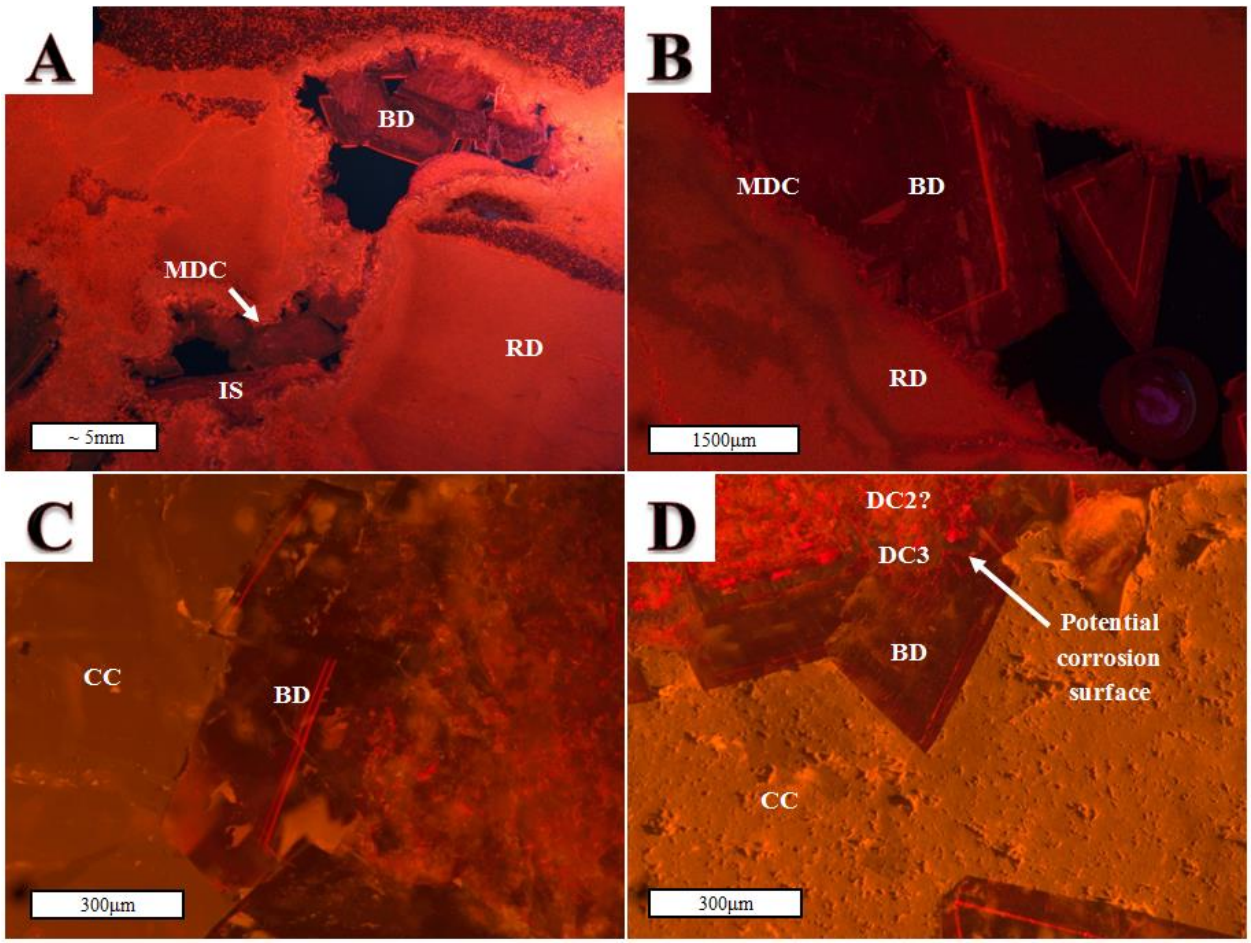

**Figure 2.14:** All images are CL photomicrographs: (A) Replacement dolomite (RD) was affected by dissolution associated with event 8, porosity was then lined with dolomite cement 3 (DC3) and dolomite cement 4 (DC4), then infiltrated with internal sediment (IS), and subsequently lined with baroque dolomite (BD) displaying thick dull-red bands and the double red-orange band as the last stage of crystal growth (sample 4524.8 from Wellington 1-32); (B) Brecciated material (event 9) lined with dolomite cement 3 (DC3) and dolomite cement 4 (DC4) and then filled with baroque dolomite (BD) displaying dull-red bands and only one band from the double red-orange band (sample 4755.4 from Wellington 1-32); (C) Pore lined with baroque dolomite (BD) displaying double red-orange band, followed by dull-yellow luminescence of calcite cement (CC) (sample 3-14 (3979.1ft) from Vulcan); (D) Porosity lined with dolomite cement 2 (DC2), dolomite cement 3 (DC3), and baroque dolomite (BD), with a potential corrosion surface between DC3 and BD; calcite cement (CC) subsequently fills porosity (sample 3-11 (3983.2ft) from Vulcan).

## 5. SEM Analysis

SEM-BSE analysis was performed on four baroque dolomite (BD) samples, with at least one sample obtained from the bottom, middle, and top of the Arbuckle Group (Appendix II). BSE-imaging was performed to support or refute the potential for BD recrystallization, and to illustrate the impact recrystallization may have had on microthermometric data obtained from fluid inclusions. The images collected reveal at least four separate dolomite growth zones with rare patches of calcite, as well as extensive fracturing and subsequent recrystallization associated with what appears to be the latest stage of crystal growth (Fig. 2.15). Additional growth zones may be present, but these were difficult to discern with certainty throughout the samples.

### *5.1. Early dark-grey zone (EDZ)*

The early dark-grey zone appears to have formed during precipitation of finer-grained individual dolomite crystals; this is most notable when compared to the larger-scale growth bands associated with single dolomite crystals in successive growth zones (Fig. 2.15A). The general lack of patchiness or mottling implies that recrystallization has likely not affected this early stage of cement growth or that BSE does not allow its detection.

### *5.2. Middle light-grey zone (MLZ)*

The middle light-grey zone is the thickest growth zone observed; there are likely multiple vague concentric subzones that are also present but these were not observed with certainty. Microfractures have shattered this zone in every sample observed (Fig. 2.15B, 2.15C, 2.15D). Extensive darker BSE appears to propagate from the microfractures, displaying dark-grey streaks and mottling that appear to be associated with the recrystallization along microfractures during precipitation of the late dark-grey zone (Fig. 2.15B, 2.15C, 2.15D). There also appears to be evidence for preferential recrystallization along certain subzones (Fig. 2.15D). Calcite has replaced small patches of this zone as very small (<10μm), localized bright BSE inclusions (Fig. 2.15D, 2.16). If compared to the average size of fluid inclusions within baroque dolomite, fluid inclusions within this zone appear to be slightly larger (~20μm); smaller fluid inclusions are concentrated within the darker recrystallized fabric, typically appearing to be <10μm (Fig. 2.15C).

### *5.3. Middle medium-grey zone (MMZ)*

The middle medium-grey zone is a growth band that is approximately 150μm thick (Fig. 2.15A, 2.15B); this zone can be recognized in all of the baroque dolomite samples that were imaged. Similar to the middle light-grey zone, this zone has been cross-cut by microfractures that appear to have acted as conduits for fluids associated with precipitation of the late dark-grey zone (Fig. 2.15B). Small (<10μm) fluid inclusions appear to be concentrated within the dark BSE fabric associated with microfractures.

*5.4. Late dark-grey zone (LDZ)*

The late dark-grey zone is a thin growth band that is approximately 40µm thick (Fig. 2.15A, 2.15B); this zone appears to be the last stage of baroque dolomite crystal growth. Because this growth band was so thin, it was only recognized in one sample. The dark-grey BSE of this zone appears to correspond with the dark-grey BSE of the recrystallized fabric associated with microfractures, suggesting recrystallization of earlier zones occurred during precipitation of this zone as a cement. Fluid inclusions are most abundant in this zone and are concentrated in recrystallization along microfractures that appear to be associated with this last stage of dolomite precipitation and recrystallization (Fig. 2.15C, 2.15D).

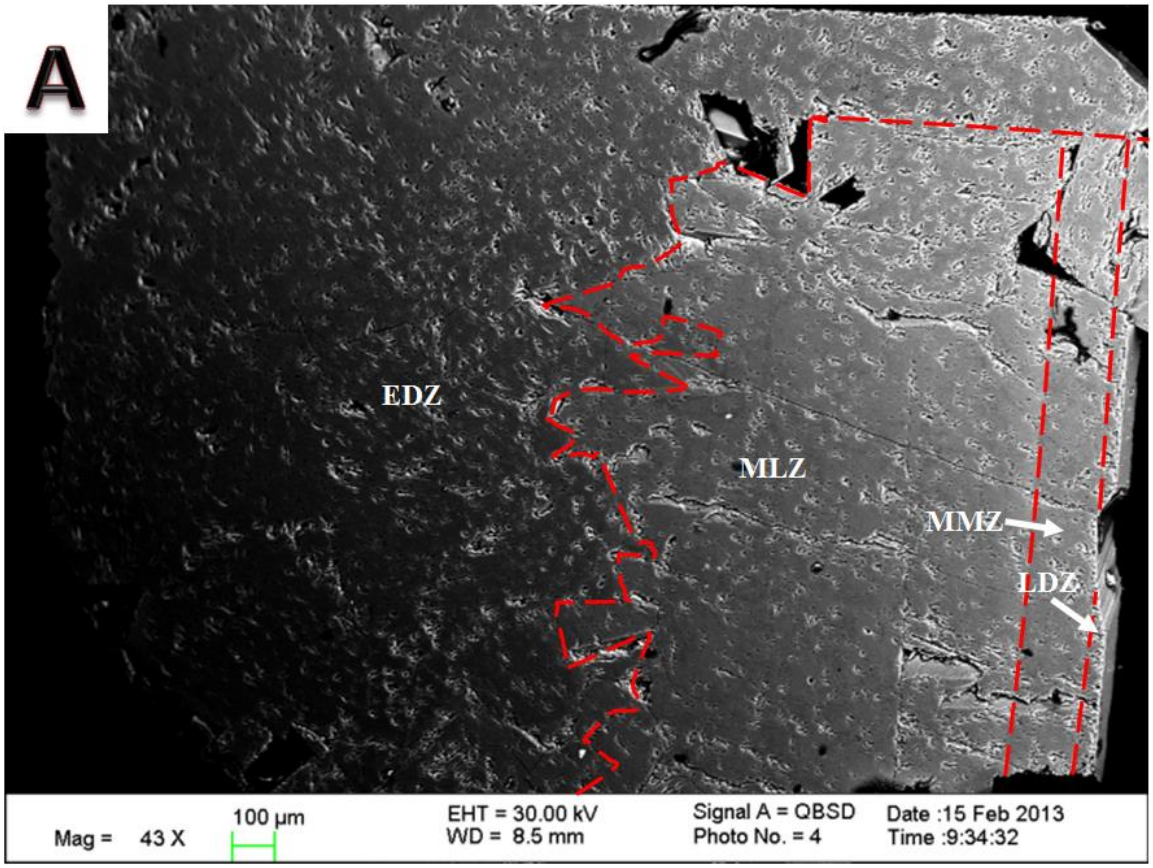

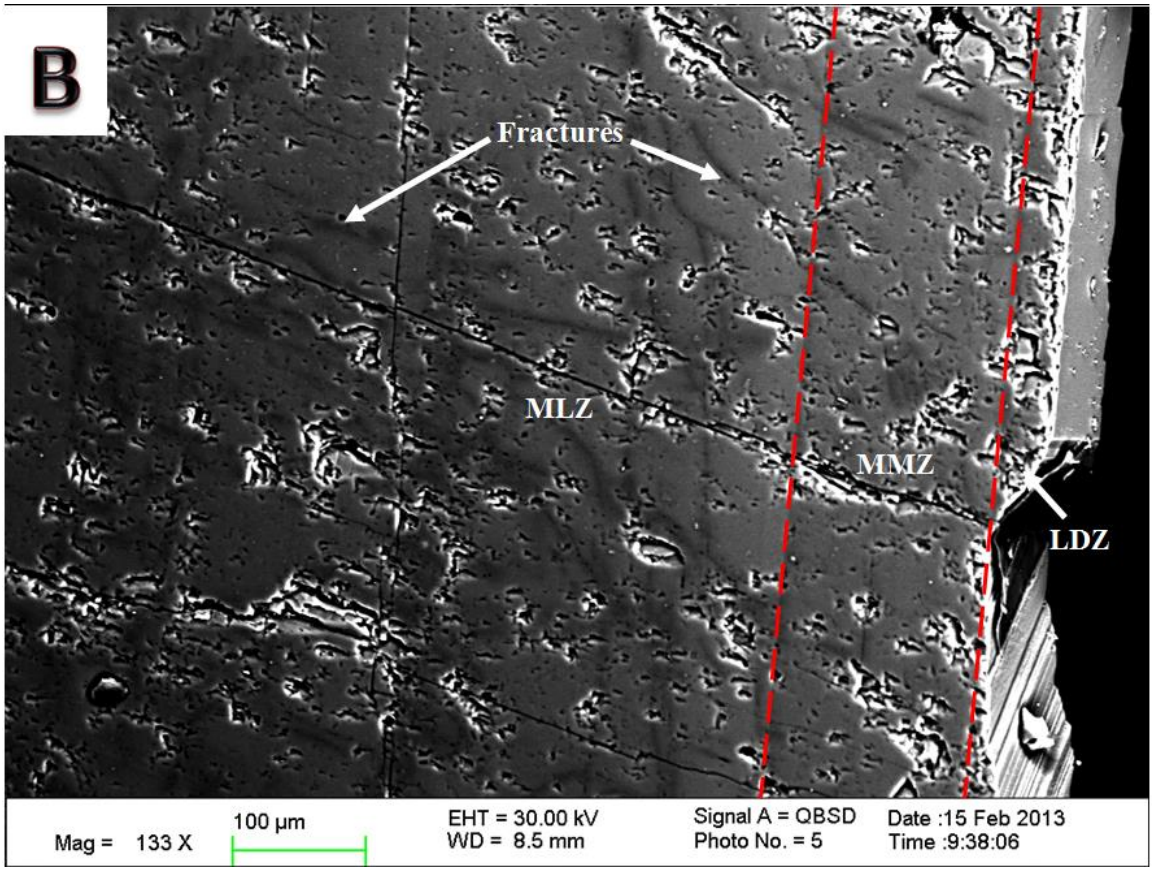
B
Fractures
MLZ
MMZ
LDZ
Mag = 133 X
100 µm
EHT = 30.00 kV
WD = 8.5 mm
Signal A = QBSD
Photo No. = 5
Date :15 Feb 2013
Time :9:38:06

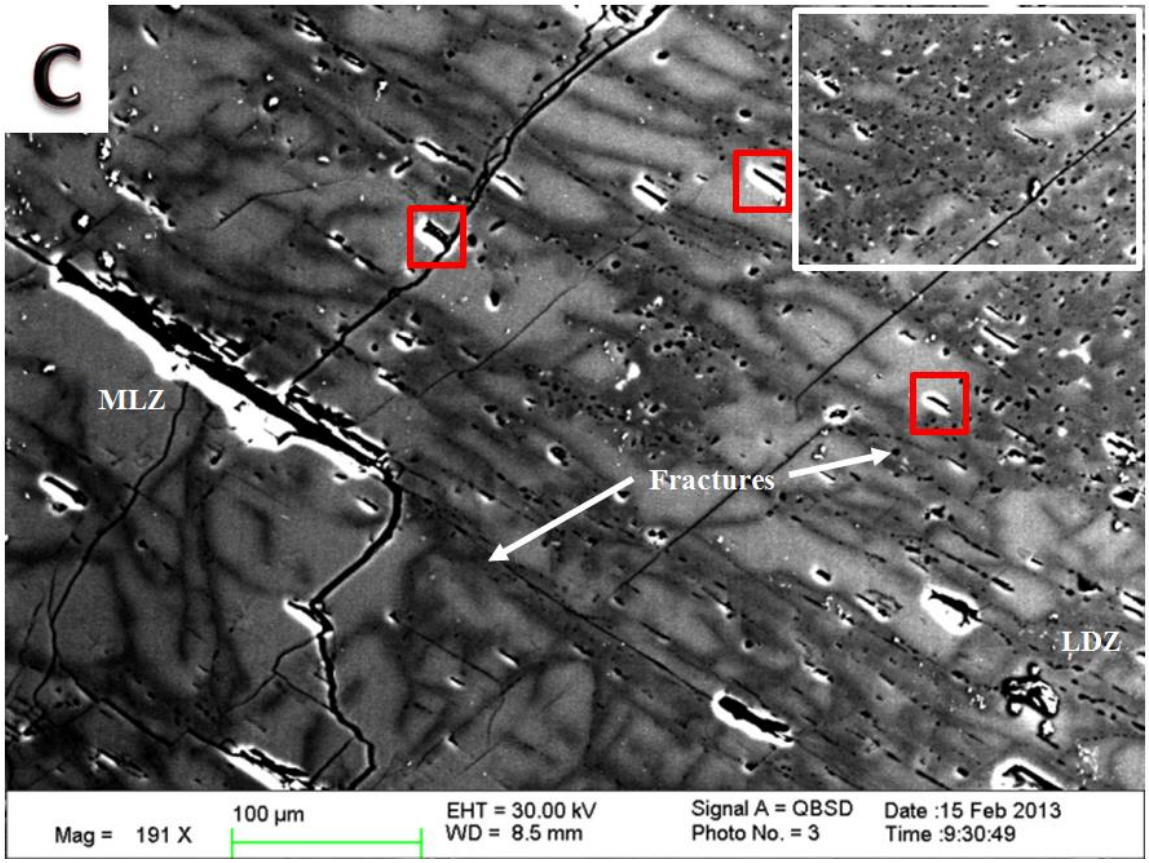
C
MLZ
Fractures
LDZ
Mag = 191 X
100 µm
EHT = 30.00 kV
WD = 8.5 mm
Signal A = QBSD
Photo No. = 3
Date :15 Feb 2013
Time :9:30:49

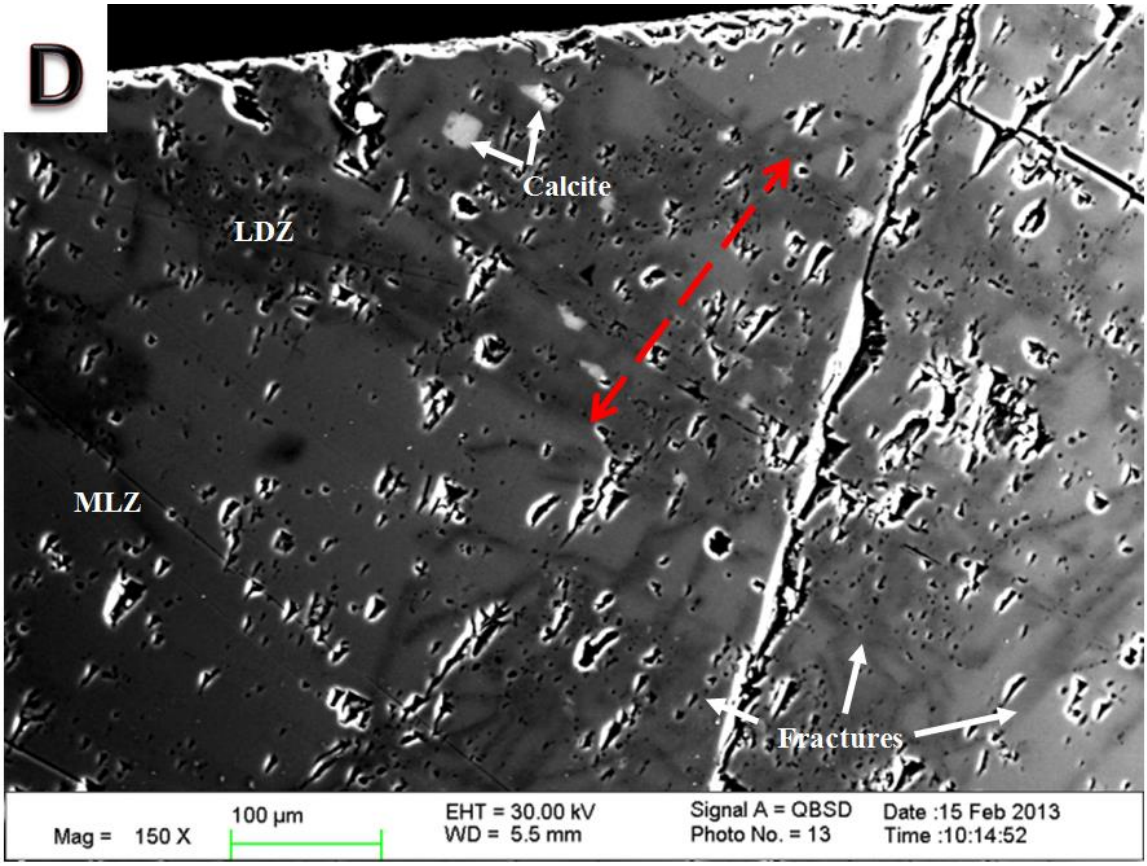


**Figure 2.15:** All images are SEM-BSE photomicrographs: (A) The entire range of observed growth zones can be seen here, initial finer-grained crystal growth is illustrated by irregular red line delineating extent of early dark-grey zone (EDZ), this is followed by coarser-grained crystal growth associated with middle light-grey zone (MLZ), middle medium-grey zone (MMZ), and late dark-grey zone (LDZ); (B) Higher magnification photo displaying microfractures and distinction between middle light-grey zone (MLZ), middle medium-grey zone (MMZ), and late dark-grey zone (LDZ); (C) High magnification photo of middle light-grey zone (MLZ) showing extensive fracturing and subsequent recrystallization by late dark-grey zone (LDZ); (D) Image of middle light-grey zone (MLZ) with extensive microfracturing, followed by preferential recrystallization along fractures and ambiguous growth zone; image also shows white calcite domains likely resulting from recrystallization of dolomite during later precipitation of calcite.

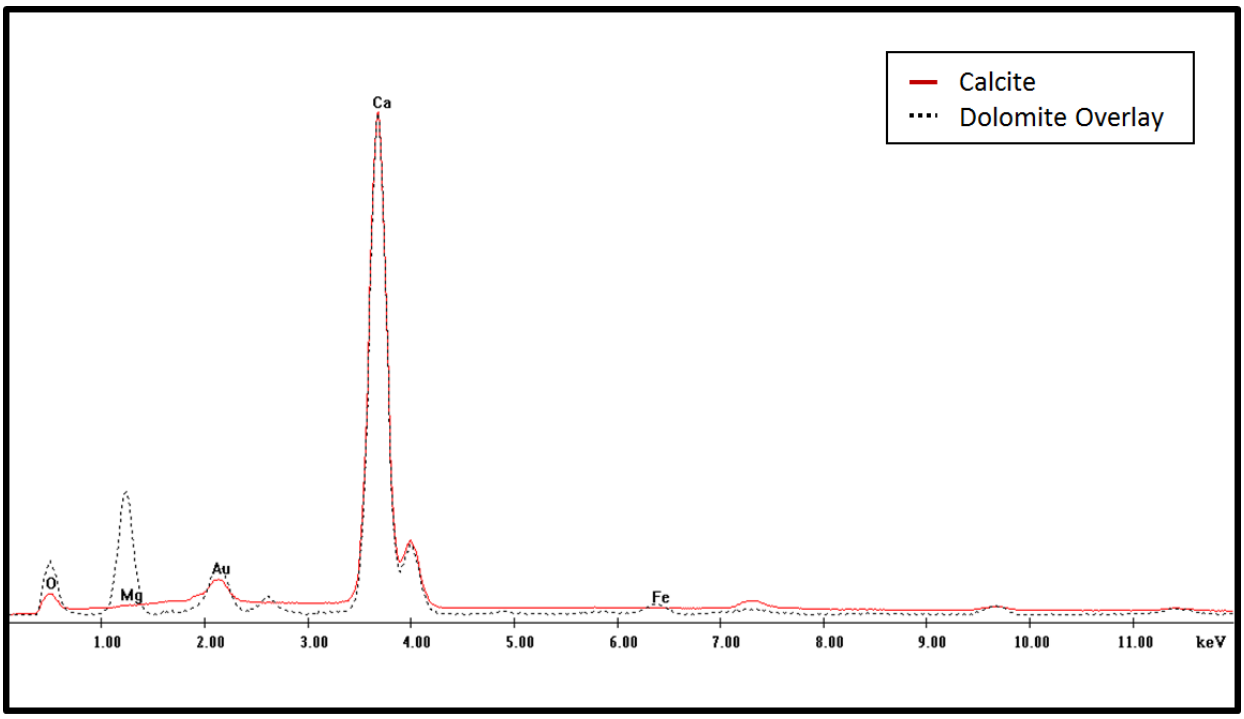


**Figure 2.16:** Compositional analysis of small calcite domain is illustrated by the red line and compositional analysis of baroque dolomite is illustrated by the dashed line. Note the lack of a magnesium (Mg) peak in the calcite analysis.

## 6. Fluid Inclusion Analysis

The following section discusses fluid inclusion petrography and microthermometry of early dolomite cements (DC1 and DC2), middle dolomite cements (DC3 and DC4), early megaquartz (MQ1), late megaquartz (MQ2), baroque dolomite (BD), and calcite cement (CC) (Appendix III). Discussions are in paragenetic order. The methodology and terminology proposed by Goldstein and Reynolds (1994) is used for fluid inclusion analysis. The term fluid inclusion assemblage (FIA) is used throughout and is defined as "the most finely discriminated, petrographically distinguishable group of inclusions" within a given mineral phase (Goldstein and Reynolds, 1994; Goldstein, 2003). Goldstein and Reynolds (1994) define a consistent FIA as one in which ≥ 90% of homogenization temperature (Th) data fall within a range of 10º-15ºC; and an inconsistent FIA as one that yields more variable Th data. Consistent Th data are

interpreted to mean that thermal reequilibration of fluid inclusions has not occurred (Goldstein and Reynolds, 1994). The microthermometric data provided consist of homogenization temperatures (Th) and final melting temperatures of ice ($Tm_{ice}$). $Tm_{ice}$ are translated to salinity in weight percent NaCl equivalent (wt. % NaCl eq.). Salinity was calculated from $Tm_{ice}$ measurements using the AqSoVir program from Bakker (2008) and the equation from Bodnar (1993):

*Equation 2.1*: Salinity (wt. % NaCl eq.) = $0.00 + 1.78\theta - 0.0442\theta^2 + 0.000557\theta^3$

where $\theta$ equals the depression of the freezing point in °C (Bodnar, 1993). $Tm_{ice}$ data were only collected from fluid inclusions with gas bubbles present before final melting. Th data was preferentially measured from fluid inclusions that appeared to result from homogeneous entrapment or were likely the liquid-rich end member of an FIA with evidence for heterogeneous entrapment (Goldstein and Reynolds, 1994). The first melting temperature of several samples was approximated in some instances and is considered to have some degree of uncertainty due to petrographic limitations. An interpretation of fluid inclusion data is provided for each diagenetic event.

### *6.1. Early dolomite cements*

*Petrography:* Early dolomite cements (event 5) consist of dolomite cement 1 (DC1) and dolomite cement 2 (DC2). DC1 and DC2 both appear clear under transmitted light and contain primary FIAs mimicking concentric growth of dolomite rhombohedra. Fluid inclusions are relatively abundant within both early cements and vary in size and shape, with the long axis of fluid inclusions running parallel to crystal growth direction. Two-phase fluid inclusions consisting of an aqueous liquid and gas bubble are common, with variable liquid-gas ratios in

FIAs; all-liquid inclusions are common alongside the two-phase fluid inclusions (Fig. 2.17B). Evidence for necking-down after a phase change is not readily observable, though the high abundance of inclusions may mask petrographic pairing (Goldstein and Reynolds, 1994). Both cements appear patchy under cathodoluminescence, indicating potential for recrystallization (Fig. 2.13A, 2.13B, 2.13C, 2.13D).

*Microthermometry:* The presence of all-liquid inclusions in both cements implies formation of inclusions at low-temperatures (<50ºC); the lack of a gas bubble prevented Th measurements (Goldstein and Reynolds, 1994). Attempts were made to overcome nucleation metastability and generate gas bubbles in all-liquid samples by placing samples in a freezer for 4-5 weeks; this method resulted in no bubble generation. Several Th measurements from two-phase fluid inclusions resulted in a temperature range of 89-183ºC. Although many inclusions contained gas bubbles, additional measurement was avoided because of the potential for heterogeneous entrapment and thermal reequilibration (Goldstein and Reynolds, 1994).

A total of three inconsistent primary FIAs were subjected to freezing for the purpose of obtaining $Tm_{ice}$ values (Fig. 2.18). $Tm_{ice}$ measurements were conducted on two-phase fluid inclusions, rather than all-liquid fluid inclusions that had been heated and stretched to generate a gas bubble. $Tm_{ice}$ values ranged from -21.3 to -23.0ºC for DC1 and -17.5 to -22.3ºC for DC2 (Fig. 2.18). Melting was observed as consolidation of low-relief, rounded crystals into a larger crystal that slowly melted until completely disappearing; this was commonly accompanied by sudden movement of the gas bubble. $Tm_{ice}$ data resulted in salinities ranging from 23.2-24.3 wt. % NaCl eq. for DC1 and 20.6-23.9 wt. % NaCl eq. for DC2.

*Interpretation:* Th measurements of two-phase fluid inclusions range from 89-183ºC and large all-liquid aqueous inclusions are commonly observed. Large all-liquid inclusions strongly

suggest entrapment during low-temperature diagenetic conditions (when large in size and petrographic pairing is not observed), but the presence of two-phase inclusions and elevated Th measurements suggests some complexity (Goldstein and Reynolds, 1994). Possible explanations include: (1) heterogeneous entrapment at low-temperatures, (2) homogeneous entrapment at low-temperature conditions followed by thermal reequilibration, (3) homogeneous entrapment at low-temperatures followed by recrystallization, or (4) a combination of each scenario. Scenario (1) would provide all-liquid, low-temperature inclusions and allow for the Th measurements if the two-phase fluid inclusions measured represented variable end-members of inconsistent liquid-gas ratios entrapped during heterogeneous conditions; however, the patchiness under CL-imaging suggests that recrystallization likely affected early dolomite cements sometime in the past. Scenario (2) would provide all-liquid, low-temperature inclusions but Th measurements associated with late hydrothermal cements did not reach values as high as 183ºC, necessitating another process to produce such values. Scenario (3) would provide all-liquid, low-temperature inclusions and allow for the Th measurements if recrystallization occurred during heterogeneous entrapment conditions and measurements were conducted on variable liquid-gas end-members; this would also account for the patchiness observed in CL-imaging, but the onset of hydrothermal activity late in the paragenesis suggests potential for thermal reequilibration resulting in leaking and refilling of inclusions. Whereas scenario (3) could result in the characteristics of early dolomite cements, a combination (scenario 4) of all three scenarios remains a possibility.

High salinity values (20.6-24.3 wt. % NaCl eq.) in early dolomite cements strongly indicate an association with evaporites (Hanor, 1979), either through (1) dissolution of evaporites during fluid migration or (2) reflux of evaporative fluids. The fact that the $Tm_{ice}$ measurements

were conducted on two-phase fluid inclusions, and not all-liquid fluid inclusions that were heated and stretched to generate a gas bubble, leaves potential for these measurements to have been taken from fluid inclusions that had reequilibrated with later diagenetic fluids. If the salinity values do represent original diagenetic fluids, the elevated salinities could be attributed to refluxing evaporative fluids or dissolution of Arbuckle Group evaporites. Similar to the findings of other authors, through reflux of high density evaporative brines, fluids seeping down through the Arbuckle Group would have replaced original carbonate facies and precipitated early dolomite cements; these fluids may have even increased in salinity through evaporite dissolution during fluid migration (Garcia-Fresca et al., 2012; Shelton et al., 2009; Jones and Xiao, 2005; Franseen et al., 2004; Machel, 2004; Gao et al., 1995; Gao and Land, 1991; Land, 1985; Ross, 1976; Harris, 1973). Alternatively, these values could represent late diagenetic fluids; these are discussed in more detail in later sections.

### *6.2. Middle dolomite cements*

*Petrography:* Middle dolomite cements (event 10-11) consist of dolomite cement 3 (DC3) and dolomite cement 4 (DC4). DC3 and DC4 appear mostly clear under transmitted light (17A, 17B, 17C, 17D). DC3 generally lacks fluid inclusions with scattered large inclusions present at the contact between DC2 and DC3; these inclusions are typically elongate in crystal growth direction, vary in size and shape, and can be two-phase or all-liquid (Fig. 2.17C). In cases where two phases are present in an inclusion, the liquid-gas ratios of the FIAs appear fairly consistent. Petrographic pairing is not observed in fluid inclusions, indicating necking down after a phase change is not the explanation for the all-liquid fluid inclusions (Goldstein and Reynolds, 1994). DC4 lacks fluid inclusions but solid pyrite inclusions can be observed in the

later growth zones of this cement. Pyrite inclusions occur as assemblages of opaque cubes under transmitted light (Fig. 2.17D). Vague patchiness can be observed in DC3 when exposed to cathodoluminescence, allowing for the possibility of recrystallization (Fig. 2.13C).

*Microthermometry:* The general lack of fluid inclusions and even greater paucity of two-phase inclusions resulted in limited microthermometric data for middle dolomite cements; no data was acquired for DC4 due to the lack of measureable fluid inclusions. Similar to early dolomite cements, the presence of all-liquid inclusions implies formation of inclusions at low-temperatures (<50ºC), and the lack of a gas bubble prohibited Th measurements of such inclusions (Goldstein and Reynolds, 1994). Attempts were made to generate gas bubbles in all-liquid samples by placing samples in a freezer for 4-5 weeks; this method resulted in no bubble generation. Several attempts were made to gather Th data from two-phase fluid inclusions, resulting in temperatures ranging from 99.0-106.1ºC. Additional Th measurements were abandoned due to the potential for thermal reequilibration (Goldstein and Reynolds, 1994).

A total of three inconsistent primary FIAs were subjected to freezing for the purpose of obtaining $Tm_{ice}$ values. $Tm_{ice}$ measurements were conducted on two-phase fluid inclusions, and not all-liquid fluid inclusions that were heated and stretched to generate a gas bubble. Freezing of fluid inclusions typically resulted in a sudden jerk or decrease in size of the gas bubble. Upon warming the inclusions, first melting is estimated to have occurred between -43 and -57ºC for DC3, recognized by the occurrence of an "orange peel" texture (Goldstein and Reynolds, 1994). $Tm_{ice}$ occurred between -19.0 and -22.9ºC in DC3 (Fig. 2.18). Melting was observed as consolidation of low-relief, rounded crystals into a larger crystal that slowly melted until completely disappearing. This was commonly accompanied by sudden movement of the gas bubble. $Tm_{ice}$ data resulted in salinities ranging from 21.7 – 24.3 wt. % NaCl eq.

*Interpretation:* Th measurements of two-phase fluid inclusions range from 99-106ºC and large all-liquid aqueous inclusions are commonly observed. Large all-liquid inclusions strongly suggest entrapment during low-temperature diagenetic conditions (when large in size and petrographic pairing is not observed), but the presence of two-phase inclusions and elevated Th measurements suggests some complexity (Goldstein and Reynolds, 1994). Possible explanations include: (1) homogeneous entrapment at low-temperature conditions followed by thermal reequilibration, (2) homogeneous entrapment at low-temperatures followed by recrystallization, or (3) a combination of each scenario. Scenario (1) would provide all-liquid, low-temperature inclusions and the range of Th measurements, but patchiness observed in DC3 would still require some recrystallization. Scenario (2) would provide all-liquid, low-temperature inclusions and allow for the Th measurements if recrystallization occurred during later dolomite precipitation with elevated temperature conditions; this would also account for the patchiness observed in CL-imaging, but the onset of hydrothermal activity late in the paragenesis suggests potential for thermal reequilibration. Whereas scenario (2) could result in the characteristics of middle dolomite cements, a combination (scenario 3) of both scenarios remains a possibility.

As with early dolomite cements, high salinity values (21.7 – 24.3 wt. % NaCl eq.) in middle dolomite cements strongly indicate an association with evaporites (Hanor, 1979), either through (1) dissolution of evaporites during fluid migration or (2) reflux of evaporative fluids. Also similar to early dolomite cements, $Tm_{ice}$ measurements were conducted on two-phase fluid inclusions, and not all-liquid fluid inclusions that were heated and stretched to generate a gas bubble, thus, it is possible that measurements were from fluid inclusions that reequilibrated with later diagenetic fluids. The timing of middle dolomite cement precipitation is interpreted to have occurred during sea-level fluctuations possibly associated with the major post-Sauk subaerial

exposure event but prior to burial (see Paragenesis section 3.). Fluctuations in sea level during the subaerial exposure event could have provided evaporative seawater that was capable of seeping down through the Arbuckle Group and precipitating the middle dolomite cements (Garcia-Fresca et al., 2012; Shelton et al., 2009; Jones and Xiao, 2005; Franseen et al., 2004; Machel, 2004; Gao et al., 1995; Gao and Land, 1991; Land, 1985; Ross, 1976; Harris, 1973). Alternatively, measurements may have been taken from fluid inclusions that have reequilibrated with later diagenetic fluids responsible for baroque dolomite precipitation; these are discussed in later sections.

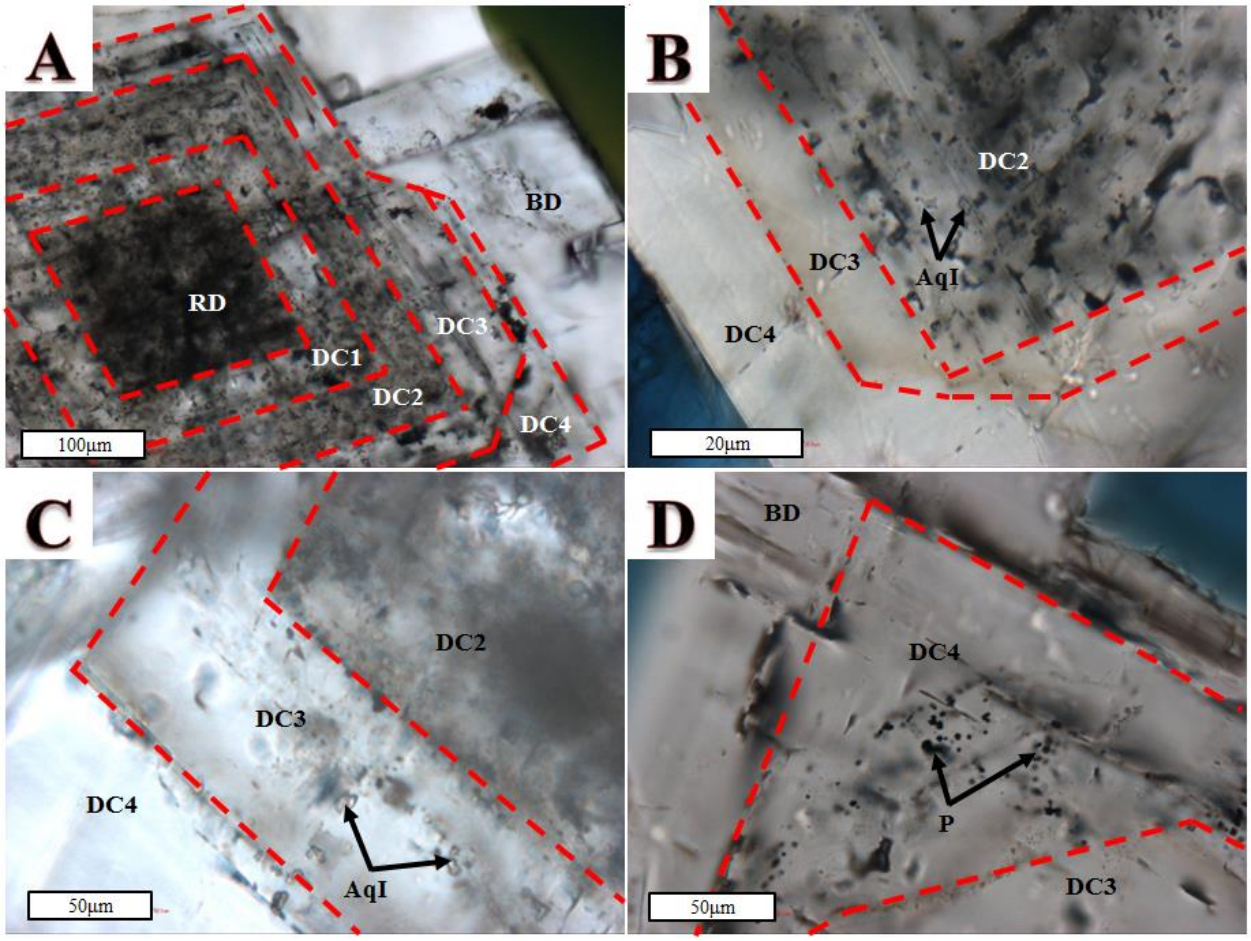

**Figure 2.17:** All images are transmitted light photomicrographs: (A) Growth zoning with primary FIAs in replacement dolomite (RD), dolomite cement 1 (DC1), dolomite cement 2 (DC2), dolomite cement 3 (DC3), dolomite cement 4 (DC4), and baroque dolomite (BD) (sample 3-16 (3969.5ft) from Vulcan); (B) All-liquid aqueous inclusions (AqI) in primary FIAs of dolomite cement 2 (DC2) and common brown tint marking transition from dolomite cement 3 (DC3) to dolomite cement 4 (DC4) (sample 4467.8 from Wellington 1-32); (C) Large all-liquid aqueous inclusions (AqI) within primary FIAs of dolomite cement 3 (DC3) (sample 3-15 (3971.8ft) from Vulcan); (D) Brown tint between dolomite cement 3 (DC3) and dolomite cement 4 (DC4) and pyrite inclusions (P) following growth zones of dolomite cement 4 (DC4) (sample 3-12 (3980.4ft) from Vulcan).

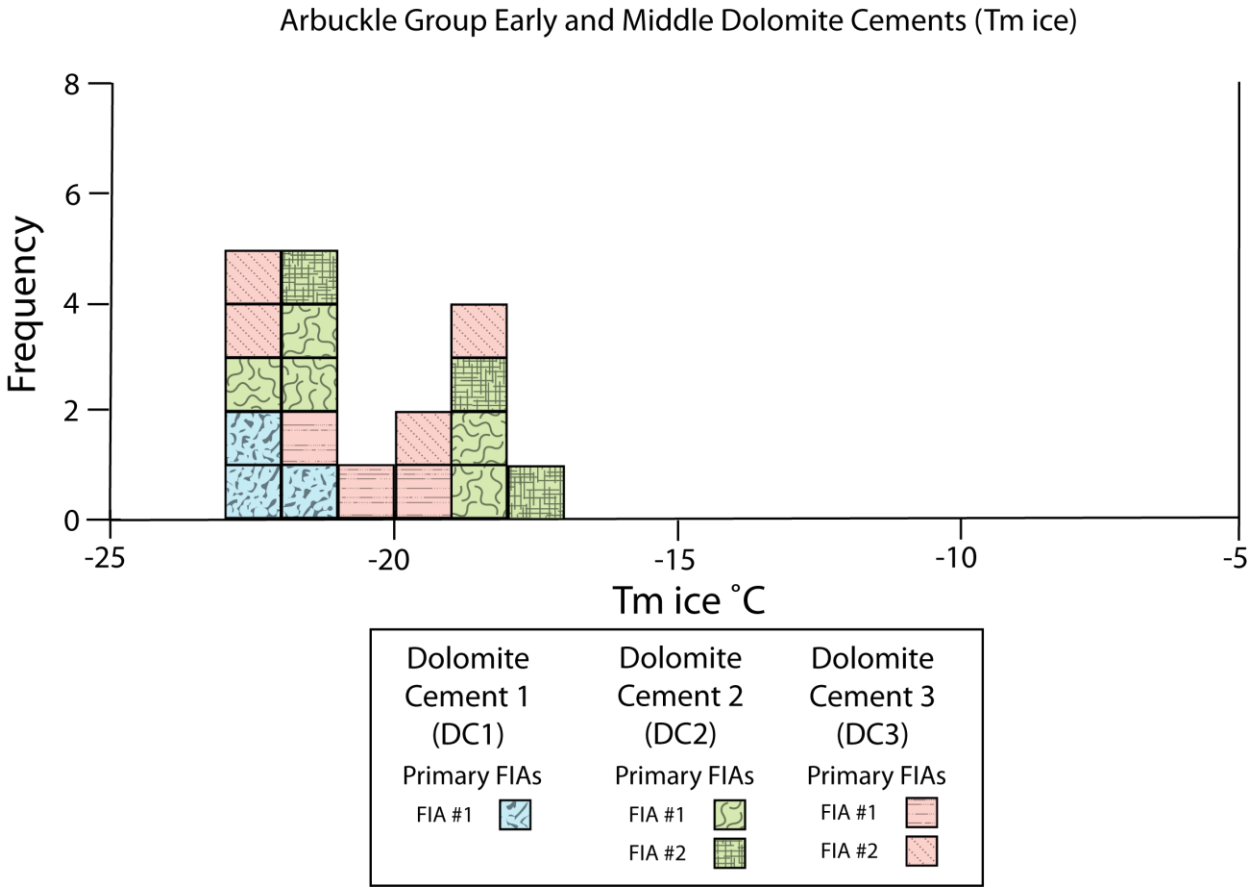


**Figure 2.18:** Final melting temperature of ice ($Tm_{ice}$) of dolomite cement 1 (DC1), dolomite cement 2 (DC2), and dolomite cement 3 (DC3). Data are plotted in degrees celsius versus the frequency of measurements.

### *6.3. Megaquartz 1*

*Petrography:* Megaquartz 1 (MQ1) appears clear under transmitted light and contains primary FIAs that contain fluid inclusions elongated in the direction of crystal growth (Fig. 2.19A, 2.19B). Fluid inclusions vary significantly in size and shape. Some FIAs contain two-phase inclusion and have variable ratios of gas and aqueous liquid; large all-liquid fluid inclusions are common (Fig. 2.19A). Solid anhydrite inclusions are readily observed and occur as rounded rectangular laths that appear clear under transmitted light; anhydrite inclusions are easily distinguished from other inclusions by their distinct birefringence under crossed-polars (Fig. 2.19B). Petrographic pairing is not readily observed in FIAs, indicating necking down after a phase change was not the cause of the variability in liquid:gas ratio (Goldstein and Reynolds, 1994).

*Microthermometry:* The presence of all-liquid inclusions implies formation of inclusions at low temperatures (<50ºC) and the lack of a gas bubble prohibited Th measurements of such inclusions (Goldstein and Reynolds, 1994). Attempts were made to generate gas bubbles in all-liquid samples by placing samples in a freezer for 4-5 weeks; this method resulted in no bubble generation. Th measurements were avoided because of the likelihood for low-temperature heterogeneous entrapment.

A total of three inconsistent primary FIAs were subjected to freezing for the purpose of obtaining $Tm_{ice}$ values. All-liquid inclusions were not stretched and then measured, but inclusions that were gas-dominated, likely resulting from original heterogeneous entrapment, were subjected to freezing runs. Freezing of inclusions was typically accompanied by a sudden jerk and decrease in size of the gas bubble. Upon warming the inclusions, $Tm_{ice}$ occurred between -20.0 and -25.1ºC (Fig. 2.20). Melting was accompanied by consolidation of low-relief, rounded crystals into a larger crystal that slowly melted until completely disappearing. This was

commonly accompanied by sudden movement of the gas bubble. $Tm_{ice}$ data resulted in salinities ranging from 22.6-25.6 wt. % NaCl eq.

*Interpretation:* Large all-liquid inclusions strongly suggest entrapment during low-temperature diagenetic conditions (<50ºC), especially when large in size and petrographic pairing is not observed (Goldstein and Reynolds, 1994). The presence of all-liquid and gas-dominated inclusions within the same FIAs necessitates heterogeneous entrapment.

High salinity values (22.6-25.6 wt. % NaCl eq.) in megaquartz cement 1 strongly indicate an association with evaporites (Hanor, 1979), either through (1) dissolution of evaporites during fluid migration or (2) reflux of evaporative fluids. The timing of MQ1 precipitation is interpreted to have occurred after extensive dissolution related to the major post-Sauk subaerial exposure event but before burial (see Paragenesis section). Similar to early and middle dolomite cements, fluctuations in sea-level could have allowed for reflux of high density evaporative brines that seeped down through the Arbuckle Group, replacing carbonates and anhydrite, and precipitating megaquartz 1. Dissolution of evaporites within the Arbuckle Group may have provided another source if they were dissolved during fluid migration. Also, a combination of both reflux and evaporite dissolution could account for the high salinities. Evaporitic and hypersaline fluids formed after flooding of the subaerial exposure surface on the Arbuckle Group; this may have been the source for refluxing fluids responsible for megaquartz precipitation.

### *6.4. Megaquartz cement 2*

*Petrography:* Megaquartz cement 2 (MQ2) appears clear under transmitted light and rarely contains primary FIAs that appear to be distributed in a feather-like pattern, oriented in the

direction of crystal growth (Fig. 2.19C, 2.19D). Fluid inclusions are typically small in size (<5μm) and display a round shape, with slight elongation in the direction of crystal growth (Fig. 2.19C, 2.19D). Fluid inclusions can be observed as two-phase inclusions containing a gas bubble and aqueous liquid, or as small, all-liquid aqueous inclusions (Fig. 2.19D). Liquid-gas ratios among inclusions in an FIA appear inconsistent, and there are some gas-dominated inclusions (Fig. 2.19C, 2.19D). Petrographic pairing is not observed in fluid inclusions, indicating necking down after a phase change has not caused the variability in liquid:gas ratio (Goldstein and Reynolds, 1994).

*Microthermometry:* The general paucity of fluid inclusions limited the number of microthermometric measurements. The relatively small size (<5μm) of inclusions led to petrographic limitations and likely resulted in nucleation metastability effects, restricting bubble generation in the smallest inclusions (Goldstein and Reynolds, 1994). A total of nine inconsistent primary FIAs were subjected to heating for the purpose of obtaining Th data. Heating of fluid inclusions resulted in a gradual decrease in gas bubble size, until the two phases homogenized and the bubble disappeared. The resulting Th data varied significantly, with values ranging from 87.0-157.0ºC (Fig. 2.21).

A total of five inconsistent primary FIAs were subjected to freezing for the purpose of obtaining $Tm_{ice}$ values. Freezing of inclusions was typically accompanied by a sudden jerk and decrease in size of the gas bubble. Upon warming the inclusions, $Tm_{ice}$ occurred between -1.8 and -3.7ºC (Fig. 2.20). Melting involved the consolidation of low-relief, round crystals into a larger crystal that slowly melted until completely disappearing. This was commonly accompanied by sudden movement of the gas bubble. $Tm_{ice}$ data resulted in salinities ranging from 3.1-6.0 wt. % NaCl eq.

*Interpretation:* Th measurements of two-phase fluid inclusions within inconsistent FIAs range from 87.0-157.0ºC and small all-liquid inclusions can be observed. The fact that all-liquid inclusions are small in size suggests nucleation metastability may play a role in the absence of a gas bubble (Goldstein and Reynolds, 1994); if small all-liquid inclusions are attributed to metastability, then megaquartz precipitation is most likely dominated by high-temperature conditions. Possible explanations for Th measurements include: (1) homogeneous entrapment at variably high temperatures and (2) heterogeneous entrapment at high temperatures. Inconsistent liquid-gas ratios in FIAs, with gas-dominated inclusions and no evidence for petrographic pairing, require entrapment during heterogeneous conditions, eliminating the potential for scenario (1). Heterogeneous entrapment in scenario (2) would account for the variability in Th measurements. Because the fluid inclusions within FIAs contain liquid-rich and gas-rich end members of the heterogeneous system, liquid-rich end-members would provide the actual temperatures during entrapment (Goldstein and Reynolds, 1994); in an attempt to collect Th data from liquid-rich end members (two-phase fluid inclusions with the smallest gas bubbles) it is inevitable that data collection from inclusions that formed with miniscule amounts of gas would have occurred. If this is the case, the lowest measured temperatures (~90ºC) would represent actual temperature of entrapment, whereas the higher temperature range would represent heterogeneous entrapment of gas along with liquid.

Salinities measured in late megaquartz cement are lower than that recorded in dolomite and calcite inclusions, but still high enough (3.1-6.0 wt. % NaCl eq) to suggest some dissolution of evaporites. Alternatively, these values could represent connate seawater and evaporated seawater that was present in the basin. When considering the elevated Th measurements, a basin-sourced fluid is the best candidate to account for high temperature-moderate salinity fluids

(Young, 2010; Hanor, 1979). A discussion regarding potential hydrologic models is provided in section 9.5.

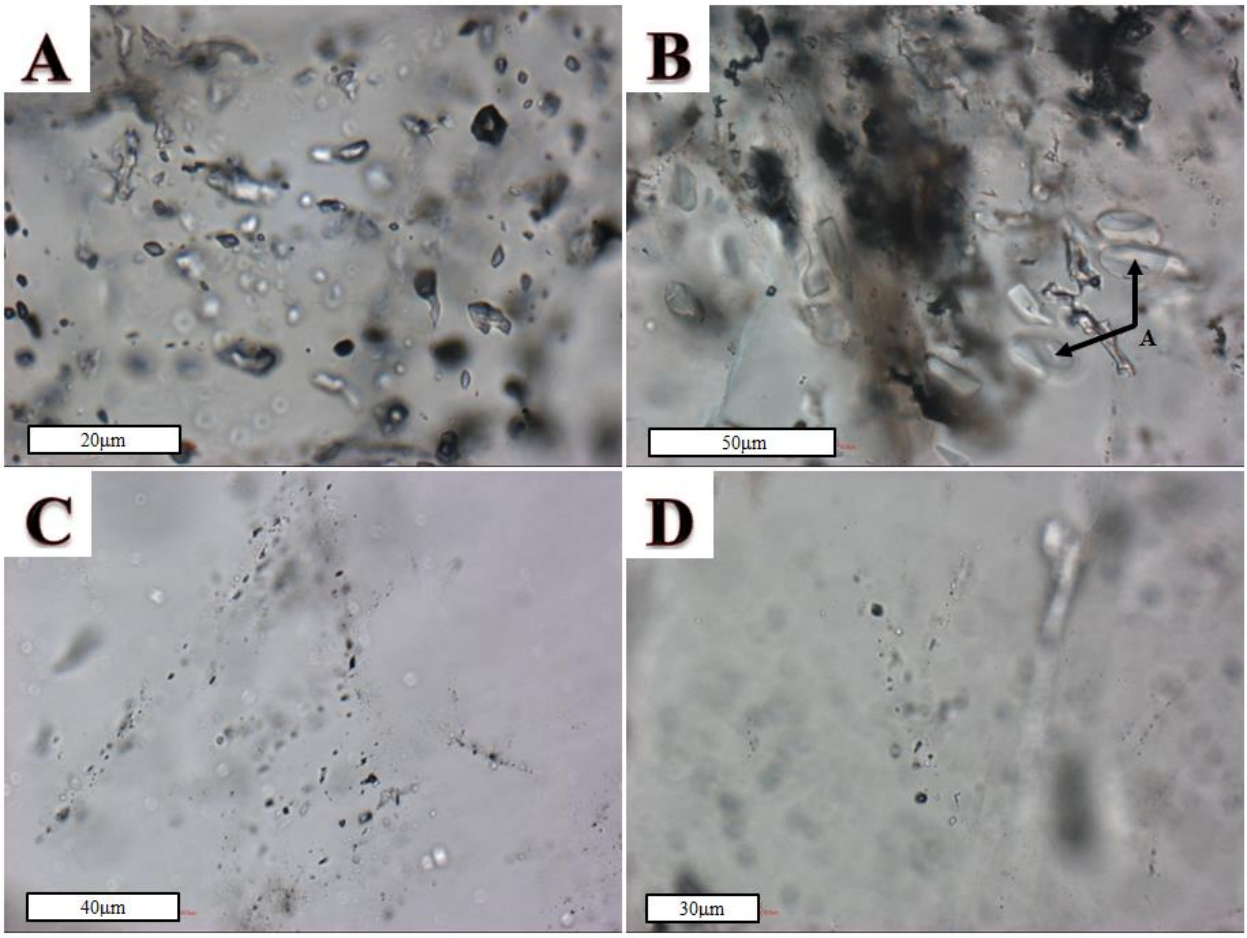


**Figure 2.19:** All images are transmitted light photomicrographs: (A) Variable liquid-gas ratios within megaquartz 1 (MQ1), with gas-rich inclusions and large all-liquid inclusions within primary FIAs (sample 4276.5 from Wellington 1-32); (B) Solid anhydrite (A) inclusions common within megaquartz 1 (MQ1) (sample 4382.9 from Wellington 1-32); (C) Feather-like distribution of primary FIAs parallel to growth direction in megaquartz cement 2 (MQ2), with variable liquid-gas ratios (sample 5083.7 from Wellington 1-32); (D) Fluid inclusions displaying gas-rich and liquid-rich end members in primary FIAs within megaquartz cement 2 (MQ2) (sample 3-5A (4005.5ft) from Vulcan).

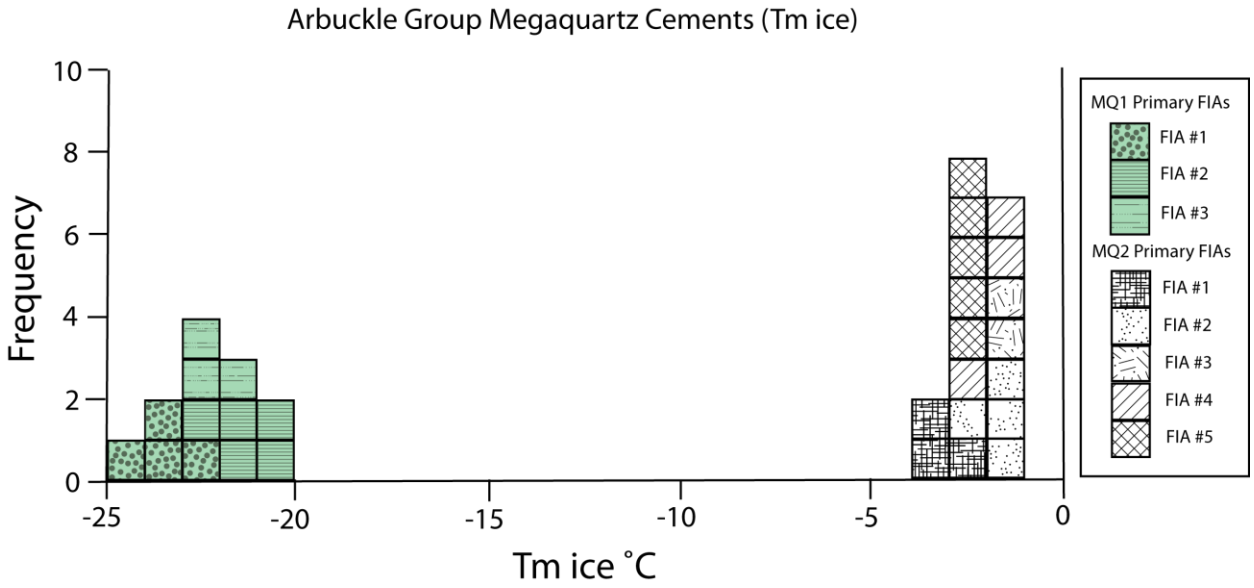


**Figure 2.20:** Final melting temperature of ice ($Tm_{ice}$) of megaquartz 1 (MQ1) and megaquartz cement 2 (MQ2). Data are plotted in degrees celsius versus the frequency of measurements. The most noticeable trend is the drastic decrease in salinity from early diagenetic cement (MQ1) to late (MQ2).

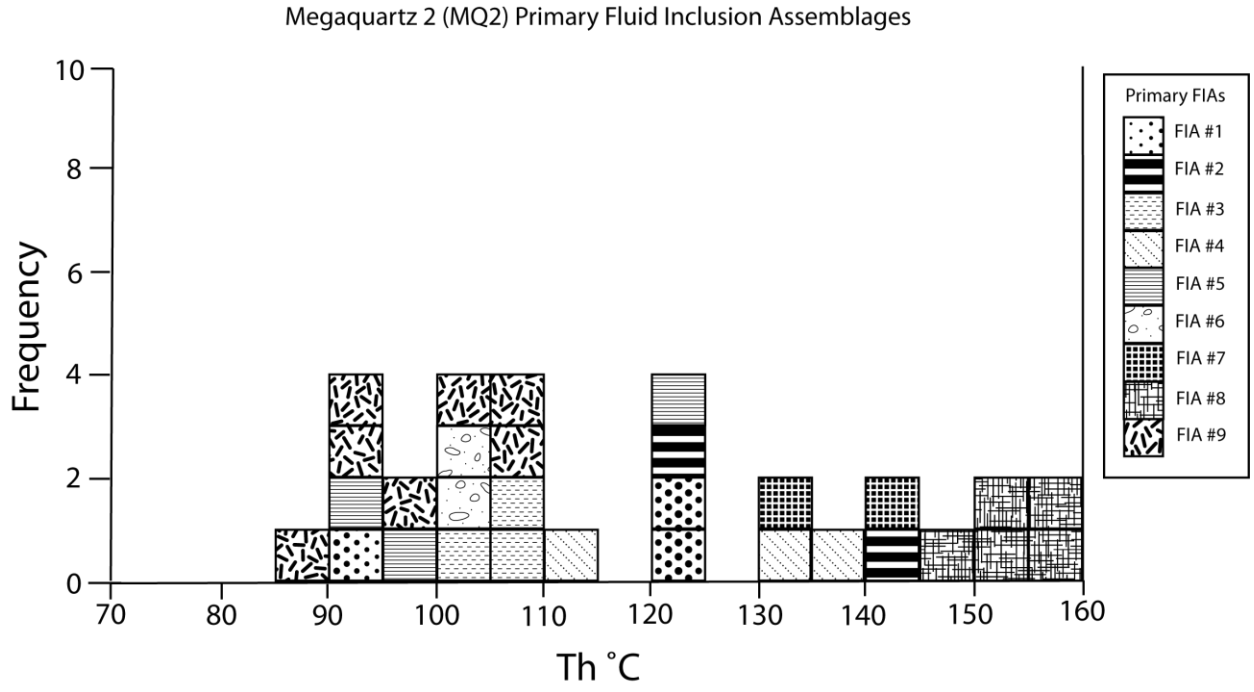


**Figure 2.21:** Homogenization temperatures (Th) measured in primary FIAs of megaquartz cement 2 (MQ2). Data ranges significantly, likely due to measurement of various end members of inclusions entrapped during heterogeneous conditions.

### *6.5. Baroque dolomite*

*Petrography:* Baroque dolomite (BD) typically appears clear under transmitted light with a cloudy core and concentric growth bands defined by high abundance of fluid inclusions (Fig. 2.22A). Primary FIAs can commonly be observed mimicking concentric crystal growth of dolomite samples in the Wellington core (Fig. 2.22A, 2.22B). Pseudosecondary or secondary FIAs were observed within BD present in Vulcan core samples and occur as curviplanar, three-dimensional features cross-cutting dolomite crystals. Fluid inclusions within primary FIAs are typically two-phase inclusions with a small gas bubble in aqueous liquid. They vary in size and shape; liquid-gas ratios are consistent among fluid inclusions in each FIA (Fig. 2.22B). All-liquid inclusions can be observed within primary FIAs but are only the relatively small-sized inclusions of the FIA (<5μm). Fluid inclusions within pseudosecondary or secondary FIAs appear as two-phase inclusions with gas bubbles and aqueous liquid and as all-liquid aqueous inclusions. Some pseudosecondary or secondary FIAs appear to contain two-phase inclusions with consistent liquid-gas ratios, whereas others display two-phase inclusions with variable liquid-gas ratios and all-liquid inclusions. Petrographic pairing is not present in primary FIAs but can be clearly observed in pseudosecondary or secondary FIAs where large all-liquid inclusions are present, indicating necking-down after a phase change may be responsible for the presence of all-liquid inclusions (Goldstein and Reynolds, 1994). No patchiness was observed in BD when exposed to cathodoluminescence, but SEM analysis revealed extensive evidence for recrystallization during precipitation of the latest growth zone, along microfractures in earlier growth zones (Fig. 2.14A, 2.14B, 2.14C, 2.14D, 2.15B, 2.15C, 2.15D). Additionally, BD contains UV-fluorescent fluid inclusions, indicating entrapment of oil. These hydrocarbon inclusions occur as two-phase fluid inclusions in pseudosecondary or secondary FIAs entrapped

during crystal growth later recrystallization of baroque dolomite rhombs; there are some hydrocarbon inclusions that may be primary in origin as well (Fig. 2.22C, 2.22D). These inclusions appear clear to light-yellow under transmitted light and display a bright blue color when exposed to UV-epifluorescence (Fig. 2.22C, 2.22D).

SEM-BSE imaging supplied insight into the crystal growth history of the baroque dolomite, allowing for four distinct growth zones to be identified. The onset of baroque dolomite precipitation was preserved as relatively fine-grained crystal growth and was followed by considerably coarser-grained crystal growth (Fig. 2.15A). Following precipitation of the middle medium-grey zone, extensive microfracturing produced a highly fractured, brecciated, fabric that is definitively observable in the middle light-grey and middle medium-grey zones; the fractured fabric may also be present in the early dark-grey zone, but contrasting shades were difficult to distinguish. Following the extensive fracturing of earlier crystal growth zones, the late dark-grey zone, believed to be the last stage of crystal growth, appears to have precipitated as cement whereas previous growth zones recrystallized along a network of microfractures (Fig. 2.15B, 2.15C, 2.15D)

Recrystallization of early growth zones by the latest stage of precipitation appears to have had a major impact on the location of fluid inclusions (Fig. 2.15C, 2.15D). Fluid inclusions are most concentrated in the late dark-grey zone. Inclusions preferentially formed during recrystallization of the earlier growth zones, either along micro-fractures or vague growth zones within the middle light-grey zone (Fig. 2.15C, 2.15D). Though some fluid inclusions can still be observed within the earlier growth zones, most are slightly larger and isolated; this has resulted in the majority of the fluid inclusion data being derived from the latest stage of crystal growth, rather than spanning the entire history of crystal growth.

*Microthermometry:* A total of seventeen consistent primary FIAs and three consistent pseudosecondary or secondary FIAs were subjected to heating for the purpose of obtaining Th data. SEM analysis revealed that rare, larger inclusions (~20μm) appear to be preserved within the earlier growth zones that predated the recrystallization. Four of the primary FIAs were focused on larger fluid inclusions interpreted to represent early baroque dolomite precipitation. Heating of fluid inclusions resulted in a gradual decrease in gas bubble size, until the two phases homogenized and the bubble disappeared. Measurements focused on the larger inclusions in the early baroque dolomite provided Th values ranging from 97.0-113.0ºC. SEM analysis of baroque dolomite revealed that the majority of the fluid inclusions measured were trapped during the latest stage of crystal growth, due to extensive fracturing and recrystallization of previous dolomite growth zones. In these growth zones, the values collected from primary FIAs ranged from 93.0-130.6ºC and Th values collected from pseudosecondary or secondary FIAs ranged from 107.0-131.0ºC (Fig. 2.23, 2.24). Th values collected from the Vulcan core ranged from 97.0-124.0ºC in primary FIAs and 107.0-128.0 ºC in pseudosecondary or secondary FIAs, whereas Th values collected from the Wellington core ranged from 93.0-130.6ºC in primary FIAs. Several crystal transects were completed, measuring Th values in primary FIAs while progressing from the inner to the outer crystal margin of baroque dolomite rhombs. Th values measured along early to late transects did not display any readily observable trends, with temperatures increasing or decreasing from the inner to the outer crystal margin (Fig. 2.26).

A total of seven consistent primary FIAs and three consistent psuedosecondary or secondary FIAs were subjected to freezing for the purpose of obtaining $Tm_{ice}$ values. Four of the primary FIAs were interpreted to represent early baroque dolomite precipitation. Freezing of inclusions was typically accompanied by a sudden jerk and decrease in size of the gas bubble.

Upon warming the inclusions, first melting is estimated to have occurred between -42 and -56ºC, recognized by the occurrence of an "orange peel" texture (Goldstein and Reynolds, 1994). $Tm_{ice}$ measurements from larger inclusions interpreted as representing earlier dolomite growth zones ranged from -12.4 to -14.5ºC, resulting in salinities ranging from 16.3-18.2 wt. % NaCl eq. $Tm_{ice}$ measurements obtained from later baroque dolomite precipitation occurred between -13.2 and -17.3ºC, resulting in salinities ranging from 17.1-20.4 wt. % NaCl eq. (Fig. 2.25). Melting was observed as the consolidation of low-relief, well-rounded, small crystals into a larger crystal that slowly melted until completely disappearing. This was commonly accompanied by a sudden movement of the gas bubble.

*Interpretation:* Th measurements of two-phase fluid inclusions within consistent FIAs range from 93.0-131.0ºC and crystal transects show rises and falls of Th values from the inner to outer margin of individual crystals. Small all-liquid inclusions can be observed. The fact that all-liquid inclusions are small in size suggests nucleation metastability may play a role in the absence of a gas bubble (Goldstein and Reynolds, 1994). If small all-liquid inclusions are attributed to metastability, then fluid inclusion entrapment most likely occurred during homogeneous conditions at high temperatures. Possible explanations for variability in Th measurements include: (1) homogeneous entrapment followed by thermal reequilibration at variable high temperatures for each growth zone, (2) homogeneous entrapment followed by recrystallization at variable high temperatures for each growth zone, or (3) homogeneous entrapment during rising and falling high temperatures for each growth zone. Thermal reequilibration would typically lead to significant Th variability in FIAs; the fact that all FIAs are consistent eliminates scenario (1). SEM analysis has revealed that recrystallization during the latest stage of crystal growth trapped the majority of the fluid inclusions measured (Fig. 2.15B,

2.15C, 2.15D). As most fluid inclusion data are confined to those recrystallized areas, and FIAs are not a mixture of recrystallized and unrecrystallized dolomite, homogeneous entrapment of fluid inclusions during multiple fluid migration events likely occurred at variably high temperatures. This is strongly supported by the consistent nature of FIAs. Recrystallization was likely so prevalent that most fluid inclusions reflect conditions during the latest stage of crystal growth. Only the larger inclusions contained in the earlier growth zones represent the earlier conditions, and they are only a minor part of the data set.

Early baroque dolomite precipitated from fluids with 16.3-18.2 wt. % NaCl eq. and later baroque dolomite precipitated from fluids with 17.1-20.4 wt. % NaCl eq. High salinity fluids (16.3-20.4 wt. % NaCl eq.) in baroque dolomite suggest dissolution of evaporites at some point during the fluid migration history or reflux of evaporative fluids. First melting temperatures between -42 and -56ºC fall within the observed range of both NaCl-$CaCl_2$-$H_2O$ and NaCl-$MgCl_2$-$H_2O$ fluids (Goldstein and Reynolds, 1994). When considering the elevated Th values and first melting temperatures of fluids responsible for baroque dolomite precipitation, a basinal-sourced fluid is the best candidate to account for hydrothermal fluids in the study area (Young, 2010). A discussion regarding potential hydrologic models is provided in section 9.5.

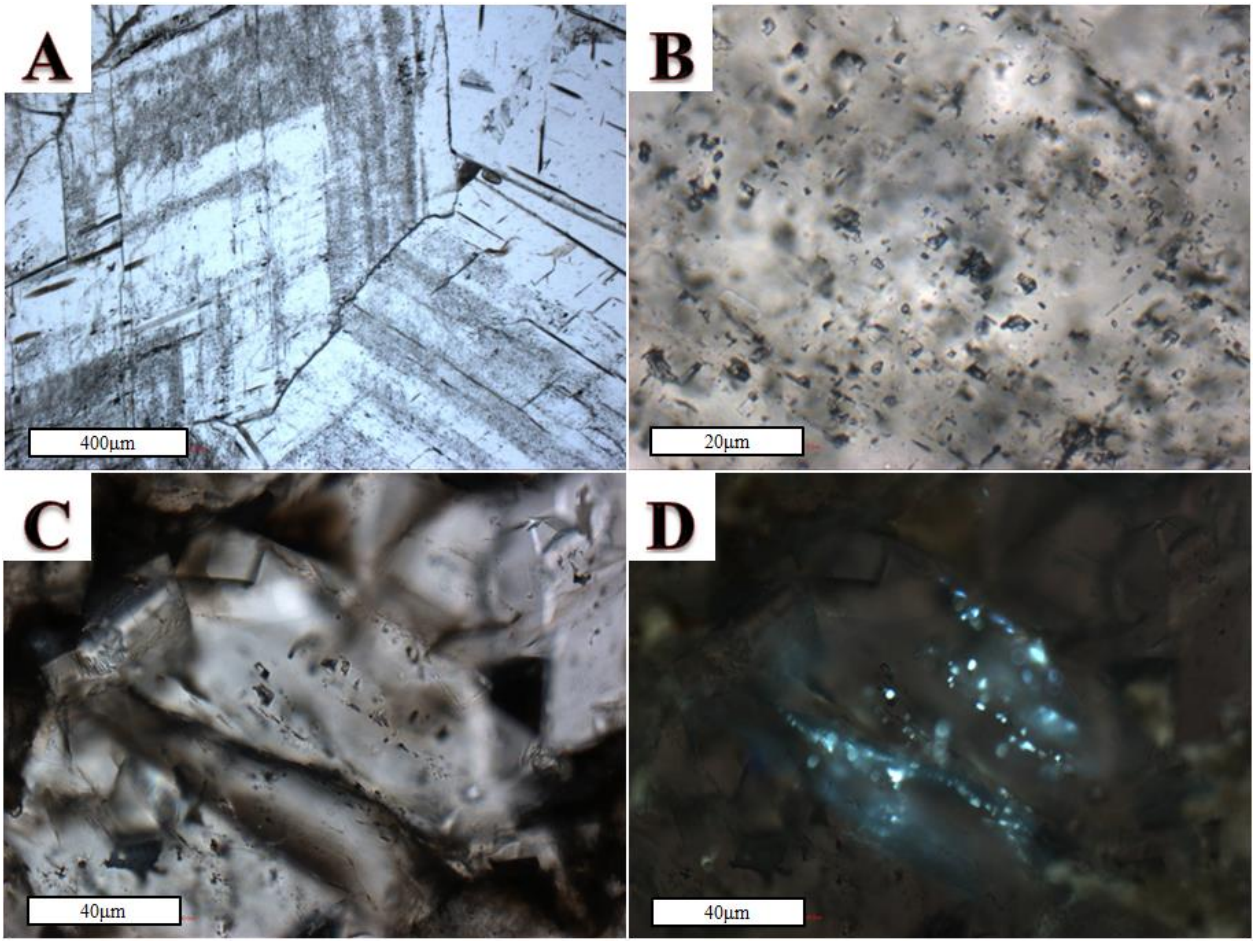


**Figure 2.22:** (A) Transmitted light photomicrograph of primary FIAs running perpendicular to growth direction in baroque dolomite (BD) (sample 5063.6A from Wellington 1-32); (B) Transmitted light photomicrograph of higher magnification image of 22A, displaying two-phase fluid inclusions within primary FIAs of baroque dolomite (BD) (sample 5063.6A from Wellington 1-32); (C) Transmitted light photomicrograph of pseudosecondary, secondary, and possibly primary FIAs containing hydrocarbon fluid inclusions in baroque dolomite (BD) crystals (sample 4382.9 from Wellington 1-32); (D) UV-epifluorescence photomicrograph of pseudosecondary, secondary, and possibly primary FIAs containing hydrocarbon fluid inclusions in baroque dolomite (BD) crystals (sample 4382.9 from Wellington 1-32).

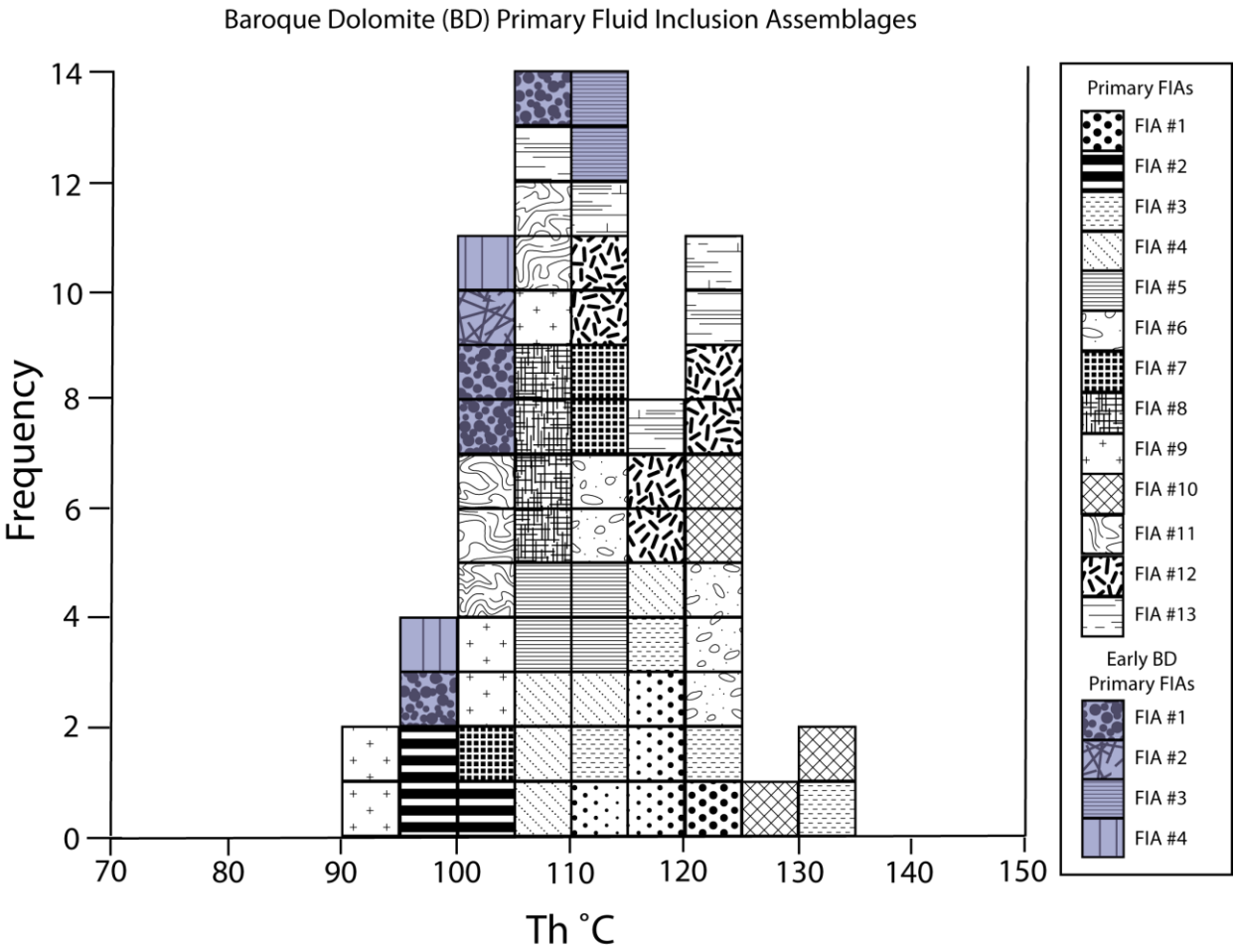


**Figure 2.23:** Homogenization temperatures (Th) measured in primary FIAs of baroque dolomite (BD). Blue shaded data points are Th values for large inclusions that appear to be related to the earliest stages of baroque dolomite precipitation. Data points occur most frequently between 100 and 125ºC.

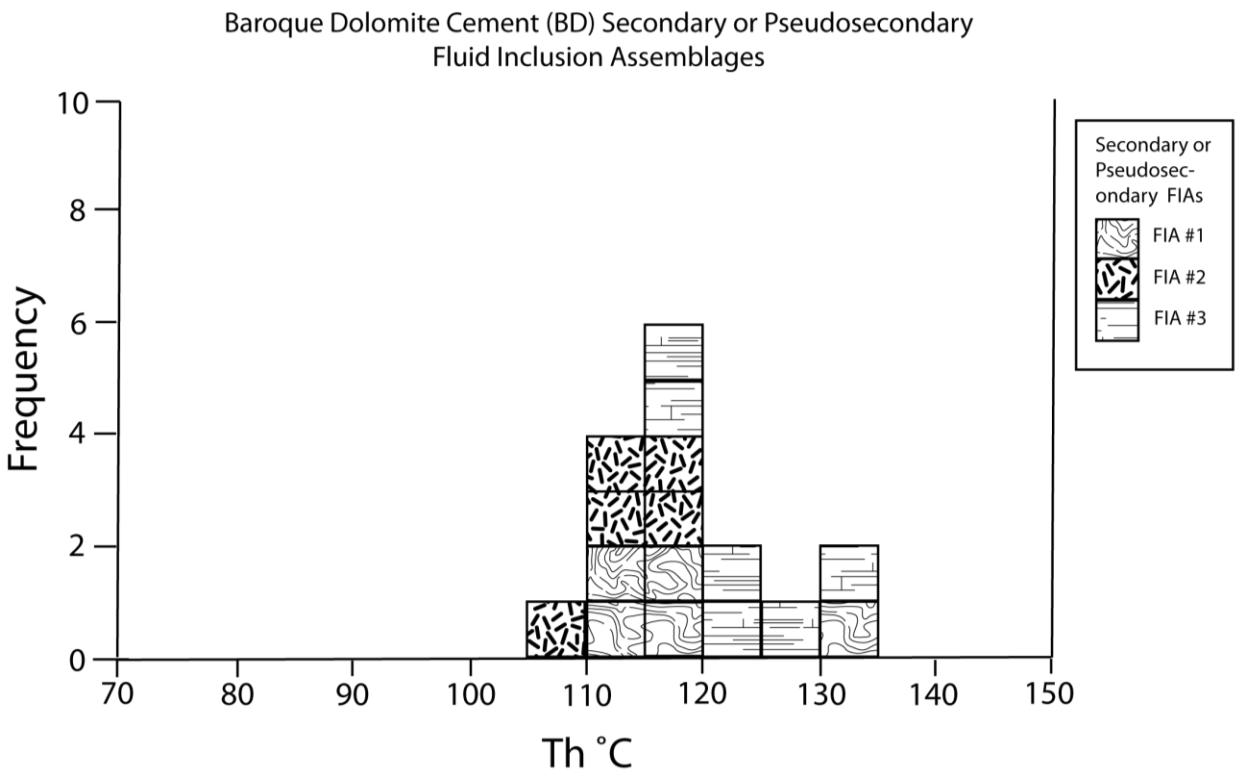


**Figure 2.24:** Homogenization temperatures (Th) measured in secondary FIAs of baroque dolomite (BD). The highest frequency of data points occurs within the same range as primary FIAs, indicating similar conditions during entrapment.

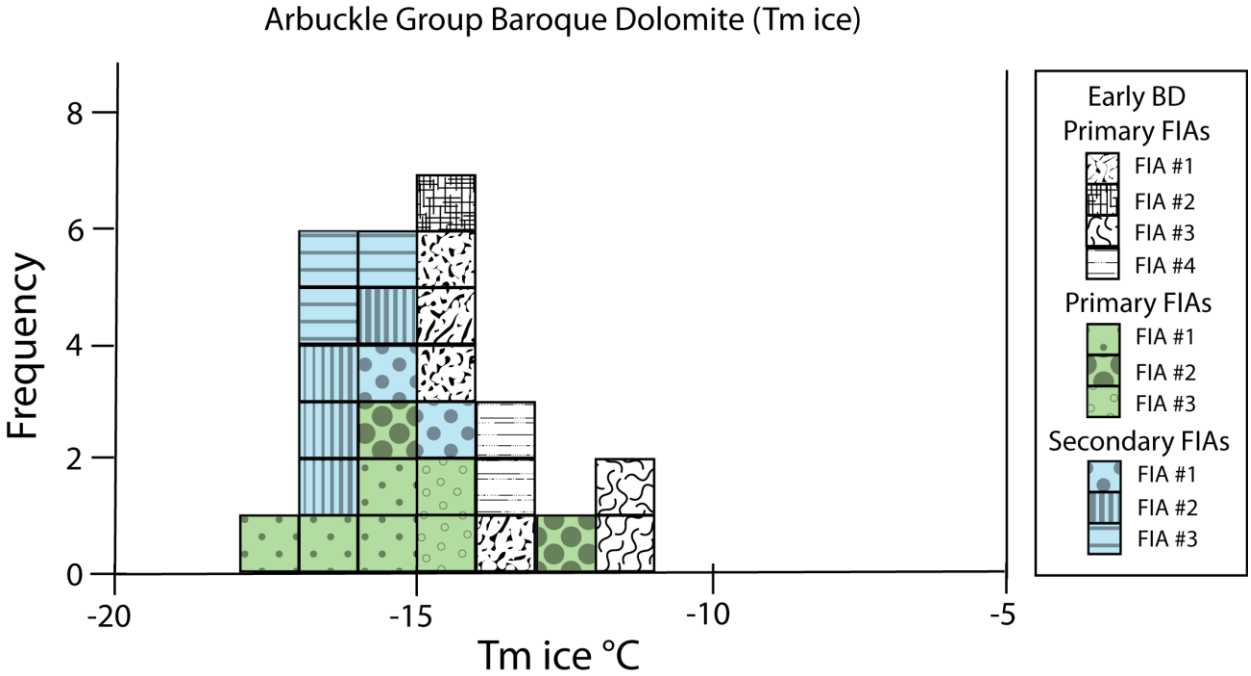


**Figure 2.25:** Final melting temperature of ice ($Tm_{ice}$) of baroque dolomite (BD). Data are plotted in degrees celsius versus the frequency of measurements. The most noticeable trend is lower salinity during the earliest stage of baroque dolomite precipitation.

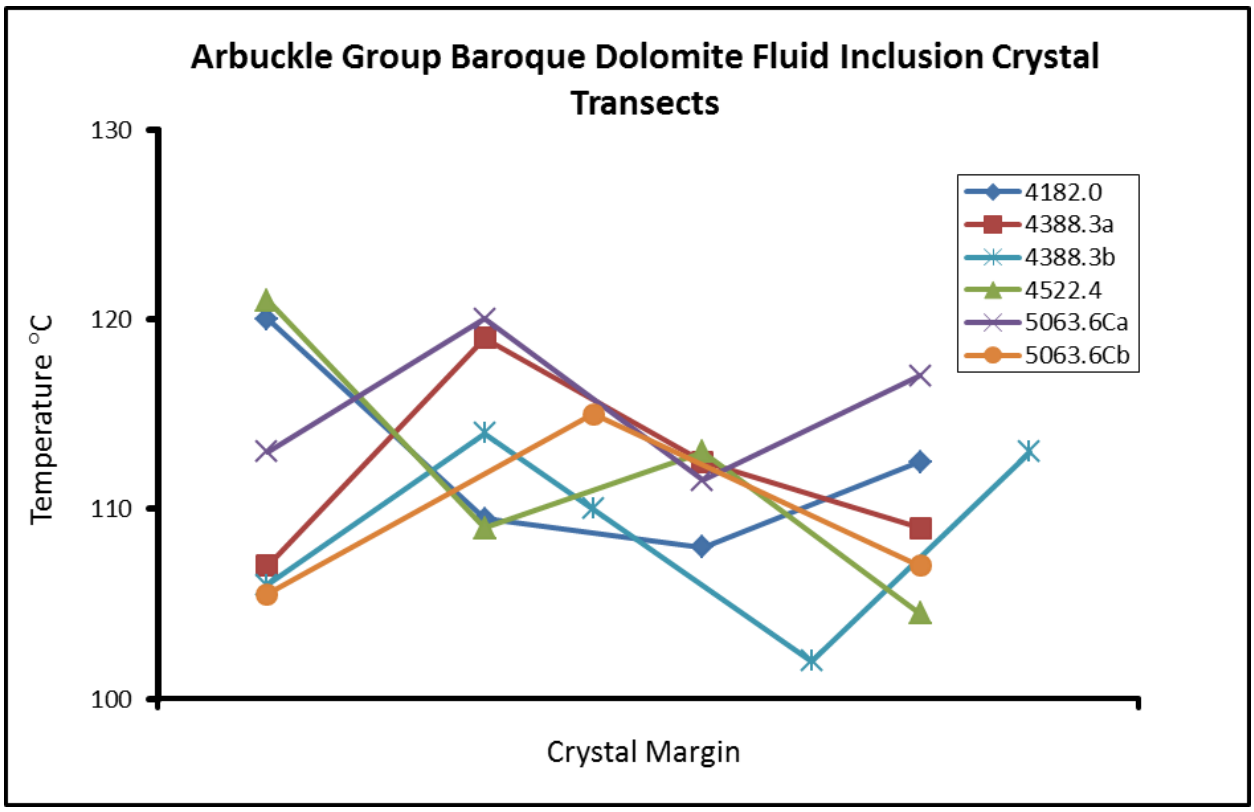


**Figure 2.26:** Transects in baroque dolomite measuring homogenization temperatures progressing from the inner to outer margin of individual crystals. All transects display rises and falls in temperature of entrapment as crystal growth continued. Transects were conducted in samples spanning the entire thickness of the Arbuckle Group, suggesting the entire unit was affected by these temperature fluctuations.

### *6.6. Calcite cement*

*Petrography:* Calcite cement (CC) appears clear under transmitted light with no observable primary FIAs. Secondary FIAs can be observed as curviplanar, three-dimensional features cutting across entire calcite crystals (Fig. 2.27A). Fluid inclusions within secondary FIAs are generally the same size and occur as rounded negative crystal-shaped inclusions with small gas bubbles surrounded by an aqueous liquid; liquid-gas ratios in FIAs appear consistent (Fig. 2.27B). All-liquid inclusions can be observed but are only those that are relatively small in size (<5μm). Petrographic pairing of all-liquid and two-phase inclusions is not observed,

indicating that fluid inclusions did not neck down after a phase change (Goldstein and Reynolds, 1994). No patchiness was observed in CC when exposed to cathodoluminescence, indicating that recrystallization is unlikely (Fig. 2.14C, 2.14D).

*Microthermometry:* A total of five consistent secondary FIAs were subjected to heating for the purpose of obtaining Th data. Heating of fluid inclusions resulted in a gradual decrease in gas bubble size, until the two phases homogenized and the bubble disappeared. The values collected from secondary FIAs ranged from 70.5-89.8ºC (Fig. 2.28). Th values were collected only from the Vulcan core because of the absence of measureable fluid inclusions in the samples from the Wellington core.

A total of three consistent secondary FIAs were subjected to freezing for the purpose of obtaining $Tm_{ice}$ values. Freezing of inclusions was typically accompanied by a sudden jerk and decrease in size of the gas bubble. Upon warming the inclusion, $Tm_{ice}$ occurred between -14.6 and -16.2ºC (Fig. 2.29). During warming low-relief, rounded, small crystals merged into a larger crystal that slowly melted until completely disappearing. This was accompanied by a sudden movement of the gas bubble. $Tm_{ice}$ data resulted in salinities ranging from 18.2-19.6 wt. % NaCl eq.

*Interpretation:* Th measurements of two-phase fluid inclusions within consistent secondary FIAs range from 70.5-89.8ºC. The fact that all-liquid inclusions are relatively small in size suggests nucleation metastability may play a role in the absence of a gas bubble (Goldstein and Reynolds, 1994). If small all-liquid inclusions are attributed to metastability, then secondary fluid inclusion entrapment most likely occurred during homogeneous conditions at the moderate homogenization temperatures measured. Due to the lack of primary inclusions, temperature conditions during mineral growth were impossible to derive from inclusion analysis. Th

measurements from secondary FIAs only give temperature of fluids during fracture healing after mineral growth, indicating conditions had cooled down at some point following precipitation of baroque dolomite, but remained moderately high following precipitation of calcite cement.

High salinity fluids (18.2-19.6 wt. % NaCl eq.) in fractures in calcite cement suggest evaporite dissolution or reflux during the fluid migration history. High salinities could represent continued fluid migration of similar basin-sourced fluids. A discussion regarding potential hydrologic models is provided in section 9.5.

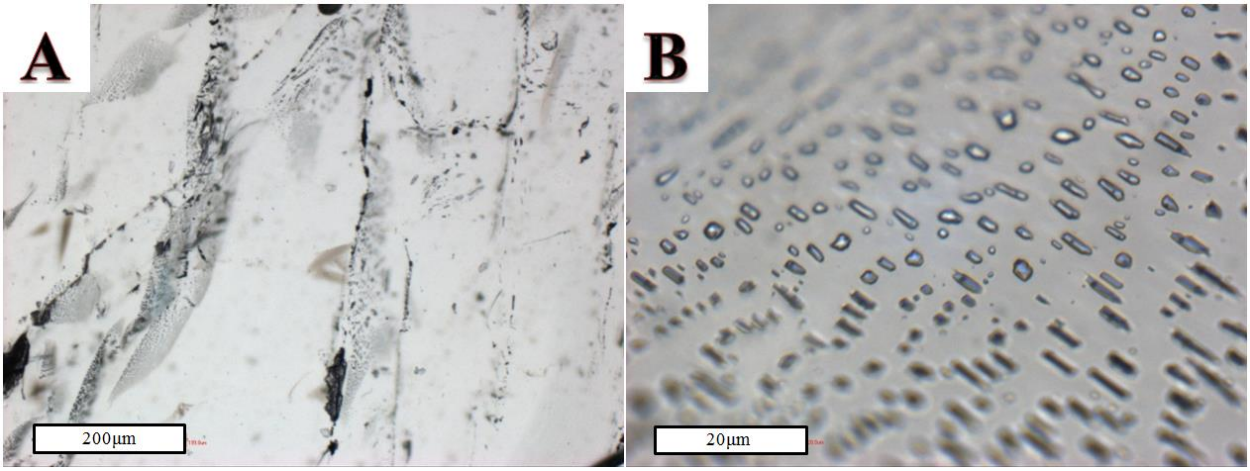


**Figure 2.27:** All images are transmitted light photomicrographs: (A) Secondary FIAs cross-cutting calcite cement (CC) crystals (sample 3-14 (3979.1ft) from Vulcan); (B) Higher magnification image of 22C, displaying two-phase inclusions with consistent liquid-gas ratios within secondary FIAs of calcite cement (CC) (sample 3-14 (3979.1ft) from Vulcan).

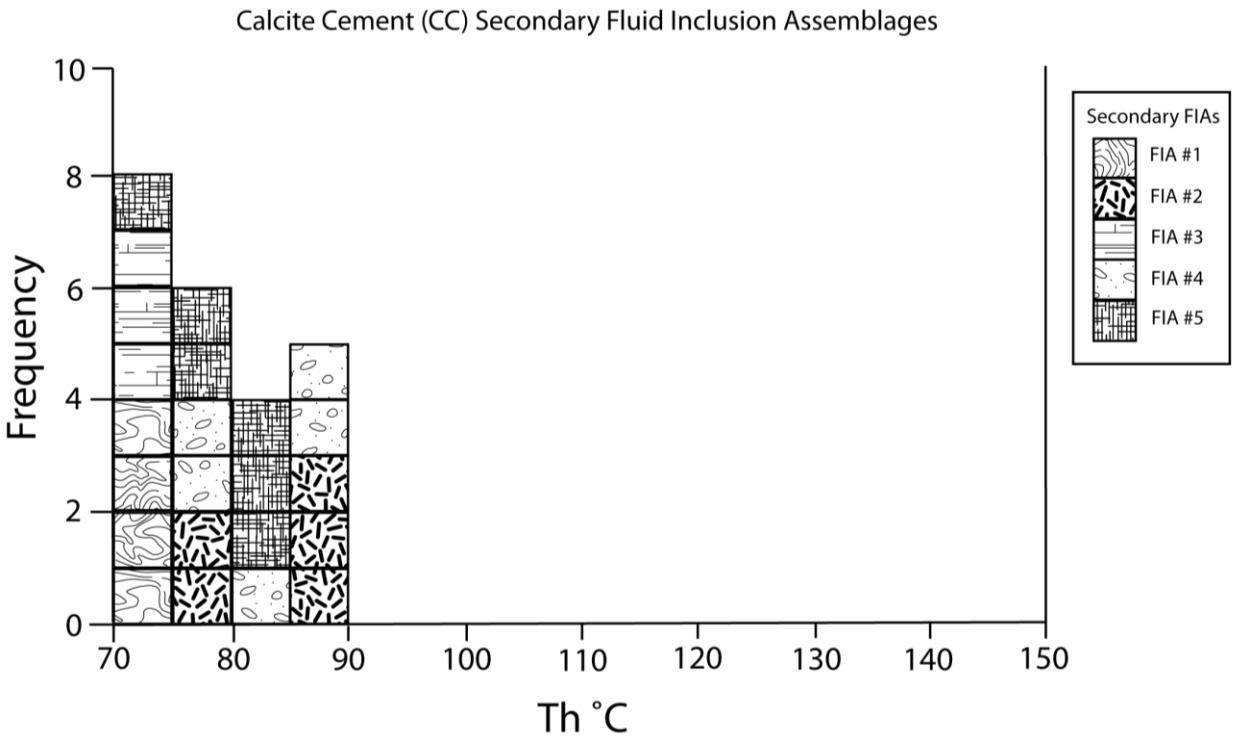


**Figure 2.28:** Homogenization temperatures (Th) measured in secondary FIAs of calcite cement (CC). Though inclusions were trapped after mineral growth, they still indicate a decrease in temperature after precipitation of baroque dolomite.

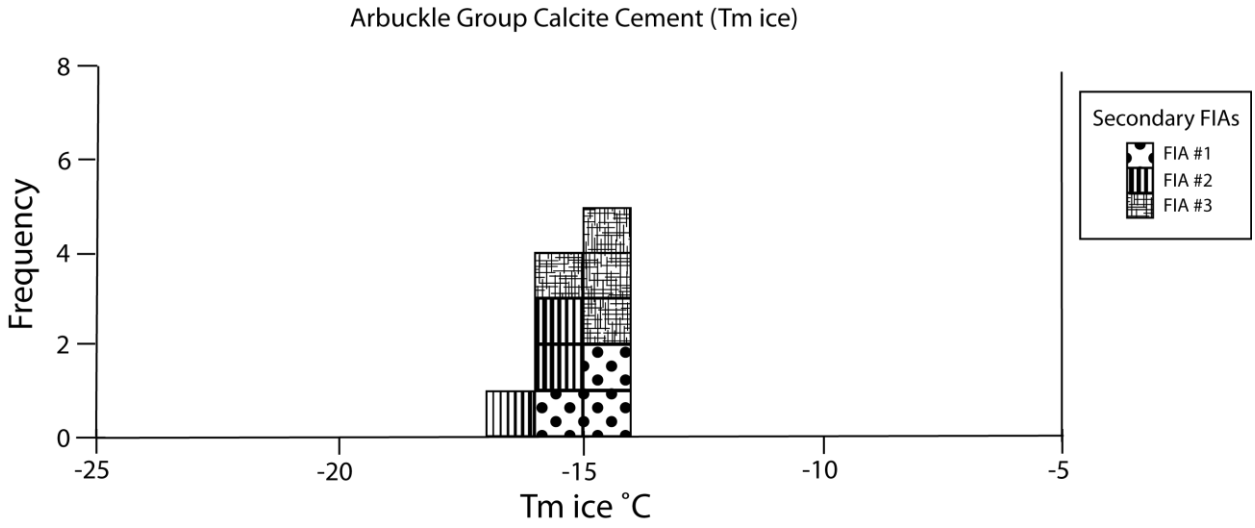


**Figure 2.29:** Final melting temperature of ice ($Tm_{ice}$) of calcite cement (CC). Data are plotted in degrees celsius versus the frequency of measurements. The most noticeable trend is the slight decrease in salinity from precipitation of BD to the entrapment of secondary fluid inclusions in calcite.

### *6.7. Fluid Inclusion Discussion*

Low-temperature (<50ºC) interpretations of fluid inclusion data from early dolomite cements (event 5), middle dolomite cements (event 10-11), and megaquartz 1 (event 12) compare well with their placement as early diagenetic events in the paragenesis (Fig. 2.4, 2.30). Precipitation prior to burial, due to shallow fluid-flow processes, would account for the low-temperature interpretation. Early reflux during evaporative conditions could have provided the high salinities measured in the early-stage diagenetic cements (although these may have come from reequilibrated fluid inclusions), and dissolution of Arbuckle Group evaporites during fluid migration could have increased salinity further (Garcia-Fresca et al., 2012; Shelton et al., 2009; Jones and Xiao, 2005; Franseen et al., 2004; Machel, 2004; Gao et al., 1995; Gao and Land, 1991; Land, 1985; Ross, 1976; Harris, 1973; Goldstein, in press).

The current temperature of the Arbuckle Group ranges from 43.9ºC at the top to 54.4ºC at the base (recorded from bottom-hole temperatures in Wellington 1-32 core), requiring a substantially higher reservoir temperature some time in the geologic past to produce the Th values recorded in megaquartz cement 2 (interpreted to be ≥87ºC), early baroque dolomite (97.0-113.0 ºC), late baroque dolomite (93.0-131.0ºC), and secondary fluid inclusions in calcite cement (70.5-89.8ºC) (Fig. 2.30). Potential hypotheses that could account for the increase in temperature include: (1) increased burial, (2) elevated geothermal gradient, or (3) injection of hydrothermal fluids. Both hypothesis (1) and (2) can be evaluated using a model of the burial history of Arbuckle Group strata. The thickness of Cretaceous sediment prior to extensive erosion, as well as estimates of geothermal gradients, generates uncertainty regarding the burial history of Paleozoic strata in Kansas (Newell, 1997; Merriam, 1963). Newell (1997) produced a burial history model for Phanerozoic strata in McPherson and Harper Counties in Kansas (north

and west of study area) (Fig. 2.31). Using the surface temperatures and geothermal gradients, Newell used in his estimates, the McPherson County model (30°C/km and 1,500ft of Cretaceous strata) suggests a maximum temperature of approximately 74°C and the Harper County model (25°C/km and 500ft of Cretaceous strata) suggests a maximum temperature of approximately 73°C, both achieved early in Permian time (30°C surface temperature). According to Newell (1997), the highest reasonable geothermal gradient in both counties is 40°C/km, and Cretaceous thickness likely does not exceed 3,000ft in McPherson County and 500ft in Harper County. For comparison purposes, the maximum geothermal gradient (40°C/km) and thickness (3,000ft) were also used for each model. McPherson County produced a maximum temperature of approximately 109°C during the Cretaceous and Harper County produced a maximum temperature of approximately 113°C during the Cretaceous. Homogenization temperatures in baroque dolomite are still greater than even the higher end estimates suggested by Newell (1997). Additionally, the rises and falls in temperature observed in baroque dolomite fluid inclusion transects (Fig. 2.26), as well as changes in salinity (Fig. 2.30), would be difficult to produce by fluctuating burial depth or a higher geothermal gradient, rendering hypothesis (1) and (2) unlikely.

Injection of hydrothermal fluids (hypothesis 3) would produce the elevated fluid inclusion measurements, and if migration of fluids occurred multiple times at different temperatures and variable salinities, it would also account for fluctuating Th values in transects and the changes in salinity. The xenotopic-C texture, curved crystal faces, and undulating extinction under crossed-polars are indicators of elevated temperatures during baroque dolomite precipitation (Davies and Smith, 2006; Gregg, 1985; Gregg and Sibley, 1984; Radke and Mathis, 1980). Moreover, the mineral assemblage of late cements in the Arbuckle Group are remarkably

similar to that of MVT deposits in the mid-Continent, widely believed to be associated with regional migration of hydrothermal fluids from nearby basins (e.g., Leach and Sangster, 1995; Garven, 1993; Bethke and Marshak, 1990; Sverjensky, 1986; Oliver, 1986). Similar mineral assemblages and fluid inclusion data found by others around the southern Midcontinent, as well as similar mineral assemblages found by others in higher stratigraphic intervals in the study area (Young, 2010; Wojcik, 1992; 1994; 1997), support the idea of a regional aquifer during migration of hydrothermal fluids. High fluid inclusion temperatures argue for basin-sourced hydrothermal fluids that migrated laterally and into less-deeply buried regions. Secondary fluid inclusion data derived from calcite suggests that fluids in the Arbuckle Group continued to have high salinity values and remained at elevated temperatures for some time after calcite precipitation, though values were lower than temperatures recorded during baroque dolomite precipitation.

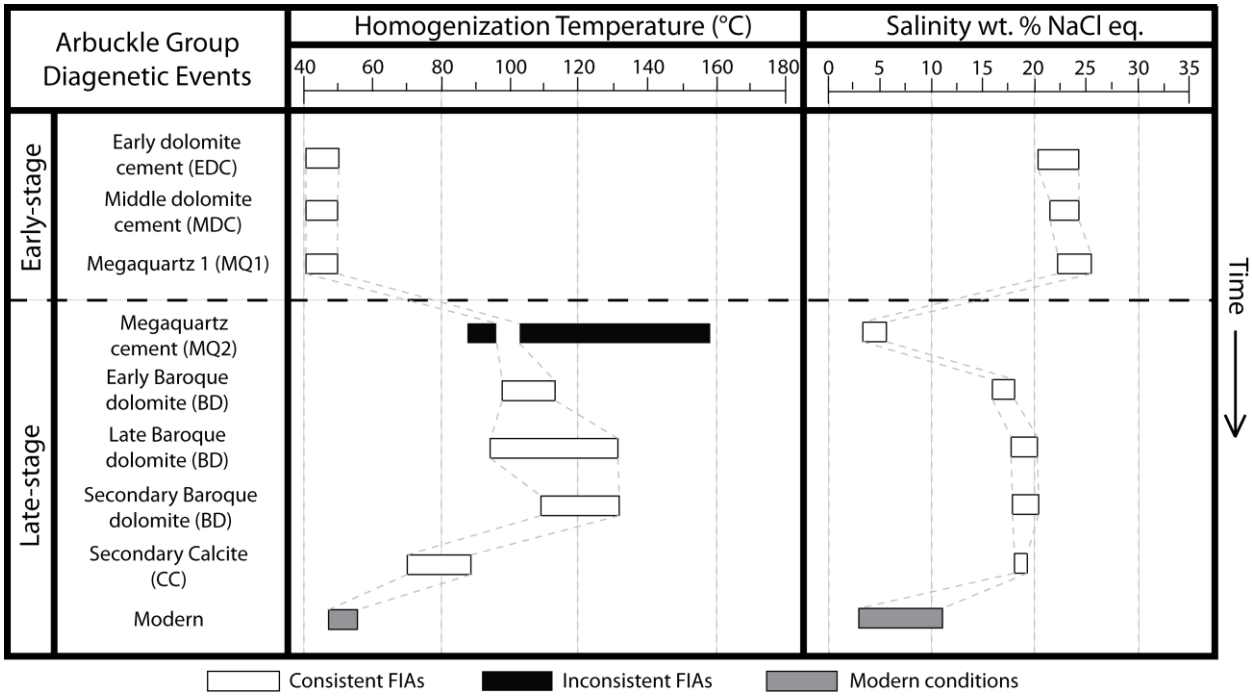


**Figure 2.30:** Fluid evolution illustration that uses fluid inclusion data (Th and $Tm_{ice}$) to display changes in reservoir fluid temperature and salinity from early stage cements, to late stage cements, to modern time. Values are fairly consistent during early-stage diagenesis, with temperatures likely representing reservoir temperature due to burial, geothermal gradient, and Ordovician surface temperature. The precipitation of megaquartz cement 2 (MQ2) signifies a drastic decrease in salinity and increase in temperature, possibly linked to migration of high-temperature connate fluids from the Anadarko Basin. During baroque dolomite (BD) precipitation, salinity increases while temperatures continue to climb; this is thought to represent continued sourcing of hydrothermal fluids from the Anadarko Basin after Permian reflux. Secondary fluid inclusions in calcite cement (CC) record a decline in temperature and salinity at some point after precipitation of calcite. Modern values yield temperatures that are significantly lower than what was seen by the reservoir during late-stage diagenesis, but still slightly higher than early-stage temperatures, likely due to increased burial since the time of early-stage diagenesis. Modern salinity values fall between the range observed in megaquartz cement 2 and baroque dolomite, suggesting a continued influence of evaporites along the current fluid migration pathway.

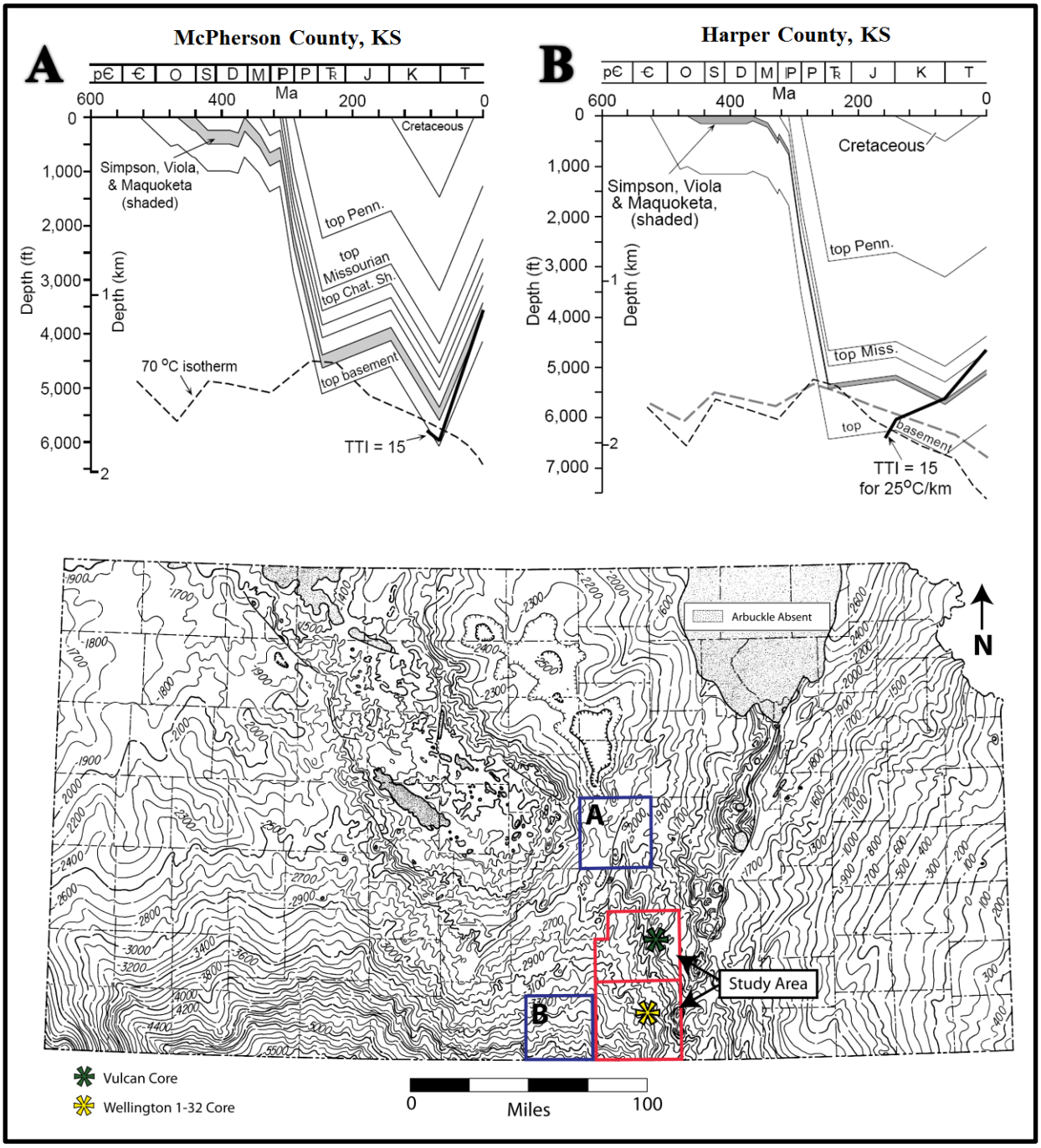


**Figure 2.31:** Burial history models for Phanerozoic strata in McPherson and Harper Counties in Kansas (north and west of study area). Assuming the thickness of Cretaceous strata and geothermal gradients to be 1500ft (460m) and 30°C/km for McPherson County and 500ft (150m) and 25°C/km for Harper County, a 70°C geotherm was also calculated for both models (modified from Newell 1997). When considering Cambrian-Ordovician strata, the McPherson County model suggests a maximum temperature of approximately 74°C and the Harper County suggests a maximum temperature of approximately 73°C, both achieved early in Permian time. The bottom image is a structural map of the Arbuckle Group with county and study area locations; contour interval is 100ft (modified from Franseen et al. 1994).

## 7. Oxygen and Carbon Isotopic Data

The following section discusses oxygen ($\delta^{18}O$) and carbon ($\delta^{13}C$) isotopic values provided from 44 isotopic analyses of samples from 11 stratigraphic horizons for dolomite and 4 stratigraphic horizons for calcite (Appendix IV). Isotopic values are given in ‰ VPDB. Baroque dolomite (event 19) is discussed first, followed by calcite (event 21-22-23). The range and average of data, as well as any observable trends, are listed first. Interpretations of $\delta^{18}O$ and $\delta^{13}C$ isotopic values, spatial variations of values, and potential fluid flow models are discussed for each precipitate.

### *7.1. Baroque dolomite*

A total of eleven stratigraphic horizons containing baroque dolomite were micro-sampled and processed for $\delta^{18}O$ and $\delta^{13}C$ isotopic values relative to VPDB; all of the micro-samples were taken from the Wellington 1-32 core. Ten of the eleven horizons were sampled in transects extending from the inner to outer margin of individual crystals, providing a total of twenty-seven analyses (Fig. 2.32, 2.33, 2.34) (Appendix IV). The $\delta^{18}O$ values range from the most negative value of -10.2‰ to the most positive value of -6.6‰, with an average of -8.4‰ (Fig. 2.32) (Appendix IV). The $\delta^{13}C$ values range from the most negative value of -3.6‰ to a slightly more enriched value of -2.4‰, with an average of -2.8‰ (Fig. 2.32) (Appendix IV). Nine of the twenty-seven microsamples were collected from baroque dolomite present in relatively late fractures (event 14-15) and are noted with sample names printed in red in the sample list for each image. The $\delta^{18}O$ values collected from fractures provide the most negative value of -9.5‰ and the most enriched value of -7.3‰, with an average of -8.2‰ (Fig. 2.32) (Appendix IV). Of the

$\delta^{13}C$ values collected from fractures, the most negative is -3.5‰ and the most positive is -2.5‰, with an average of -2.8‰ (Fig. 2.32) (Appendix IV).

There are several notable trends that can be observed in the baroque dolomite data. $\delta^{18}O$ values become more depleted from the base to the top of the Arbuckle Group, with an overall decrease of -3.5‰ (-6.6‰ to -10.1‰) (Fig. 2.35). $\delta^{13}C$ values remain fairly constant except for a decrease between 4500 and 4400ft of -0.9‰ (-2.7‰ to -3.6‰) to values that remain fairly constant through the upper Arbuckle Group (Fig. 2.36). Isotopic data from crystal transects with more than two isotopic analyses appear to fluctuate from the inner to outer crystal margin (Fig. 2.33, 2.34). The apparent fluctuations in data from transects may support the hypothesis mentioned in the fluid inclusion discussion that suggests multiple pulses of hydrothermal fluids at variable temperatures.

*Interpretation:* Baroque dolomite $\delta^{18}O$ values range from -6.6‰ -10.2‰, with an average of -8.4‰. Although a low-temperature origin for this dolomite is unlikely, it is useful to rule out low-temperature dolomite on the basis of multiple observations. According to Lohmann and Walker (1989), primary Cambrian-Ordovician marine calcites preserved initial $\delta^{18}O$ values with a maximum negative value of -7.0‰. Land (1980; 1985) established that dolomite forming coeval to calcite would likely be enriched by approximately 3‰, allowing for estimations of low-temperature dolomite precipitated from Cambrian-Ordovician seawater to be as low as -4.0‰. Not surprisingly, all of the $\delta^{18}O$ values in baroque dolomite are more negative than this value (by at least 2.6‰), eliminating a low-temperature seawater model.

A low-temperature mixture of seawater and meteoric water may also be proposed as a potential explanation for the depleted $\delta^{18}O$ values of the baroque dolomite as well as the apparent correlation between $\delta^{18}O$ and $\delta^{13}C$ (Gill et al., 1995; Muchez and Viaene, 1994). Though a

meteoric influence would provide a mechanism for further depleting the $\delta^{18}O$ values (Arthur et al., 1983; Land, 1985), fluid inclusion data has clearly demonstrated elevated homogenization temperatures (93.0-131.0ºC) during baroque dolomite precipitation, making the influence of low-temperature meteoric water unlikely.

The $\delta^{18}O$ values, when integrated with petrographic, fluid inclusion, and additional geochemical data, are best explained by a high-temperature model (e.g., Davies and Smith, 2006; Goldstein and Reynolds, 1994; Land et al., 1988; Land, 1985; Gregg and Sibley, 1984). The xenotopic-C texture, curved crystal faces, and undulating extinction under crossed polars are indicators of elevated temperatures during baroque dolomite precipitation (Davies and Smith, 2006; Gregg and Sibley, 1984; Radke and Mathis, 1980). Fluid inclusion temperatures ranging from 93.0-131.0ºC necessitate a hydrothermal environment to acquire such elevated values in the study area (see Fluid Inclusion Discussion) (Goldstein and Reynolds, 1994; Goldstein, in press). Homogenization temperatures and $\delta^{18}O_{dolomite}$ data allow for an approximation of $\delta^{18}O_{water}$ (Land, 1985 published equation):

$$\textit{Equation 2.2:}\quad 10^3 \ln \alpha = 2.78 * 10^6 / T^2 + 0.91$$

where ($10^3 \ln \alpha$) is approximately equal to ($\delta^{18}O_{dolomite} - \delta^{18}O_{water}$) and T is temperature in Kelvin (Land, 1985). The $\delta^{18}O_{water}$ PDB was then converted to $\delta^{18}O_{water}$ SMOW (Arthur et al., 1983). Thermal fractionation would lead to the most depleted $\delta^{18}O_{dolomite}$ values being associated with the highest temperatures, and the most enriched $\delta^{18}O_{dolomite}$ values associated with the lowest temperatures. The $\delta^{18}O$ values of fluids responsible for precipitating baroque dolomite may have ranged from -1.9 to +5.6‰. Enriched $\delta^{18}O_{water}$ values are common in residual evaporite brines (Epstein and Mayeda, 1953; Heimstra, 2003). Also, extensive rock-water interaction with material in the basin or along the fluid migration pathway could have provided enrichment of

$\delta^{18}O$ values. High salinities, depleted $\delta^{18}O_{dolomite}$ values, and enriched $\delta^{18}O_{water}$ values support the hypothesis of a basin-derived hydrothermal brine migrating through the Arbuckle Group (e.g., Davies and Smith, 2006; Banner, 1995; Land et al., 1988; Hanor, 1979). If one assumes a consistent isotopic composition of the fluid during baroque dolomite precipitation (2.0‰), the range in isotopic composition yields a temperature range of about 37 ºC, a range consistent with that of the fluid inclusion data. Given such an assumption, the values near the top of the Arbuckle, at times, may have been 37 ºC warmer than the base of the Arbuckle.

There are several hypotheses that could be explored to explain the spatial variation of $\delta^{18}O$ values. Extensive fluid-rock interaction is a possible hypothesis, but an unreasonably high fluid-rock ratio would be required to alter the $\delta^{18}O$ value of pore fluids to produce the observed variation (Lohmann, 1988). Spatial variation in fluid composition can also be ruled out by the consistent nature of the cathodoluminescence signature in the baroque dolomite cement stratigraphy (Goldstein, 1991; Machel and Burton, 1991), as well as the relatively consistent fluid inclusion salinity data. Given the previously established high-temperature influence on the depleted $\delta^{18}O$ values, an increase in temperature is most likely responsible for the decrease in $\delta^{18}O$ values as one progresses up section from the lower to the upper Arbuckle Group. The potential for preferential fluid flow, a temperature-controlled density gradient, or a combination of both is addressed in the discussion (Section 9.).

The geochemical characteristics of the fluids imply a basinal source for a hydrothermal brine that either migrated laterally from deeper portions of the basin or along deep-seated faults and fractures, very similar to many models for MVT deposits (e.g., Davies and Smith, 2006; Leach and Sangster, 1995; Garven, 1993; 1995; Sverjensky, 1986). The Anadarko basin has been suggested as a primary source for such fluids (e.g., Gao and Land, 1991; Gao, 1990a;

Garven, 1993; Musgrove and Banner, 1993) and encompasses the necessary depth and strata to produce the data values found in the baroque dolomite (Gallardo and Blackwell, 1999; Johnson et al., 1988).

The $\delta^{13}C$ values of the baroque dolomite range from the most negative value of -3.6‰ to the most positive value of -2.4‰, with an average of -2.8‰ (Appendix IV). Given the previous interpretation for $\delta^{18}O$ values, the spatial variation of the $\delta^{13}C$ values will be the focus. The slightly depleted $\delta^{13}C$ values indicate potential organic influences and the minor variability could be due to differences in fluid-rock interaction along the fluid migration pathway (Anderson and Arthur, 1983; Land, 1983; Machel, 1987; 2001; Davies and Smith, 2006); variable fluid source has already been ruled out above through evaluation of cement stratigraphy and fluid inclusion data.

Extensive fluid-rock interaction of the brine is plausible, given that even minor dissolution of rock during the migration history of the basinal brine could have a significant impact on the $\delta^{13}C$ values observed (Anderson and Arthur, 1983; Lohmann, 1988). The spatial variation of $\delta^{13}C$ values could be attributed to fluid-rock interaction because there is a positive correlation between $\delta^{13}C$ and $\delta^{18}O$ values ($\delta^{13}C$ values are most negative where $\delta^{18}O$ values are most negative). The fact that the Arbuckle Group is a reservoir for hydrocarbons, most notably in the upper part of the unit, suggests organic matter in the top portion of the unit could have supplied depleted $\delta^{13}C$ values in the uppermost samples.

Elevated temperatures observed in fluid inclusions indicate the contribution of light carbon may also be influenced by abiotic reactions, presumably thermochemical sulphate reduction (TSR) (Machel, 1987; 2001). The majority of homogenization temperatures fall within the most common range observed in sites altered by TSR reactions (100-140ºC) (Machel, 2001).

The presence of anhydrite, one of the most prominent sources for sulphate when dissolved in solution, provides the needed catalyst for TSR reactions to exist and the most common products of TSR reactions can be observed throughout the Arbuckle Group (dolomite, calcite, galena, pyrite, and sphalerite) (Machel, 1987; 2001). The spatial variation could be due to a slight increase in temperature in areas of increased fluid flow in the upper Arbuckle Group, providing conditions conducive to TSR reactions (Machel, 2001). The positive correlation between $\delta^{13}C$ and $\delta^{18}O$ values ($\delta^{13}C$ values decrease where $\delta^{18}O$ values decrease), as one progresses up in section from the lower to the upper Arbuckle Group, supports a greater TSR influence in the upper portion of the unit and is also likely controlled by temperature.

Another notable observation is the fact that both oxygen and carbon isotopic values do not appear to correlate with the low porosity/permeability zone that Scheffer (2012) hypothesized to be responsible for modern separation of fluids between the upper and lower Arbuckle Group and the rest of the unit (Fig. 2.35 and 2.36); this may mean migration of fluids in the ancient was not affected by the same low porosity/permeability zone present today.

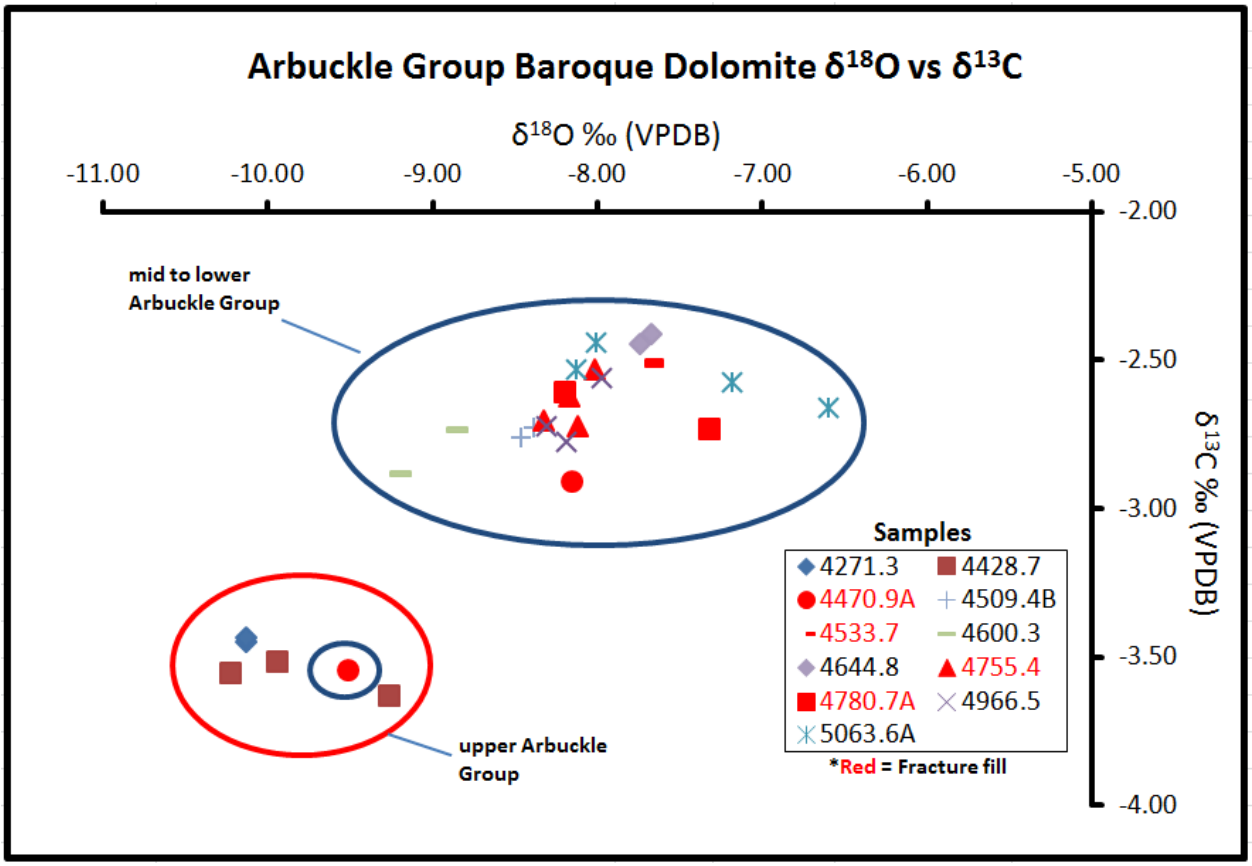


**Figure 2.32:** Cross-plot of $\delta^{18}O$ and $\delta^{13}C$ values for Arbuckle Group baroque dolomite. $\delta^{18}O$ and $\delta^{13}C$ values are the most depleted in the same samples, possibly illustrating hotter temperatures producing depleted $\delta^{18}O$ values, as well as allowing for TSR reactions to slightly deplete $\delta^{13}C$ values. An enhanced porosity zone at the top of the unit or rising lower density fluids may have produced the observed trend.

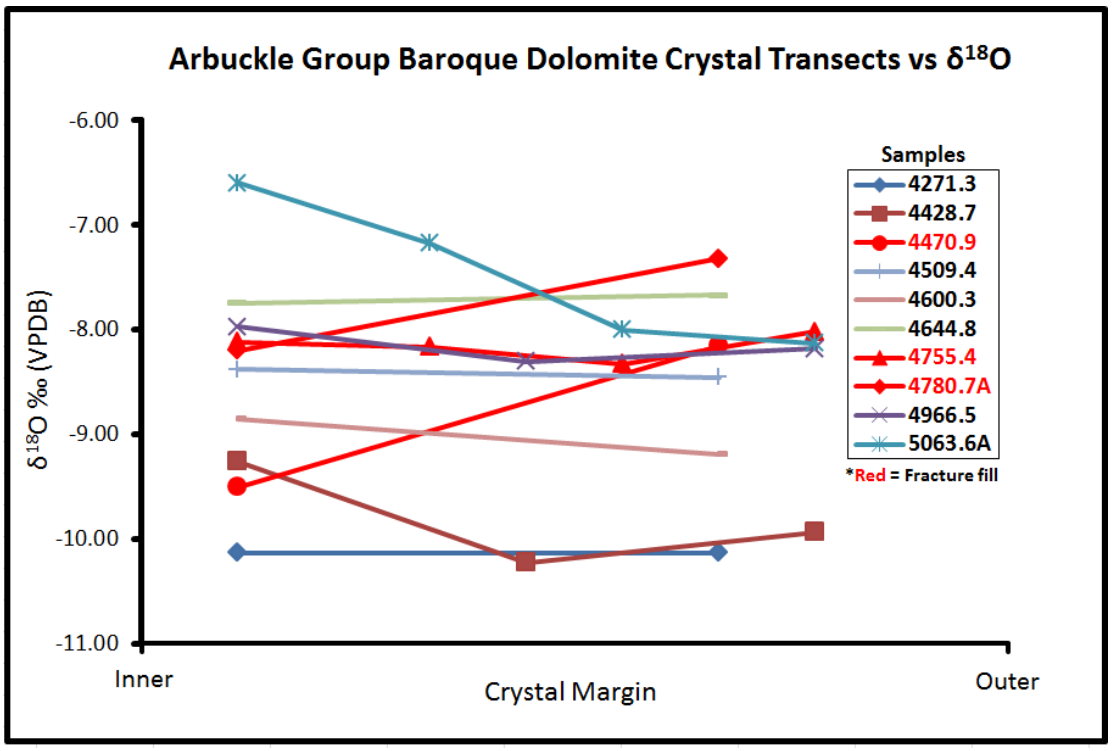


**Figure 2.33:** Cross-plot of $\delta^{18}O$ values and crystal margin for Arbuckle Group baroque dolomite. Fluctuations in samples with more than two analyses support the idea of multiple pulses of hydrothermal fluids proposed in the Fluid Inclusion Discussion.

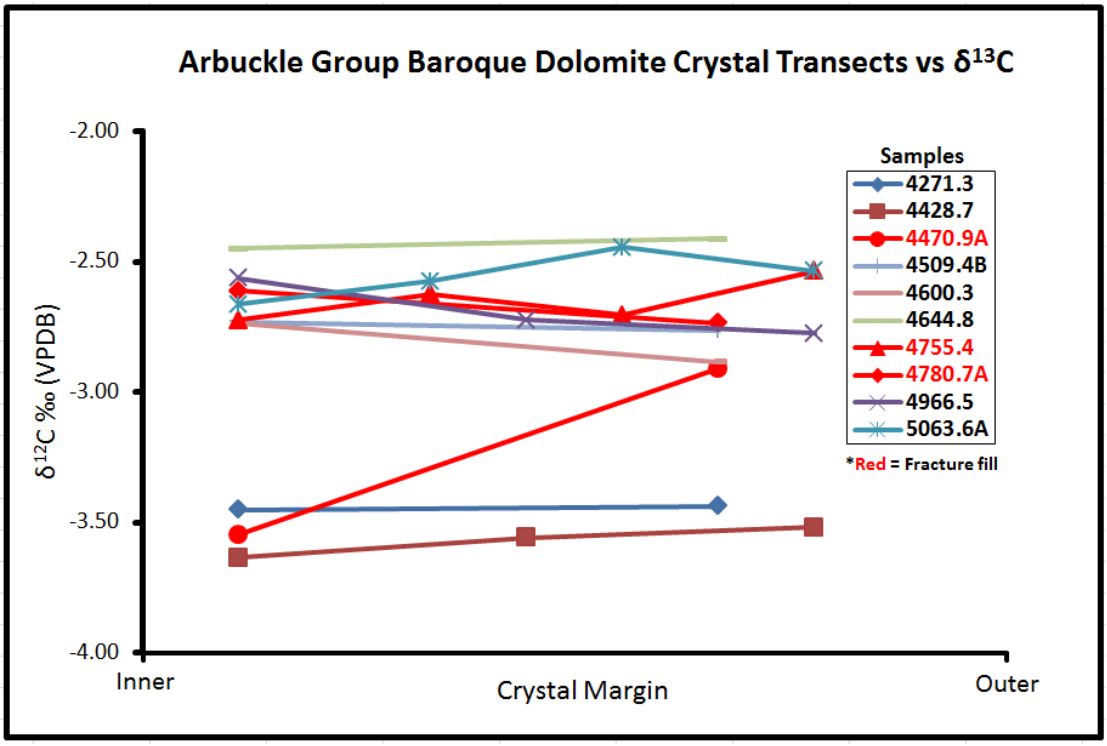


**Figure 2.34:** Cross-plot of $\delta^{13}C$ values and crystal margin for Arbuckle Group baroque dolomite. There is no discernible trend in the data.

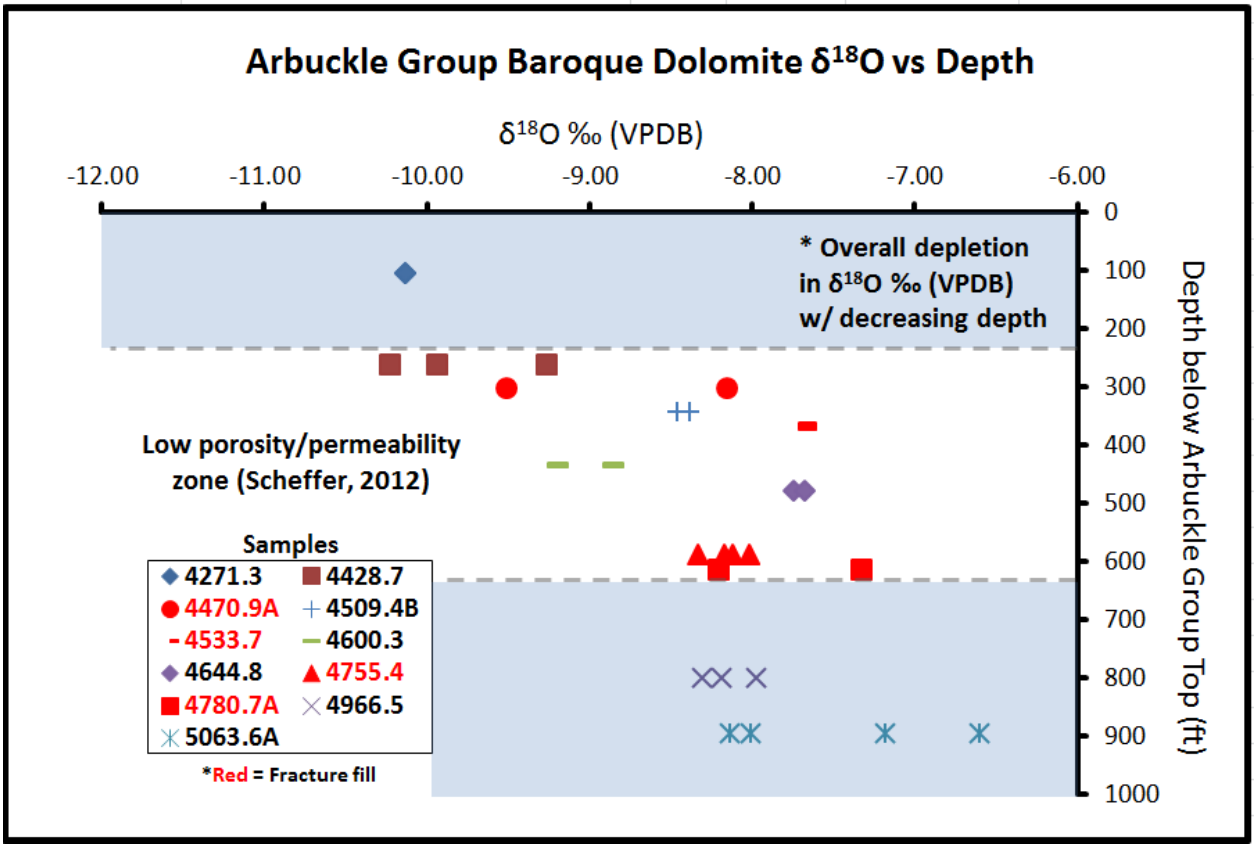


**Figure 2.35:** Cross-plot of $\delta^{18}O$ values and depth of samples. $\delta^{18}O$ values clearly become more depleted with decreasing depth, likely illustrating higher temperatures, potentially caused by preferential fluid flow or temperature-controlled density stratification in the Arbuckle Group. The gradual depletion of $\delta^{18}O$ with decreasing depth, especially within Scheffer's (2012) low porosity/permeability zone, supports a temperature-controlled density gradient affecting the entire unit at the time of baroque dolomite precipitation. Blue boxes represent modern zones of higher porosity/permeability due to solution enhanced fractures and brecciated zones (Scheffer 2012). The data appears to follow a trend of increasingly depleted values towards the top of the unit, regardless of modern reservoir conditions.

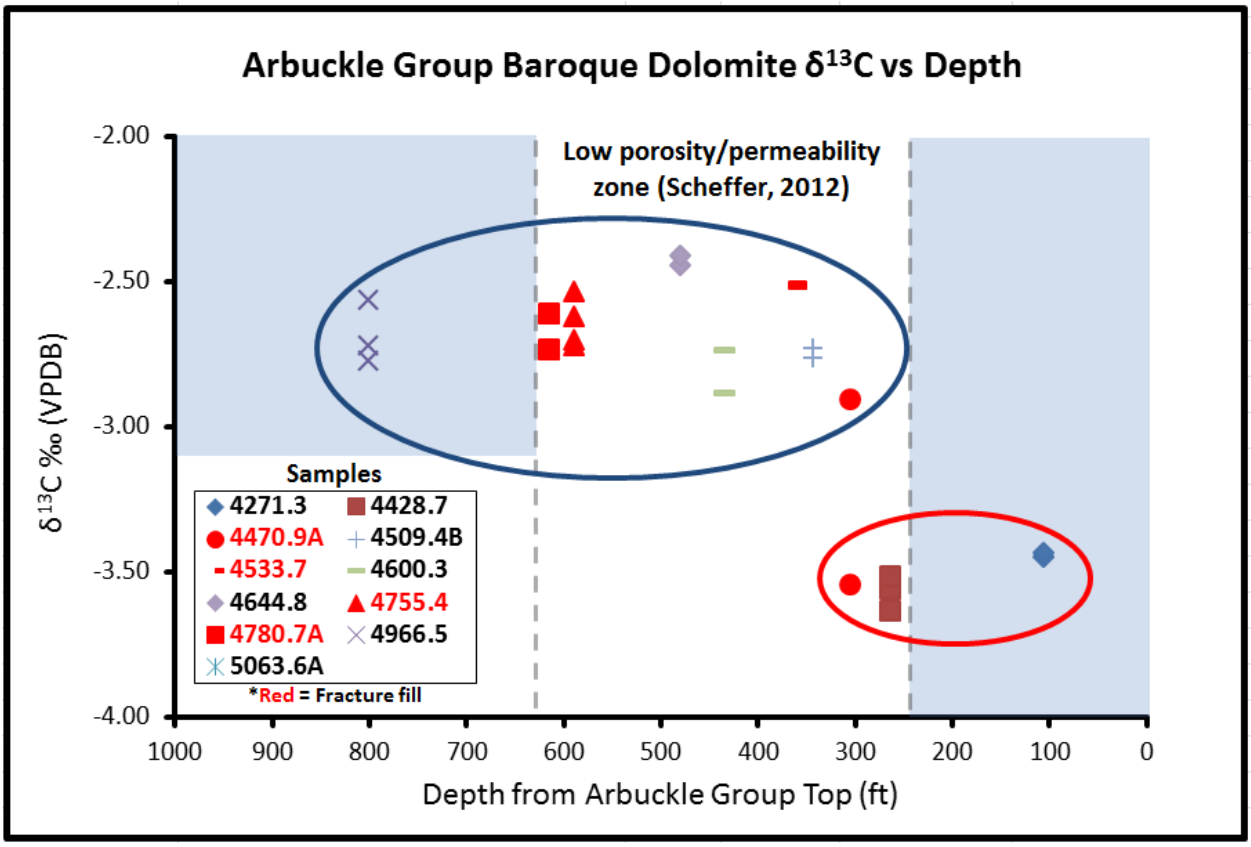


**Figure 2.36:** Cross-plot of $\delta^{13}C$ values and depth of samples for Arbuckle Group baroque dolomite. The upper Arbuckle Group (red circle) displays slightly more depleted $\delta^{13}C$ values than the lower and middle portions of the unit (blue circle). Higher temperatures at the top of the unit may have allowed for TSR to deplete the carbon values. The more depleted carbon values can be found within and outside of Scheffer's (2012) low porosity/permeability zone, again suggesting fluid flow during baroque dolomite precipitation may not have been affected by current formation conditions. Blue boxes represent modern zones of higher porosity/permeability (Scheffer, 2012).

### *7.2. Calcite cement*

A total of four stratigraphic horizons containing calcite were microsampled and processed for $\delta^{18}O$ and $\delta^{13}C$ isotopic values; three samples were taken from the Wellington 1-32 core and one was taken from the Vulcan core. All of the samples were sampled in transects extending from the core to outer margin of individual crystals, providing a total of seventeen isotopic analyses (Fig. 2.37, 2.38, 2.39) (Appendix IV). The $\delta^{18}O$ values range from the most negative value of -9.8‰ to the most positive value of -7.0‰, with an average of -8.7‰ (Fig.

2.37) (Appendix IV). The $\delta^{13}C$ values range from the most negative value of -18.5‰ to the most positive value of -3.7‰, with an average of -11.5‰ (Fig. 2.37) (Appendix IV).

The most readily observable trend in the data is the drastic difference that exists between values of the Vulcan and Wellington 1-32 cores, with the Wellington 1- 32 producing significantly more depleted values relative to $\delta^{18}O$ and $\delta^{13}C$ (Fig. 2.37, 2.40, 2.41). The Wellington 1-32 calcite $\delta^{18}O$ values range from -8.6‰ to -9.8‰, whereas the Vulcan core values range from -7.0‰ to -7.7‰ (Appendix IV). The $\delta^{13}C$ values of the Wellington core range from -12.3‰ to -18.6‰, whereas the Vulcan core values ranged from -3.7‰ to -3.9‰ (Appendix IV). Transects in calcite crystals resulted in what appears to be overall depletion of isotopic values from the beginning to the culmination of calcite precipitation (Fig. 2.38, 2.39).

*Interpretation:* The $\delta^{18}O$ values of calcite range from the most negative value of -9.8‰ to the most positive value of -7.0‰, with an average of -8.7‰ (Appendix IV). According to Lohmann and Walker (1989), primary Cambrian-Ordovician marine calcites preserve initial $\delta^{18}O$ values with a maximum negative value of -7.0‰. As only the most enriched $\delta^{18}O$ value is -7.0‰, a low-temperature seawater model is eliminated; this is not surprising given the late placement in the paragenesis (event 21-22-23).

A model consisting of a mixture of seawater and meteoric water could also be proposed, with meteoric water providing the depleted $\delta^{18}O$ values (Anderson and Arthur, 1983). If one assumes that original calcite precipitation occurred below the highest temperature recorded in baroque dolomite (131.0°C) and above the highest temperature recorded in secondary FIAs in calcite (89.8°C), then temperatures during calcite precipitation likely would have been higher than can be explained by normal burial conditions or geothermal gradient. The influence of low-temperature meteoric water would be eliminated if calcite precipitated at such high temperatures.

One can calculates the $\delta^{18}O_{water}$ of fluids responsible for calcite precipitation using the estimated temperature range. O'Neil et al. (1969) provide the equation:

$$\textit{Equation 2.3:}\quad 10^3 \ln \alpha = 2.78 * 10^6 / T^2 - 2.89$$

where ($10^3 \ln \alpha$) is approximately equal to ($\delta^{18}O_{calcite}$ - $\delta^{18}O_{water}$) and T is temperature in Kelvin (Land, 1985). The $\delta^{18}O_{water}$ PDB was then converted to $\delta^{18}O_{water}$ SMOW (Arthur et al., 1983). With a temperature range from 89.9-131.0°C and a $\delta^{18}O_{calcite}$ range from -7.0 to -9.8‰, $^{18}O_{water}$ for original calcite precipitation ranges from about +1.9 to +9.1‰. This range of fluid compositions is also enriched in comparison to the fluids responsible for baroque dolomite precipitation, suggesting a potential link in fluid source or migration pathway. Given an assumed constant isotopic composition of the fluid (5.0‰), the temperature would have ranged approximately 22ºC.

As with the baroque dolomite, the combination of petrographic observations, fluid inclusion data, and geochemical data can most adequately be explained by the continued influence of high temperatures. The late-stage precipitation of calcite (potentially the latest event (23) in the paragenesis), correlates well with other authors' interpretations that calcite precipitated in the later stages of cement precipitation in MVT deposits (Coveney et al., 2000; Brannon et al., 1996; Garven, 1993; Voss et al., 1989; Hagni and Grawe, 1964). Further discussion regarding potential fluid flow models is addressed in the discussion (Section 9.).

Limited sample depths of calcite inhibit the interpretation of spatial variation of $\delta^{18}O$ values and fluid flow, but several points of speculation can be made. As mentioned earlier, the main observable trend within the plotted calcite isotope data is the drastic difference between values of the Vulcan and Wellington 1-32 cores, with the Wellington 1-32 producing significantly more depleted $\delta^{18}O$ values. Assuming the calcite samples are of the same age,

several hypotheses can be offered. Extensive fluid-rock interaction is a possible hypothesis, but an unreasonably high fluid-rock ratio would be required to alter the $\delta^{18}O$ value of pore fluids to produce the observed variation (Lohmann, 1988). Calcite $\delta^{18}O$ values are more enriched in the Vulcan core, near the top of the Arbuckle Group. The fact that the isotope data are from different cores, separated by more than fifty miles, could support preferential fluid flow near the Wellington 1-32 core, resulting in warmer fluids and more depleted $\delta^{18}O$ values than that recorded in the Vulcan core. A basin-derived hydrothermal fluid-flow model could be applied to the precipitation of calcite. In contrast to the regional advective fluid flow model proposed for the baroque dolomite, the difference in isotopic composition between cores, and lack of an upward depletion in $\delta^{18}O$ in the Wellington 1-32 core, suggests other variables controlling fluid flow (Fig. 2.40, 2.41). One potential hypothesis is that calcite precipitation was affected by a fracture-controlled system occurring after baroque dolomite precipitation. If fracturing after baroque dolomite did play a role in fluid flow, then it is possible that the spatial variability could be associated with location relative to fractures or faults. Another trend of note is the fact that transects through calcite crystals displayed minor progressive depletion in isotopic values as crystal precipitation progressed, but the overall variation is greater from sample to sample than within samples. If depleted values are controlled by temperatures, the trend observed in transects could represent an increase in temperature with time. Further discussion regarding fluid flow will be supplied in Sections 8 and 9 following the presentation of strontium isotopic data.

The $\delta^{13}C$ values range from the most negative value of -18.5‰ to the most positive value of -3.7‰, with an average of -11.5‰. There is significant depletion of $\delta^{13}C$ values from the Wellington 1-32 core (-12.3‰ to -18.6‰) when compared to the Vulcan core values (-3.7‰ to -3.9‰), with variability between $\delta^{13}C$ values from samples in the Wellington core. Similar to

$\delta^{18}O$ data, transects through calcite crystals display increasingly depleted $\delta^{13}C$ values as crystal precipitation progressed (Fig. 2.38, 2.39).

The previously established presence of elevated temperature conditions indicates that the contribution of light carbon may also be influenced by abiotic reactions, presumably TSR (Machel, 1987; 2001). As is the case with the baroque dolomite, the presence of anhydrite, one of the most prominent sources for sulphate when dissolved in solution, provides the needed catalyst for TSR reactions to exist (Machel, 1987; 2001). The most common products of TSR reactions can be observed throughout the Arbuckle Group (dolomite, calcite, galena, pyrite, and sphalerite) (Machel, 1987; 2001). The assumption that original calcite precipitation took place at temperatures somewhere between values recorded in baroque dolomite (93.0-131.0°C) and in secondary FIAs in calcite (70.5-89.8°C) places the fluids within a range of temperatures conducive for TSR to occur (Machel, 2001). Alternatively, the fact that $\delta^{13}C$ values are much more depleted than the values observed in baroque dolomite may also illustrate the impact that organic matter can have on depletion of carbon. Petroleum migration occurred during and possibly some time after the precipitation of baroque dolomite, likely providing an abundance of organic matter in the reservoir when calcite precipitated at a later time. Another hypothesis could be that a fracture-controlled system is influencing the precipitation of calcite. The more negative $\delta^{13}C$ values could represent less rock-water interaction and the dominance of flow along fractures.

Alternatively, previous studies have shown evidence for multiple generations of calcite cement near the study area (Coveney, 2000; Wojcik, 1992; 1994; 1997). If the calcite sampled is actually representative of different generations of calcite precipitation then more research is required to shed light on isotopic values and data trends.

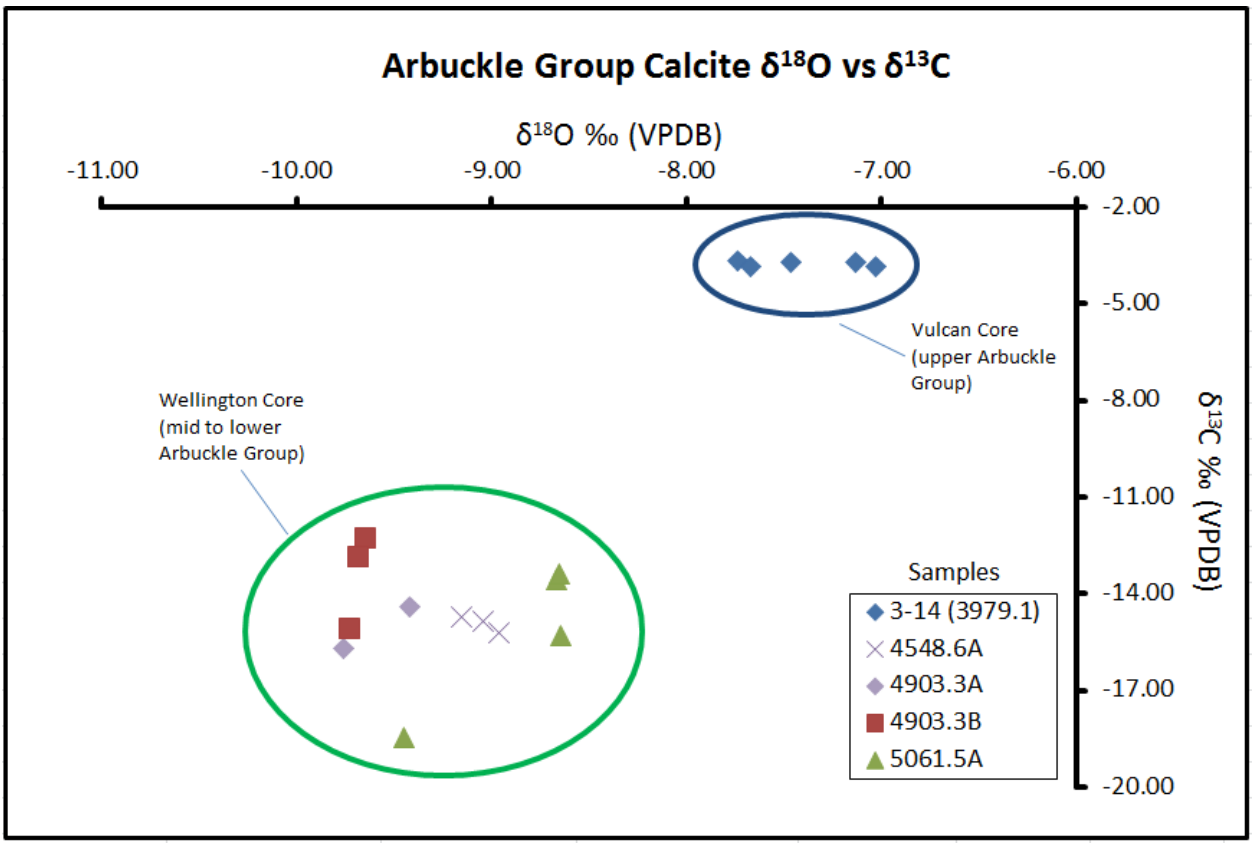


**Figure 2.37:** Cross-plot of $\delta^{18}O$ and $\delta^{13}C$ values for Arbuckle Group calcite cement. Samples from the Wellington core display more depleted isotopic values, requiring variability in fluids between the two locations.

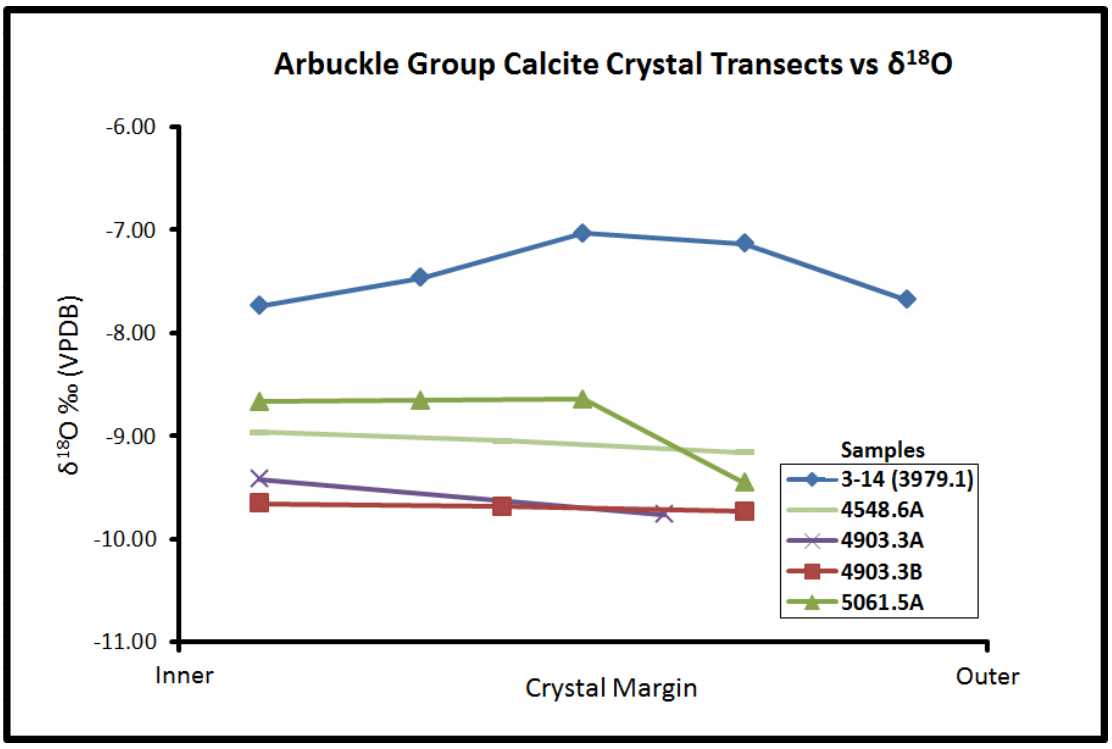


**Figure 2.38:** Cross-plot of $\delta^{18}O$ and crystal margin for Arbuckle Group calcite cement. Overall, fluids responsible for calcite precipitation appear to become more depleted or temperatures increase as crystal precipitation progressed.

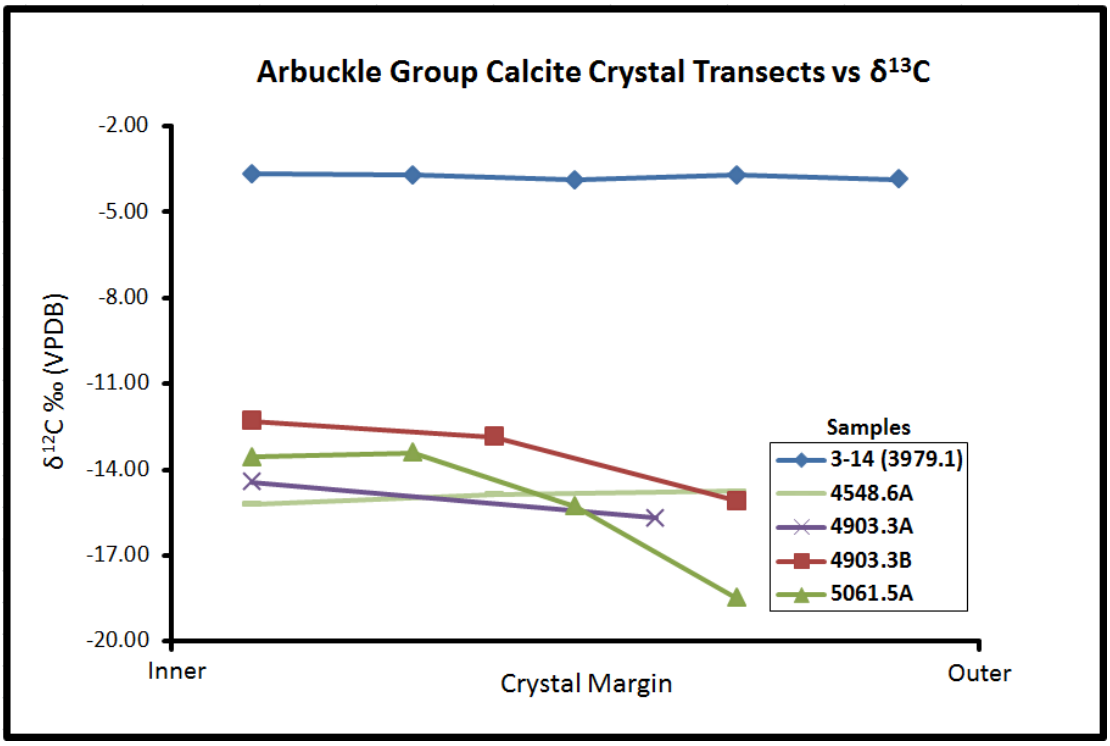


**Figure 2.39:** Cross-plot of $\delta^{13}C$ values and crystal margin for Arbuckle Group calcite cement. Similar to $\delta^{18}O$ data, $\delta^{13}C$ values also appear to become more depleted as crystals

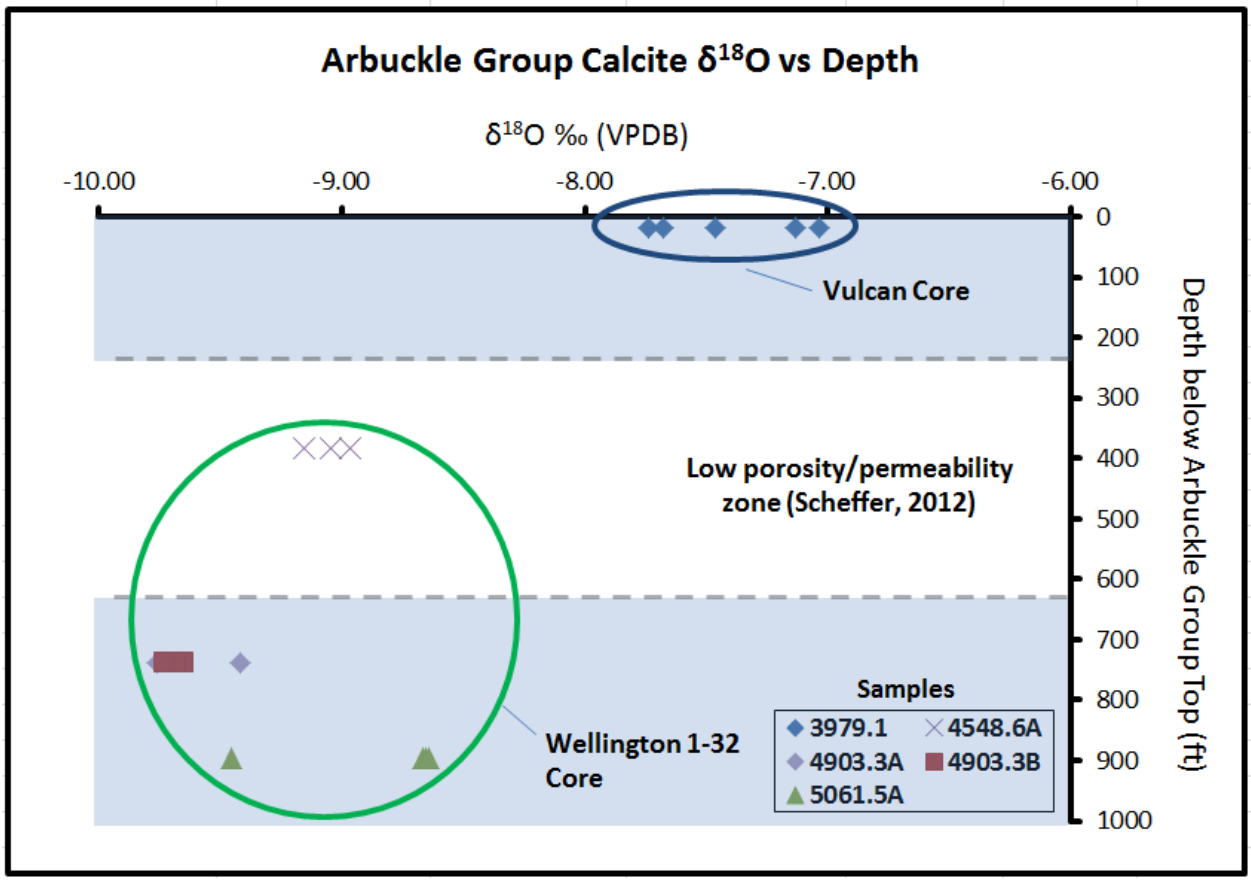


**Figure 2.40:** Cross-plot of $\delta^{18}O$ values and depth of samples. The only noticeable trend remains the more depleted nature of the Wellington core. Also, the $\delta^{18}O$ values do not appear to be influenced by preferential fluid flow or a density gradient, as appeared to be the case with baroque dolomite; this may provide support for the influence of a fracture-controlled fluid flow system affecting the unit at the time of calcite precipitation. Scheffer's (2012) low porosity/permeability zone does not appear to affect the isotopic values of calcite throughout the Arbuckle Group. Blue boxes represent zone of higher porosity/permeability in the upper and lower Arbuckle Group (Scheffer, 2012).

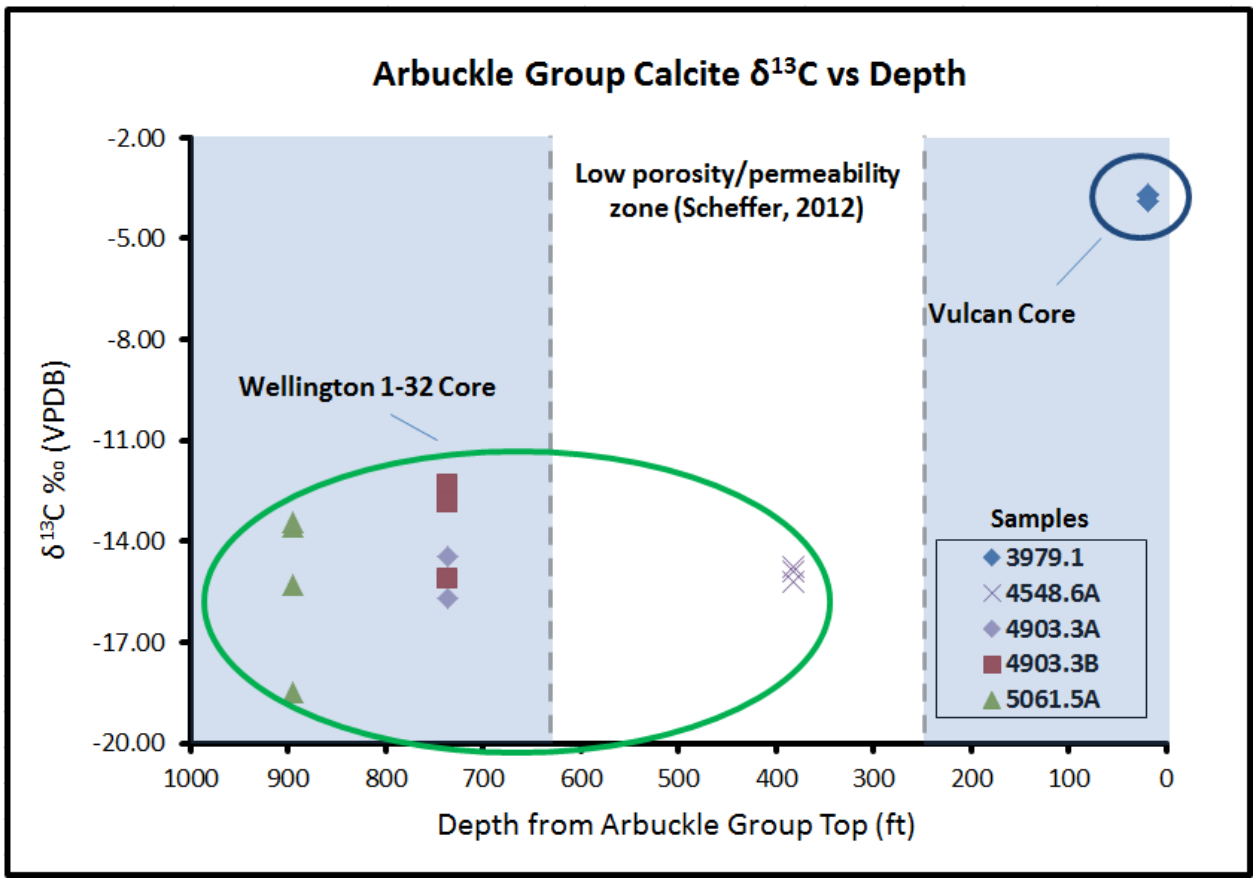


**Figure 2.41:** Cross-plot of $\delta^{13}C$ values and depth of samples. The only noticeable trend is the more depleted nature of the Wellington core samples. As with $\delta^{18}O$ data, $\delta^{13}C$ data does not appear to correlate with the modern zone of low porosity/permeability proposed by Scheffer (2012). Blue boxes represent zones of higher porosity/permeability in the upper and lower Arbuckle Group (Scheffer, 2012).

## 8. Strontium Isotopic Data

The following section discusses strontium concentration and isotopic ratios ($^{87}Sr/^{86}Sr$) provided from the analysis of nine dolomite samples and four calcite samples (Appendix IV). Baroque dolomite (event 19) is discussed first, followed by calcite (event 21-22-23). The range and average of data, as well as any observable trends, are presented first. Discussions of observed values and trends are offered at the end of each section. For comparison purposes, all values mentioned from previous authors' work have been normalized to NBS 987 = 0.710250.

### *8.1. Baroque dolomite*

A total of nine occurrences of baroque dolomite were sampled from the Wellington 1-32 core; all samples but one were also paired with carbon and oxygen isotope analyses. Samples ranged from the depth of 4190.5' to 5063.6', nearly encompassing the entire extent of the Arbuckle Group. Strontium concentrations varied from 34.68 to 68.33ppm with an average of 49.11ppm, whereas $^{87}Sr/^{86}Sr$ ranged from 0.70908 to 0.71019 with an average of 0.70948 (Appendix IV). When cross-plotted with the depth of each sample, $^{87}Sr/^{86}Sr$ values become more radiogenic and variable as depth decreases, with the most radiogenic value (0.71019) belonging to the shallowest sample (4271.3') (Fig. 2.42). $^{87}Sr/^{86}Sr$ values were also cross-plotted with the $\delta^{13}C$ and $\delta^{18}O$ values derived from the same samples. The cross-plot with $\delta^{18}O$ data displays a trend of increasingly radiogenic values being associated with increasingly depleted $\delta^{18}O$, with the most radiogenic value (0.71019) being linked with the most depleted value (-10.1‰) (Fig. 2.43). The cross-plot with $\delta^{13}C$ data also displays a trend of increasingly radiogenic values being associated with increasingly depleted $\delta^{13}C$ values, with the most depleted $\delta^{13}C$ data correlating with the most radiogenic values (Fig. 2.44).

*Interpretation:* Early Ordovician seawater values yield $^{87}Sr/^{86}Sr$ ranging from approximately 0.70864 to 0.70892 (Denison et al., 1998). Every baroque dolomite sample produced values more radiogenic than unmodified Ordovician seawater (Fig. 2.42). In fact, the entire data range (0.70908-0.71019) is more radiogenic than any seawater values recorded from Cambrian (0.70904) to modern (0.70896) (Denison et al., 1998). The radiogenic nature of the baroque dolomite samples suggests rock-water interaction with siliciclastic material or basement at some point during the fluid migration history (Davies and Smith, 2006; Banner, 1995). The $^{87}Sr/^{86}Sr$ values provide additional support to the earlier interpretation of oxygen isotopic data,

supporting a basinal source for the fluids responsible for late-stage baroque dolomite precipitation (see Section 7.1.).

The spatial variability in the data provides two informative trends that further support the previous interpretations (Section 7.1. and 7.2.). The presence of hydrothermal fluids migrating through the Arbuckle Group has been well-established through petrographic observations, fluid inclusion microthermometry, and carbon and oxygen isotopic analysis. The highly porous and permeable upper portion of the Arbuckle Group has been hypothesized as a preferential fluid flow conduit (this study; Scheffer, 2012; Jorgensen et al., 1993), but the depletion of $\delta^{18}O$ with decreasing depth supports the idea of a temperature-controlled density gradient affecting the unit as well (Section 6 and 7). $^{87}Sr/^{86}Sr$ values become more radiogenic and variability increases moving up through the Arbuckle Group; this trend appears to support the idea of a temperature-controlled density gradient pushing hotter, less dense, fluids toward the top of the unit, whereas the enhanced porosity and permeability at the top of the unit may have allowed for preferential fluid flow at the same time. The enhanced fluid flow and higher temperatures could result in less rock-water interaction at the top of the Arbuckle Group. The $^{87}Sr/^{86}Sr$ from this portion of the unit would yield water-dominated values (more radiogenic) whereas ratios obtained from lower in the section would yield rock-dominated values (less radiogenic). Cross-plots of $^{87}Sr/^{86}Sr$ values with $\delta^{13}C$ and $\delta^{18}O$ data provide additional support to the idea of hotter fluids towards the top of the unit. The cross-plot with $\delta^{18}O$ data displays a trend of increasingly radiogenic values being associated with increasingly depleted $\delta^{18}O$ values, with the most radiogenic value (0.71019) being linked with the most depleted $\delta^{18}O$ value (-10.1‰) (Fig. 2.43); this correlation follows the idea of preferential fluid flow or a density gradient producing higher temperatures and less rock-water interaction higher in the section. The cross-plot with $\delta^{13}C$ data also displays

a trend of increasingly radiogenic values being associated with increasingly depleted $\delta^{13}C$ values, with the most depleted $\delta^{13}C$ values correlating with most radiogenic samples (Fig. 2.44); this correlation agrees with the idea of higher temperatures and less rock-water interaction toward the top of the Arbuckle Group being responsible for TSR, which can account for the depletion of the $\delta^{13}C$ values.

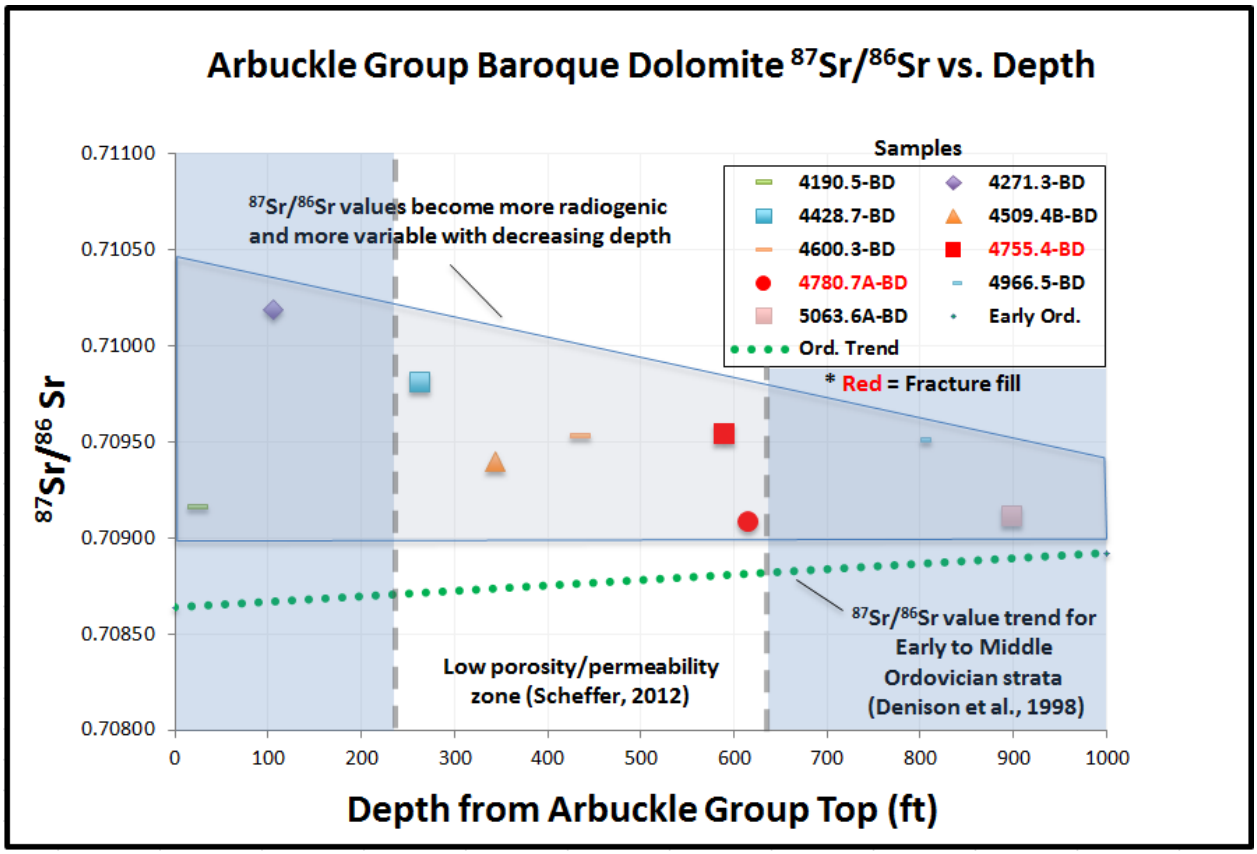


**Figure 2.42:** Cross-plot of $^{87}Sr/^{86}Sr$ versus depth of samples from Arbuckle Group baroque dolomite. Estimated Early Ordovician samples are also provided from Denison et al., 1998. Values become more radiogenic and more variable with decreasing depth, supporting the idea of enhanced fluid and temperature toward the top of the unit. As with isotopic data, $^{87}Sr/^{86}Sr$ data does not appear to be affected by Scheffer's (2012) low porosity/permeability zone. Blue Blue boxes represent zones of higher porosity/permeability in the upper and lower Arbuckle Group.

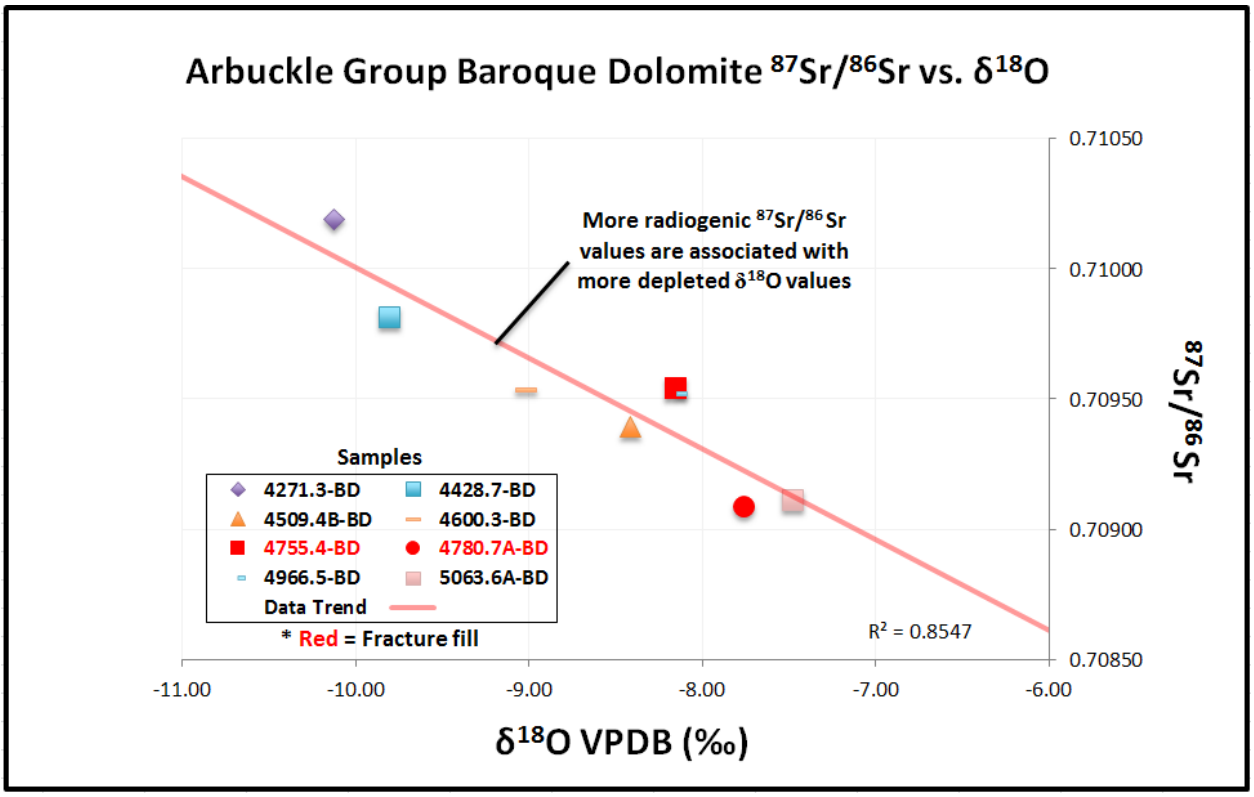


**Figure 2.43:** Cross-plot of $^{87}Sr/^{86}Sr$ versus $\delta^{18}O$ values for Arbuckle Group baroque dolomite. Plot displays more radiogenic values correlating with more depleted $\delta^{18}O$ values.

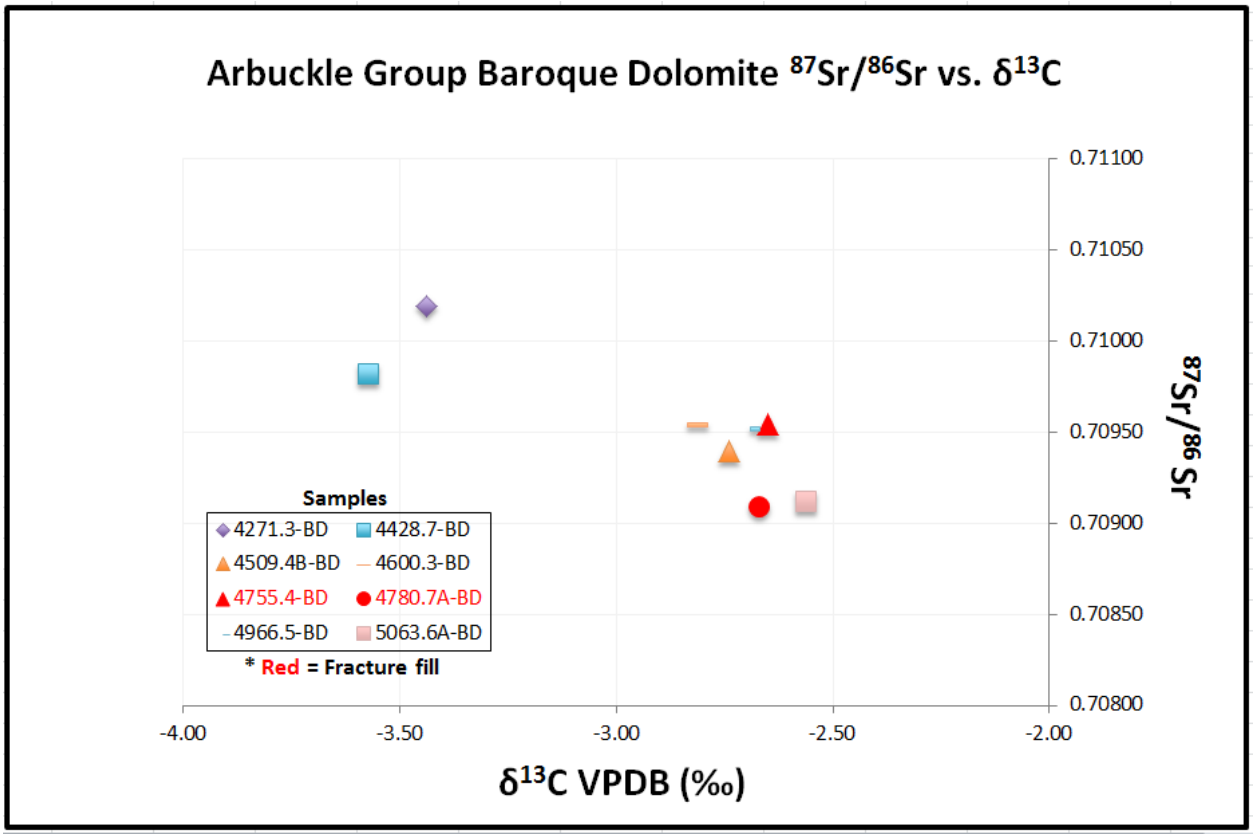

**Figure 2.44:** Cross-plot of $^{87}Sr/^{86}Sr$ versus $\delta^{13}C$ values for Arbuckle Group baroque dolomite. Plot displays more radiogenic values correlating with more depleted $\delta^{13}C$ values. Data support the idea of higher temperature fluids preserving more radiogenic values, and being capable of sustaining TSR, which in turn depletes the $\delta^{13}C$ values.

### *8.2. Calcite cement*

Three locations were sampled from the Wellington 1-32 core and one was sampled from the Vulcan core; all samples were also paired with carbon and oxygen isotope analysis. Sample depths are discussed relative to the top of the Arbuckle Group because they were taken from more than one core. Sample depths ranged from 17.5' to 895.5' below the top of the Arbuckle Group, providing data points that span nearly the entire extent of the unit. Strontium concentrations varied from 50.09 to 92.47ppm with an average of 73.80ppm, whereas $^{87}Sr/^{86}Sr$ ranged from 0.71257 to 0.71716 with an average of 0.71546 (Appendix IV). The cross-plot of $^{87}Sr/^{86}Sr$ with depth shows that Wellington 1-32 core samples are more radiogenic than Vulcan core samples, but there is no trend relative to depth (Fig. 2.45). Cross-plots with $\delta^{13}C$ and $\delta^{18}O$ values provide additional trends of note. The cross-plot with $\delta^{18}O$ data displays a trend of increasingly radiogenic values being associated with increasingly depleted $\delta^{18}O$ values, with the most radiogenic value (0.71716) being linked to the most depleted value (-9.6‰ VPDB) (Fig. 2.46). The cross-plot with $\delta^{13}C$ data also displays a trend of increasingly radiogenic values being associated with increasingly depleted $\delta^{13}C$ values, but the correlation is not as strong, generally showing that the Wellington 1-32 core has more radiogenic values associated with the more depleted $\delta^{13}C$ values (Fig. 2.47).

*Interpretation:* The radiogenic $^{87}Sr/^{86}Sr$ values (0.71257 to 0.71716) produced from the calcite are well above any value measured from seawater in any part of the Phanerozoic, clearly

suggesting extensive rock-water interaction with siliciclastic or basement material during the fluid migration history. When comparing the calcite values to those observed in baroque dolomite (0.70908-0.71019), the more radiogenic nature of the calcite suggests that the fluids responsible for calcite precipitation in each of the two localities may have followed different fluid migration pathways than the dolomite-precipitating fluids. If calcites in the two locations are the same age, their different geochemical compositions suggest localized fluid flow rather than regional advective flow. One possible hypothesis could be that tectonism that occurred after baroque dolomite precipitation may have opened different fluid conduits via additional open fracture networks, possibly allowing for changes in rock-water interaction along the fluid migration pathway and the more evenly distributed $\delta^{18}O$ values.

The spatial variability of the data differs from that observed in the baroque dolomite. There appears to be no direct correlation between $^{87}Sr/^{86}Sr$ values and the depth of the sample (Fig. 2.45). A possible explanation for this is that fracturing could have localized fluid flow instead of having regional lateral fluid flow through the Arbuckle Group. The cross-plot with $\delta^{18}O$ data follows the trend observed in the baroque dolomite of increasingly radiogenic values being associated with increasingly depleted $\delta^{18}O$ values, with the most radiogenic value (0.71716) being linked with the most depleted value (-9.6‰ VPDB) (Fig. 2.46). Though this correlation does not display a link to the depth of the sample, it still demonstrates that areas with higher temperatures (more depleted $\delta^{18}O$ values) also produced more radiogenic $^{87}Sr/^{86}Sr$ values. The disparity between the Wellington 1-32 core and the Vulcan core matches well with the $\delta^{13}C$ data discussed earlier (Fig. 2.47); these differences likely reflect preferential fluid flow in the area of the Wellington 1-32 core, allowing for less rock-water interaction and producing more

radiogenic values in the area. The difference between cores may also be directly linked to the mechanisms responsible for the difference in $\delta^{13}C$ values (discussed in Section 8.2.).

Conversely, the correlation between $^{87}Sr/^{86}Sr$ and $\delta^{18}O$ data may represent two-component mixing (Fig. 2.46). This type of mixing would have consisted of a physical mixture of two end-member calcites, one with depleted $\delta^{18}O$ and radiogenic $^{87}Sr/^{86}Sr$, and the other with enriched $\delta^{18}O$ and less radiogenic $^{87}Sr/^{86}Sr$. The potential clearly exists for sampling of multiple generations of calcite (e.g., Coveney, 2000; Wojcik, 1992; 1994; 1997). If this is the case, interpretations based on this data set would need to be reconsidered following additional research on calcite cements in the study area. Alternatively, the correlation may represent mixing of two different fluids at the time of calcite precipitation. If fluid mixing produced the linear relationship between $^{87}Sr/^{86}Sr$ and $\delta^{18}O$, then it is possible that one fluid that was slightly hotter and more radiogenic was mixing with a slightly lower temperature fluid with less radiogenic values. This type of mixing could mean that fluids were being sourced from multiple sources or along different fluid migration pathways at the time of calcite precipitation.

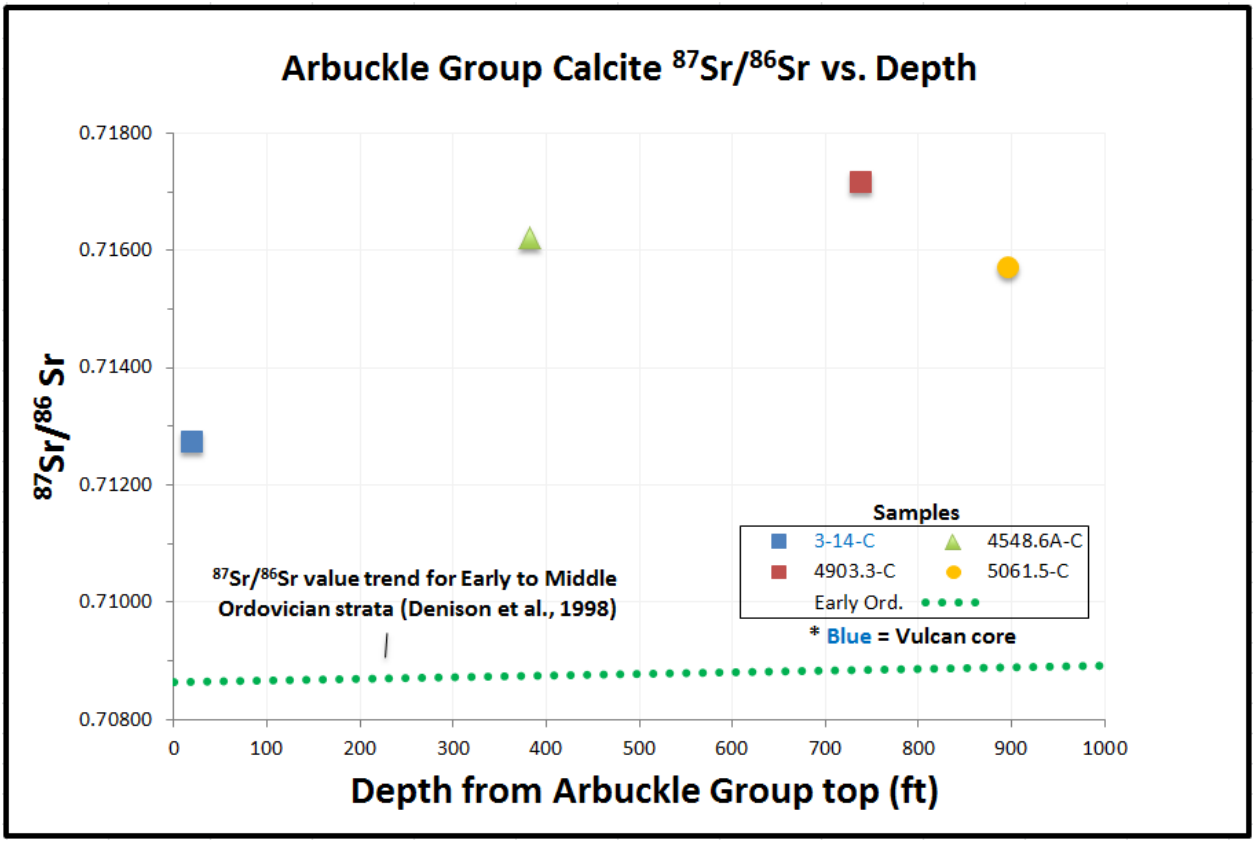


**Figure 2.45:** Cross-plot of $^{87}Sr/^{86}Sr$ data versus depth of samples from Arbuckle Group calcite cement. Estimated Early Ordovician samples are also provided from Denison et al., 1998. All samples are more radiogenic than Early Ordovician estimates, and the most radiogenic values are from Wellington 1-32 samples.

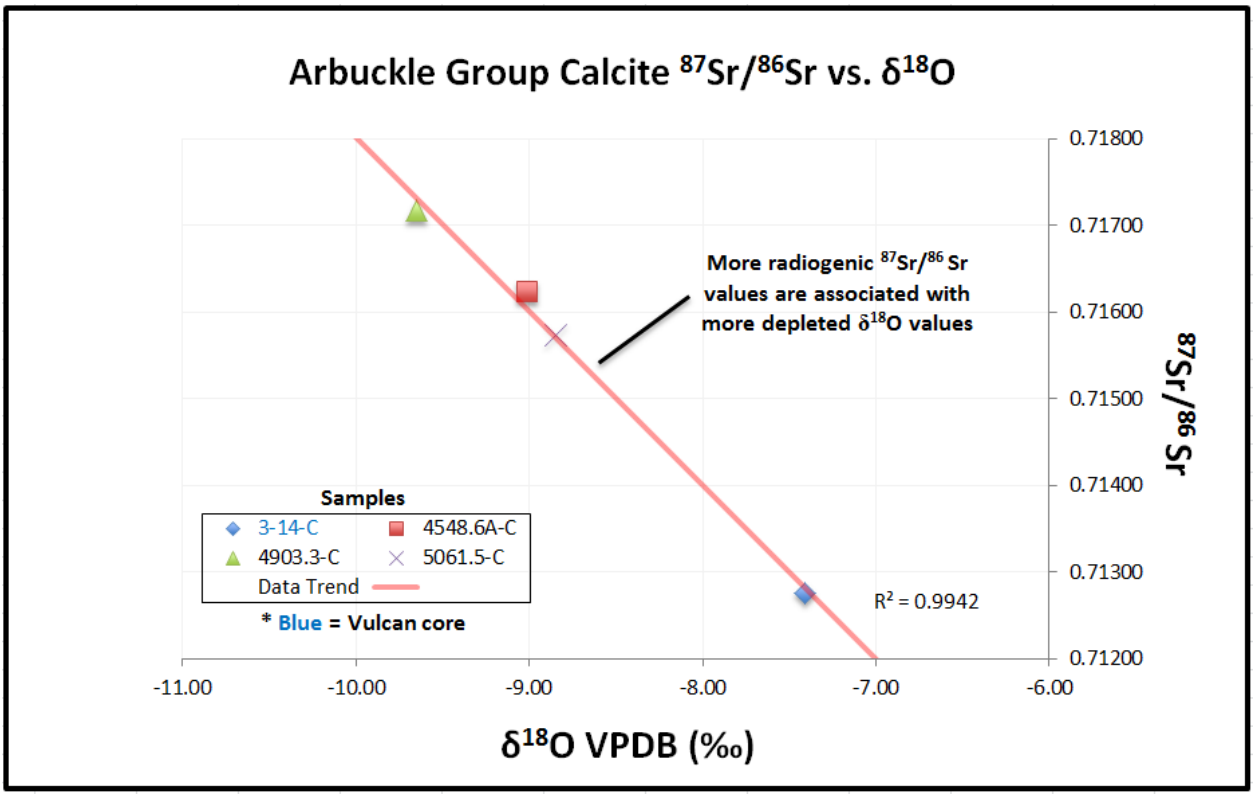


**Figure 2.46:** Cross-plot of $^{87}Sr/^{86}Sr$ ratio versus $\delta^{18}O$ values of Arbuckle Group calcite. Plot displays more radiogenic values correlating with more depleted $\delta^{18}O$ values. Data supports the idea of higher temperature fluids preserving more radiogenic values (Vulcan core sample is highlighted in blue).

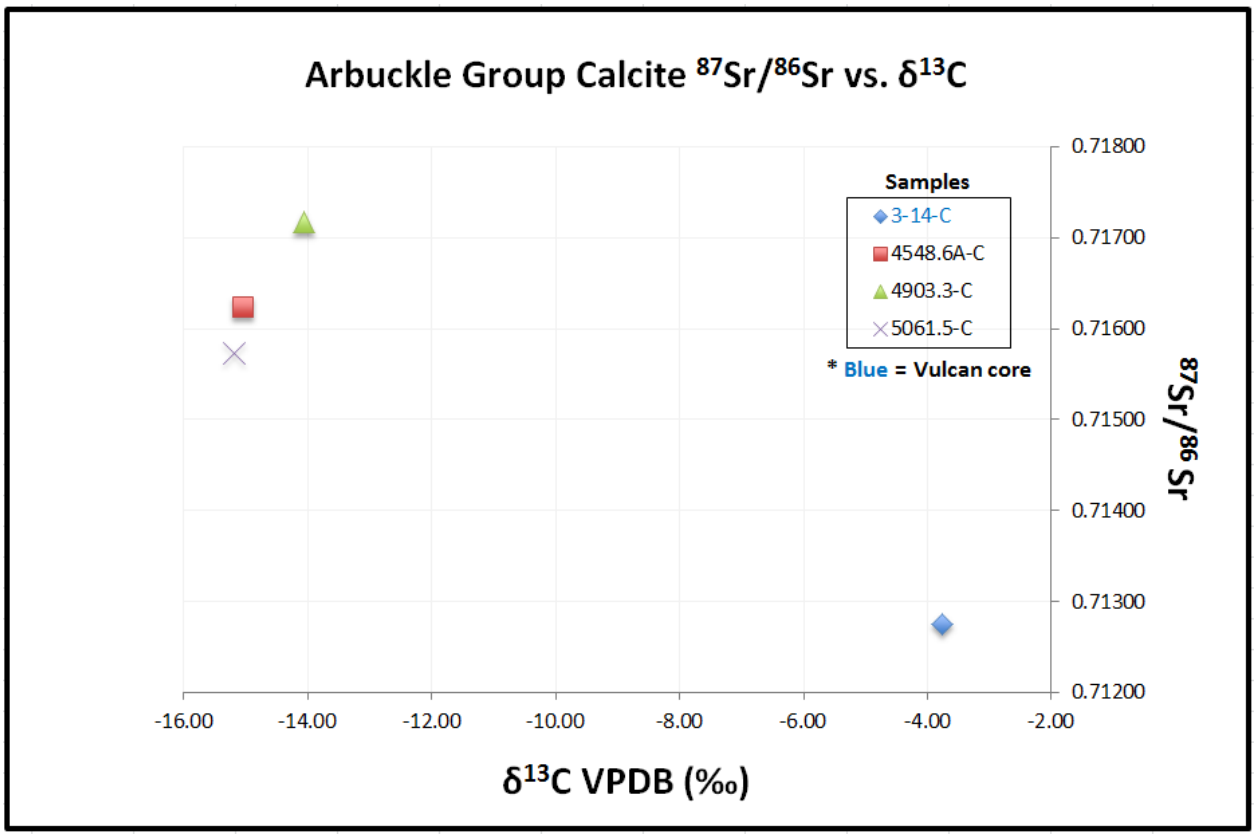


**Figure 2.47:** Cross-plot of $^{87}Sr/^{86}Sr$ versus $\delta^{13}C$ values of Arbuckle Group calcite. Plot displays more radiogenic values correlating with more depleted $\delta^{13}C$ values. The plot also displays the difference in $\delta^{13}C$ values between the Wellington 1-32 and Vulcan cores (Vulcan core sample is highlighted in blue).

## 9. Discussion

### *9.1. Porosity evolution and fluid flow conduits*

Porosity of the Arbuckle Group has been significantly altered by early and late diagenetic events (see Paragenesis section and Fig. 2.4), producing a variety of secondary pore types dominated by vugs, caverns, and fractures. Still, primary porosity has been preserved within the section in some instances, mostly in the form of fenestral and interparticle porosity (e.g. Franseen et al. 2004). Early replacement dolomite (event 2-3-4) appears to have decreased overall porosity, replacing existing carbonate sediment and reducing interparticle pores. Early

dissolution events, likely due to intraformational sea-level oscillations, temporarily enhanced porosity and created vugs and caverns (Franseen et al., 2004; Ross and Ross, 1988). These early dissolution features appear to have created preferential fluid flow conduits for fluids responsible for subsequent precipitation of cements and are reduced with early and late diagenetic cements. Primary and secondary porosity, as well as extensive brecciation, in the lower Arbuckle Group represents a zone of high porosity and permeability. At the culmination of Arbuckle Group deposition, a regionally extensive subaerial exposure event during Middle Ordovician time led to extensive erosion, karsting, and collapse breccias (Franseen et al., 2004; Simo and Smith, 1997; Gao and Land, 1991; Gao et al., 1995; Kerans, 1988; Kupecz and Land, 1991; Montanez and Read, 1992); this exposure event produced a substantial increase in porosity and is recognized as vugs, caverns, and brecciated fabrics that are most prevalent in the upper portions of the unit. Pores associated with this event are commonly reduced with middle to late diagenetic cements, and likely acted as enhanced fluid flow conduits for the fluids that precipitated those cements.

Following the major subaerial exposure event, burial resulted in compaction and stylolitization. Though stylolitization produced a decrease in porosity, fractures emanating from stylolites temporarily enhanced it. Fractures associated with stylolitization were largely filled with late diagenetic cements. Later fracturing likely associated with the Ouachita orogeny also temporarily enhanced porosity, but was subsequently reduced with late cements as well. The injection of hydrothermal fluids, responsible for late cementation, appears to have created some secondary porosity as evidenced by silica and carbonate dissolution, as well as vugs that are only filled with later cements. Existing primary and secondary porosity, including late fracturing, acted as excellent conduits for hydrothermal fluid flow throughout the unit, resulting in reduction of porosity by high-temperature cement precipitation. As discussed earlier, trends in $\delta^{18}O$ data

suggest fluid temperatures may have increased from the base to the top of the Arbuckle Group by as much as 37 °C, with the highest temperatures existing in the upper section of the unit (see Stable isotope interpretation sections 7.2 and 7.3). Scheffer (2012) found evidence for a modern low porosity/permeability zone in the middle of the Arbuckle Group that separates the upper Arbuckle Group fluids from the lower Arbuckle Group fluids. Baroque dolomite can be observed from the base to the top of the unit, but with more depleted $\delta^{18}O$ values at the top suggesting higher temperatures. This likely means the middle low porosity/permeability zone was not important at the time of fluid migration, and that a temperature-controlled density gradient, which may have also been influenced by enhanced fluid flow in the upper section of the unit, existed at the time of baroque dolomite precipitation. High-temperature and high-salinity, coupled with radiogenic $^{87}Sr/^{86}Sr$ and enriched $\delta^{18}O_{water}$ values, support a regional advective fluid flow system with fluids sourced from the nearby Anadarko basin.

Conversely, $\delta^{18}O$ data from calcite cements do not follow the same kind of depth-dependent trend. Assuming that the $\delta^{18}O$ range observed in calcite (-7.0 to -9.8‰) is the result of elevated temperature values that ranged between those of the inclusion values in the baroque dolomite (93.0-131.0 ºC) and secondary inclusions in calcite (70.0-89.9 ºC) data, temperatures remained too high to be accounted for by burial conditions or geothermal gradients during calcite precipitation. Highly radiogenic $^{87}Sr/^{86}Sr$ values suggest a different fluid source or migration pathway than fluids responsible for baroque dolomite precipitation. It is unlikely that the same system, with fluids being sourced from the Anadarko basin, would be able to produce the more radiogenic values without at least altering the migration pathway. Tectonic activity following the precipitation of baroque dolomite could have altered migration pathways by creating fluid-flow through newly created fracture networks. Fracturing in the study area could have altered

the connectivity between the Arbuckle Group and underlying stratigraphic units, possibly enabling interaction with radiogenic fluids present in the underlying Cambrian Reagan sandstone or basement rock. Though the Reagan sandstone is absent in the study area, the basal sand could have acted much like the Arbuckle Group for regional advective fluid flow of hydrothermal fluids out of the Anadarko basin, with later fracturing allowing for migration of fluids in underlying units into the overlying Arbuckle Group. It is also possible that the fluids responsible for calcite precipitation may have been sourced from basement rock, using fractures that connected the basement with overlying strata. If fluids responsible for calcite precipitation did use fracture networks as fluid conduits, then calcite precipitation could be expected to be an event controlled by structural deformation.

### *9.2. Hydrothermal fluids*

The late-stage mineral assemblage of the Arbuckle Group, including megaquartz, baroque dolomite, calcite, galena, and sphalerite, is similar to MVT deposits believed by most to be the result of basin-derived hydrothermal fluids (Young, 2010; Leach and Sangster, 1995; Garven, 1993; Wojcik et al., 1992; Bethke and Marshak, 1990; Garven and Freeze, 1984a; 1984b; Leach and Rowan, 1986; Sverjensky, 1986; Oliver, 1986; Cathles and Smith, 1983). Moreover, overlying units in the study area have been interpreted as being modified by multiple migration events of hydrothermal fluids sourced from nearby basins (Wojcik et al., 1992; Young, 2010). The existence of basin-derived hydrothermal fluid flow within the Arbuckle Group has been methodically established through petrographic observations, fluid inclusion analysis, and geochemical data (see Fluid inclusion discussion section 6.7. and Stable isotope interpretation sections 7.1. and 7.2.).

The presence of baroque dolomite, with a xenotopic-C texture, is in itself an indicator of elevated temperatures during cement precipitation (Davies and Smith, 2006; Gregg and Sibley, 1984; Radke and Mathis, 1980). Fluid inclusion analysis produced elevated homogenization temperatures in late diagenetic cements (≥87ºC for megaquartz and as high as 131°C for baroque dolomite). Depleted $\delta^{18}O$ values recorded in baroque dolomite and calcite cement also suggest thermal fractionation that resulted from high temperatures commonly associated with heating of basin-derived brines (Davies and Smith, 2006). According to Newell (1997), a burial history model using a reasonable geothermal gradient and Cretaceous thickness values would produce a maximum formation temperature of around 74ºC during Permian time in counties just outside the study area; this value is 20°C below Th values measured in late megaquartz cement and nearly 50°C below Th values measured in baroque dolomite. Newell (1997) also explored the possibility of both higher geothermal gradients and Cretaceous thicknesses than were thought to be geologically reasonable. Even with the unreasonably high values, temperature estimates remain approximately 20-30ºC lower than Th values observed in baroque dolomite. Moreover, Th values and $\delta^{18}O$ data recorded in baroque dolomite support multiple pulses of hydrothermal fluids during precipitation; fluctuations in burial depth or geothermal gradient cannot reasonably account for short-term pulses in reservoir temperature. More depleted $\delta^{18}O$ values near the top of the Arbuckle indicate the inverse of what would normally be expected for a normal burial system. During baroque dolomite precipitation, temperatures at the top of the Arbuckle were 37 ºC warmer than the base, evidence against a normal burial system and in favor of a hydrothermal system. In calcite cement, depleted $\delta^{18}O$ values also support thermal fractionation resulting from temperatures close to the same values that were recorded in fluid inclusion data from baroque dolomite (93.0-131.0°C) (Davies and Smith, 2006). The only reasonable explanation for

temperatures higher than can be modeled from burial, repeated rises and falls in temperature, and higher temperatures at the top of the Arbuckle is the pulsed injection of hydrothermal fluids.

### *9.3. Potential sources*

The nearby Anadarko basin would appear to be the most likely source for hydrothermal fluids in the study area, as has been suggested by others in the past (Gao and Land, 1991; Gao, 1990a; Musgrove and Banner, 1993). High salinities have commonly been attributed to reflux of evaporative brines into deeper portions of basins, and radiogenic $^{87}Sr/^{86}Sr$ values support the presence of basinal brines that have undergone extensive rock-water modification during contact with siliciclastic material or basement rock (Banner, 1995; Hanor, 1979). The Anadarko basin has been proven to contain the necessary siliciclastic strata to produce such fluid compositions (Johnson et al., 1988) and Permian-age evaporites are thought to be potential sources for reflux of highly saline fluids into deeper portions of mid-Continent basins (Wojcik et al., 1994; Young, 2010). Alternatively, evaporite dissolution either in the basin or along the migration pathway may have also played an important role in producing the high salinity fluids; Silurian evaporites, or rift-salts in the Anadarko basin associated with Cambrian tectonic activity, are potential candidates. Thermal studies of the Anadarko basin have proven that substantial heating of such fluids could easily be attained through burial heating, producing temperatures ranging from 175-220°C at the top of the Arbuckle Group in the deepest portions of the basin (Gallardo and Blackwell, 1999); these conditions would provide the necessary environment for generation of hydrothermal brines. Additionally, the presence of hydrocarbon fluid inclusions within baroque dolomite further supports the idea that fluids were sourced from the Anadarko basin because

hydrocarbons present in the Arbuckle Group are thought to have been primarily sourced from the nearby basin (Price, 1980).

Whereas fluids from the Anadarko basin would appear to account for the majority of the characteristics observed in the late diagenetic fluids, the more radiogenic nature of calcite samples necessitates a change in source or migration pathway from time of baroque dolomite to calcite precipitation. As suggested in previous sections, an alternative source for such radiogenic fluids may be fluids migrating vertically out of underlying sand units or basement rock through fracture networks. Previous studies have shown evidence for Ouachita and Laramide tectonism reactivating basement faults, and extending them into overlying Paleozoic strata (Elebiju et al., 2011; Jorgensen et al., 1993; Tweto, 1980). Potential mechanisms for fluid flow are discussed in section 9.5.

### *9.4. Multiple migration events*

The geochemical characteristics of calcite and baroque dolomite have already been interpreted as requiring different fluid sources or migration pathways, clearly demanding more than one fluid migration event. In addition, microthermometric data observed in megaquartz (event 18) and baroque dolomite (event 19) also supply observations worthy of discussion when considering the potential for multiple migration events. Homogenization temperatures display fluctuations in temperature during baroque dolomite precipitation (Fig. 2.26), suggesting multiple pulses of hydrothermal fluids. Additionally, the introduction of a single fluid migration event would likely result in an increase in temperature with time (Young, 2010). Though this is supported by an increase in temperature from precipitation of megaquartz to baroque dolomite, the observed fluctuations in homogenization temperatures recorded in crystal transects in

baroque dolomite clearly conflicts with what would be characteristic of a single migration event. Moreover, numerous authors have been able to date multiple fluid migration events producing MVT deposits that are thought to be genetically linked to hydrothermal fluids responsible for late cementation (Table 2.1) (Brannon et al., 1996; Coveney et al., 2000; Blackburn et al., 2008). Also, $Tm_{ice}$ values produce salinities that increase from precipitation of megaquartz (3.1-6.0 wt. % NaCl eq.) to precipitation of baroque dolomite (16.3-20.4 wt. % NaCl eq.). It would be unlikely for a single fluid to increase by at least 10.0 wt. % NaCl eq. during a single migration event. Similar to the precipitation of calcite, either a different fluid source or migration pathway appears to be necessary for such an increase in salinity to occur. Multiple migration events of hydrothermal fluids, fluids that likely followed different migration pathways or were sourced from different areas, most adequately explain the mineralogy, fluid inclusion data, and geochemical data related to late-stage hydrothermal activity.

### *9.5. Hydrologic models*

Potential hypotheses regarding fluid flow mechanisms must account for multiple migration events of fluids sourced from areas that would produce high temperatures, variably high salinities, and radiogenic $^{87}Sr/^{86}Sr$ values, as well as the known tectonic and stratigraphic history of the study area. Previous authors have explored several hydrologic models that may account for regional fluid migration, including: (1) compaction-driven pore fluid flow and free convection, (2) tectonically controlled, episodic dewatering of basins and (3) gravity-driven fluid flow (Kupecz and Land, 1991; Garven, 1993; 1995; Garven and Freeze, 1984a; 1984b; Leach and Rowan, 1986; Bethke, 1986; Oliver, 1986; Cathles and Smith, 1983; Sharp, 1978; Dozy, 1970).

Hypothesis (1) is the least likely scenario, given that it involves relatively slow fluid flow and is not thought to be capable of the heating necessary to produce observed fluid inclusion temperatures or the volume of fluid needed for regionally extensive deposits (Garven, 1993; Kupecz and Land, 1991; Bethke, 1986).

For hypothesis (2), tectonically controlled, episodic dewatering of multiple zones in basins is thought to be capable of expelling hot fluids (Kupecz and Land, 1991; Oliver, 1986; Cathles and Smith, 1983; Sharp, 1978), but it is also believed to produce too little fluid volume to account for high homogenization temperatures in regionally extensive hydrothermal deposits (Garven, 1993; Leach and Rowan, 1986). This limitation conflicts with the alleged regional extent of late-stage hydrothermal cements. Even so, hypothesis (2) could account for migration of hydrothermal fluids if combined with faulting occurring at increasingly deeper intervals of the Anadarko basin as time progressed. Young (2010) proposed that initial stages of orogenic activity associated with the Ouachita orogeny may have caused relatively shallow faulting of Arkoma basin strata, resulting in the earliest migration of hydrothermal fluids into Mississippian strata near the study area. If a similar process was invoked for the Arbuckle Group, the initial stage of hydrothermal activity (low-salinity megaquartz cement) could have been caused by shallow faulting in the Anadarko basin during the Ouachita orogeny, releasing connate fluids lower in salinity and potentially cooler by being sourced from shallower levels in the basin. Young (2010) also proposed that deeper faulting occurred as tectonic activity progressed, tapping into deeper, and subsequently hotter, sections of the basin; this allowed discharge of refluxed Permian-age evaporitic fluids that are thought to be responsible for late-stage dolomite precipitation. If the same process is considered for late-stage dolomite precipitation in the Arbuckle Group, continued tectonic activity along the Ouachita orogenic belt would tap into

deeper portions of the Anadarko basin that had been recharged by highly saline fluids derived from Permian-age evaporation, allowing for subsequent precipitation of baroque dolomite from slightly hotter and more saline fluids. Alternatively, thrusting along the Ouachita orogenic belt could also produce multiple events of fluid migration if faulting evolved from thin-skinned to thick-skinned faulting, forcing fluids out of the basin in a type of "squeegee" effect (Young, 2010; Oliver, 1986). For calcite, the radiogenic Sr and differing compositions in different areas requires additions to the tectonic and fluid model. As discussed earlier, the underlying Reagan sandstone or basement rock may be the most likely source for the radiogenic Sr in calcite cements. Fracturing associated with either the Ouachita or Laramide orogeny could have provided conduits for high-temperature brines migrating into overlying strata from either underlying sandstone or basement rock. There was no direct evidence of fracturing that could be placed between baroque dolomite and calcite precipitation, leaving some uncertainty regarding this interpretation. Changing Sr chemistry for calcite precipitation would require a change in the overall fluid-flow system and driving force, but could still be related to tectonic activity, which supplies the needed fluid flow conduits. Both Ouachita and Laramide orogenies are thought to have produced strike-slip faulting, likely linked with reactivation of basement faults (Watney et al., 2013; Wharton, 2012; Elebiju et al., 2011; Watney et al., 2008; Ohlmacher and Berendsen, 2005; Jorgenson et al., 1993; Tweto 1980). Davies and Smith (2006) propose that this type of deformation could result in pumping of fluids from underlying strata, which could either be the Reagan sandstone or the basement in this case. Though orogenic activity could potentially explain initial fluid migration responsible for late-stage cements, volume restrictions would still likely rule this out as the sole source for hydrothermal fluids migrating through the Arbuckle Group.

Hypothesis (3), gravity-driven fluid flow resulting from uplift of adjacent mountains, could also account for basin-sourced hydrothermal fluids facilitating precipitation of late-stage cements (Garven and Freeze, 1984a; 1984b; Garven, 1993; 1995). Tectonic uplift during the Ouachita orogeny was associated with deepening of the Anadarko basin (Fig. 2.1B, 2.48) (Burgess, 1976; Ye et al., 1996; Gallardo and Blackwell, 1999). In this scenario, the Anadarko basin (source of heat) and the surrounding uplifts (hydraulic head source) would have set the stage for regional hydrothermal fluid migration across the study area; this is comparable to previous interpretations of regionally extensive hydrothermal deposition related to other midcontinent basins (Garven, 1995; 1993; 1985; Leach and Sangster, 1995; Leach and Rowan, 1986). This process could produce initial expulsion of relatively low salinity connate fluids from the basin during the precipitation of megaquartz 2. Ouachita deformation and uplift began before Permian reflux, and highly saline brines might not have been available until after the Permian. During the Permian, the hydrologic system of head in the mountains adjacent to a deep basin still existed. This system could have continued driving hydrothermal fluids northward during and after the Permian reflux, which may have charged the basin with the more saline brines observed during baroque dolomite precipitation. The heated fluids would have migrated laterally out of the basin through multiple carbonate aquifers (Mississippian as well as Cambrian-Ordovician Arbuckle Group) (Fig. 2.41) (Garven, 1995; 1993; Leach and Sangster, 1995; Leach and Rowan, 1986). Gravity-driven fluid flow requires a freshwater hydraulic head, and there is no direct evidence in late-stage Arbuckle Group cements that shows a decrease in salinity with time. The absence of evidence for decreasing salinity could mean that mixing of refluxed fluids and freshwater fluids occurred prior to or during fluid migration, causing salinities to actually be lower in the study area than they would have been without a freshwater source. On the other

hand, Shelton et al. (2009) found evidence for evaporated seawater as the only source for basinal brines responsible for late-stage dolomite occurrences related to MVT deposition. If the area of this study experienced a similar history of fluid flow to Shelton et al.'s (2009) study area, then gravity-driven fluid flow is only tenable if fluids responsible for late-stage dolomite represent the early stages of hydrothermal fluid flow, before break-through of meteoric waters. As will be discussed in Chapter 3, Mississippian calcite cement may show the influence of freshwater later in the paragenesis, supporting the hypothesis that gravity-driven fluid flow could have been an important driving force behind fluid migration. The gravity-driven hydrologic model can account for the initial low-salinity fluids (connate fluids) and later high salinity fluids (acquired from Permian evaporite reflux), positive $\delta^{18}O_{water}$ values (acquired from enrichment during evaporation process or through extensive rock-water interaction), radiogenic $^{87}Sr/^{86}Sr$ data (rock-water interaction with siliciclastics or basement), relatively high homogenization temperatures (basinal heating), and the widespread occurrence of baroque dolomite. Repeated deformation could have given rise to pulses of fluid flow. The radiogenic nature of calcite samples requires a different source or fluid migration pathway to account for later calcite precipitation. Obtaining more radiogenic values from the same basinal source during later precipitation seems unlikely.

Tectonically valved, gravity-driven fluid flow appears to be the most reasonable explanation for the migration of hydrothermal fluids into the study area. Gravity-driven fluids (related to the Ouachita orogeny), varying in flux associated with deformation events, were likely the driving forces behind migration of fluids out of the Anadarko basin and into the study area, producing late-stage precipitation of megaquartz and baroque dolomite. The migration of connate fluids responsible for megaquartz precipitation occurred prior to Permian reflux, likely some time in the Pennsylvanian (Fig. 2.48A). The fact that fluids responsible for megaquartz

precipitation recorded much lower salinities requires migration prior to the hypothesized reflux of evaporative Permian fluids. Either during or after Permian reflux (Fig. 2.48B), the migration of highly saline fluids responsible for baroque dolomite precipitation occurred (Fig. 2.48C). Lower salinity values in early baroque dolomite suggest fluid migration may have occurred during Early-Mid Permian time, with early reflux fluids potentially mixing with lower salinity connate fluids or fluids along the migration pathway. Precipitation of the highest salinity baroque dolomite may represent migration after the basin was completely flushed by refluxing fluids later in the Permian. Strike-slip faulting occurring after baroque dolomite precipitation in the study area may have pumped underlying fluids into overlying strata and allowed for vertical migration of high temperature and highly radiogenic fluids responsible for late-stage calcite precipitation (Fig. 2.49). The fact that calcite precipitates after baroque dolomite, and the fact that fluids responsible for baroque dolomite precipitation are hypothesized as being derived from Permian-age reflux, implies that the Ouachita orogeny may be an unlikely timing for the strike-slip faulting because, for the most part, Ouachita deformation ended by Early Permian time (Marshak et al., 2003; Kluth and Coney, 1981; Frezon and Dixon, 1975; Flawn, 1961). Coveney et al. (2000) summarized radiometric dates of multiple calcite cements in the Tri-State area that included 251±11Ma, 137±3Ma, 66±2Ma, and 39±2Ma (Brannon et al., 1996a; 1996b; Blasch and Coveney, 1988). 251±11Ma and 137±3Ma both appear to fall between the Ouachita and Laramide orogenies. If the calcite observed in the Arbuckle Group is related to these cements, it is possible that it may be related to Mesozoic rifting in the Gulf of Mexico. The two youngest dates (66±2Ma and 39±2Ma) coincide with the estimated timing of the Laramide orogeny (Coveney et al., 2000; Tweto, 1980). If the calcite observed in the Arbuckle Group is associated with the younger dates then strike-slip faulting or reactivation of basement faults during the

Laramide orogeny could be a plausible mechanism for fluid-flow. The potential for the late-stage calcite in the Arbuckle Group to be unrelated to the calcites addressed in Coveney et al. (2000) remains. Further research on the calcite cements is required to obtain a more complete understanding of the origin of the calcite.

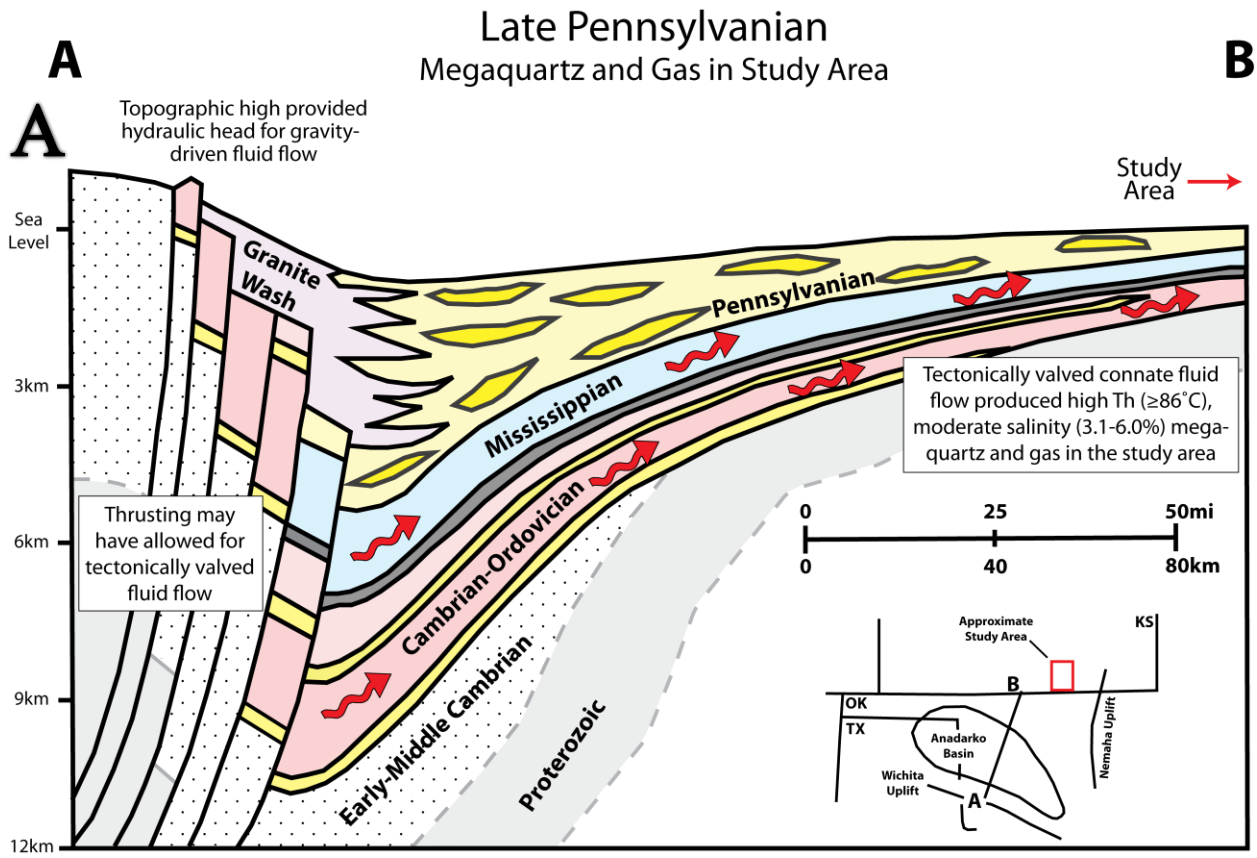

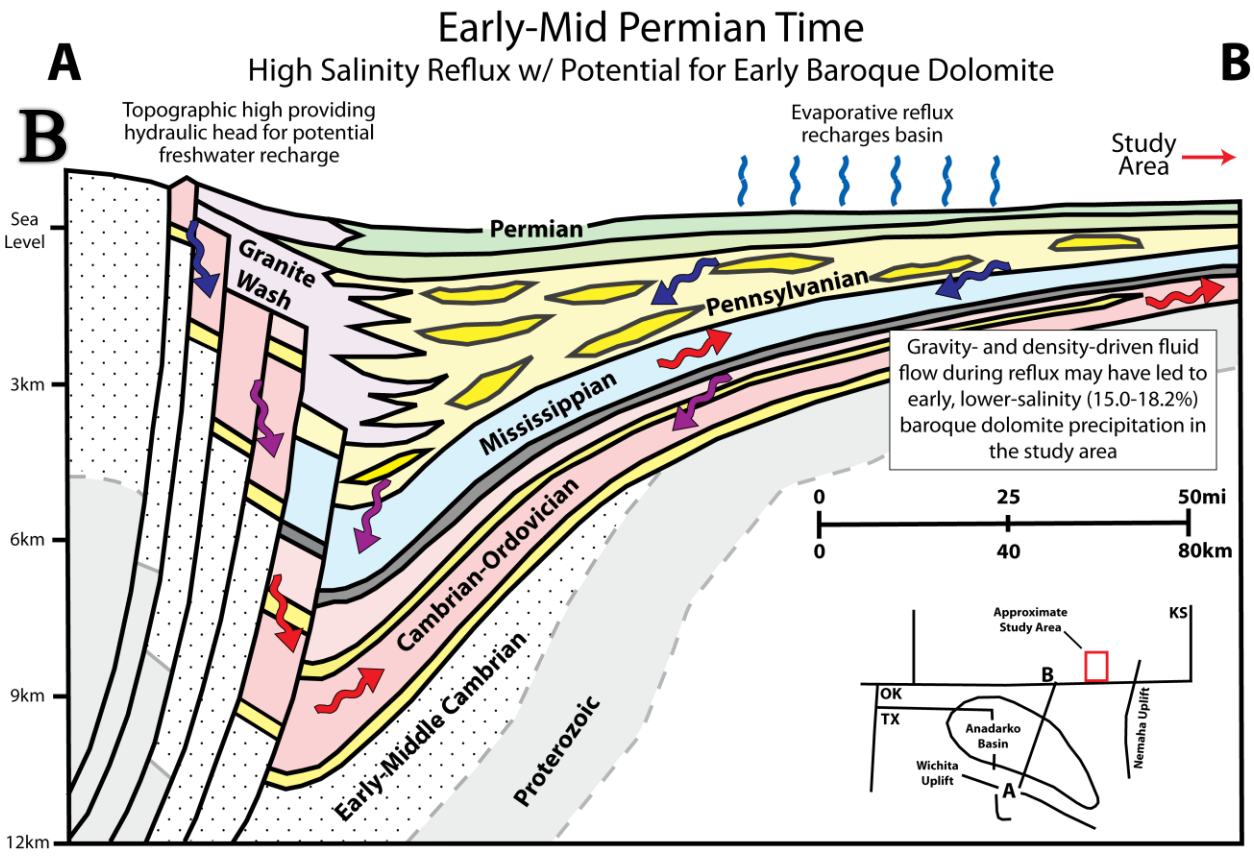
Early-Mid Permian Time
High Salinity Reflux w/ Potential for Early Baroque Dolomite
A
B
B
Topographic high providing hydraulic head for potential freshwater recharge
Evaporative reflux recharges basin
Study Area
Sea Level
3km
6km
9km
12km
Permian
Granite Wash
Pennsylvanian
Mississippian
Cambrian-Ordovician
Early-Middle Cambrian
Proterozoic
Gravity- and density-driven fluid flow during reflux may have led to early, lower-salinity (15.0-18.2%) baroque dolomite precipitation in the study area
0 25 50mi
0 40 80km
Approximate Study Area
KS
B
OK
TX
Anadarko Basin
Wichita Uplift
Nemaha Uplift
A

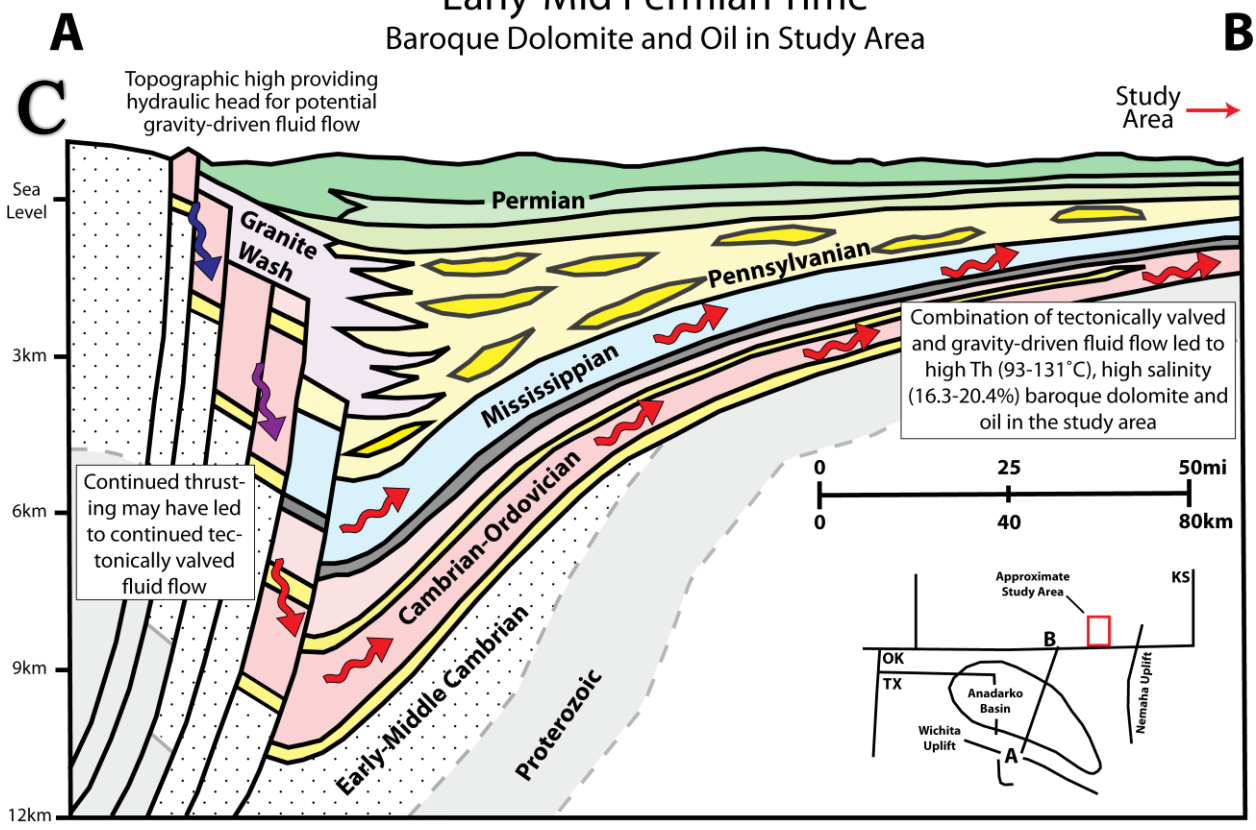
Early-Mid Permian Time
Baroque Dolomite and Oil in Study Area
A
B
C
Topographic high providing hydraulic head for potential gravity-driven fluid flow
Study Area
Sea Level
3km
6km
9km
12km
Permian
Granite Wash
Pennsylvanian
Mississippian
Cambrian-Ordovician
Early-Middle Cambrian
Proterozoic
Continued thrust-ing may have led to continued tec-tonically valved fluid flow
Combination of tectonically valved and gravity-driven fluid flow led to high Th (93-131˚C), high salinity (16.3-20.4%) baroque dolomite and oil in the study area
0 25 50mi
0 40 80km
Approximate Study Area
KS
B
OK
TX
Anadarko Basin
Wichita Uplift
Nemaha Uplift
A

**Figure 2.48:** (A) Initial expulsion of connate fluids from the Anadarko Basin strata may have occurred with the onset of orogenic activity related to the Ouachita orogeny during Late Pennsylvanian time. Tectonic activity could have tectonically valved fluids or provided a topographic high and set the scene for gravity-driven fluid flow out of the basin. This initial stage of fluid migration would have consisted of 3.1-6.0 wt. % NaCl equivalent connate fluids at temperatures ≥87°C, along with gas, migrating into the study area and precipitating megaquartz cement 2 (MQ2). (B) During Permian time, evaporitic conditions would have provided highly saline fluids refluxing through permeable strata and fractures associated with the earlier orogenic activity; this fluid could have actively recharged the basin with saline fluids. Besides tectonic valving and gravity-driven fluid flow, density-driven fluid flow may have played an active role in fluid migration as well, with high density fluids migrating downward and pushing out lower density fluids. (C) After Permian reflux, continued tectonic activity, gravity-driven fluid flow, or even density-driven fluid flow could have been the driving forces behind continued fluid migration out of the basin and into the study area during Permian time. This stage of fluid migration would have consisted of the 16.3-20.4 wt. % NaCl eq. fluid, ranging from 93-131°C, which was responsible for baroque dolomite (BD) precipitation and petroleum migration in the study area. Images modified from Gallardo and Blackwell (1999).

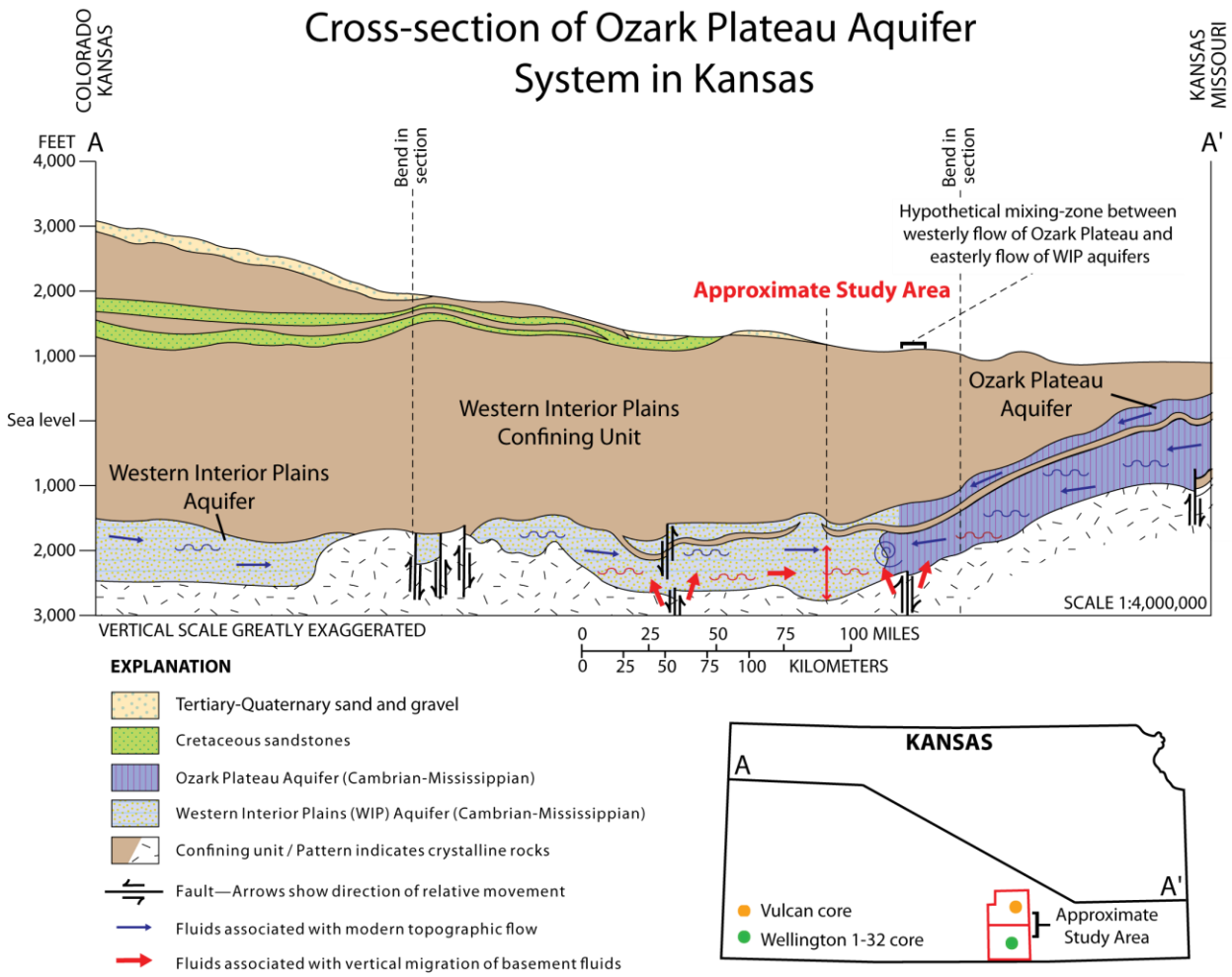

**Figure 2.49:** Cross-section of the Ozark Plateau aquifer system (OPAS), the Cambrian-Ordovician Arbuckle Group is the basal component of this system (Carr et al., 2005). Illustration depicts easterly flow associated with the OPAS throughout the majority of Kansas, as well as the potential mixing-zone between the WIP aquifer and westerly flow from the Ozark Plateau aquifer in the eastern part of the state (Carr et al., 2005). Following strike-slip faulting (hypothesized as occurring during Ouachita or Laramide tectonic activity), and extension of faults into overlying strata, high-temperature, highly radiogenic Reagan sandstone or basement fluids migrate along fractures into overlying strata (illustrated by red symbols). The proximity of specific areas to fractures may have resulted in enhanced fluid flow in areas directly affected by fracturing (Wellington 1-32 core in the case of this study), while areas located further from fractures would display lower temperatures and more rock-dominated isotopic values (Vulcan core in the case of this study). The injected fluids precipitated high-temperature, highly radiogenic calcite cement (CC) in the Arbuckle Group. Fluid flow associated with tectonic activity could mark the transition of an advective system with fluids sourced from the Anadarko Basin, to a fracture-controlled fluid flow system with fluids sourced from underlying sandstone or basement rock. Image is modified from Miller and Appel (1997).

### *9.6. Relationship to $CO_2$ sequestration*

The establishment of the porosity evolution and fluid migration history of the Arbuckle Group is supplementary to previous and current studies regarding the $CO_2$ sequestration potential of the Arbuckle Group. Though a more complete evaluation is provided in Chapter 3, several general deductions can be made from findings in the Arbuckle Group. Stratigraphic trapping, solubility trapping, capillary trapping, and mineral trapping enable $CO_2$ storage in underground geologic formations (Benson and Cole, 2008; Gunter et al., 1997). Overlying shale-rich units (Devonian and Pennsylvanian age) appear to provide the stratigraphic trap necessary, but further analysis of seal integrity is required (Chapter 3). Though the Arbuckle Group is considered to be under-pressured, pressure is high enough for sequestration of supercritical $CO_2$, confirming the potential for dissolution of $CO_2$ into the aquifer brine (3-11 wt. % NaCl Eq.) (Scheffer, 2012). Investigation of porosity evolution in this chapter has proven that, even with extensive early and late-stage cementation, considerable primary (fenestral and interparticle) and secondary (vugs

and fractures) porosity currently exists in the Arbuckle Group. Existing porosity in fractures should suggest potential for high permeability and effective migration of $CO_2$ following injection, but the fact that fractures typically appear isolated, relatively short, and facies-dependent indicates little potential for connectivity (Scheffer, 2012). Even so, high permeabilities are observed in the Arbuckle Group through primary and secondary porosity connectivity (Scheffer, 2012).

The initial phase of $CO_2$ injection could result in carbonate dissolution, assumedly resulting in substantial increases in porosity and permeability, allowing for even greater lateral migration of injected $CO_2$, but also causing concern for reservoir and overlying seal integrity (Scheffer, 2012; Gunter et al., 1997; Benson and Cole, 2008). Subsequent occurrences of mineral carbonation, despite taking a relatively long time to occur, are the most desired processes for $CO_2$ capture and storage (Scheffer, 2012; Oelkers et al., 2008; Benson and Cole, 2008). Scheffer (2012) found that current Arbuckle Group formation brines are saturated with respect to carbonate minerals, indicating potential for long-term storage via precipitation of calcite, dolomite, and magnesite (Oelkers et al., 2008; Metz et al., 2005). The common presence of pyrite also generates interest (Fig. 2.9A, 2.9B, 2.17D); when $CO_2$ is injected into units containing pyrite, gypsum is commonly precipitated (Scheffer, 2012). The effect of secondary mineral precipitation would successfully account for some of the injected $CO_2$, but would also fill pore space, potentially decreasing storage capacity (Scheffer, 2012; Gunter et al., 1997; Oelkers et al., 2008).

Scheffer's (2012) work also suggests that a modern day low porosity/permeability zone exists between fluids in the upper and middle to lower Arbuckle Group (Fig. 2.35, 2.36, 2.40, 2.41, 2.42), restricting vertical fluid flow within the unit and potentially creating an additional

seal, but also decreasing storage capacity unless $CO_2$ was injected into both zones. The results of this study provide evidence for an ancient fluid flow system that was dominated by advective fluid flow during Late Pennsylvanian and Permian time, and was possibly influenced by tectonic and gravity-driven processes associated with fracturing and uplift during the Ouachita orogeny. This system took advantage of primary and secondary porosity, precipitating late-stage megaquartz and baroque dolomite cement throughout the entire Arbuckle Group. Geochemical data trends illustrate the influence of a temperature-controlled density gradient that, along with enhanced fluid flow at the top of the unit, focused the hottest fluids toward the upper Arbuckle Group. Much more radiogenic $^{87}Sr/^{86}Sr$ values in subsequent calcite cement signify a change in fluid source and migration pathway. It is hypothesized that tectonic activity extended fractures from underlying sandstone or basement into the Arbuckle Group, allowing for migration of high-temperature, highly radiogenic fluids into the unit to cause calcite precipitation, presumably during the Late Cretaceous or Early Tertiary. Because calcite cement has been observed in vug porosity, in samples that span the entire length of the core, it appears that even though vertical fractures may have been the original conduits for these fluids, lateral migration emanating from these fractures is also likely.

Significantly lower temperatures and salinity of modern reservoir fluids imply the system is drastically different than what was present at the time of late-stage cement precipitation (Carr et al., 2005). The dependency of both of the interpreted fluid-flow systems on tectonic activity associated with major orogenies suggests that the ancient systems are no longer extant. It is more likely that these late-stage hydrothermal events were exceptional events, producing the late-stage cements and spikes in temperature and salinity. Thus, migration behavior of sequestered $CO_2$ would most adequately be modeled with the use of modern topographic

groundwater flow, with a focus on overlying seal integrity (Chapter 3). Modern fluids are primarily sourced from the Front Ranges of the Rocky Mountains to the west (Fig. 2.49) (Garven, 1993; Jorgensen et al., 1993; Musgrove and Banner, 1993; Miller and Appel, 1997; Macfarlane, 2000). There is also evidence of mixing with fluids sourced from the east, resulting from east-west flow associated with the topographic high of the Ozark Plateau, and northern flow of basinal fluids into southern Kansas due to thermal expansion (Fig. 2.49) (Garven, 1993; Jorgensen et al., 1993; Miller and Appel, 1997; Macfarlane, 2000; Carr et al., 2005; KGS, 2012). A more complete contribution to the ongoing study of $CO_2$ sequestration potential requires additional evaluation of overlying units; this is provided in Chapter 3.

## 10. Conclusions

The Arbuckle Group was originally deposited as shallow shelf carbonate strata with primary fenestral and interparticle porosity. A total of 22 diagenetic events altered the porosity and mineralogy of the unit, reducing and generating porosity in a series of dissolution and cementation events. Transmitted light, UV-epifluorescence, and cathodoluminescence display distinctive features within the Arbuckle Group mineral assemblage, enabling the generation of a paragenesis that can be separated into early- and late- stage diagenetic events, based on timing relative to compaction. Early diagenetic events primarily enhanced porosity, mainly due to pervasive karsting and brecciation associated with the regionally extensive post-Sauk subaerial exposure event at the end of Early Ordovician Arbuckle Group deposition. The Middle Ordovician post-Sauk subaerial exposure event created a porous, highly permeable interval in the upper Arbuckle Group. Porosity was reduced with middle- to late-stage cements, but then enhanced again by fracturing associated with late Paleozoic tectonic activity. At some point

after the commencement of fracturing, hydrothermal brines were injected into the unit, initially resulting in silica and carbonate dissolution, and then precipitation of late-stage cements. Though pore space throughout the Arbuckle Group appears to be lined with either early- or late-stage cements in every example, substantial primary and secondary porosity persists in the unit today.

Fluid inclusion analysis supplemented petrographic observations, displaying distinct differences between early and late stage cements. All-liquid aqueous fluid inclusions present in early dolomite cements, middle dolomite cements, and early megaquartz cement strongly suggest formation of inclusions at low-temperatures (<50ºC), and possibly from high salinities (20.6-25.6 wt. % NaCl eq.) suggesting interaction with evaporites. These characteristics coincide with occurrence early in the diagenetic history, either during Arbuckle Group deposition or during sea-level fluctuations post-dating marine inundation of the Sauk unconformity, when low-temperature and evaporative fluids would have been most likely to exist. Homogenization temperatures measured in late stage megaquartz cement (≥87ºC), baroque dolomite (93.0-131.0ºC), and calcite cement (70.5-89.8ºC) reveal entrapment temperatures higher than expected from elevated geothermal gradients or normal burial conditions, necessitating a hydrothermal influence during late-stage cementation. Lower salinities measured in late megaquartz cement (3.1-6.0 wt. % NaCl eq.) also mark the transition from early- to late-stage cementation, whereas an increase in salinity of subsequent baroque dolomite (16.3-20.4 wt. % NaCl eq.) and secondary inclusions in calcite cements (18.2-19.6 wt. % NaCl eq.) imply interaction with Permian-age evaporated fluids or evaporite dissolution within the Anadarko basin during the fluid migration history. Both high temperature and high salinities support a basinal or basement source for hydrothermal brines.

Geochemical data further support the migration of basin-derived hydrothermal fluids within Arbuckle Group strata. Depleted $\delta^{18}O_{\text{baroque dolomite and calcite}}$ values observed in baroque dolomite and calcite cement can be attributed to thermal fractionation produced from elevated fluid temperatures, whereas enrichment of $\delta^{18}O_{water}$ supports an origin as evaporative brines. $\delta^{18}O_{dolomite}$ values become more depleted with decreasing depth, supporting higher temperatures with decreasing depth in the Arbuckle Group, temperature-controlled density stratification, and possibly some preferential fluid flow in the upper Arbuckle Group. Slightly more depleted $\delta^{13}C$ values in the upper Arbuckle Group may record thermochemical sulfate reduction that could have persisted along with higher temperatures produced in the upper portion of the unit. Radiogenic $^{87}Sr/^{86}Sr$ values imply rock-water interaction with siliciclastics or basement, likely during migration through various stratigraphic sections of a sedimentary basin before migration into the study area or, in the case that fluids were basement derived, interaction with basement rock before vertical migration into overlying strata.

The most likely source for hydrothermal basinal brines responsible for late-stage megaquartz and baroque dolomite precipitation appears to be the Anadarko basin. The believed association of hydrocarbon production in the basin with hydrocarbons present in the Arbuckle Group of Kansas supports migration of fluids from the basin into the study area. The immense depth of the basin, especially Cambrian-Ordovician strata (approx. 9km (~29,500ft) in the deepest portions of basin), would easily provide the heat necessary for the most elevated homogenization temperatures (131ºC) and prevalent siliciclastic material within the basin could have caused the radiogenic $^{87}Sr/^{86}Sr$ values. Initial discharge of lower salinity (3.1-6.0 wt. % NaCl eq.) connate fluids would account for late megaquartz cement. Reflux of evaporative fluids generated during Permian time could have recharged the basin, accounting for discharge of

high salinity (16.3-20.4 wt. % NaCl eq.) fluids responsible for later precipitation of baroque dolomite and calcite cements.

A combination of tectonically valved and gravity-driven fluid flow most adequately accounts for the petrographic observations, fluid inclusion analysis, and geochemical data derived from megaquartz and baroque dolomite, especially when linked to the stratigraphic and tectonic history of the Anadarko basin and the study area. Though compaction due to overburden and tectonic activity may have played a role in the initial expulsion of low-salinity connate fluids, these forces would not have been able to produce the volume of fluid necessary for the regionally extensive nature of high temperature-high salinity baroque dolomite. Fracturing during the Ouachita orogeny would have allowed for tectonic valving of basin fluids, and uplifts would have provided a topographic high adjacent to the deep Anadarko basin, setting the stage for gravity-driven fluid flow. Migration likely began with fracturing of basinal strata, discharging connate fluids first, and then continued following reflux and recharge of evaporative fluids during Permian time.

The precipitation of calcite cement appears to mark a transition from an advective fluid-flow system, with fluids being sourced from the Anadarko basin, to a vertical fluid-flow system with fluids being sourced from the underlying Cambrian Reagan sandstone or the basement. $^{87}Sr/^{86}Sr$ values recorded in late calcite cement are much more radiogenic than the values observed in baroque dolomite, necessitating an alternative source or fluid migration pathway, and $\delta^{18}O$ values in calcite do not appear to be dependent on depth or the enhanced porosity zone at the top of the Arbuckle Group. Fracturing related to the Laramide orogeny may have reactivated fractures present in basement rock and extended those fractures into overlying strata,

providing the needed conduits for high temperature, highly radiogenic Reagan sandstone or basement fluids to migrate into the Arbuckle Group.

Observations of the Arbuckle Group support long-term sequestration of $CO_2$, especially through mineral formation and reaction with formation brines. Substantial porosity and permeability would allow for extensive migration of the $CO_2$ throughout the aquifer, providing widespread interaction and storage. Evaluation of seal integrity and connectivity with overlying units in the geologic past provides insight into potential leakage. Past hydrothermal migration of fluids appears to be related to tectonic events in the distant geologic past, and bear little relation to the current system of fluid flow. Elaboration on this topic, as well as characterization of the late mineral assemblage in overlying units, is provided in Chapter 3.

## References

Arne, D.C., 1992, Evidence from apatite fission-track analysis for regional Cretaceous cooling in the Ouachita mountain fold belt and Arkoma Basin of Arkansas: AAPG Bulletin, v. 76, p. 392-402.

Arne, D.C., Duddy, I.R., and Sangster, D.F., 1990, Thermochronologic constraints on ore formation at the Gays River Pb-Zn deposit Nova Scotia, Canada, from apatite fission track analysis: Canadian Journal of Earth Sciences, v. 27, p. 1013-1022.

Arthur, M.A., Anderson, T.F., Kaplan, I.R., Veizer, J., and Land, L.S., 1983, Stable isotopes in sedimentary geology: SEPM Short Course 10.

Bachtadse, V., Van der Voo, R., Haynes, F.M., and Kesler, S.E., 1987, Late Paleozoic

magnetism of mineralized and unmineralized Ordovician carbonates from East Tennessee: evidence for post-ore chemical event: Journal of Geophysical Research, v. 92, p. 14165-14176.

Bakker, R.J., 2008, AqSoVir software package fluids: Fluid Inclusion Laboratory Leoben, http://fluids.unileoben.ac.at

Banner, J.L., 1995, Application of the trace element and isotope geochemistry of strontium to studies of carbonate diagenesis: Sedimentology, v. 42, p. 805-824.

Banner, J.L., Hanson, G.N., and Meyers, W.J., 1988, Water-rock interaction history of regionally extensive dolomites of the Burlington-Keokuk Formation (Mississippian): Isotopic evidence: SEPM Special Publication, n. 43, p. 97-113.

Belitz, K. and Bredehoeft, J.D., 1988, Hydrodynamics of Denver Basin: Explanation of subnormal fluid pressures: AAPG Bulletin, v. 72, n. 11, p. 1334-1359.

Benson, S.M. and Cole, D.R., 2008, Carbon dioxide sequestration: $CO_2$ sequestration in deep sedimentary formations: Elements, v. 4, p. 325-331.

Bethke, C.M., 1986, Hydrologic constraints on the genesis of the upper Mississippi valley mineral district from Illinois Basin brines: Economic Geology, v. 81, n. 2, p. 233-249.

Bethke, C.M. and Marshak, S., 1990, Brine migrations across North America - The plate tectonics of groundwater: Annual Review of Earth and Planetary Sciences, v. 18, p. 287-315.

Blackburn, T.J., D.F. Stockli, R.W. Carlson, and P. Berendsen, 2008, (U-Th)/He dating of kimberlites-A case study from north-eastern Kansas: Earth and Planetary Science Letters, v. 275, p. 111-120.

Blasch, S.R. and Coveney, R.M., 1988, Goethite-bearing brine inclusions, petroleum inclusions, and the geochemical conditions of ore deposition at the Jumbo mine, Kansas: Geochimica et Cosmochimica Acta, v. 52, p. 1007-1017.

Bodnar, R.J., 1993, Revised equation and table for determining the freezing point depression of $H_20$-NaCl solutions: Geochimica et Cosmochimica Acta, v. 57, n. 3, p. 683-684.

Brannon, J.C., S.C. Cole, F.A. Podosek, V.M. Ragan, R.M. Jr. Coveney, M.W. Wallace, and A.J. Bradley, 1996a, Th-Pb and U-Pb dating of ore-stage calcite and Paleozoic fluid flow: Science, v. 271, p. 491-493.

Brannon, J.C., Podosek F.A., Cole, S.C., 1996b, Radiometric dating of Mississippi Valley-type ore deposits, in Sangster, E.D., ed., Carbonate-hosted lead-zinc deposit: SEG Special Publication, v. 4, p. 546-554.

Burgess, W.J., 1976, Geologic evolution of the mid-Continent and Gulf Coast areas – a plate tectonics view: Transactions-Gulf Coast Association of Geological Societies, v. 26, p. 132-143.

Burruss, R.C., 1991, Practical aspects of fluorescence microscopy of petroleum fluid inclusions, in Barker, C. E., and Kopp, O. C., eds., Luminescence Microscopy and Spectroscopy: Society of Economic Paleontologists and Mineralogists Short Course, v. 25, p. 1-7.

Cantrell, D. L., Swart, P. K., and Hagerty, R. M., 2004, Genesis and characterization of dolomite, Arab-D reservoir, Ghawar field, Saudi Arabia: GeoArabia, v. 9, no. 2, p. 1– 26.

Carr, T.R., Merriam D.C., and Bartley, J.D., 2005, Use of relational databases to evaluate regional petroleum accumulation, groundwater flow, and $CO_2$ sequestration potential in Kansas: AAPG Bulletin, v. 89, n. 12, p. 1607-1627.

Carter, L.S., Kelley, S.A., Blackwell, D.D., and Naesar, N.D., Heat flow and thermal history of the Anadarko Basin, Oklahoma: AAPG Bulletin, v. 82, n. 2, p. 291-316.

Cathles, L.M. and Smith, A.T., 1983, Thermal constraints on the formation of the Mississippi Valley-type lead-zinc deposits and their implications for episodic basin dewatering and deposit genesis: Economic Geology, v. 78, p. 983-1002.

Choquette, P.W. and Pray, L.C., 1970, Geologic nomenclature and classification of porosity in sedimentary carbonates: AAPG Bulletin, v. 54, n. 2, p. 207-250.

Coveney Jr., R.M., 1992, Evidence for expulsion of hydrothermal fluids and hydrocarbons in the Midcontinent during the Pennsylvanian, in K.S. Johnson and B.J. Cardott, eds., Source Rocks in the Southern Midcontinent, 1990 Symposium: Oklahoma Geological Survey Circular 93, p. 133-143.

Coveney Jr., R.M., Ragan, V.M., and Brannon, J.C., 2000, Temporal benchmarks for modeling Phanerozoic flow of basinal brines and hydrocarbons in the southern Midcontinent based on radiometrically dated calcite: Geology, v. 28, n. 9, p. 795-798.

Davies, G. R., and Smith, T., 2006, Structurally controlled hydrothermal dolomite reservoir facies: An overview: American Association of Petroleum Geologists Bulletin, v. 90, p. 1641– 1690.

Denison, R.E., Koepnick, R.B., Burke, W.H., and Hetherington, E.A., 1998, Construction of the Cambrian and Ordovician seawater $^{87}Sr/^{86}Sr$ curve: Chemical Geology, v. 152, p. 325-340.

Dickson, J.A.D., 1965, A modified staining technique for carbonates in thin section: Nature, v. 205, p. 587.

Dozy, J.J., 1970, A geological model for the genesis of lead-zinc ores of the Mississippi valley, U.S.A.: Transactions-Applied Earth Science, v. 79, n. 765, p. B163-B170.

Elebiju, O.O., Matson, S., Keller, G.R., and Marfurt, K.J., 2011, Integrated geophysical studies of the basement structures, the Mississippian chert, and the Arbuckle Group of Osage County region, Oklahoma: American Association of Petroleum Geologists, v. 95, n. 3, p. 371-393.

Emery, D. and Robinson, A., 1993, Inorganic geochemistry: applications to petroleum Geology: Blackwell Scientific Publications.

Epstein, S. and Mayeda, T., 1953, Variation of $^{18}O$ content of waters from natural sources: Geochimica et Cosmochimica Acta, v. 4, p. 213-224.

Farr, M.R., 1989, Compositional zoning characteristics of late dolomite cement in the Cambrian Bonneterre Formation, Missouri, implications for parent fluid migration pathways: Carbonates and Evaporites, v. 4, n. 2, p. 177-194.

Folk, R.L., 1965, Some aspects of recrystallization in ancient limestones, in L.C. Pray and R.C. Murray, eds., Dolomitization and limestone diagenesis: a symposium: SEPM Special Publication 13, p. 14-48.

Franseen, E.K., Byrnes, A.P., Cansler, J., Steinhauff, D.M., and Carr, T.R., 2004, The Geology of Kansas -Arbuckle Group: Current Research in Earth Sciences, Kansas Geological Survey Bulletin 250, part 2, 43 p., http://www.kgs.ku.edu/Current/2004/franseen/franseen1.html.

Franseen, E.K., 2000, A review of Arbuckle Group strata in Kansas from a sedimentologic perspective: insights for future research from past and recent studies: The Compass, Journal of Earth Sciences Sigma Gamma Epsilon, v. 75, n. 2 and 3, p. 68-89.

Flawn, P.T., Goldstein, A. Jr., King, P.B., and Weaver, C.E., 1961, The Ouachita System: Bureau of Economic Geology, The University of Texas, Austin, Texas, p. 401.

Frezon, S.E. and Dixon, G.H., 1975, Texas panhandle and Oklahoma paleotectonic investigations of the Pennsylvanian system in the United States; Part I, Introduction and regional analyses of the Pennsylvanian System: U.S. Geological Survey Professional Paper, p. 177-195.

Gallardo, J. and Blackwell, D.D., 1999, Thermal structure of the Anadarko Basin: AAPG Bulletin, v. 83, n. 2, p. 333-361.

Gao, G., Land, L.S., and Elmore, R.D., 1995, Multiple episodes of dolomitization in the Arbuckle Group, Arbuckle Mountains, south-central Oklahoma: Field, petrographic, and geochemical evidence: Journal of Sedimentary Research, v. A65, n. 2, p. 321-331.

Gao, G. and Land, L.S., 1991, Early Ordovician Cool Creek Dolomite, middle Arbuckle Group, Slick Hills, SW Oklahoma, U.S.A.: origin and modification: Journal of Sedimentary Petrology, v. 61, n. 2, p. 161-173.

Gao, G., 1990a, Geochemical and isotopic constraints on the diagenetic history of a massive stratal, late Cambrian (Royer) dolomite, lower Arbuckle Group, Slick Hills, SW Oklahoma, USA: Geochimica et Cosmochimica Acta, v. 54, p. 1979-1989.

Garcia-Fresca, B., Lucia, F.J., Sharp Jr., J.M., and Kerans, C., 2012, Outcrop-constrained hydrogeological simulations of brine reflux and early dolomitization of the Permian San Andres Formation: AAPG Bulletin, v. 96, n. 9, p. 1757-1781.

Garven, G., 1995, Continental-scale groundwater flow and geologic processes: Annual Review of Earth and Planetary Sciences, v. 23, p. 89-117.

Garven, G., 1993, Genesis of stratabound ore deposits in the Midcontinent basins of North America; 1, the role of regional groundwater flow: The American Journal of Science, v.293, n. 6, p. 497-568.

Garven, G. and Freeze R.A., 1984a, Theoretical analysis of the role of groundwater flow in the genesis of stratabound ore deposit: 1 . Mathematical and numerical model: The American Journal of Science, v. 284, n. 10, p. 1085-1124.

Garven, G. and Freeze, R.A., 1984b, Theoretical analysis of the role of groundwater flow in the

genesis of stratabound ore deposits: 2. Quantitative results: The American Journal of Science, v. 284, n. 10, p. 1125-1174.

Gill, I.P., Moore, C.H., and Aharon, P., 1995, Evaporitic mixed-water dolomitization on St. Croix, USVI: Journal of Sedimentary Research, v. A65, p. 591-604.

Goldstein, R.H., (in press) Fluid inclusion geothermometry in sedimentary systems: from paleoclimate to hydrothermal *in* N. Harris (ed.) SEPM Special Publication, Thermal History Analysis of Sedimentary Basins.

Goldstein, R.H., 1991, Practical aspects of cement stratigraphy with illustrations from Pennsylvanian limestone and sandstone, New Mexico and Kansas, in Barker, C. E., and Kopp, O. C., eds., Luminescence Microscopy and Spectroscopy: Society of Economic Paleontologists and Mineralogists Short Course, v. 25, p. 123-132.

Goldstein, R.H. and Reynolds, T.J., 1994, Systematics of fluid inclusions in diagenetic minerals: SEPM Short Course 31.

Goldstein, R.H., 2003, Ch. 2: Petrographic analysis of fluid inclusions, in I. Samson, A. Anderson, and D. Marshall, eds., Fluid Inclusions: Analysis and Interpretation, Mineralogical Association of Canada Short Course 32, p. 9-53.

Gregg, J.M, 1985, Regional epigenetic dolomitization in the Bonneterre Dolomite (Cambrian), southeastern Missouri: Geology, vol. 13, p. 503-506.

Gregg, J.M. and Hagni, R.D., 1987, Irregular cathodoluminescent banding in late dolomite cements: Evidence for complex faceting and metalliferous brines: GSA Bulletin, v. 98, p. 86-91.

Gregg, J.M. and Shelton, K.L., 1989, Geochemical and petrographic evidence for fluid sources

and pathways during dolomitization and lead-zinc mineralization in southeast Missouri: A review: Carbonates and Evaporites, vol. 4, p. 153-175.

Gregg, J.M. and Sibley, D.F., 1984, Epigenetic dolomitization and the origin of xenotopic dolomite texture: Journal of Sedimentary Petrology, v. 54, n. 3, p. 908-931.

Gunter, W.D., Wiwchar, B., and Perkins, E.H., 1997, Aquifer storage of CO2-rich greenhouse gases: extension of the time scale of experiment for CO2-sequestering reactions by geochemical modeling: Mineralogy and Petrology, v. 59, p. 121-140.

Hagni, R.D. and Grawe, O.R., 1964, Mineral paragenesis in the Tri-state district Missouri, Kansas, Oklahoma: Economic Geology, v. 59, p. 449.457.

Hanor, J.S., 1979, The sedimentary genesis of hydrothermal fluids: Geochemistry of Hydrothermal Ore Deposits, 2nd edition, 137-172.

Harris, L.D., 1973, Dolomitization model for upper Cambrian and lower Ordovician carbonate rocks in the eastern United States: U.S. Geological Survey, Journal of Research, v. 1, p. 63-78.

Heimstra, E.J., 2003, The diagenesis and fluid migration history of the Indian Basin field, Eddy County, New Mexico: University of Kansas Master's Thesis, p. 1-359.

Johnson, K.S., Amsden, T.W., Denison, R.E., Dutton, S.P., Goldstein, A.G., Rascoe, B., Sutherland, B.K., and Thompson, D.M., 1988, Southern Midcontinent region, in Sloss, L.L., ed., Sedimentary Cover – North American craton; U.S.: Boulder, Colorado, Geological Society of America, The Geology of North America, v. D-2, p. 307-359.

Jones, G.D. and Xiao, Y., 2005, Dolomitization, anhydrite cementation, and porosity evolution in a reflux system: Insights from reactive transport models: AAPG Bulletin, v. 89, n. 5, p. 577-601.

Jorgensen, D.G., Helgesen, J.O., and Imes, J.L., 1993, Regional aquifers in Kansas, Nebraska, and parts of Arkansas, Colorado, Missouri, New Mexico, Oklahoma, South Dakota, Texas, and Wyoming – Geohydrologic framework: U.S. Geological Survey Professional Paper, v. 1414-B, p. 1-68.

Kansas Geological Survey (KGS), 2012, South-Central Kansas $CO_2$ Project, http://www.kgs.ku.edu/PRS/Ozark/Reports/Activities/2012_04_09.html.

Kerans, C., 1988, Karst-controlled reservoir heterogeneity in Ellenburger Group carbonates of West Texas: The American Association of Petroleum Geologists Bulletin, v. 72, n. 10, p. 1160-1183.

Kluth, C.F. and Coney, P.J., 1981, Plate tectonics of the Ancestral Rocky Mountains: Geology, v. 9, p. 10-15.

Kupecz, J.A. and Land, L.S., 1991, Late-stage dolomitization of the Lower Ordovician Ellenburger Group, West Texas: Journal of Sedimentary Petrology, v. 61, n. 4, p. 551-574.

Land, L.S., 1985, The origin of massive dolomite: Journal of Geological Education, v. 33, n. 2, p. 112-125.

Land, L.S., 1983, The application of stable isotopes to studies of the origin of dolomite and to problems of diagenesis of clastic sediments, in Arthur, M.A., ed., Stable isotopes in sedimentary geology: SEPM Short Course, n. 10, p. 4-1 – 4-21.

Land, L.S., 1980, The isotopic and trace element geochemistry of dolomite: The state of the art: SEPM Special Publication, n. 28, p. 87-110.

Land, L.S., Macpherson, G.L., and Mack, L.E., 1988, The geochemistry of saline formation

waters, Miocene, offshore Louisiana: Transactions-Gulf Coast Association of Geological Societies, v. 38, p. 503-511.

Lange, S., Chaudhuri, S., and Clauer, N., 1983, Strontium isotopic evidence for the origin of barites and sulfides from the Mississippi Valley-type ore deposits in southeast Missouri: Economic Geology, v. 78, p. 1255-1261.

Leach, D.L. and Rowan, E.L., 1986, Genetic link between Ouachita foldbelt tectonism and the Mississippi valley-type lead-zinc deposits of the Ozarks: Geology, v. 14, no. 11, p. 931-935.

Leach, D.L. and Sangster, D.F., 1995, Mississippi Valley-type lead-zinc deposits, in Kirkham, R.V., Sinclair, W.D.,Thorp, R.I., and Duke, J.M., eds., Mineral Deposit Modeling: Geological Association of Canada Special Paper 40, p. 289-314.

Leach D.L., Bradley, D., Lewchuk, M.T., Symons, D.T.A., Marsily, G., and Brannon, J., 2001, Mississippi Valey-type lead-zinc deposits through geological time: implications from recent age-dating research: Mineralium Deposita, v. 36, p. 711-740.

Lewchuk, M.T., and Symons, D.T.A., 1996, Paleomagnetism and Mississippi Valley-type ore genesis in the Ordovician Knox Supergroup of Central Tennessee, in Sangster, D.F., ed., Carbonate-hosted lead-zinc deposits: SEG Special Publication, v. 4, p. 567-576.

Lohmann, K.C., 1988, Geochemical patterns of meteoric diagenetic systems and their application to studies of paleokarst, in James, N.P. and Choquette, P.W., eds., Paleokarst, Ch. 2, p. 58-80.

Lohmann, K.C. and Walker, C.G., 1989, The $\delta^{18}O$ record of Phanerozoic abiotic marine calcite cements: Geophysical Research Letters, v. 16, n. 4, p. 319-322.

Luczaj, J.A., 2006, Evidence against the Dorag (mixing-zone) model for dolomitization along

the Wisconsin arch – A case for hydrothermal diagenesis: Introduction: America Association of Petroleum Geologists Bulletin, v. 90, p. 1719-1738.

Macfarlane, P.A., 2000, Revisions to the nomenclature for Kansas aquifers: Current Research in Earth Sciences, Kansas Geological Survey Bulletin 244, part 2. <http://www.kgs.ku.edu/Current/2000/macfarlane1.html>

Machel, H. G., 2004, Concepts and models of dolomitization: A critical reappraisal, in C. J. R. Braithwaite, G. Rizzi, and G. Darke, eds., The geometry and petrogenesis of dolomite hydrocarbon reservoirs: Geological Society (London) Special Publication 235, p. 7–63.

Machel, H.G., 2001, Bacterial and thermochemical sulfate reduction in diagenetic settings - old and new insights: Sedimentary Geology, v. 140, p. 143-175.

Machel, H.G., 1999, Effects of groundwater flow on mineral diagenesis, with emphasis on carbonate aquifers: Hydrogeology Journal, v. 7, p. 94-107.

Machel, H.G., 1987, Saddle dolomite as a by-product of chemical compaction and thermochemical sulfate reduction: Geology, v. 15, p. 936-940.

Machel, H.G. and Burton, E.A., 1991, Factors governing Cathodoluminescence in calcite and dolomite, and their implications for studies of carbonate diagenesis, in Barker, C. E., and Kopp, O. C., eds., Luminescence Microscopy and Spectroscopy: Society of Economic Paleontologists and Mineralogists Short Course, v. 25, p. 37-57.

Machel, H.G., Mason, R.A., Mariano, A.N., and Mucci, A., 1991, Causes and emission of luminescence in calcite and dolomite, in Barker, C. E., and Kopp, O. C., eds., Luminescence Microscopy and Spectroscopy: Society of Economic Paleontologists and Mineralogists Short Course, v. 25, p. 9-25.

Marshak, S., Nelson, W.J., and McBride, J.H., 2003, Phanerozoic strike-slip faulting in the continental

interior platform of the United States: Examples from the Laramide Orogen, midcontinent, and Ancestral Rocky Mountains: Geological Society Special Publication, v. 210, p. 159-184.

McConnell, D.A., Goydas, M.J., Smith, G.N., and Chitwood, J.P., 1990, Morphology of the frontal fault zone, southwest Oklahoma: Implications for deformation and deposition in the Wichita uplift and Anadarko Basin: Geology, v. 18, p. 634-637.

Merriam, D.F., 2005, Origin and development of plains-type folds in the mid-continent (United States) during the late Paleozoic: AAPG Bulletin, v. 89, n. 1, p. 101-118.

Merriam, D.F., 1963, The geologic history of Kansas: Kansas Geological Survey Bulletin, v. 162, http://www.kgs.ku.edu/Publications/Bulletins/162/10_app_g.html

Meyers, W.J., 1991, Calcite cement stratigraphy: an overview, in Barker, C. E., and Kopp, O. C., eds., Luminescence Microscopy and Spectroscopy: Society of Economic Paleontologists and Mineralogists Short Course, v. 25, p. 37-57.

Miller, J.A. and Appel, C.L., 1997, Groundwater atlas of the United States: Kansas, Missouri, Nebraska: United States Geological Survey, Hydrologic Atlas 730-D, http://pubs.usgs.gov/ha/ha730/ch_d/D-text.html.

Montanez, I.P., and Read, J.F., 1992, Fluid-rock interaction history during stabilization of early dolomites, upper Knox Group (Lower Ordovician), U.S. Appalachians: Journal of Sedimentary Petrology, v. 62, n. 5, p. 753-778.

Mountjoy, E.W., Machel, H.G., Green, D., Duggan, J., and Williams-Jones, A.E., 1999, Devonian matrix dolomites and deep burial carbonate cements: a comparison between the Rimbey Meadowbrook reef trend and the deep basin of west-central Alberta: Bulletin of Canadian Petroleum Geology, v. 47, p. 487-509.

Muchez, P., and Viaene, W., 1994, Dolomitization caused by water circulation near the mixing

zone: an example from the lower Viséan of the Campine Basin (Northern Belgium), in Purser, B., Tucker, M., and Zenger, D., eds., Dolomites – A Volume in Honor of Dolomieu: International Association of Sedimentologists Special Publication 21, p. 155-166.

Musgrove, M. and Banner, J.L., 1993, Regional ground-water mixing and the origin of saline fluids: Midcontinent, United States: Science, v. 259, p. 1877-1882.

Nakai, S., Halliday, A.N., Kesler, S.F., and Jones, H.D., 1990, Rb-Sr dating of sphalerites from Tennessee and the genesis of Mississippi Valley-type ore deposits: Nature, v. 346, p. 354-357.

Nakai, S., Halliday, A.N., Kesler, S.F., Jones, H.D., Kyle, J.R., and Lane, T.E., 1993, Rb-Sr dating of sphalerites from Mississippi Valley-type (MVT) ore deposits: Geochimica Cosmochimica Acta, v. 57, p. 417-427.

Newell, K.D., 1997, Comparison of maturation data and fluid inclusion homogenization temperatures to simple thermal models: Implications for thermal history and fluid flow in the Midcontinent: Current Research in Earth Sciences, Kansas Geological Survey Bulletin 240, part 2, p. 13-27, http://www.kgs.ku.edu/Current/1997/newell/newell1.html.

Oelkers, E.H., Gislason, S.R., and Matter, J., 2008, Mineral carbonation of $CO_2$: Elements, v. 4, p. 333-337.

Ohlmacher, G.S. and Berendsen, P., 2005, Kinematics, mechanics, and potential earthquake hazards for faults in Pottawatomie County, Kansas, USA: Tectonophysics, v. 396, p. 227-244.

Oliver, J., 1986, Fluids expelled tectonically from orogenic belts: Their role in hydrocarbon migration and other geologic phenomena: Geology, v. 14, p. 99-102.

O'Neil, J.R., Clayton, R.N., and Mayeda, T.K., 1969, Oxygen isotope fractionation in divalent metal carbonates: Journal of Chemical Physics, v. 51, n. 12, p. 5547-5558.

Pan, H., Symons, D.T.A., and Sangster, D.F., 1990, Paleomagnetism of Mississippi Valley-type ore and host rocks in the northern Arkansas and Tri-State districts: Canadian Journal of Earth Sciences, v. 27, p. 923-931.

Price, L., 1980, Shelf and shallow basin oil as related to hot-deep origin of petroleum; Journal of Petroleum Geology, v. 3, n. 1, p. 91-116.

Radke, B.M. and Mathis, R.L., 1980, On the formation and occurrence of saddle dolomite: Journal of Sedimentary Petrology, v. 50, n. 4, p. 1149-1168.

Ross, R.J. Jr., 1976, Ordovician sedimentation in the western United States; in, The Ordovician System: Proceedings of a Palaeontologic Association Symposium, Birmingham, September 1974, M.G. Bassett, ed.: University of Wales Press and Natural Museum of Wales, Cardiff, p. 73-106.

Ross, C.A. and Ross, J. R., 1988, Late Paleozoic transgressive-regressive deposition; in, Sea Level Changes - An Integrated Approach, C.K. Wilgus, B.S. Hastings, C.G. Kendall, H.W. Posamentier, C.A. Ross, and J.C. Van Wagoner, eds: Society of Economic Paleontologists and Mineralogists (SEPM) Special Publication, n. 42, p. 227-247.

Rossi, C., Goldstein, R.H., Ceriani, A., and Marfil, R., 2002, Fluid inclusions record thermal and fluid evolution in reservoir sandstones, Khatatba Formation, Western Desert, Egypt: A case for fluid injection: American Association of Petroleum Geologists Bulletin, v. 86, p. 1773-1799.

Scheffer, A., 2012, Geochemical and microbiological characterization of the Arbuckle saline

aquifer, a potential CO2 storage reservoir; Implications for hydraulic separation and caprock integrity: University of Kansas Master's Thesis, p. 1-88.

Scholle, P.A. and Ulmer-Scholle, D.S., 2003, A color guide to the petrography of carbonate rocks: grains, textures, porosity, diagenesis: AAPG Memoir 77, 474 p.

Sharp, J.M., 1978, Energy and momentum transport model of the Ouachita basin and its possible impact on formation of economic mineral deposits: Economic Geology, v. 73, p. 1057-1068.

Shelton, K.L., J.M. Reader, L.M. Ross, G.W. Viele, and D.E. Seidemann, 1986, Ba-rich adularia from the Ouachita Mountains, Arkansas: Implications for a post-collisional hydrothermal system: American Mineralogist, v. 71, p. 916-923.

Shelton, K.L., Gregg, J.M., and Johnson, A.W., 2009, Replacement dolomites and ore sulfides as recorders of multiple fluids and fluid sources in the Southeast Missouri Mississippi Valley-Type District: Halogen-$^{87}Sr/^{86}Sr$- $\delta^{18}O$-$\delta^{34}S$ Systematics in the Bonneterre Dolomite: Economic Geology, v. 104, p. 733-748.

Simo, G. L. and Smith, J. A., 1997, Carbonate diagenesis and dolomitization of the lower Ordovician Prairie du Chien Group: Geoscience Wisconsin, v. 16, p. 1-16.

Smith Jr., L. B. and Davies, G. D., 2006, Structurally controlled hydrothermal alteration of carbonate reservoirs: Introduction: American Association of Petroleum Geologists Bulletin, v. 90, p. 1635-1640.

Sverjensky, D.A., 1986, Genesis of Mississippi valley-type lead-zinc deposits: Annual Review of Earth and Planetary Sciences, vol. 14, p. 177-199.

Symons, D.T.A., Lewchuk, M., and Leach, D.L., 1998a, Age and duration of the Mississippi

Valley-type mineralizing fluid flow events in the Viburnum Trend, southeast Missouri, USA, from paleomagnetism: Geological Society Special Publications, v. 144, p. 27-39.

Symons, D.T.A. and Sangster D.F., 1991, Paleomagnetic age of the Central Missouri barite deposits and its genetic implications: Economic Geology, v. 86, p. 1-12.

Symons, D.T.A. and Stratakos, 2000, Palaeomagnetic dating of dolomitization and Mississippi Valley-type zinc mineralization in the Mascot-Jefferson City district of eastern Tennessee: a preliminary analysis, in Pueyo, J.J., Cardellach, E., Bitzer, K., and Taberner, C., eds., Proceedings of geofluids III; third international conference on fluid evolution, migration, and interaction in sedimentary basins and orogenic belts: Journal of Geochemical Exploration, v. 69-70, p. 373-376.

Tweto, Ogden, 1980, Summary of Laramide orogeny in Colorado, in Kent, H.C., and Porter, K.W., eds., Colorado geology: Rocky Mountain Association of Geologists Symposium on Colorado, p. 129-134.

Voss, R.L., Hagni, R.D., and Gregg, J.M., 1989, Sequential deposition of zoned dolomite and its relationship to sulfide mineral paragenetic sequence in the Vibernum Trend, southeast Missouri: Carbonates and Evaporites, v. 4, n. 2, p. 195-210.

Watney, W.L. and Bhattacharya, S., 2009, Modeling $CO_2$ sequestration in saline aquifer and depleted oil reservoir to evaluate regional $CO_2$ sequestration potential of Ozark Plateau Aquifer System, South-Central Kansas: DOE Grant Proposal 076248616.

Watney, W.L., Franseen, E.K., Byrnes, A.P., and Nissen, S.E., 2008, Contrasting styles and common controls on Middle Mississippian and Upper Pennsylvanian carbonate platforms in the Northern midcontinent, U.S.A.: in Lukasik, J., and Simo, A., eds., Controls on

Carbonate Platform and Reef Development, SEPM Special Publication 89, Society of Sedimentary Geology, Tulsa, p. 125-145.

Watney, W.L., Youle, J., Hedke, D., Gerlach, P., Sorenson, R., Dubois, M., Nicholson, L., Hansen, T., Koger, D., and Baker, R., 2013, Sedimentologic and stratigraphic effects of episodic structural activity during the Phanerozoic in the Hugoton Embayment, Kansas USA: AAPG Annual Meeting, Pittsburgh, PA.

Wharton, G.C., 2012, Transitional tectonics: Early Laramide strike-slip deformation of the northeastern Front Range, Colorado: University of Texas-Austin Master's Thesis, p. 1-122.

Wisniowiecki, M.J., Van der Voo, R., McCabe, C., and Kelly, W.C., 1983, A Pennsylvanian paleomagnetic pole from the mineralized Late Cambrian Bonneterre Formation, southeast Missouri: Journal of Geophysical Research, v. 88, p. 6540-6548.

Wojcik, K.M., M.E. McKibben, R.H. Goldstein, and A.W. Walton, 1992, Diagenesis, thermal history, and fluid migration, Middle and Upper Pennsylvanian rocks, southeastern Kansas: Oklahoma Geological Survey Circular, v. 93, p. 144-159.

Wojcik, K.M., Goldstein, R.H., and Walton, A.W., 1994, History of diagenetic fluids in a distant foreland area, Middle and Upper Pennsylvanian, Cherokee Basin, Kansas, USA: Fluid inclusion evidence: Geochimica et Cosmochimica Acta, v. 58, n. 3, p. 1175-1191.

Wojcik, K.M., R.H. Goldstein, and A.W. Walton, 1997, Regional and local controls of diagenesis driven by basin-wide flow system: Pennsylvanian sandstones and limestones, Cherokee basin, southeastern Kansas, in I.P. Montaneez, J.M. Gregg, and K.L. Shelton, eds., Basin-wide diagenetic patterns; integrated petrologic, geochemical, and hydrologic considerations: SEPM Special Publication No. 57, p. 235-252.

Ye, H., Royden, L., Burchfiel, C., and Schuepbach, M., 1996, Late Paleozoic deformation of interior North America: The Greater Ancestral Rocky Mountains: AAPG Bulletin, v. 80, n. 9, p. 1397-1492.

Young, E.M., 2010, Controls on reservoir character in carbonate-chert strata, Mississippian (Osagean-Meramecian), southeast Kansas: University of Kansas Master's Thesis, p. 1-207.

# Chapter 3

## Fluid Flow, Thermal History, and Diagenesis of Middle Ordovician Simpson Group to Middle Pennsylvanian Cherokee Group in South-Central Kansas


### Abstract

The Cambrian-Ordovician Arbuckle Group in south-central Kansas appears to qualify for successful sequestration of $CO_2$. Analysis of late-stage cements in this study provides insight into the ancient fluid-flow history of the stratigraphic interval from the Cambrian-Ordovician Arbuckle Group to the Middle Pennsylvanian Cherokee Group.

Similar late-stage mineral assemblages in the Arbuckle Group and overlying units of southern Kansas suggest genetically related fluids may have migrated through the entire stratigraphic interval at some time. Fluid inclusion microthermometric data derived from Middle Ordovician Simpson Group and Mississippian strata produce homogenization temperatures higher than can be explained by normal burial conditions or geothermal gradients. The record of inclusion salinities, which fall near the same range of values observed in the Arbuckle Group, illustrate an evolution of the fluid composition associated with hydrothermal fluid flow. Similar ranges of $\delta^{18}O$, $\delta^{13}C$, and $^{87}Sr/^{86}Sr$ data from the Middle Ordovician Simpson Group, Mississippian strata, and Middle Pennsylvanian Cherokee Group further supports a relation between fluids. Elevated homogenization temperatures, variable $Tm_{ice}$ values, depleted $\delta^{18}O_{dolomite\ and\ calcite}$, enriched $\delta^{18}O_{water}$, and radiogenic $^{87}Sr/^{86}Sr$ all point to the Anadarko basin as the origin of hydrothermal fluids, with regional advective fluid flow utilizing the entire stratigraphic interval as an aquifer system for such fluids, leading to warmer temperatures near the top of the aquifer. The Late Paleozoic Ouachita orogeny is the most likely mechanism capable of driving basinal fluids out of the basin and into platform deposits in south-central Kansas. More radiogenic $^{87}Sr/^{86}Sr$ values recorded from Arbuckle Group calcite support the

transition from an advective fluid-flow system to a fracture-controlled fluid system that allowed for fluids to migrate into the stratigraphic interval from either underlying sandstone or basement rock. The transition of the system toward normal burial temperatures may be preserved in healed microfractures in late-stage calcite in both Arbuckle Group and Mississippian calcite that record lower temperatures and high salinities.

Though the potential seals appear to have had a negligible impact on migration of fluids in the ancient, modern studies support integrity of the overlying seals today. Modern reservoir fluids are much cooler than diagenetic fluids preserved in hydrothermal cements and the salinity similarities that existed in the past are no longer extant. This suggests migration of injected $CO_2$ is best modeled using modern topographic groundwater flow, with continued investigation of potential seals.

## 1. Introduction and Purpose

The Cambrian-Ordovician Arbuckle Group is believed to qualify as a stable storage reservoir for sequestered carbon dioxide ($CO_2$) (Fig. 3.1) (Chapter 2 of this study; Scheffer, 2012; Watney and Bhattacharya, 2009). The overlying Middle Ordovician Simpson Group, Devonian-Mississippian Chattanooga Shale, and the Lower Mississippian Kinderhookian Stage are believed to be potential seals (Fig. 3.1; KGS, 2012). The Middle Pennsylvanian Cherokee Group and Permian evaporites also serve as potential seals (Fig. 3.1). An accurate assessment of the potential for geologic $CO_2$ storage in the Arbuckle Group requires a comprehensive study that evaluates the ability of fluids to migrate across potential seals via connected pore systems between the Arbuckle Group and overlying units. Chapter 2 focuses on the characteristics of the late-stage diagenetic events that have altered the Arbuckle Group, as well as the fluid migration

history responsible for such events. Similar characterization of the late-stage fluid migration history that has affected the overlying units will provide a basis for comparison between the reservoir and potential seals. This will facilitate an interpretation of seal integrity in the geologic past, which can then be applied to seal integrity predictions in the future. Hydrothermal fluid migration appears to have affected the study area (Chapter 2 of this study; Young, 2010; Wojcik et al., 1992; 1994; 1997), and similarities in late-stage mineral paragenesis, fluid inclusion microthermometric data, and geochemical data in stratigraphic units ranging from the Middle Ordovician Simpson Group to the Middle Pennsylvanian Cherokee Group, the Arbuckle Group, and MVT deposits support a potential connection in mechanisms behind regional fluid flow (Table 3.1; Garven, 1993; Leach and Sangster, 1995; Garven and Freeze, 1984a; 1984b; Leach and Rowan, 1986; Sverjensky, 1986; Oliver, 1986; Sharp, 1978; Cathles and Smith, 1983; Coveney et al. 2000).

Late-stage cements studied within Middle Ordovician Simpson Group, Mississippian strata, and Middle Pennsylvanian Cherokee Group have produced fluid inclusion and geochemical data similar to data derived from analysis of late-stage cements in the Arbuckle Group and nearby study areas (Chapter 2 of this study; Young, 2010; Wojcik, 1992; 1994; 1997). The Wellington 1-32 core provided the opportunity for core observations and petrographic analysis of the overlying units (Fig. 3.2). Data collection methods included transmitted-light, reflected light, and UV epifluorescence petrography, back-scattered electron microscopy (BSE), and fluid inclusion analysis. The above mentioned methods have been merged with carbon, oxygen, and strontium isotope analyses to aid in understanding the history of fluid flow in the stratigraphic interval spanning from the Middle Ordovician Simpson Group to the Middle Pennsylvanian Cherokee Group in southeast Kansas.

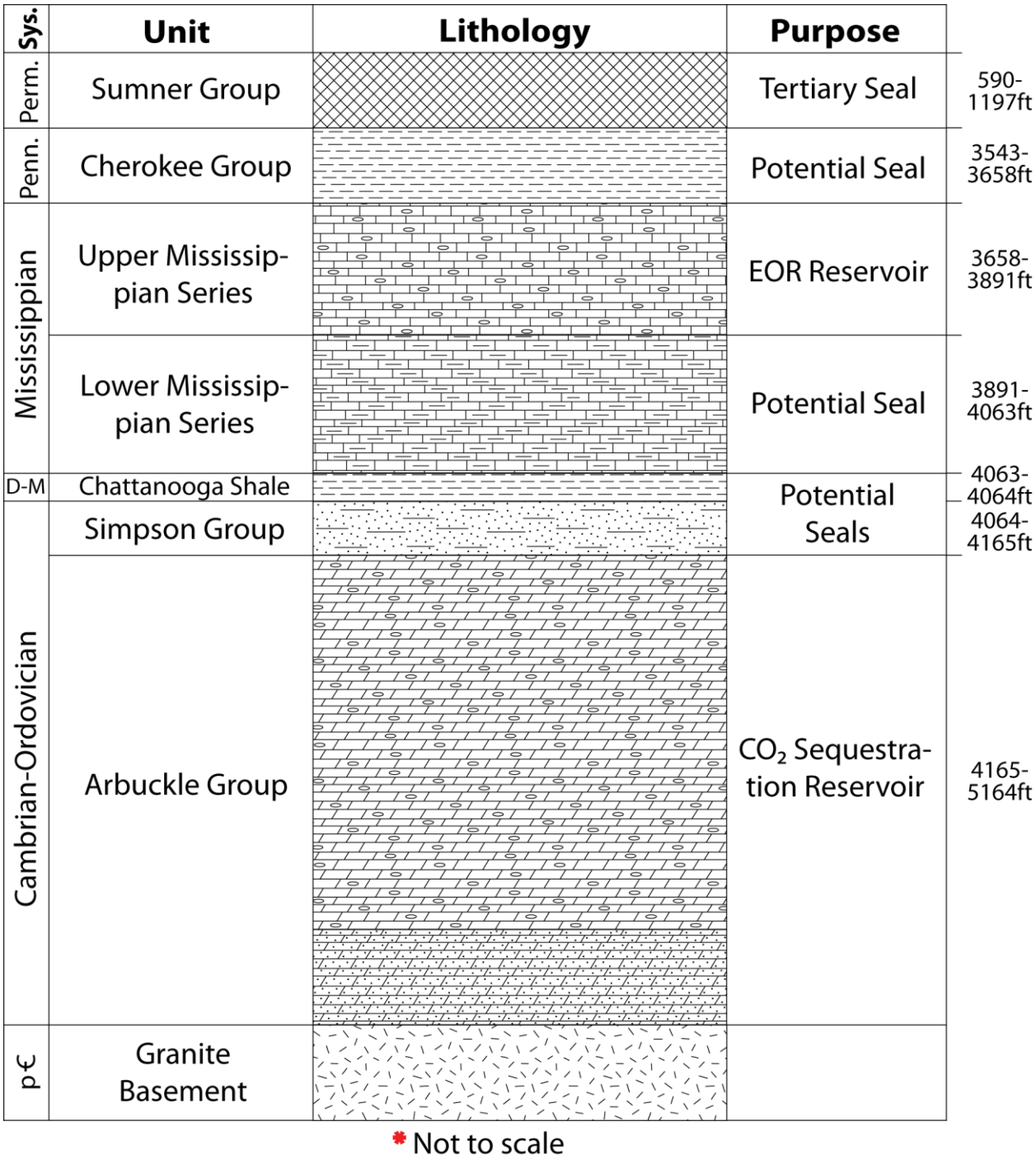


**Figure 3.1:** Stratigraphic section of Precambrian through Pennsylvanian strata, displaying units of note in this study and the larger-scale $CO_2$ sequestration project. Depth markers correlate with depths observed in the Wellington 1-32 core (based on Scheffer, 2012).

| Region of Study | Hydrothermal Fluid Flow Mechanism | Specific Driving Forces | Interpreted Age of Hydrothermal Deposit | Radiometric or Paleomagnetic Dates | Authors |
|---|---|---|---|---|---|
| SE Kansas | Late-Paleozoic Ouachita orogeny | Progressively deeper thrust faulting | Late Pennsylvanian-Early Permian | N/A | Young, 2010 |
| | Late-Paleozoic Ouachita orogeny | N/A | Late Pennsylvanian | N/A | Wojcik et al., 1992, 1994, 1997 |
| Tri-State | Late-Paleozoic to Late-Mesozoic tectonic activity | Expelled pore fluids or gravity-driven flow | Pennsylvanian-Late Cretaceous | 251±11 Ma; 137±3 Ma; 66±2 Ma; 39±2 Ma | Coveney et al., 2000 |
| | Late Paleozoic Alleghenian-Ouachita orogeny | Gravity-driven flow | Late Permian-Early Triassic | 251±11 Ma | Brannon et al., 1996b |
| | Late-Paleozoic Ouachita orogeny | N/A | >Late Jurassic | >183 Ma | Arne et al., 1992; Leach et al., 2001 |
| SE Missouri | Late-Paleozoic Alleghenian-Ouachita orogeny | N/A | Late Pennsylvanian-Early Permian | 286±20 Ma | Wisniowiecki et al., 1983; Leach et al., 2001 |
| | Late-Paleozoic Alleghenian-Ouachita orogeny | N/A | Early Permian | 273±10 Ma | Symons et al., 1998a; Leach et al., 2001 |
| | N/A | N/A | Late Permian-Eocene | 241±10 Ma; 203±10Ma; 100-50Ma | Arne et al., 1990; Leach et al., 2001 |
| | N/A | N/A | Devonian | 392±21 Ma | Lange et al., 1983; Leach et al., 2001 |
| North Arkansas | Late-Paleozoic Alleghenian-Ouachita orogeny | N/A | Permian | 265±20 | Pan et al., 1990; Leach et al., 2001 |
| Central Missouri | Late-Paleozoic Alleghenian orogeny | N/A | Pennsylvanian | 303±17 Ma | Symons and Sangster, 1991; Leach et al., 2001 |
| Central Tennessee | Late-Paleozoic Alleghenian orogeny | N/A | Late Permian-Early Triassic | 245±10 Ma | Lewchuck and Symons, 1996 |
| | Late-Paleozoic Alleghenian orogeny | Gravity-driven flow | Late Permian | 260±42 Ma | Brannon et al., 1996a |
| East Tennessee | Late-Paleozoic Alleghenian orogeny | N/A | Late Pennsylvanian-Early Permian | 286±20 Ma | Bachtadse et al., 1987; Leach et al., 2001 |
| | Late-Paleozoic Alleghenian orogeny | N/A | Pennsylvanian | 316±8 Ma | Symons and Stratakos, 2000 |
| | Middle-Paleozoic Acadian orogeny | Thrust faulting | Devonian | 377±29 Ma | Nakai et al., 1990; Leach et al., 2001 |
| | Middle-Paleozoic Acadian orogeny | Thrust faulting | Mississippian | 347±20 Ma | Nakai et al., 1990; 1993; Leach et al., 2001 |

**Table 3.1:** Table first lists the studies of overlying units in the study area (S Kansas). The table then lists study areas in the U.S. and the details of the hydrothermal system, including absolute ages of late-stage cements.

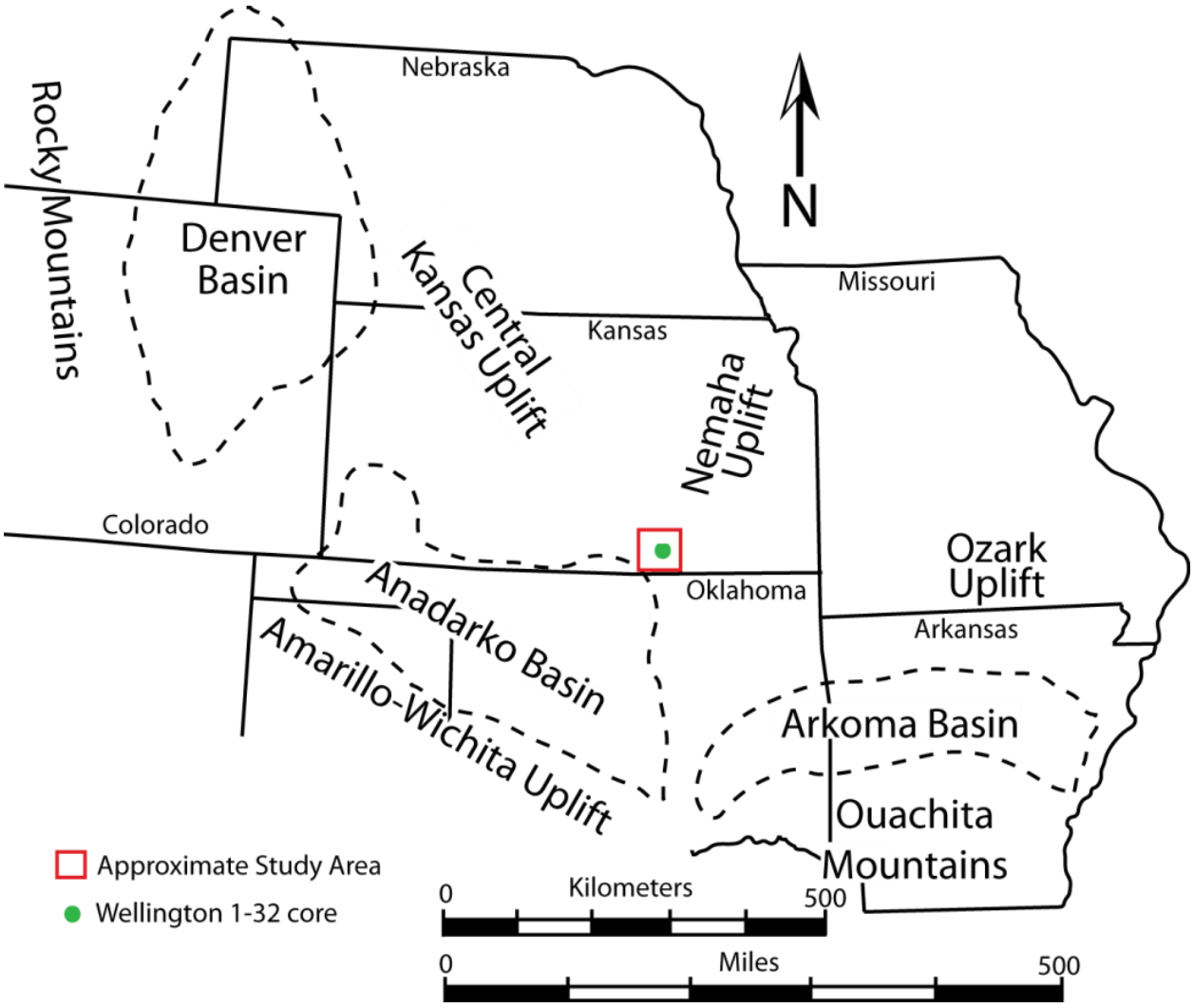


**Figure 3.2:** Regional map displaying location of approximate study area and Wellington 1-32 core. The general locations of notable basins and uplifts are noted as well. Modified from Garven (1993).

## 2. Stratigraphy and Late-stage Cements

All samples used for observations and collection of data were acquired from the Wellington 1-32 core. A total of 34 stratigraphic horizons were sampled and are listed in Appendix I.

### *2.1. Ordovician (Simpson Group)*

The Middle Ordovician Simpson Group unconformably overlies the Cambrian-Ordovician Arbuckle Group (Fig. 3.1). The Simpson Group is primarily a package of sandstone with smaller amounts of limestone, dolomite, and shale becoming more prevalent toward the top of the unit (KGS, 2012; Merriam, 1963; Zeller, 1968). The shale present in the Simpson Group is believed to represent a potential seal overlying the Arbuckle Group, likely being the first unit above the Arbuckle Group to hamper vertical migration of injected $CO_2$ (KGS, 2012). Though extensive erosion is believed to have removed portions of the Simpson Group in the state of Kansas (Merriam, 1963; Zeller, 1968), the unit maintains a thickness of approximately 100 feet in the Wellington 1-32 core (4,064-4,165ft subsurface). Megaquartz cement, interpreted as a late-stage diagenetic event, can be observed filling interparticle porosity as overgrowths on individual sandstone grains. Baroque dolomite cement, also interpreted as a late-stage diagenetic event, can be observed reducing primary porosity and lining fractures. Baroque dolomite was subjected to isotopic analysis and fluid inclusion analysis for comparison purposes with baroque dolomite present in the Arbuckle Group.

### *2.2. Devonian-Mississippian (Chattanooga Shale)*

The Devonian-Mississippian Chattanooga Shale unconformably rests on the Simpson Group and has been suggested as another seal for $CO_2$ storage (Fig. 3.1). The Chattanooga Shale is black to dark grey and can be silty, dolomitic and pyrite-rich (KGS, 2012; Scheffer, 2012; Zeller, 1968). The unit can be observed throughout most of eastern Kansas but varies widely in thickness, ranging from 0 to 250 feet (Zeller, 1968). The Chattanooga Shale is only 6 inches thick in the Wellington 1-32 core. Significant variability in thickness is clearly noted when compared to a thickness of approximately 50 feet observed in wire-line logs in the nearby

Wellington 1-28 log (~2/3 mile away) (Scheffer, 2012). Late-stage cements were not observed filling fractures and vugs within the small segment of the unit in the Wellington 1-32 core, eliminating the possibility of a direct comparison with the cements studied in the Arbuckle Group.

### *2.3. Mississippian*

Currently, Mississippian strata in the Wellington 1-32 core has only been separated into lower and upper stratigraphic intervals, primarily based on porosity and permeability. The lower Mississippian interval unconformably rests on the Chattanooga Shale and is identified as another potential seal (Fig. 3.1); this zone is approximately 170 feet thick in the Wellington 1-32 core (3,891-4,063ft subsurface). The lower Mississippian interval is primarily composed of cherty dolomite with variable abundance of shale and limestone (KGS, 2012; Zeller, 1968). Recognition as a potential seal is due to the overall tight nature of the Kinderhookian Stage, with an especially low-porosity segment present from 3,975-4,064ft (Scheffer, 2012; KGS, 2012). The upper Mississippian interval is primarily composed of limestone and dolomite, with minor amounts of sandstone, shale, and chert (KGS, 2012; Zeller, 1968); this zone is approximately 230 feet thick in the Wellington 1-32 core (3,658-3,891ft subsurface). The upper Mississippian interval is the oil-producing unit in the Wellington oilfield and is currently being examined for enhanced oil recovery via injection of $CO_2$ (Scheffer, 2012). Megaquartz cement, baroque dolomite, and calcite cements, all of which were interpreted as late-stage diagenetic events, can be observed reducing vugs and fractures in the lower and upper Mississippian intervals. Late-stage cements were subjected to isotopic analysis and fluid inclusion analysis for comparison purposes with cements in the Arbuckle Group.

### *2.4. Pennsylvanian (Cherokee Group)*

The Middle Pennsylvanian Cherokee Group was the only portion of Pennsylvanian strata preserved in the Wellington 1-32 core; this unit is approximately 115 feet thick (3,543-3,658ft subsurface). The Cherokee Group is identified as another seal in the $CO_2$ sequestration study of the Arbuckle Group and as a primary seal in the enhanced oil recovery project in the upper Mississippian interval (Fig. 3.1). The Cherokee Group in the Wellington 1-32 core includes the Cherokee Shale portion of the group and is primarily composed of paleosols, ranging from pale yellowish-brown massive chert to dark greenish-gray blocky mudstones (KGS, 2012; Scheffer, 2012). One example of calcite cement filling a fracture is the only late-stage cement observed in the Cherokee Group; this sample was analyzed for oxygen and carbon isotopes for comparison purposes. Additional comparison of late-stage diagenetic events to underlying units was aided by previous author's diagenetic work in the study area (Walton et al., 1995; Wojcik et al., 1992; 1994; 1997).

## 3. Late-stage Paragenesis

Although early diagenetic events have clearly affected overlying units in the study area, only diagenetic events that have been interpreted as occurring late in the paragenesis are addressed here. A late-stage interpretation was primarily based on the presence of cement as the latest cement in pore space. Within this study, the purpose of evaluating overlying units was for comparison with late-stage cements that were analyzed in the Arbuckle Group, as well as evaluating the degree of vertical connectivity between units. Late-stage cements are described for Middle Ordovician, Mississippian, and Pennsylvanian strata. Five events are believed to

have resulted from late-stage diagenesis in the Middle Ordovician Simpson Group. A total of nine events were described in Mississippian strata. The Pennsylvanian Cherokee Group in Wellington 1-32 displayed only two examples of what may be late-stage diagenetic events, but several more events are described with the aid of Wojcik et al. (1992; 1994; 1997) and Walton et al. (1995). Pore types are classified using Choquette and Pray (1970). Folk (1965) was used to describe calcite textures and Gregg and Sibley (1984) was used to describe dolomite textures. For each stratigraphic unit, the affect that each event has had on porosity is illustrated in Figure 3.3. Any percentages provided are visual estimates from the core and should be viewed with uncertainty.

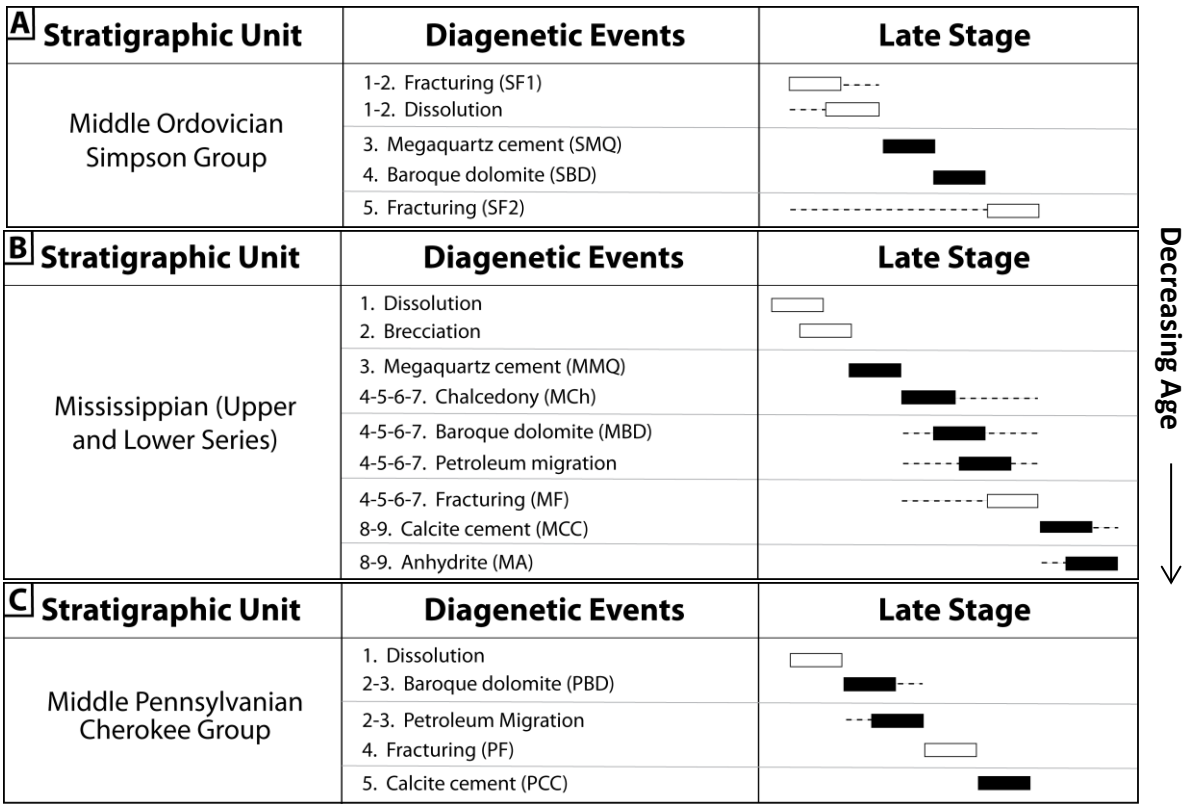


**Figure 3.3:** Images illustrate the established paragenesis for (A) Middle Ordovician Simpson Group, (B) Mississippian strata (Upper and Lower Series), and (C) Pennsylvanian strata. Open rectangles represent porosity enhancing events and filled rectangles represent events that decreased porosity. Dashed lines represent a degree of uncertainty associated with the relative timing of some events.

### *3.1. Ordovician (Simpson Group)*

*Event 1-2: Fracturing* – Fracturing (SF1) of Simpson Group strata can be observed as nearly vertical fractures cross-cutting entire samples. Fractures associated with this event appear to fracture around individual detrital quartz grains, without cutting across megaquartz cement (SMQ) overgrowths, suggesting fracturing occurred prior to precipitation of SMQ (Fig. 3.4A). SF1 appears to be reduced by baroque dolomite (event 3) (Fig. 3.4A), marking it as occurring prior to the precipitation of Simpson Group baroque dolomite (SBD). The exact relationship between fracturing and dissolution associated with event 1-2 is uncertain.

*Event 1-2: Carbonate dissolution* – Dissolution of carbonate strata appears to have occurred at some point prior to the precipitation of baroque dolomite (SBD), increasing porosity by <1%. This porosity is characterized by rare molds in sandstone and is almost always partially to fully occluded with SBD (Fig. 3.4B). The exact relationship of this event with the fracturing described in event 1 (SF1) is uncertain; fluids responsible for dissolving carbonate material may have used fractures as conduits, or the two events could be unrelated, with both acting as conduits for later fluid migration. Detrital quartz grains appear to be unaffected by the dissolution, supporting the idea of carbonate material being preferentially dissolved.

*Event 3: Megaquartz cement* – Megaquartz cement (SMQ) can be observed as overgrowths on detrital quartz grains, reducing interparticle porosity (Fig. 3.4C, 3.4B). Dust rims can be observed at the point where SMQ precipitates and the cement is in optical continuity with individual detrital quartz grains (Fig. 3.4B). Fracturing associated with SF1 appears to trace around individual grains without cutting across SMQ, implying precipitation of SMQ occurred after SF1 fracturing. SMQ appears to precipitate on individual grains into open pore space and fractures prior to baroque dolomite (SBD) precipitation, requiring cementation to have occurred

prior to precipitation of SBD. SMQ cement overgrowths appear to be cut across by fractures (SF2) that are thought to be the last diagenetic event observed in the Simpson Group (Fig. 3.4C).

*Event 4: Baroque dolomite* - Baroque dolomite (SBD) can be observed in the Simpson Group, reducing porosity by <1%. SBD can be found partially- to fully-occluding fractures and moldic porosity (Fig. 3.4A, 3.4B). SBD displays a xenotopic-C texture with pore- and fracture-lining, saddle-shaped crystals characterized by curved crystal terminations and sweeping extinction under crossed polars (Fig. 3.4A, 3.4B). SBD appears clear under transmitted light, with cloudy cores and bands represented by high abundance of fluid inclusions (Fig. 3.4A, 3.4B). This cement is non-fluorescent when exposed to UV-epifluorescence. Baroque dolomite can be observed filling fractures and molds related to events 1 and 2 and precipitating after the precipitation of megaquartz cement (SMQ) overgrowths, but is absent in fractures that potentially occurred later in the paragenesis, tentatively placing the cement between megaquartz cement (event 3) and later fracturing (event 5).

*Event 5: Fracturing* – Another fracturing event (SF2) can be observed as nearly vertical fractures cross-cutting entire samples and splintering detrital quartz grains and megaquartz overgrowths (Fig. 3.4C). SF2 occurs as empty fractures, appearing to cut across megaquartz cement (event 3), but lacking any relationship with baroque dolomite (event 4). The lack of baroque dolomite (SBD) suggests that the empty fractures occurred after SBD precipitation and are separate from fractures associated with SF1, though it is possible that SBD may have preferentially precipitated in some fractures instead of others for unknown reasons. If SF2 fractures are part of a separate fracturing event, it may be that these are the result of later deformation.

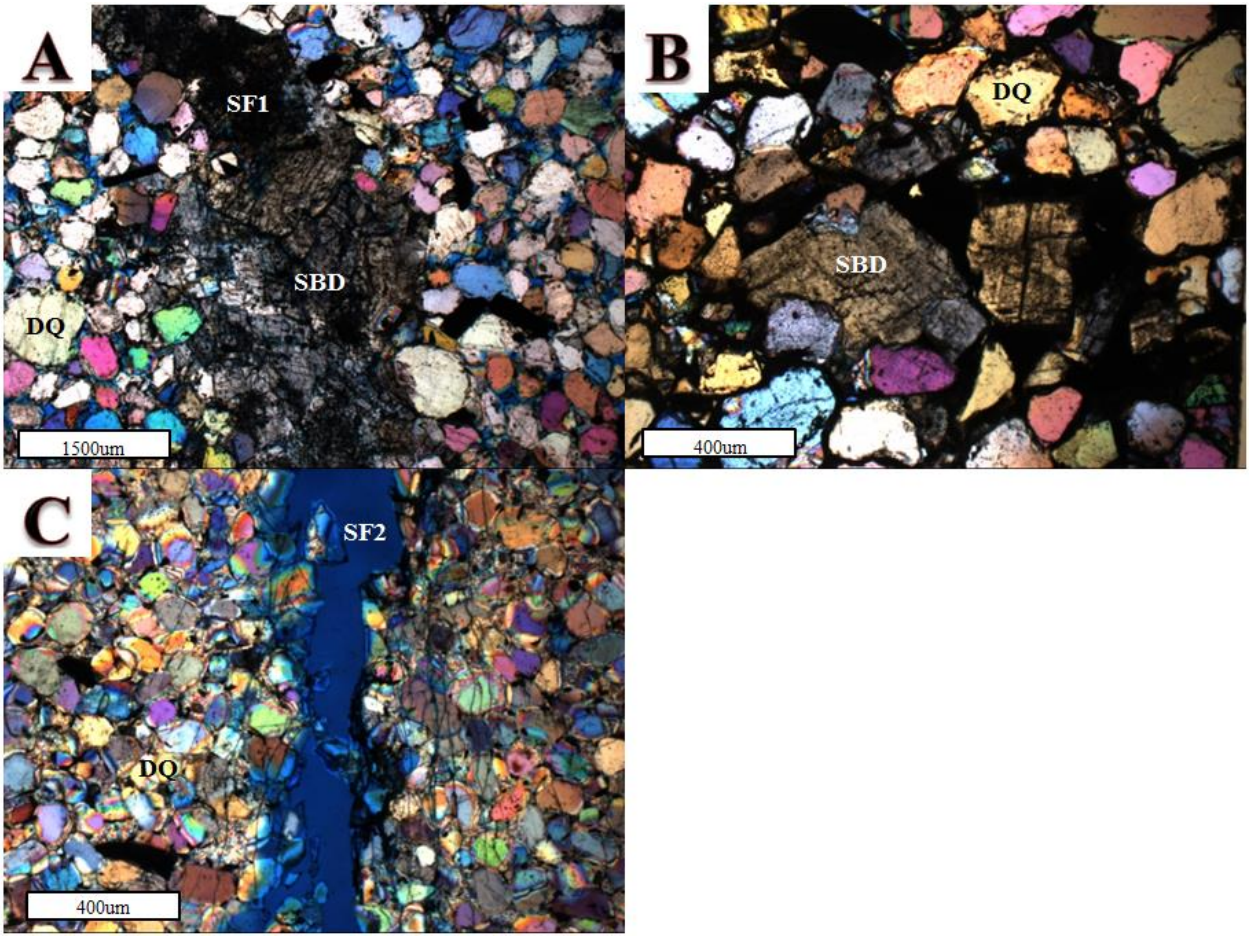


**Figure 3.4:** All images are cross-polarized light photomicrographs of thick sections: (A) Detrital quartz (DQ) grains deposited during Simpson Group deposition, this was followed by fracturing (SF1) (event 1-2), then precipitation of megaquartz cement overgrowths (SMQ), and then reduction of the fracture with baroque dolomite (SBD) (sample 4124.5 from Wellington 1-32); (B) Detrital quartz (DQ) grains deposited during Simpson Group deposition, this was followed by dissolution (event 1-2) and subsequent porosity occlusion by megaquartz cement overgrowths (SMQ) and baroque dolomite (SBD) (sample 4126.0 from Wellington 1-32); (C) Detrital quartz (DQ) grains deposited during Simpson Group deposition, this was followed by megaquartz cement overgrowths (SMQ) and then fracturing (SF2) (event 5) and splintering of DQ grains and overgrowths (SMQ); fractures were not filled with baroque dolomite (SBD) (sample 4066.3B from Wellington 1-32).

### *3.2. Mississippian*

*Event 1: Carbonate dissolution* – Dissolution of carbonate material created vug and cavern porosity within Mississippian strata, increasing porosity by <5%. This dissolution event is thought to be relatively late because the porosity generated lacks early cements but displays partial- to full-occlusion with late cements (event 3, 4, 5, 6, 8, 9) (Fig. 3.5A, 3.5B, 3.5C, 3.5D, 3.6A, 3.6C). Dissolution may have been related to under-saturated fluids accompanying the commencement of hydrothermal activity. Without a more thorough analysis of the entire paragenesis of Mississippian strata, the potential for this event to be related to the sub-Pennsylvanian unconformity remains.

*Event 2: Brecciation* – Previous dissolution, related to event 1, enhanced porosity and created an unstable fabric within Mississippian strata, resulting in brecciation and collapse features. Late-stage cements (event 3, 8-9) can be observed filling porosity after brecciation has occurred (Fig. 3.5A, 3.5B). Similar to event 1, this event could be linked to late migration of under-saturated fluids associated with hydrothermal activity or meteoric diagenesis associated with the sub-Pennsylvanian unconformity.

*Event 3: Megaquartz cement* – Megaquartz cement (MMQ) is present as euhedral quartz crystals lining vugs and occluding brecciated fabrics (Fig. 3.5A, 3.5C, 3.5D, 3.6C), reducing porosity by <5%. MMQ appears clear in transmitted light and has large groupings of fluid inclusion assemblages that feather out in the direction of crystal growth. MMQ can be observed precipitating after the precipitation of early megaquartz cement, occurring as overgrowths (Fig. 3.5D). Cementation of MMQ appears to have occurred before the precipitation of chalcedony (MCh), marking this event as a potential first event of late-stage cementation (Fig. 3.5C).

*Event 4-5-6-7: Chalcedony* – Chalcedony (MCh) can be observed as a radiating fibrous cement lining vugs. This cement is only observed in one sample, indicating it is a rare event, reducing porosity by <0.5%. Chalcedony appears light yellow to brown in color under transmitted light and has an undulating, fibrous extinction under crossed polars (Fig. 3.5C). MCh postdates megaquartz cement (MMQ) because it can be observed precipitating into pore space after MMQ (Fig. 3.5C). Calcite cement (MCC) can be observed precipitating after MCh and baroque dolomite (MBD) can be observed precipitating before MCC, tentatively placing the precipitation of MCh after MMQ but before MBD (Fig. 3.5C).

*Event 4-5-6-7: Baroque dolomite* – Baroque dolomite (MBD) is a relatively scarce late-stage cement and was observed in only two samples, reducing porosity by <0.5%. MBD displays a xenotopic-C texture with pore-lining, saddle-shaped crystals characterized by curved crystal terminations and sweeping extinction under crossed polars (Fig. 3.5D, 3.6A). MBD appears clear under transmitted light, with cloudy cores and bands represented by high abundance of fluid inclusions. MBD is the only cement that contains hydrocarbon inclusions. This cement is non-fluorescent when exposed to UV-epifluorescence. MBD does not take on any color when subjected to ARS:PF stain (Dickson, 1965) (Fig. 3.6A). Baroque dolomite can be observed precipitating after megaquartz and prior to calcite (Fig. 3.5D, 3.6A), but no direct relationship was observed with chalcedony (event 4) or fracturing associated with event 7, tentatively placing baroque dolomite as event 5.

*Event 4-5-6-7: Petroleum migration* – Hydrocarbon fluid inclusions can be observed within Mississippian baroque dolomite (MBD) crystals. The presence of what appear to be primary hydrocarbon inclusions necessitates that a petroleum migration event must have

occurred during precipitation of MBD (event 5) (Fig. 3.14C, 3.14D), though migration may have begun before or continued after.

*Event 4-5-6-7: Fracturing* – Fracturing (MF) appears to have affected Mississippian strata at some point, as evidenced by cross-cutting, nearly vertical fractures that appear as isolated features and also appear to have connected vug porosity in some instances (Fig. 3.6B). The exact timing of the fracturing relative to the paragenesis is difficult to place because of the lack of petrographic relationships. Fractures appear to only be filled with calcite (MCC) believed to be associated with event 8 (Fig. 3.6B), requiring MF to have at least begun at some point prior to event 8. MF can be observed cutting across megaquartz (event 3), indicating it occurred some point after precipitation of megaquartz.

*Event 8-9: Calcite cement* – Calcite cement (MCC) appears to be the most common late-stage precipitate in Mississippian strata, reducing porosity by <5%. MCC precipitates as coarsely crystalline equant spar and appears to exist primarily as one or two large crystals when observed in samples (Fig. 3.5B, 3.5C, 3.6A, 3.6B, 3.6C). MCC appears as a light yellow color in transmitted light, with deformation twins and partially healed micro-fractures common. MCC takes on a red tint when subjected to ARS:PF staining, indicating that it is non-ferroan (Fig. 3.6A) (Dickson, 1965). MCC can be observed filling pore space after chalcedony and baroque dolomite (Fig. 3.5C, 3.6A), but an exact relationship with anhydrite (MA) is difficult to decipher. This places precipitation after baroque dolomite and possibly before, simultaneous with, or after MA. Deformation twins in calcite cement leave potential for this calcite to have been precipitated after the onset of fracturing, as well as during the continuation of deformation.

*Event 8-9: Anhydrite* – Anhydrite (MA) can be observed commonly in Mississippian samples, reducing porosity by <5%. It appears that there were two phases of anhydrite

precipitation, with one occurring during early diagenesis and the other (event 8-9) occurring as late cement. This late event of anhydrite precipitation can be clearly observed reducing pore space after precipitation of late megaquartz cement (MMQ) (Fig. 3.6C). As discussed in calcite cement descriptions, exact placement of anhydrite in the paragenesis is difficult to place with confidence. The petrographic relationship with megaquartz cement (MMQ) places the onset of precipitation sometime after MMQ, but it is difficult to interpret when precipitation culminated.

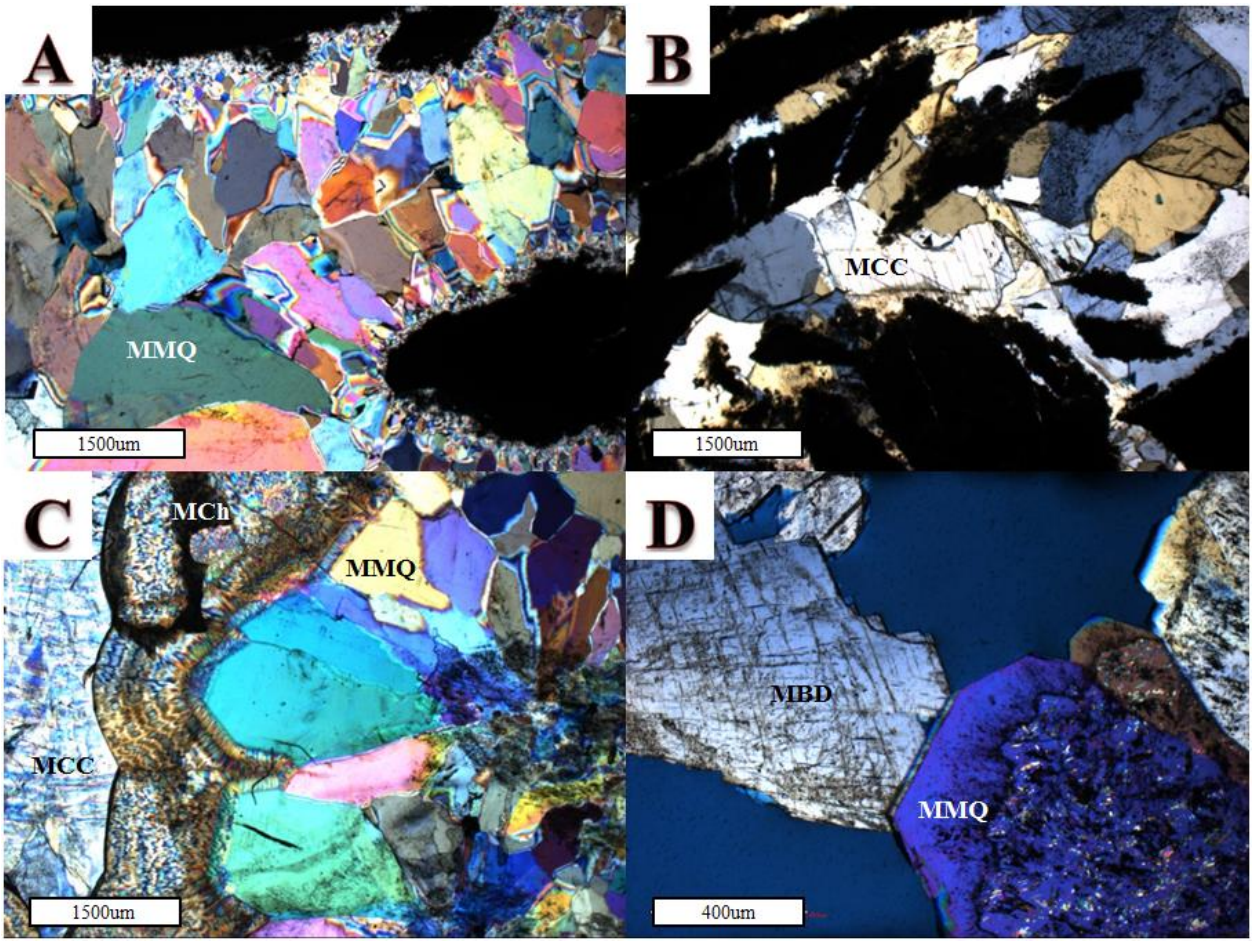

**Figure 3.5:** All images are crossed-polarized light photomicrographs of thick sections: (A) Mississippian carbonate material was subjected to dissolution (event 1) and subsequent brecciation (event 2), porosity and brecciated clasts are lined with megaquartz cement (MMQ) (sample 3770.4B from Wellington 1-32); (B) Brecciated Mississippian carbonate material that was subsequently filled with calcite cement (MCC) (sample 3775.5 from Wellington 1-32); (C) Megaquartz cement (MMQ) lines Mississippian porosity, followed by chalcedony (MCh) and then calcite cement (MCC) (sample 3844.3A from Wellington 1-32); (D) Mississippian porosity lined with megaquartz cement (MMQ) that precipitates as an overgrowth on earlier megaquartz, pore space is then reduced with baroque dolomite (MBD) (sample 3873.3 from Wellington 1-32).

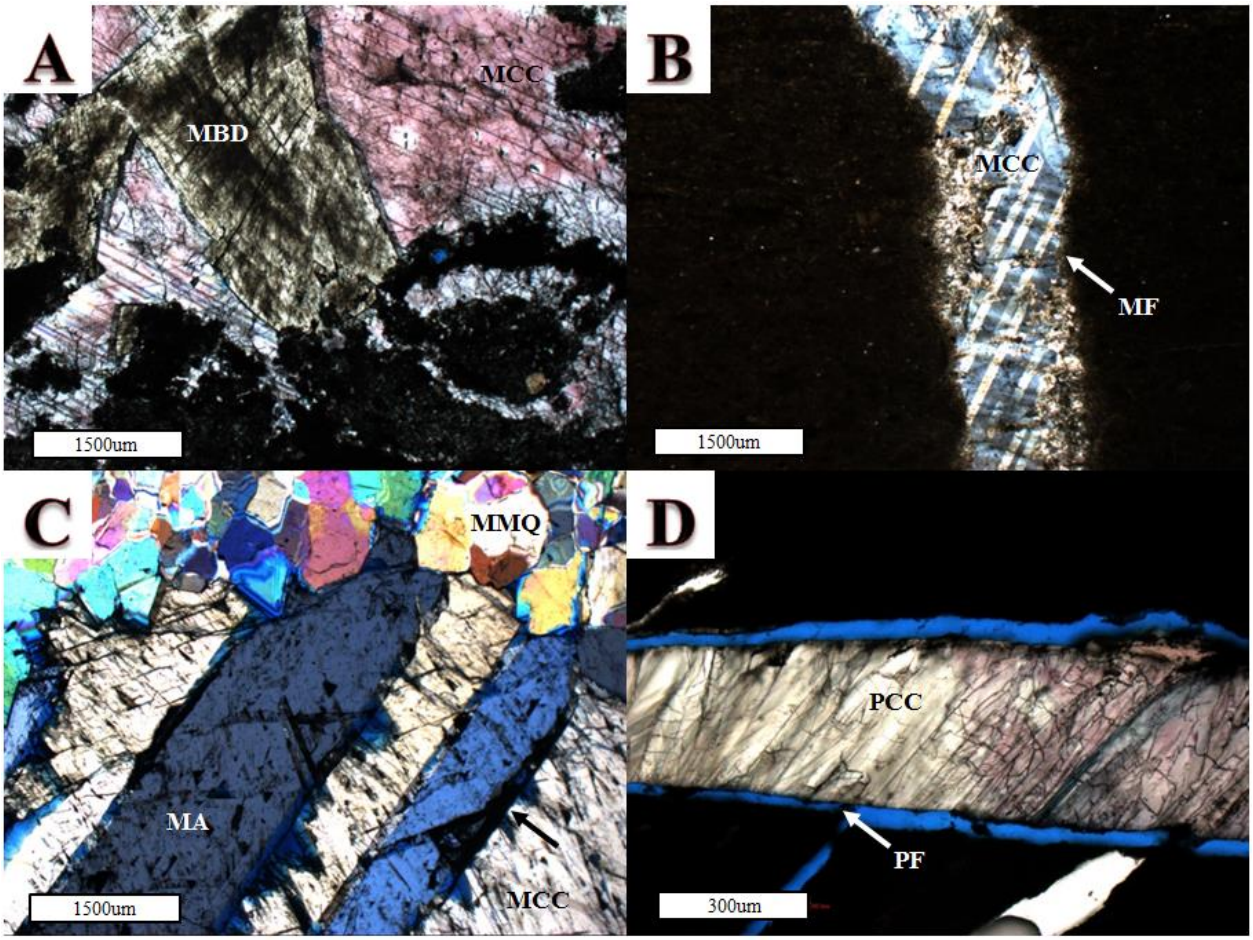

**Figure 3.6:** (A) Transmitted light photomicrograph of brecciated Mississippian strata that was first lined with baroque dolomite (MBD) and then fully occluded with calcite cement (MCC) that is stained red in this image (sample 3918.9 from Wellington 1-32); (B) Crossed-polarized light photomicrograph illustrating a nearly vertical fracture (MF) cross-cutting Mississippian strata, fracture is fully occluded by calcite cement (MCC) that displays twinning under cross-polars (sample 3771.0 from Wellington 1-32); (C) Cross-polarized light photomicrograph of Mississippian porosity lined with megaquartz cement (MMQ), then fully occluded with anhydrite (MA) and calcite cement (MCC) (sample 3787.2 from Wellington 1-32); (D) Transmitted light photomicrograph of Pennsylvanian shale that was subjected to fracturing (PF) with an unknown orientation and fracture was filled with calcite cement (PCC) that is stained pink in the right portion of the image (sample 3548.6 from Wellington 1-32).

### *3.3. Pennsylvanian (Cherokee Group)*

*Event 1: Dissolution* – Wojcik et al. (1992; 1994; 1997) and Walton et al. (1995) found evidence for a widespread dissolution event predating precipitation of baroque dolomite and petroleum migration. Large, secondary vuggy pores were created and existing pore space and fractures were enlarged or solution enhanced. Porosity associated with this event is typically reduced by baroque dolomite (Wojcik et al., 1992; 1994; 1997).

*Event 2-3: Baroque dolomite* – Baroque dolomite (and ankerite; PBD) with varying concentrations of iron and manganese can be observed reducing primary and secondary porosity in Pennsylvanian sandstone and limestone (Wojcik et al., 1992; 1994; 1997; Walton et al., 1995). PBD is very coarse-grained and displays curved crystal faces. PBD appears clear in transmitted light with some cloudiness defined by abundance of fluid inclusions (Wojcik et al., 1992; 1994; 1997). Wojcik found evidence for an earlier baroque dolomite that is partially cloudy and non-ferroan and a later baroque dolomite that is limpid and ferroan. Precipitation of PBD in pores related to event 1 dissolution places the onset of baroque dolomite precipitation after event 1.

*Event 2-3: Petroleum migration* – Wojcik et al. (1992) observed hydrocarbon inclusions in baroque dolomite (PBD) crystals. Hydrocarbon inclusions were interpreted as having a

primary and secondary origin relative to PBD crystal growth (Wojcik et al., 1992). Primary hydrocarbon inclusions suggest petroleum migration simultaneous with precipitation of PBD, whereas secondary hydrocarbon inclusions represent petroleum migration after PBD precipitation. Petroleum migration appears to have begun during baroque dolomite precipitation and to have continued for some time after (Wojcik et al., 1992; Walton et al., 1995).

*Event 4: Fracturing* – Fracturing (PF) was observed in one example within the limited portion of Pennsylvanian strata that was preserved in the Wellington 1-32 core (Fig. 3.6D). The orientation of the fracture could not be determined because the sample was a loose piece of rock within the box. The fracture appears to be isolated and cross-cuts the shale deposited during Pennsylvanian time (Cherokee Group). The fracture observed is fully occluded with calcite cement (event 5) (Fig. 3.6D).

*Event 5: Calcite cement* – Calcite cement (PCC) is the only late-stage cement observed in Pennsylvanian strata recovered in the Wellington 1-32 core, reducing porosity by <0.5%. PCC precipitates as coarsely crystalline equant spar and displays a light yellow color in transmitted light (Fig. 3.6D). It displays a red tint when exposed to ARS:PF staining, indicating that the precipitate is non-ferroan (Fig. 3.6D) (Dickson, 1965). The precipitation of PCC in fractures associated with event 4 marks this event as occurring after fracturing. Wojcik et al. (1994; 1997) found petrographic evidence for a late event of non-ferroan calcite precipitation that post-dated precipitation of baroque dolomite and petroleum migration, supporting the placement of this calcite cement as the latest stage of cement precipitation observed.

## 5. SEM Analysis

### *5.1. Mississippian baroque dolomite*

SEM-BSE analysis was performed on two Mississippian baroque dolomite (MBD) samples (Appendix II). BSE-imaging was performed to support or refute the evidence for MBD recrystallization, and to evaluate the timing of entrapment of fluid inclusions. The images collected did not provide evidence for growth zoning, but did reveal extensive fracturing of samples apparently composed of the same medium-grey phase (Fig. 3.7A, 3.7B). A dark-grey phase emanates from the fractures cutting across the medium-grey phase and likely represents recrystallization (Fig. 3.7A, 3.7B).

### *5.1.1. Medium-grey phase (MGP)*

The medium-grey phase (MGP) appears to be the zone that existed during initial growth of very coarse-grained baroque dolomite crystals. Due to a lack of internal growth zones, this phase appears to dominate entire dolomite crystals, but has been exposed to pervasive fracturing and subsequent recrystallization. Fracture networks give a shattered appearance to the MGP and may be concealing vague internal growth zones within the MGP (Fig. 3.7A, 3.7B). Much like baroque dolomite in the Arbuckle Group, fluid inclusions appear to be slightly less common within MGP, but there did not appear to be a dramatic difference in inclusion size (Fig. 3.7A, 3.7B).

### *5.1.2. Dark-grey phase (DGP)*

The dark-grey phase (DGP) appears only along fractures that have splintered the previously precipitated MGP (Fig. 3.7A, 3.7B). DGP is dolomite that exists as a recrystallization fabric propagating outward from the multitude of micro-fractures. In some instances, recrystallization appears to be following growth boundaries running perpendicular to the crystal

growth direction (Fig. 3.7A, 3.7B), but this is the only evidence for crystal growth boundaries in the samples analyzed. Fluid inclusions are generally more abundant in DGP than MGP (Fig. 3.7A, 3.7B).

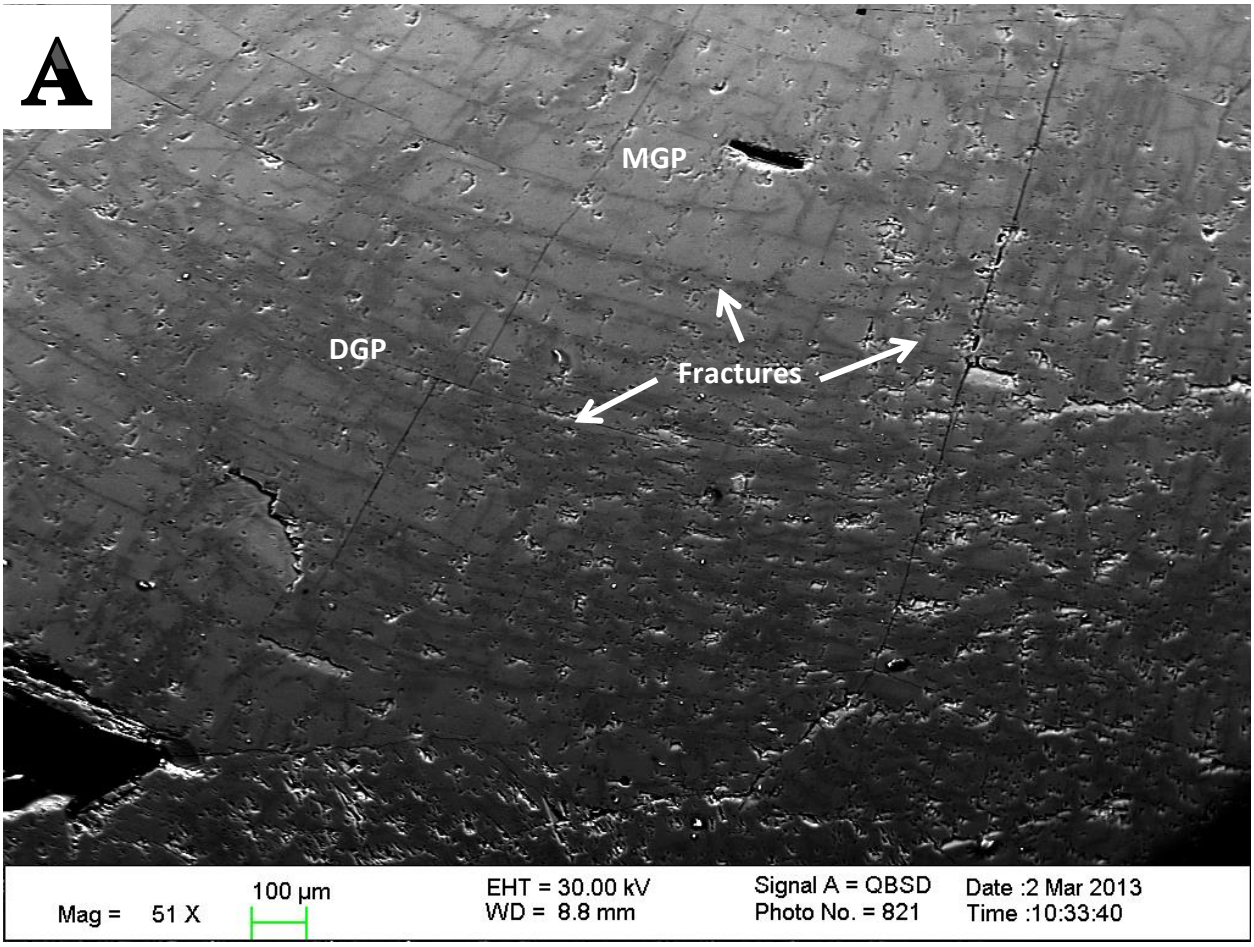

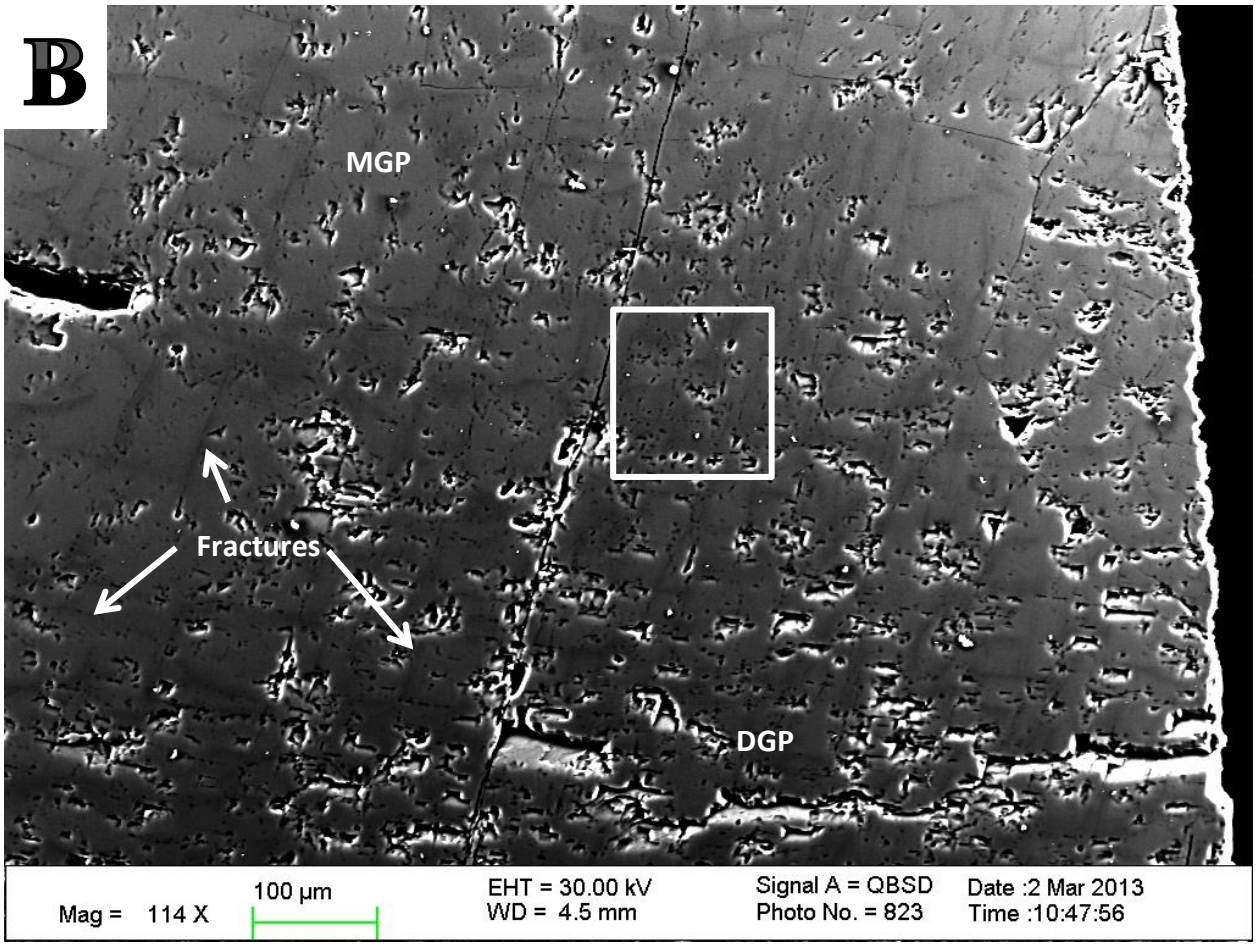


**Figure 3.7:** Both images are SEM-BSE photomicrographs taken of Mississippian baroque dolomite (MBD) at variable magnifications: (A) Mississippian baroque dolomite (MBD) lacks internal zoning, but extensive fracturing and subsequent recrystallization is represented by lineaments composed of the dark-grey phase (DGP) that cut across the earlier precipitated medium-grey phase (MGP); (B) Higher magnification view of the same sample of Mississippian baroque dolomite (MBD) displays extensive micro-fracturing of the medium-grey phase (MGP) and subsequent recrystallization by the dark-grey phase (DGP), white box shows and area with abundant dark pits that likely represent fluid inclusions, which appear to be more concentrated in the dark-grey phase (DGP); larger pits could either be large fluid inclusions or pits created during polishing of the thick section.

## 6. Fluid Inclusion Analysis

The following section discusses fluid inclusion petrography and microthermometry of the mid-Ordovician Simpson Group and Mississippian strata (Appendix III). Simpson Group baroque dolomite (SBD), Mississippian megaquartz cement (MMQ), Mississippian baroque

dolomite (MBD), and Mississippian calcite cement (MCC) were analyzed using fluid inclusion microthermometry. Discussions are in paragenetic order. The methodology and terminology proposed by Goldstein and Reynolds (1994) is used for fluid inclusion analysis. The term fluid inclusion assemblage (FIA) is used throughout the section and is defined as "the most finely discriminated, petrographically distinguishable group of inclusions" within a given mineral phase (Goldstein and Reynolds, 1994; Goldstein, 2003). Goldstein and Reynolds (1994) define a consistent FIA as one in which ≥ 90% of homogenization temperature (Th) data fall within a range of 10º-15ºC and an inconsistent FIA as one that yields more variable Th data. Consistent Th data are interpreted to mean thermal reequilibration of fluid inclusions has not occurred (Goldstein and Reynolds, 1994). The microthermometric data provided consist of homogenization temperatures (Th) and final melting temperatures of ice ($Tm_{ice}$). $Tm_{ice}$ values are translated to salinity in weight percent NaCl equivalent (wt. % NaCl eq.). Salinity was calculated from $Tm_{ice}$ measurements using the AqSoVir program from Bakker (2008) and the equation from Bodnar (1993):

*Equation 3.1:* Salinity (wt. % NaCl eq.) = $0.00 + 1.78\theta - 0.0442\theta 2 + 0.00055\theta 3$

where θ equals the depression of the freezing point in ºC (Bodnar, 1993). $Tm_{ice}$ data were only collected from fluid inclusions with gas bubbles present before final melting. Th data were preferentially measured from fluid inclusions that appeared to result from homogeneous entrapment or were likely the liquid-rich end member of an FIA with evidence for heterogeneous entrapment (Goldstein and Reynolds, 1994). An interpretation of fluid inclusion data is provided for each diagenetic event.

### *6.1. Ordovician (Simpson Group)*

### 6.1.1. Baroque dolomite

*Petrography:* Baroque dolomite (SBD) typically appears clear under transmitted light with patches of cloudiness defined by the high abundance of aqueous fluid inclusions (Fig. 3.8A, 3.8B). The vast majority of inclusions were too small (<5μm) to characterize or measure, but the general shape of larger inclusions appears to be elongated in the direction of crystal growth, which suggests a primary origin (Fig. 3.8A). Several fluid inclusions appear flat in nature, suggesting a secondary origin (Fig. 3.8B). All-liquid inclusions were observed in some samples, but were relatively small (<5μm) in size. All of the fluid inclusions measured were two-phase inclusions with small gas bubbles and an aqueous liquid, and they vary in size and shape. Liquid-gas ratios among inclusions in an FIA appear to be consistent, though the sample size was limited. Fluid inclusions that appear to belong to secondary FIAs also appear as two-phase inclusions with gas bubbles and aqueous liquid. Liquid-gas ratios appear highly inconsistent, suggesting necking down after a phase change may have occurred.

*Microthermometry:* The overall cloudiness of the dolomite crystals, as well as the general lack of samples and fluid inclusions large enough to measure, significantly limited the potential for gathering microthermometric data. A total of three FIAs, two consistent primary and one inconsistent secondary, were subjected to heating for the purpose of obtaining Th data. Heating of fluid inclusions resulted in a gradual decrease in gas bubble size, until the two phases homogenized and the bubble disappeared. The values collected from primary FIAs ranged from 119.0-132.0ºC and Th values collected from secondary FIAs ranged from 117.0-125.0ºC, with some inclusions retaining bubbles well above these temperatures (Fig. 3.9). Th values of Simpson Group baroque dolomite fall within the upper end of the range of values observed in Arbuckle Group baroque dolomite (93.0-131.0ºC).

Two consistent primary FIAs were subjected to freezing for the purpose of obtaining $Tm_{ice}$ values. Freezing of inclusions was typically accompanied by a sudden jerk and decrease in size of the gas bubble. $Tm_{ice}$ values were measured between -21.3 and -21.8ºC (Fig. 3.10); melting was accompanied by consolidation of low-relief, rounded crystals into a larger crystal that slowly melted until completely disappearing. The melting of ice was commonly accompanied by sudden movement of the gas bubble. $Tm_{ice}$ data resulted in salinities ranging from 23.2-23.7 wt. % NaCl eq. Salinities of Simpson Group baroque dolomite are approximately 3% higher than values measured in Arbuckle Group baroque dolomite (16.3-20.4%).

*Interpretation:* Th measurements of two-phase fluid inclusions within consistent primary FIAs range from 119.0-132.0ºC, whereas measurements from inconsistent secondary FIAs range from 117.0-125.0ºC. Small (<5μm) all-liquid inclusions can be observed. The fact that all-liquid inclusions are small in size suggests nucleation metastability may play a role in the absence of a gas bubble (Goldstein and Reynolds, 1994). If small all-liquid inclusions are attributed to metastability, then fluid inclusion entrapment most likely occurred during homogeneous conditions at high temperatures. Possible explanations for variability in Th measurements include: (1) homogeneous entrapment followed by thermal reequilibration at variable high temperatures for each growth zone, (2) homogeneous entrapment followed by recrystallization at variable high temperatures for each growth zone, or (3) homogeneous entrapment at variable high temperatures for each growth zone. Thermal reequilibration would typically lead to significant Th variability in FIAs; the fact that all primary FIAs are consistent eliminates scenario (1). The fact that recrystallization is commonly observed in baroque dolomite samples in the study area leaves potential for recrystallization to have occurred in

baroque dolomite samples in the Simpson Group as well. Thus, scenario (2) cannot be eliminated. Homogeneous entrapment of fluid inclusions during multiple fluid migration events at variable high temperatures, without changes after entrapment, could also provide a plausible explanation for Th measurements in baroque dolomite. If baroque dolomite is assumed to be genetically related to baroque dolomite in the Arbuckle Group, homogeneous entrapment during multiple migration events at variably high temperatures, along with recrystallization, is the most reasonable explanation for Th values.

High salinity fluids (23.2-23.7 wt. % NaCl eq.) in baroque dolomite strongly suggest basinal brines. When considering the elevated Th values and the potential genetic link with Arbuckle Group baroque dolomite, a basin-sourced fluid is the best candidate to account for such fluids (Chapter 2 of this study; Young, 2010; Heimstra, 2003; Smith and Davies, 2006; Banner, 1995; Land, 1985; Hanor, 1979). The fact that salinities are slightly higher than values observed in Arbuckle Group baroque dolomite may suggest increased interaction with evaporites, or mixing with higher salinity connate fluids present in the Simpson Group prior to fluid migration into the study area. A discussion regarding potential hydrologic models is provided in section 9.3.

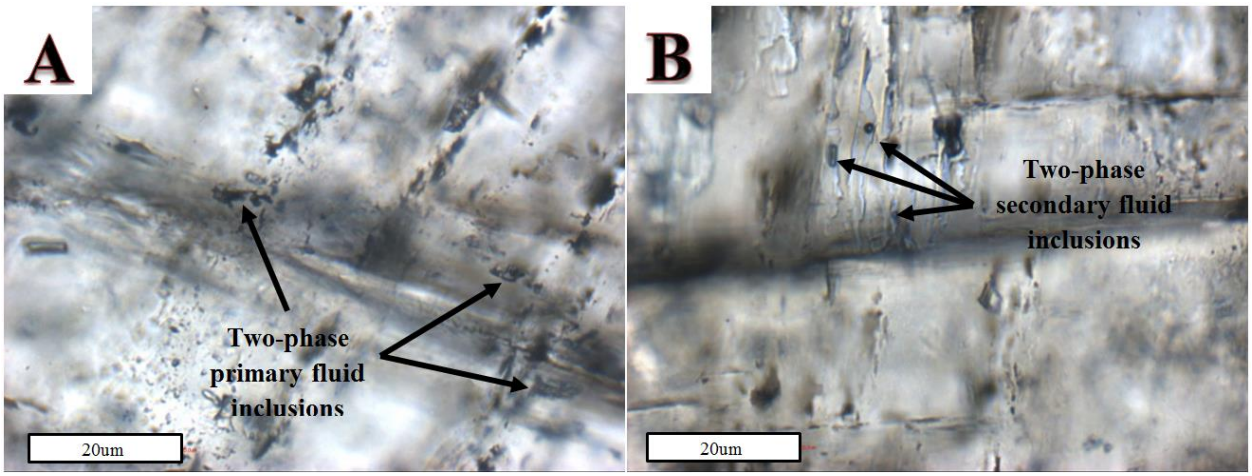

**Figure 3.8:** Transmitted light photomicrographs of SBD: (A) Primary FIAs in Simpson Group baroque dolomite (SBD) displaying two-phase fluid inclusions that are slightly elongated in the direction of crystal growth (sample 4126.0 from Wellington 1-32); (B) Secondary FIAs in Simpson Group baroque dolomite (SBD) displaying two-phase fluid inclusions that appear flat in nature (sample 4124.0 from Wellington 1-32).

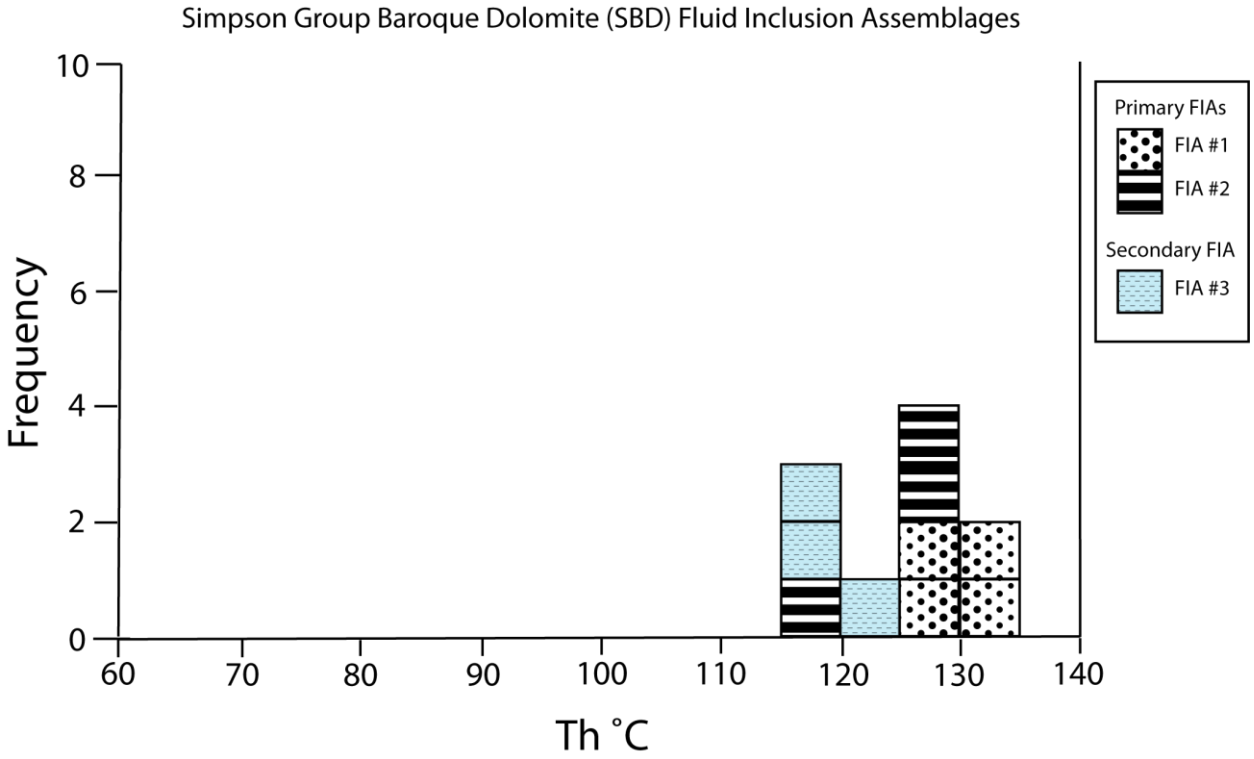


**Figure 3.9:** Histogram of homogenization temperatures (Th) measured from primary and secondary FIAs in Simpson Group baroque dolomite (SBD).

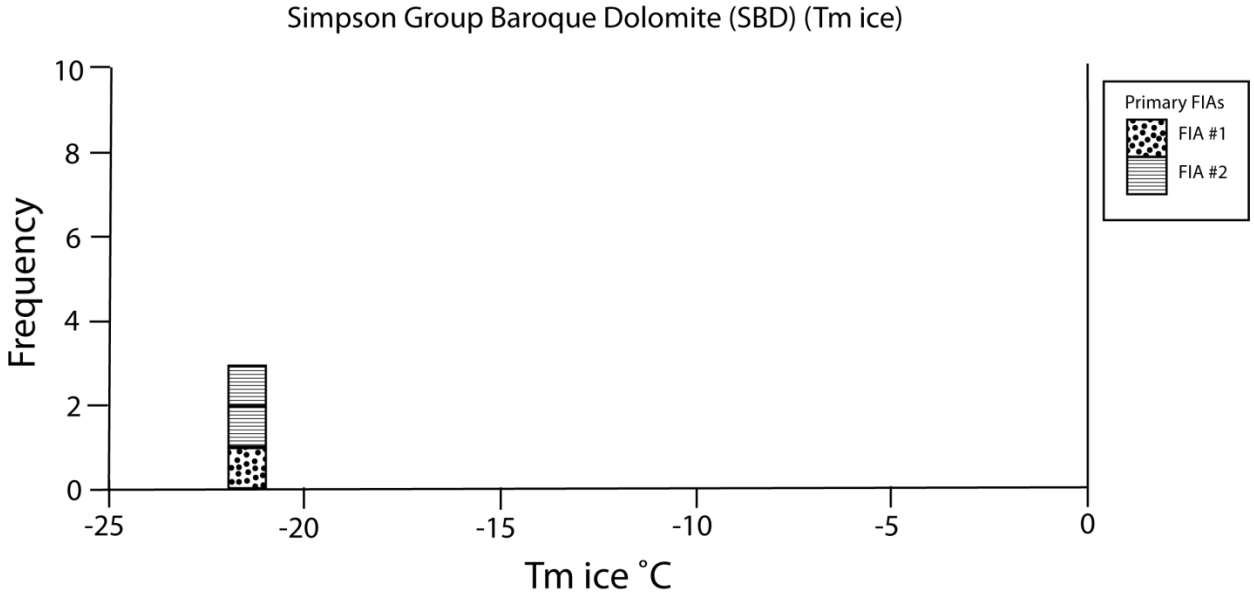

**Figure 3.10:** Histogram of the final melting temperatures of ice ($Tm_{ice}$) from primary FIAs in Simpson Group baroque dolomite (SBD).

## *6.2. Mississippian*

### 6.2.1. Megaquartz

*Petrography:* Megaquartz cement (MMQ) appears clear under transmitted light and contains abundant primary FIAs that appear to be distributed in a feather-like pattern, oriented in the direction of crystal growth (Fig. 3.11A). Fluid inclusions are typically very small in size (<5μm) and display a rounded shape, with slight elongation in the direction of crystal growth (Fig. 3.11B). Fluid inclusions can be observed as two-phase inclusions with a gas bubble and aqueous liquid, and as small, all-liquid aqueous inclusions (Fig. 3.11B). Liquid-gas ratios among inclusions in an FIA appear inconsistent with a small percentage of gas-dominated inclusions (Fig. 3.11B). Petrographic pairing is not observed in fluid inclusions, indicating necking down after a phase change has not caused the variability in liquid-gas ratios (Goldstein and Reynolds, 1994).

*Microthermometry:* The relatively small size of inclusions (<5μm in most cases) lead to petrographic limitations and likely resulted in nucleation metastability effects restricting bubble generation in the smallest inclusions (Goldstein and Reynolds, 1994). A total of eight inconsistent primary FIAs were subjected to heating for the purpose of obtaining Th data. Heating of fluid inclusions resulted in a gradual decrease in gas bubble size, until the two phases homogenized and the bubble disappeared. The resulting Th data varied significantly, values ranging from 86.0-161.0°C (Fig. 3.12). Nearly the same data range can be observed in late-stage megaquartz cement in Arbuckle Group samples (87.0-157.0ºC).

A total of four inconsistent primary FIAs were subjected to freezing for the purpose of obtaining $Tm_{ice}$ values. Freezing of inclusions was typically accompanied by a sudden jerk and decrease in size of the gas bubble. Upon warming the inclusions, $Tm_{ice}$ was measured between -1.9 and -2.3ºC (Fig. 3.13). Melting was accompanied by the consolidation of low-relief, rounded crystals into a larger crystal that slowly melted until completely disappearing. The melting of ice was commonly accompanied by sudden movement of the gas bubble. $Tm_{ice}$ data resulted in salinities ranging from 3.2-3.9 wt. % NaCl eq. These values fall within the values of Arbuckle Group megaquartz cement (3.1-6.0%), though they do not span the entire range.

*Interpretation:* Th measurements of two-phase fluid inclusions within inconsistent FIAs range from 86.0-161.0ºC and small all-liquid inclusions can be observed. The fact that all-liquid inclusions are small in size (<5μm) suggests nucleation metastability may play a role in the absence of a gas bubble (Goldstein and Reynolds, 1994); if small all-liquid inclusions are attributed to metastability, then megaquartz precipitation is most likely dominated by high-temperature conditions. Possible explanations for Th measurements include: (1) homogeneous entrapment at variably high temperatures and (2) heterogeneous entrapment at high temperatures. Inconsistent liquid-gas ratios in FIAs, with gas-dominated inclusions and no evidence for petrographic pairing, require entrapment during heterogeneous conditions, eliminating the potential for scenario (1). Heterogeneous entrapment in scenario (2) would account for the variability in Th measurements. Because the fluid inclusions within FIAs contain liquid-rich and gas-rich end members of the heterogeneous system, Th values from liquid-rich end-members would provide the temperatures during entrapment (Goldstein and Reynolds, 1994). In an attempt to collect Th data from liquid-rich end members (two-phase fluid inclusions with the smallest gas bubbles), it is inevitable that data collection from inclusions that formed with

miniscule amounts of a separate gas phase would have occurred. If this is the case, the lowest measured temperatures (~90ºC) would represent actual temperature of entrapment, whereas the higher temperature range would represent failed attempts at collecting Th data from liquid-rich end members.

Salinities measured in late megaquartz cement range from 3.2-3.9 wt. % NaCl eq, values very close to what would be expected from unmodified seawater. These values could represent connate seawater and slightly diluted and evaporated seawater that was present in a basin prior to fluid migration. When considering the elevated Th measurements and a potential genetic link with Arbuckle Group megaquartz, a basin-sourced fluid is the best candidate to account for high temperature and seawater-salinity fluids (Young, 2010; Hanor, 1979). A discussion regarding potential hydrologic models is provided in section 9.3.

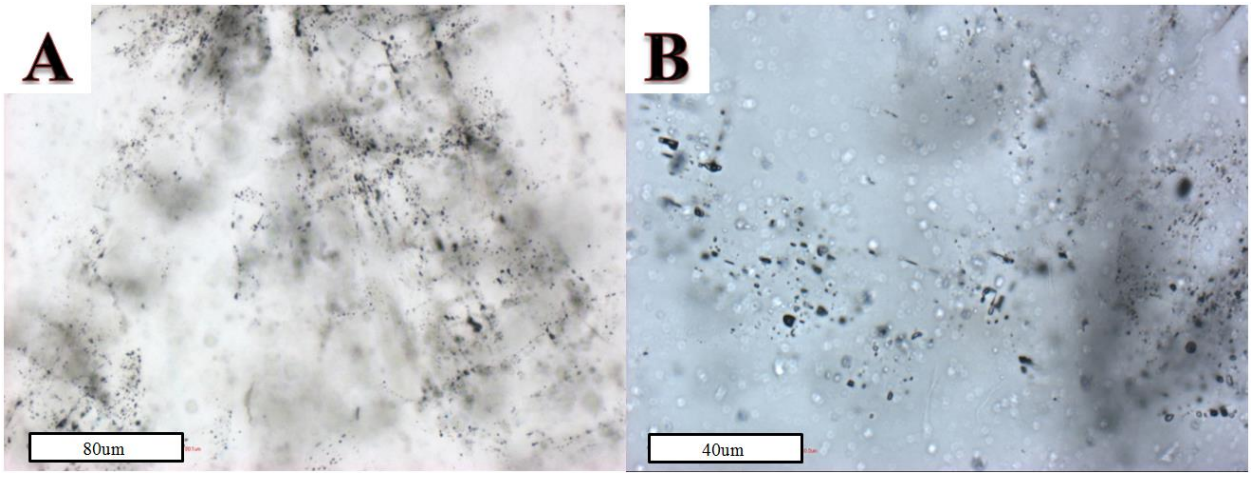


**Figure 3.11:** Transmitted light photomicrographs of MMQ: (A) Primary FIAs in Mississippian megaquartz cement (MMQ) that feather out in the direction of crystal growth (sample 3770.4A from Wellington 1-32); (B) Higher magnification view of Mississippian megaquartz cement (MMQ) displaying two-phase fluid inclusions in primary FIAs with inconsistent liquid-gas ratios (sample 3770.4A from Wellington 1-32).

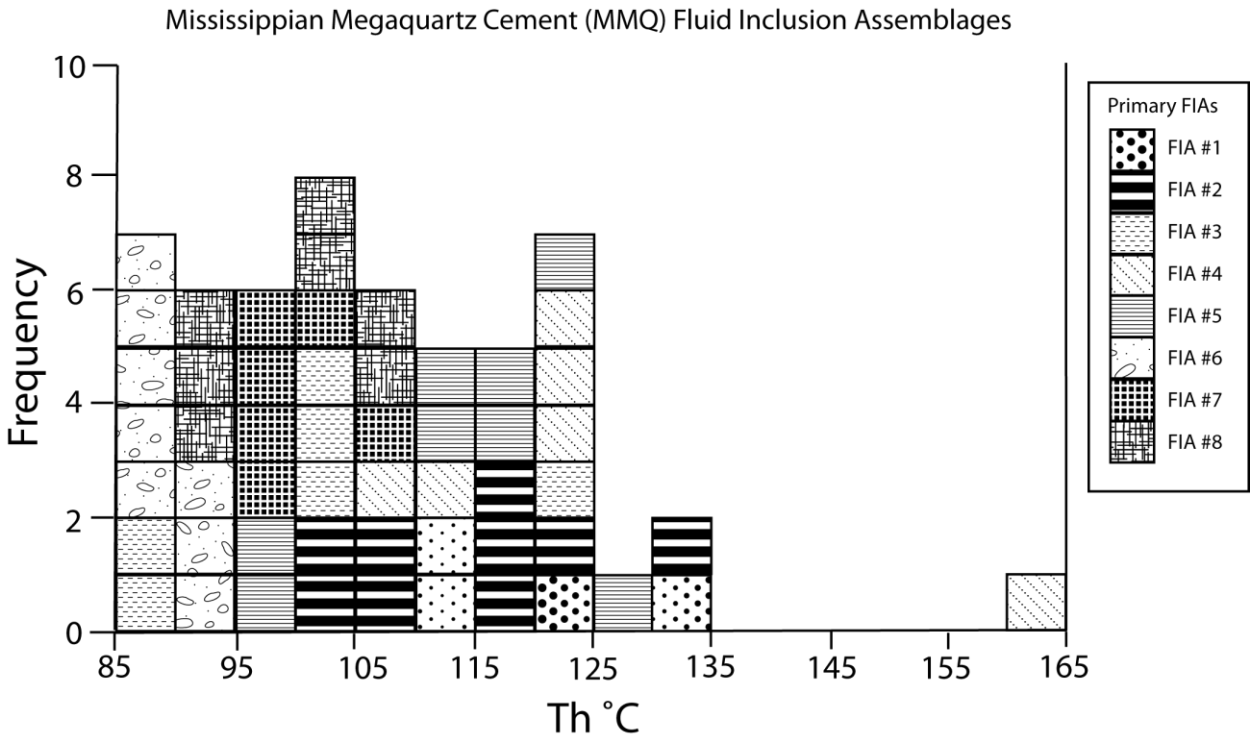


**Figure 3.12:** Histogram of homogenization temperatures (Th) measured in primary FIAs in Mississippian megaquartz cement (MMQ). Significant variability in data represents heterogeneous entrapment with liquid- and gas-rich end-members.

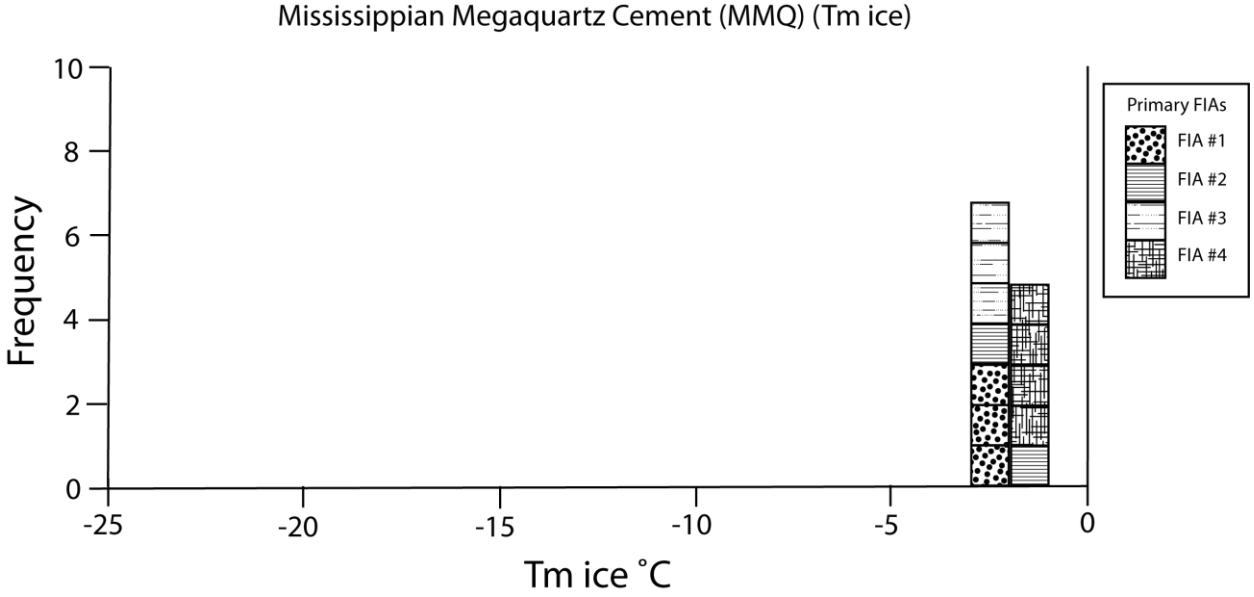


**Figure 3.13:** Histogram of final melting temperatures of ice ($Tm_{ice}$) measured in primary FIAs in Mississippian megaquartz cement (MMQ). $Tm_{ice}$ values translate to much lower salinities than that observed in Mississippian baroque dolomite (MBD) and calcite cement (MCC).

### 6.2.2. Baroque dolomite

*Petrography:* Baroque dolomite (MBD) typically appears clear under transmitted light with a cloudy core and bands defined by high abundance of fluid inclusions (Fig. 3.14A). Primary FIAs can commonly be observed mimicking concentric crystal growth of dolomite samples, with fluid inclusions appearing elongated in the direction of crystal growth (Fig. 3.14A). Fluid inclusions within primary FIAs are typically two-phase inclusions with small gas bubbles and an aqueous liquid, and they vary in size and shape. Liquid-gas ratios among inclusions in an FIA appear to be consistent (Fig. 3.14B). All-liquid inclusions can be observed within primary FIAs but are always relatively small in size (<5μm). Additionally, MBD contains primary hydrocarbon inclusions, revealing petroleum migration at the same time as fluid responsible for baroque dolomite precipitation. Hydrocarbon inclusions occur as two-phase fluid inclusions in primary FIAs that appear to have been entrapped during early crystal growth of baroque dolomite (Fig. 3.14C, 3.14D). These inclusions appear clear to light-yellow under transmitted light and display a bright blue color when exposed to UV epifluorescence (Fig. 3.14C, 3.14D).

SEM-BSE imaging supplied insight into the crystal growth history of baroque dolomite, enabling identification of two discrete phases. Initial dolomite precipitation was preserved as extremely coarse-grained crystal growth (MGP) and, because of the lack of internal growth bands, appears to have originated from a single fluid composition or compositions that did not result in BSE variation (Fig. 3.7A, 3.7B). Following precipitation of the medium-grey phase, extensive micro-fracturing produced a highly fractured, brecciated fabric that appears to be present throughout entire crystals (Fig. 3.7A, 3.7B). Following the extensive fracturing of the

earlier dolomite phase, the later dark-grey phase, believed to be the last phase of dolomite, appears as recrystallized areas following a network of microfractures (Fig. 3.7A, 3.7B).

Similar to what was observed in Arbuckle Group baroque dolomite, recrystallization of the earlier dolomite phase by the latest phase of dolomite appears to have had a major impact on the location of fluid inclusions (Fig. 3.7A, 3.7B). Fluid inclusions are most concentrated in the late dark-grey phase, indicating they were preferentially entrapped during recrystallization. Though some fluid inclusions can still be observed within the earlier phase, the majority rest within DGP. This has likely resulted in the majority of the fluid inclusion data being derived from the latest stage of crystal growth, rather than spanning the entire history of crystal growth.

*Microthermometry:* A total of fifteen consistent primary FIAs were subjected to heating for the purpose of obtaining Th data. Heating of fluid inclusions resulted in a gradual decrease in gas bubble size, until the two phases homogenized and the bubble disappeared. The values collected from primary FIAs ranged from 100.0-144.0ºC (Fig. 3.15). The highest Th values are slightly higher than the data range observed in Arbuckle Group baroque dolomite (93.0-131.0°C) and Simpson Group baroque dolomite (117.0-132.0°C). Several crystal transects were completed, measuring Th values in primary FIAs while progressing from the inner to the outer crystal margin of baroque dolomite rhombs. Th values measured during crystal transects did not display any readily observable trends, with temperatures increasing and decreasing from the inner to the outer crystal margin (Fig. 3.16).

A total of eight consistent primary FIAs were subjected to freezing for the purpose of obtaining $Tm_{ice}$ values. Freezing of inclusions was typically accompanied by a sudden jerk and decrease in size of the gas bubble. Upon warming the inclusions, $Tm_{ice}$ values were measured between -11.0 and -21.0ºC (Fig. 3.17). This was signified by the consolidation of low-relief,

rounded crystals into a larger crystal that slowly melted until completely disappearing. Melting of ice was commonly accompanied by sudden movement of the gas bubble. $Tm_{ice}$ data resulted in salinities ranging from 15.0-23.0 wt. % NaCl eq. $Tm_{ice}$ data gathered from MBD produced two end-members, with one producing values ranging from -11.0 to -12.5ºC (15.0-16.4 wt. % NaCl eq.) and the other producing values ranging from -17.5 to -21.0ºC (20.6-23.0 wt. % NaCl eq.). Arbuckle Group baroque dolomite salinities (16.3-20.4%) fall within this range, whereas Simpson Group values are slightly more saline (23.2-23.7%).

*Interpretation:* Th measurements of two-phase fluid inclusions within consistent FIAs range from 100.0-144.0ºC and crystal transects show rises and falls of Th values from the inner to outer margin of individual crystals. Small (<5μm) all-liquid inclusions can be observed. The fact that all-liquid inclusions are small in size suggests nucleation metastability may play a role in the absence of a gas bubble (Goldstein and Reynolds, 1994); if small all-liquid inclusions are attributed to metastability, then fluid inclusion entrapment most likely occurred during homogeneous conditions at high temperatures. Possible explanations for variability in Th measurements include: (1) homogeneous entrapment followed by thermal reequilibration at variable high temperatures for each growth zone, (2) homogeneous entrapment followed by recrystallization at variable high temperatures for each growth zone, or (3) homogeneous entrapment at variable high temperatures for each growth zone. Thermal reequilibration would typically lead to significant Th variability in FIAs; the fact that all FIAs are consistent eliminates scenario (1). Evidence for recrystallization is clearly observed using SEM-BSE imaging, suggesting that scenario (2) could account for at least some of the values. Homogeneous entrapment of fluid inclusions during multiple fluid migration events at variable high temperatures, without changes after entrapment (scenario (3)), cannot be the sole process

responsible because of the observed recrystallization. It is more likely that Th values represent a combination of both scenario (2) and (3).

High salinity fluids (15.0-23.0 wt. % NaCl eq.) in baroque dolomite strongly suggest basinal brines. When considering the elevated Th values and the potential genetic link with Arbuckle Group baroque dolomite, a basin-sourced fluid is the best candidate to account for such fluids (Chapter 2 of this study; Young, 2010; Heimstra, 2003; Smith and Davies, 2006; Banner, 1995; Land, 1985; Hanor, 1979). The fact that salinities are slightly higher than values observed in Arbuckle Group baroque dolomite suggests increased interaction with evaporites or different fluid pathways. A discussion regarding potential hydrologic models is provided in section 9.3.

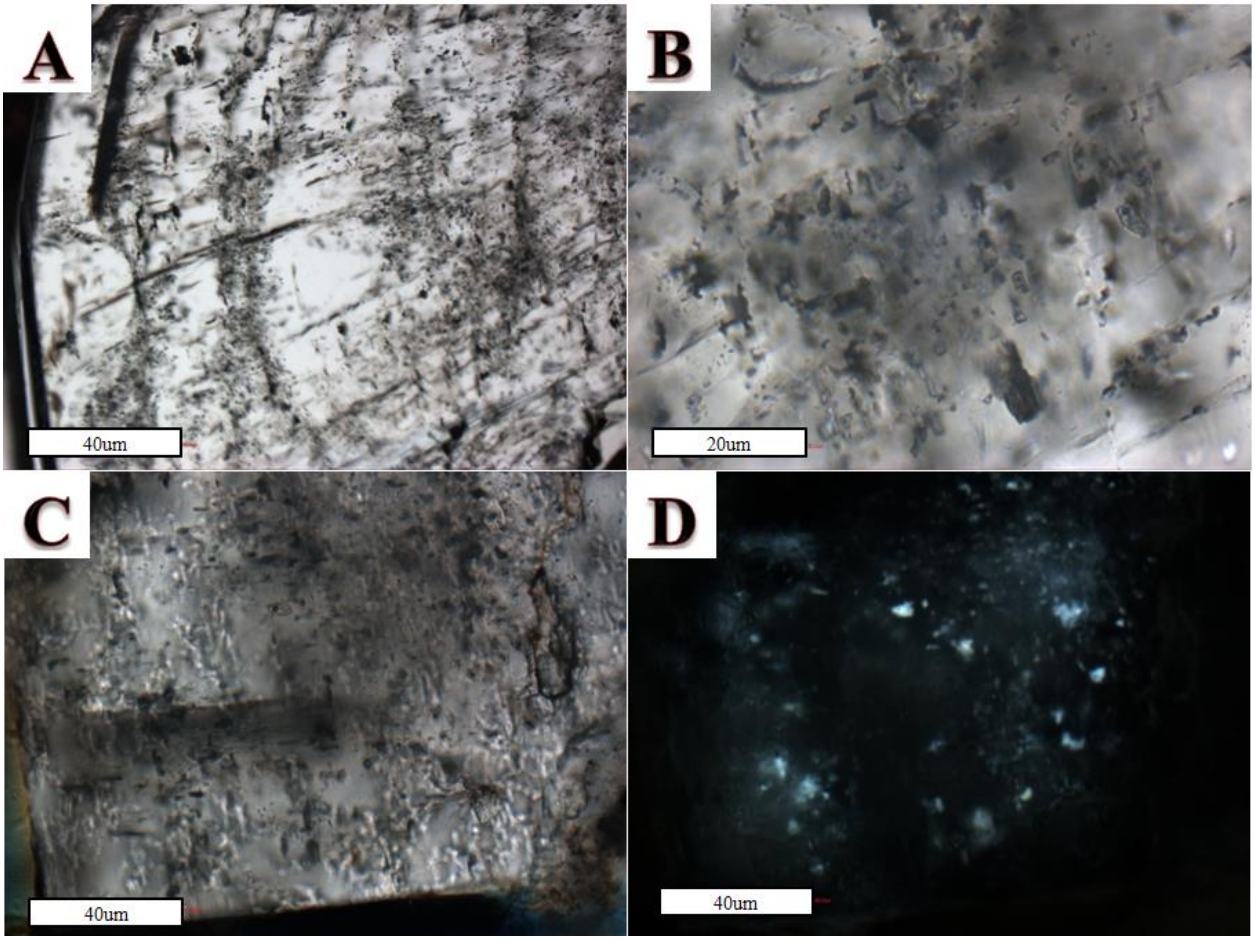

**Figure 3.14:** (A) Transmitted light photomicrograph of primary FIAs in Mississippian baroque dolomite (MBD) that appear to mimic the growth direction of the crystal (sample 3873.3 from Wellington 1-32); (B) Transmitted light photomicrograph of two-phase fluid inclusions in Primary FIAs in Mississippian baroque dolomite (MBD), inclusions appear to be slightly elongated in the direction of crystal growth (sample 3873.3 from Wellington 1-32); (C) Transmitted light photomicrograph of primary FIAs in Mississippian baroque dolomite that contain two-phase hydrocarbon inclusions (sample 3876.0 from Wellington 1-32); (D) UV-epifluorescence photomicrograph of primary FIAs in Mississippian baroque dolomite that contain two-phase hydrocarbon inclusions fluorescing a bright blue color (sample 3876.0 from Wellington 1-32).

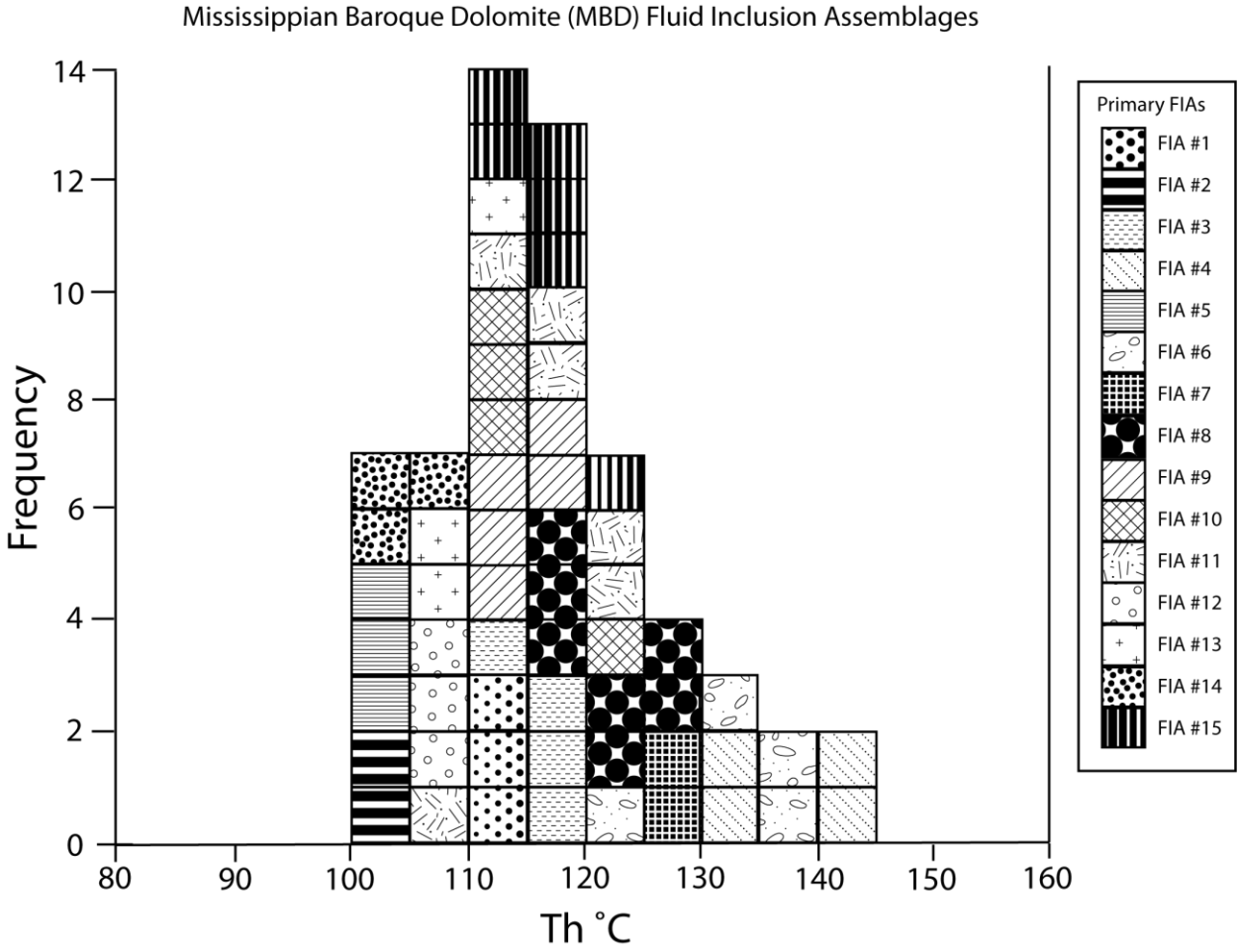


**Figure 3.15:** Histogram of homogenization temperatures (Th) measured from primary FIAs in Mississippian baroque dolomite (MBD). Measurements are most frequent between 110-120°C; the range of measurements likely reflects multiple pulses of hydrothermal fluid migration.

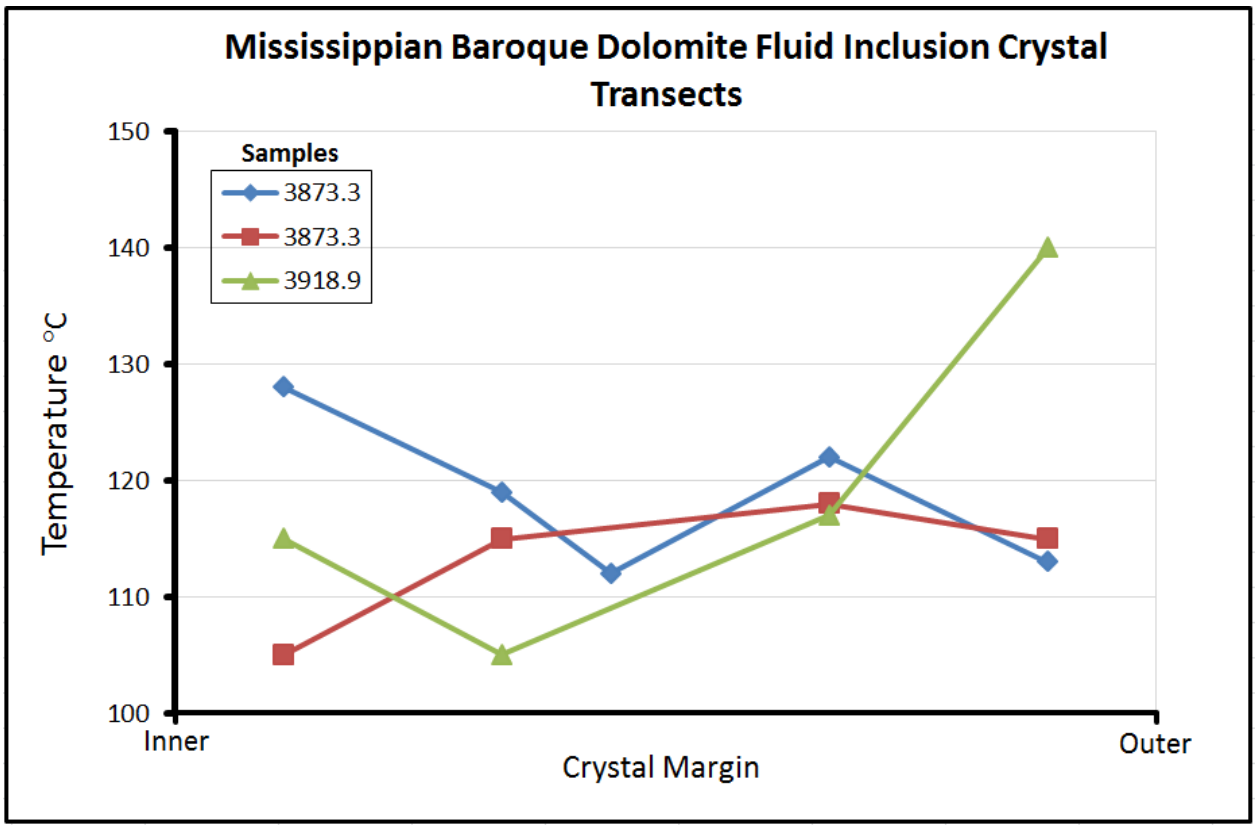


**Figure 3.16:** Homogenization temperatures measured in transects from the inner to outer crystal margin of Mississippian baroque dolomite (MBD). Fluctuations suggest migration of multiple fluid events at variable temperatures.

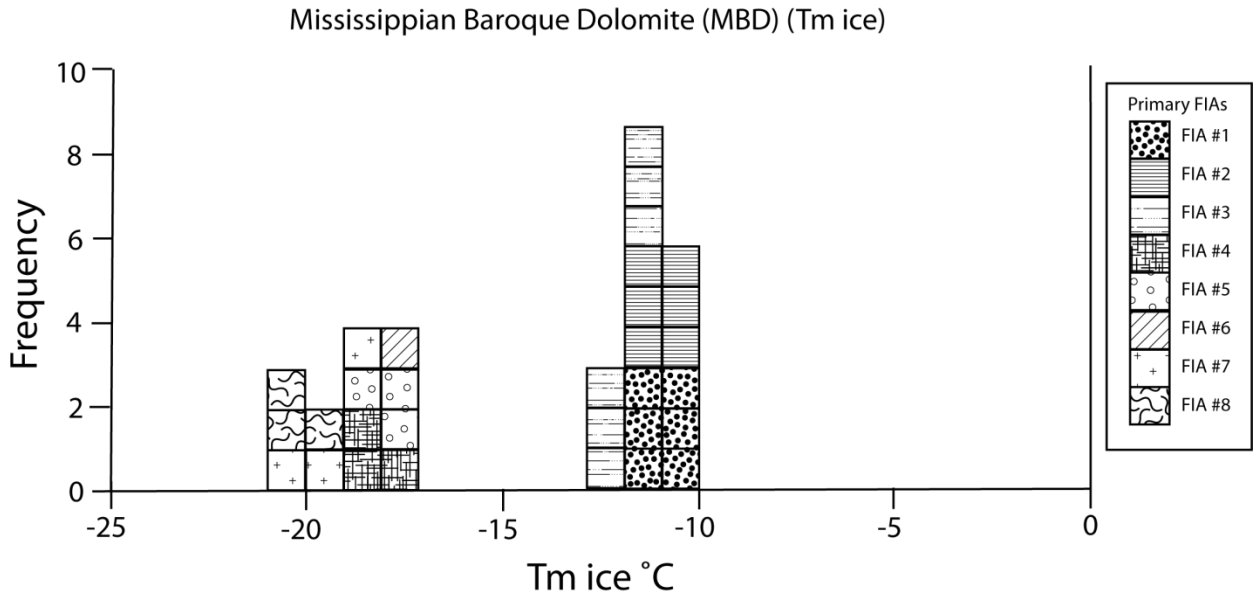


**Figure 3.17:** Histogram of final melting temperatures of ice (Tmice) measured from primary FIAs in Mississippian baroque dolomite (MBD). Range of values may represent mixing of high salinity Permian reflux with preexisting connate fluids or with later meteoric recharge.

### 6.2.3. Calcite cement

*Petrography:* Calcite cement (MCC) appears light yellow in color under transmitted light. Primary FIAs were observed as clustered fluid inclusions present in the center of individual crystals (Fig. 3.18A). Secondary FIAs can be observed as curviplanar features cutting across entire calcite crystals (Fig. 3.18C). Fluid inclusions within both FIA types are generally the same size and display irregular to negative crystal shapes, with small gas bubbles surrounded by an aqueous liquid; liquid-gas ratios among inclusions in an FIA appear consistent (Fig. 3.18B, 3.18D). All-liquid inclusions can be observed but are only those that are relatively small in size (<5μm). Petrographic pairing of all-liquid and two-phase inclusions is not observed, indicating inclusions did not neck down after a phase change (Goldstein and Reynolds, 1994).

*Microthermometry:* A total of seven consistent FIAs, four primary and three secondary, were subjected to heating for the purpose of obtaining Th data. Heating of fluid inclusions resulted in a gradual decrease in gas bubble size, until the two phases homogenized and the bubble disappeared. Primary FIAs produced the higher Th values, ranging from 93.0-103.5ºC, and secondary FIAs produced slightly lower Th values, ranging from 67.0-83.0ºC (Fig. 3.19). Th values of secondary FIAs in Arbuckle Group calcite (70.5-89.8°C) are close to that observed in secondary FIAs of Mississippian calcite.

A total of five consistent FIAs, three primary and two secondary, were subjected to freezing for the purpose of obtaining $Tm_{ice}$ values. Freezing of inclusions was typically accompanied by a sudden jerk and decrease in size of the gas bubble. Upon warming the inclusion, $Tm_{ice}$ was measured between -10.5 and -16.6ºC (Fig. 3.20). Melting involved consolidation of low-relief, rounded crystals into a larger crystal that slowly melted until completely disappearing. The melting of ice was commonly accompanied by sudden movement

of the gas bubble. $Tm_{ice}$ data resulted in salinities ranging from 14.5-19.9 wt. % NaCl eq. Similar to the Th data, $Tm_{ice}$ data produced distinct data sets for primary and secondary FIAs, with primary FIAs producing values ranging from -10.5 to -11.5ºC (14.5-15.5 wt. % NaCl eq.) and secondary FIAs producing values ranging from -16.2 to -16.6ºC (19.6-19.9 wt. % NaCl eq.).

*Interpretation:* Th measurements of two-phase fluid inclusions within consistent primary FIAs range from 93.0-103.5ºC, whereas secondary FIAs produced Th values ranging from 67.0-83.0ºC. Relatively small all-liquid inclusions can be observed, normally indicating formation at temperatures <50ºC. The fact that all-liquid inclusions are relatively small in size suggests nucleation metastability may play a role in the absence of a gas bubble (Goldstein and Reynolds, 1994). If small all-liquid inclusions are attributed to metastability, then fluid inclusion entrapment in primary FIAs most likely occurred during homogeneous conditions at least as high as the homogenization temperatures measured. Th measurements from secondary FIAs only give temperature of fluids during fracture healing after mineral growth, indicating conditions had cooled down at some point following original precipitation of calcite, but remained moderately high during the healing of microfractures.

When considering the moderately high Th values, high salinities, and believed link to Arbuckle Group baroque dolomite, a basinal-sourced fluid is the best candidate to account for the fluid inclusion data (e.g., Smith and Davies, 2006; Banner, 1995; Land, 1985; Hanor, 1979). A decrease in salinity from baroque dolomite to calcite indicates there could be freshwater mixing at the fluid source or at some point along the fluid migration pathway, gradually decreasing the salinity values. The subsequent increase in salinity during entrapment of secondary FIAs may represent a change in the fluid flow system, allowing for mixing from high

salinity fluids from a different source. A discussion regarding potential hydrologic models is provided in section 9.3.

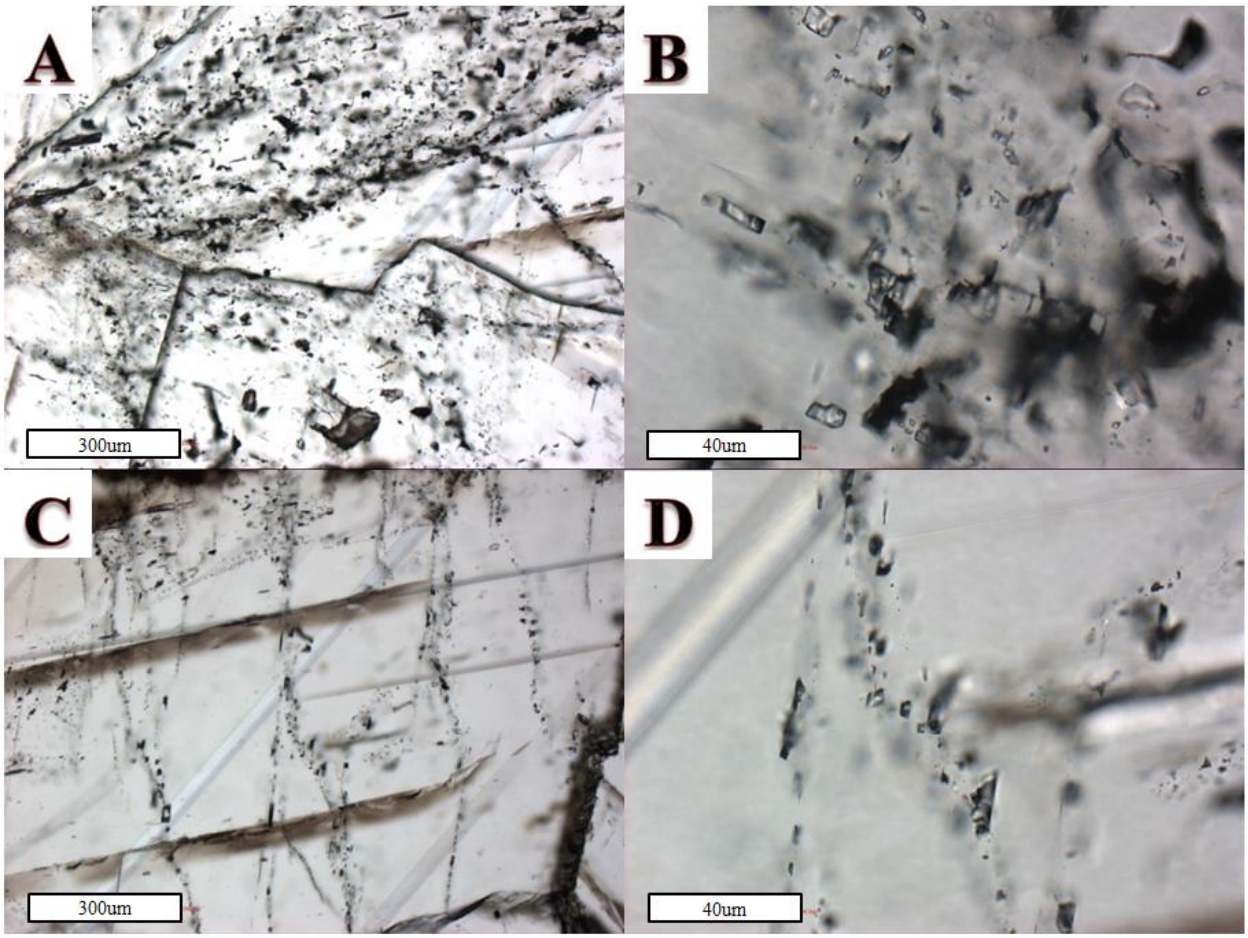


**Figure 3.18:** Transmitted light photomicrographs of fluid inclusions in MCC: (A) Primary FIAs present in the center of Mississippian calcite cement (MCC) crystals (sample 3775.5 from Wellington 1-32); (B) Two-phase fluid inclusions in primary FIAs in MCC that appear to be slightly elongated in the directions of crystal growth (sample 3775.5 from Wellington 1-32); (C) Secondary FIAs cutting across MCC crystals (sample 3775.5 from Wellington 1-32); (D) Two-phase fluid inclusions in secondary FIAs in MCC (sample 3775.5 from Wellington 1-32).

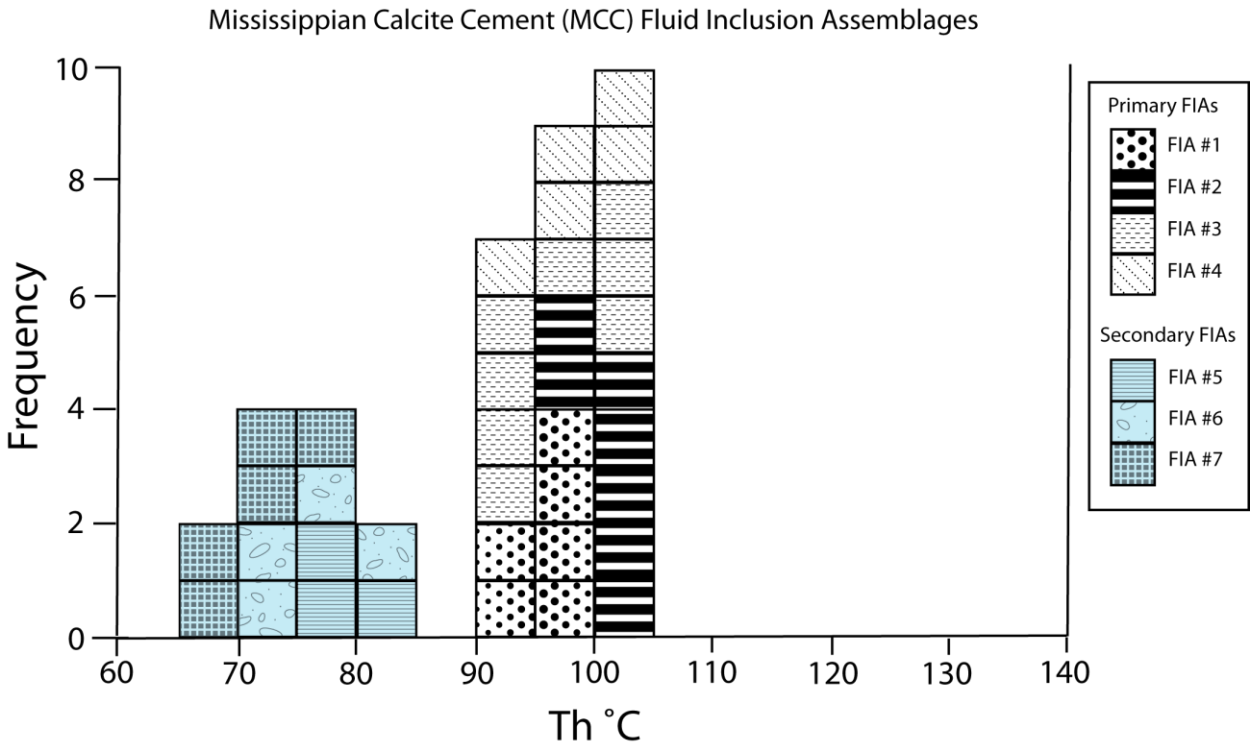


**Figure 3.19:** Histogram of homogenization temperatures (Th) from primary and secondary FIAs in Mississippian calcite cement (MCC). Primary FIAs produce temperatures noticeably higher than secondary FIAs.

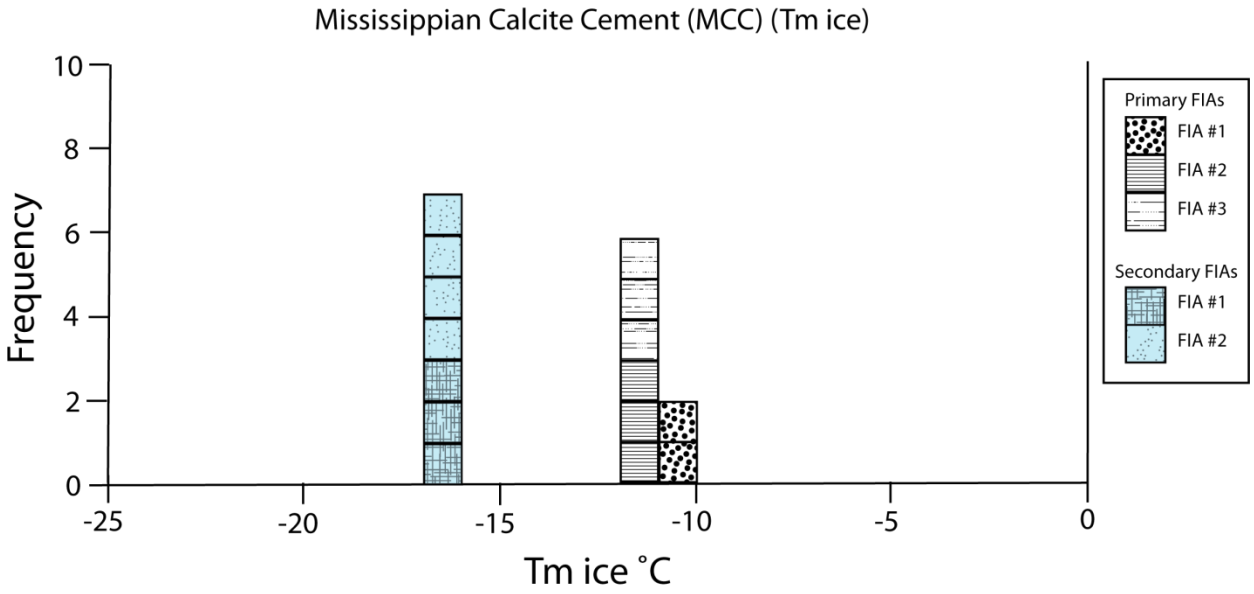


**Figure 3.20:** Histogram of final melting temperatures of ice ($Tm_{ice}$) from primary and secondary FIAs in Mississippian calcite cement (MCC). Primary FIAs are noticeably less saline than secondary FIAs.

### *6.3. Fluid Inclusion Discussion*

The current subsurface temperature at the top of the Arbuckle Group is approximately 44ºC (recorded from bottom-hole temperatures in Wellington 1-32 core), indicating that formation temperatures of the overlying units are no greater than this value. Modern formation temperatures (~44°C) require a substantially higher reservoir temperature some time in the geologic past to produce the Th values recorded in Simpson Group baroque dolomite (119.0-132.0ºC), Mississippian megaquartz cement (interpreted to be ≥86ºC), Mississippian baroque dolomite (100.0-144.0ºC), primary FIAs in Mississippian calcite cement (93.0-103.5ºC), and secondary FIAs in Mississippian calcite cement (67.0-83.0ºC) (Fig. 3.21). Potential hypotheses that could account for the increase in temperature include: (1) increased burial, (2) elevated geothermal gradient, or (3) injection of hydrothermal fluids. Both hypothesis (1) and (2) can be evaluated using a model of the burial history of strata in the study area. As discussed in Chapter 2, Newell (1997) produced a burial history model for Phanerozoic strata in McPherson and Harper Counties in Kansas (north and west of study area) (Fig. 3.22). Using the surface temperatures and geothermal gradients Newell did in his estimates, the McPherson County model (30°C/km and 1,500ft of Cretaceous strata) suggests a maximum temperature of approximately 74°C at the base of the Arbuckle Group and the Harper County model (25°C/km and 500ft of Cretaceous strata) suggests a maximum temperature of approximately 73°C at the base of the Arbuckle Group, both achieved early in Permian time (30°C surface temperature). According to Newell (1997), the highest reasonable geothermal gradient in both counties is 40°C/km, and Cretaceous thickness likely does not exceed 3,000ft in McPherson County and 500ft in Harper County. For comparison purposes, the maximum geothermal gradient (40°C/km) and thickness (3,000ft) were also used for each model. McPherson County produced

a maximum temperature of approximately 109°C at the base of the Arbuckle Group in the Cretaceous and Harper County produced a maximum temperature of approximately 113°C at the base of the Arbuckle Group in the Cretaceous. Values measured in baroque dolomite remain higher than can be explained by even the highest temperature estimates for the underlying Arbuckle Group, rendering hypothesis (1) and (2) unlikely. Moreover, the fluctuations in Th values measured in Mississippian baroque dolomite crystal transects cannot be reasonably accounted for by correlative fluctuations in burial or geothermal gradient.

Injection of hydrothermal fluids (hypothesis 3) would produce the elevated fluid inclusion measurements, and if migration of fluids occurred multiple times at different temperatures, it would also account for fluctuating Th values in transects (Fig. 3.16) and the changes in salinity in different cements (Fig. 3.21). The mineral assemblage of late cements in Simpson Group through Pennsylvanian strata are remarkably similar to the Arbuckle Group and MVT deposits in the mid-Continent, both of which are believed to be associated with migration of hydrothermal fluids from nearby basins (Chapter 2 of this study; Leach and Sangster, 1995; Garven, 1993; Bethke and Marshak, 1990; Sverjensky, 1986; Oliver, 1986). The overall fluid evolution of the fluid flow system affecting overlying strata appears to be very similar to what was interpreted from the Arbuckle Group data in Chapter 2 (Fig. 3.21), and seems to closely follow what Young (2010) interpreted from her diagenetic analysis of Mississippian strata near the study area.

Secondary fluid inclusions in calcite of both Arbuckle Group and Mississippian strata record moderate temperatures and high salinities. The secondary fluid inclusions likely represent a transition phase when temperatures were decreasing. In comparison to the modern system, the salinities in secondary fluid inclusions are similar to the high salinity values attained from

modern Mississippian fluids (<20.0%; KGS, 2010), but much higher than modern salinities observed in the Arbuckle Group (3-11%; Scheffer, 2012). This could mean that the modern Mississippian reservoir has retained fluids related to ancient fluid flow, whereas the Arbuckle Group acted as an aquifer, flushing ancient fluids and recharging the reservoir with modern fluids. Alternatively, proximity to Permian evaporites may be responsible for higher salinities in the modern Mississippian reservoir.

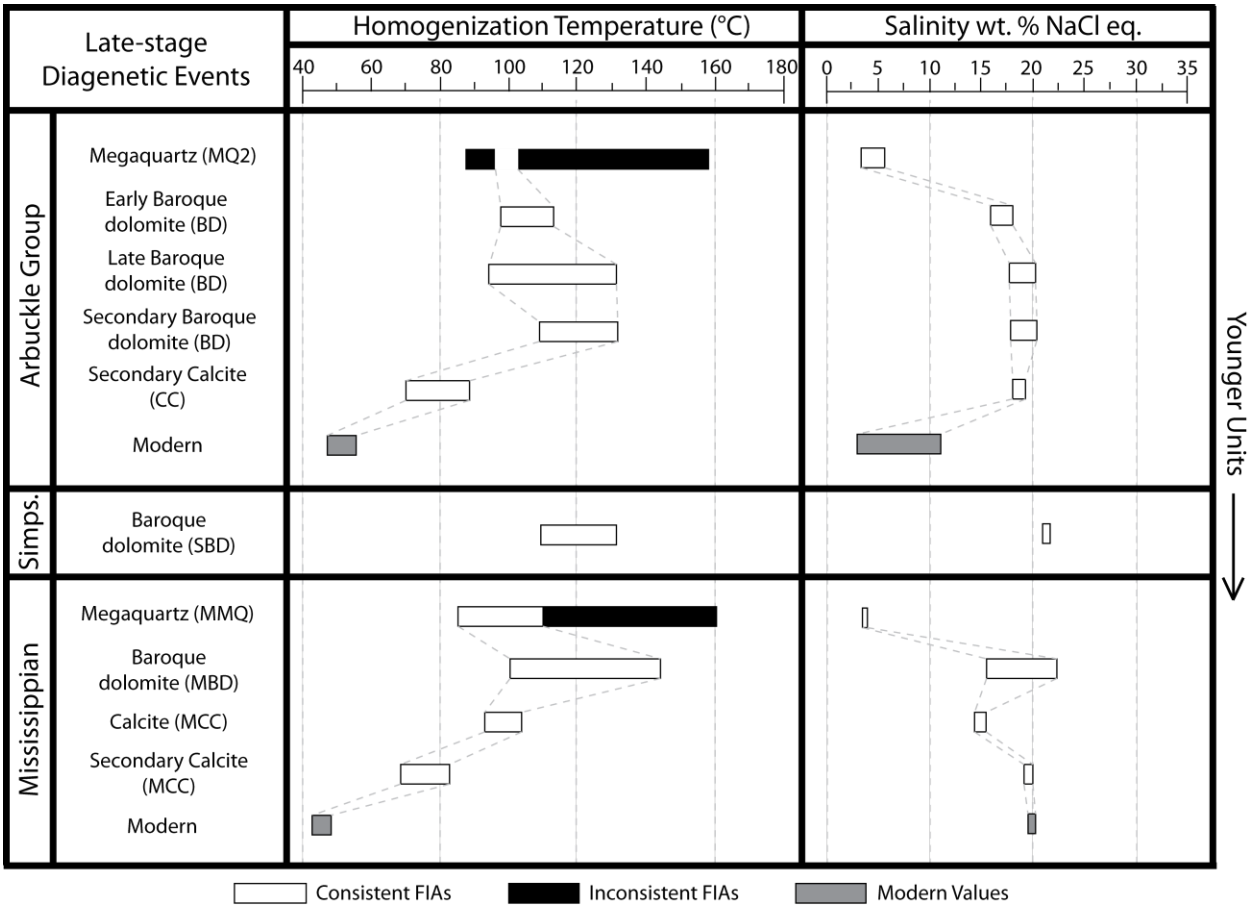

**Figure 3.21:** Diagram illustrating fluid and temperature evolution during the late-stage in Arbuckle Group, Simpson Group, and Mississippian strata. Both Arbuckle Group and Mississippian strata show elevated temperatures and relatively low salinities associated with precipitation of megaquartz cement; this is believed to be associated with initial migration of connate fluids from the Anadarko Basin. Temperatures and salinities then increase during precipitation of baroque dolomite in all three units, likely indicating fluid flow during or after evaporite precipitation in the Permian. Mississippian calcite forms in association with a slight decrease in fluid salinity and temperature, suggesting increasing influence of meteoric water associated with gravity-driven hydrothermal fluid flow. Secondary fluid inclusions in MCC are even lower temperature but show an increase in salinity; this is believed to represent the transition of the Mississippian strata to normal burial conditions. This may represent proximity to Permian evaporites and their dissolution. Modern fluids are much lower in temperature for both Arbuckle Group and Mississippian strata, while Arbuckle Group salinity decreases and Mississippian salinity remains about the same.

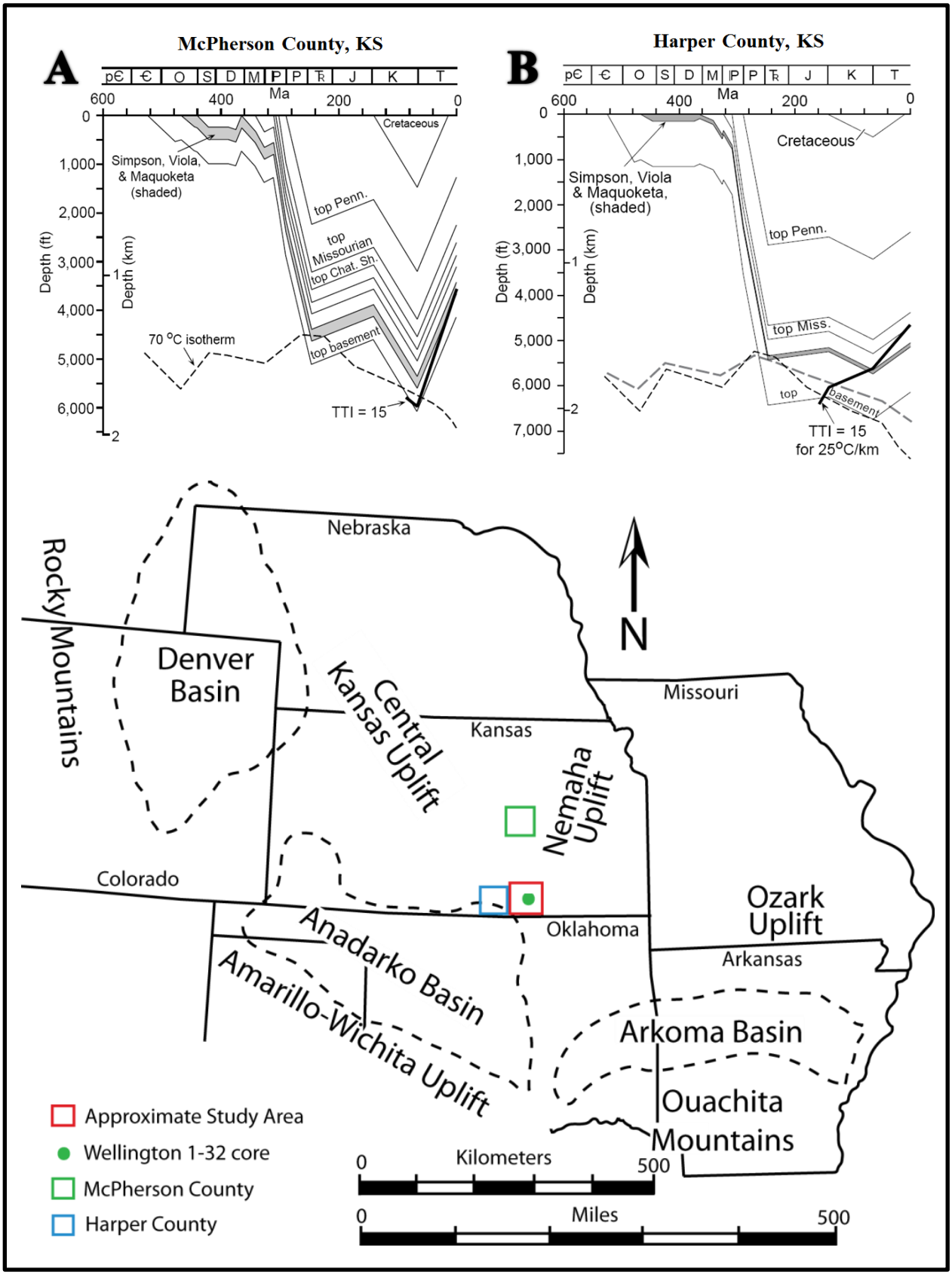
A
McPherson County, KS
pЄ Є O S D M P P Tr J K T
600 400 200 0
Ma
Cretaceous
Simpson, Viola, & Maquoketa (shaded)
top Penn.
top Missourian
top Chat. Sh.
top basement
70 °C isotherm
TTI = 15
Depth (ft)
Depth (km)
B
Harper County, KS
Cretaceous
Simpson, Viola & Maquoketa, (shaded)
top Penn.
top Miss.
top basement
TTI = 15 for 25°C/km
Nebraska
N
Rocky Mountains
Denver Basin
Central Kansas Uplift
Kansas
Missouri
Nemaha Uplift
Colorado
Oklahoma
Ozark Uplift
Arkansas
Anadarko Basin
Amarillo-Wichita Uplift
Arkoma Basin
Ouachita Mountains
Approximate Study Area
Wellington 1-32 core
McPherson County
Harper County
0 Kilometers 500
0 Miles 500

**Figure 3.22:** Top image shows burial history models for Phanerozoic strata in McPherson and Harper Counties in Kansas (north and west of study area). Assuming the thickness of Cretaceous strata and geothermal gradients to be 1500ft (460m) and 30°C/km for McPherson County and 500ft (150m) and 25°C/km for Harper County; a 70°C geotherm was also calculated for both models (modified from Newell 1997). When considering Cambrian-Ordovician strata, the McPherson County model suggests a maximum temperature of approximately 74°C and the Harper County model suggests a maximum temperature of approximately 73°C, both achieved early in Permian time. The bottom image displays the location of the counties with the burial history models, relative to the study area, significant basins, and uplifts in the region (modified from Garven, 1993).

## 7. Oxygen and Carbon Isotopic Data

The following section discusses oxygen ($\delta^{18}O$) and carbon ($\delta^{13}C$) isotopic values from carbonate samples collected from Middle Ordovician (Simpson Group), Mississippian (Lower and Upper Series), and Pennsylvanian (Cherokee Group) strata (Appendix IV). Isotopic values are presented as ‰ VPDB. Units are discussed from the deepest to the shallowest depths, beginning with the baroque dolomite present in the Simpson Group. The range and average of data, as well as any observable trends, are listed first. Interpretations of $\delta^{18}O$ and $\delta^{13}C$ isotopic values, spatial variations of values, and potential fluid flow models are discussed for each precipitate.

### *7.1. Ordovician (Simpson Group)*

#### 7.1.1. Baroque dolomite

One stratigraphic horizon containing baroque dolomite (SBD) was microsampled and processed for $\delta^{18}O$ and $\delta^{13}C$ isotopic values; the sample was taken from the Wellington 1-32 core. The $\delta^{18}O$ value was -9.0‰ and the $\delta^{13}C$ value was -2.4‰ (Fig. 3.23) (Appendix IV). Both $\delta^{18}O$ and $\delta^{13}C$ values fall within the range observed in Arbuckle Group baroque dolomite (-6.6 to -10.2‰ and -2.4 to -3.6‰) (Fig. 3.23).

Clearly, one sample cannot provide a trend, or any notable observations regarding spatial variability within the Simpson Group. However, it does provide a data point that can be compared with values recorded from baroque dolomite in the Arbuckle Group and Mississippian strata. Comparisons with isotopic values recorded in the units that bracket the Simpson Group can shed light on the fluid migration history, which is discussed next.

*Interpretation:* The $\delta^{18}O$ value of baroque dolomite is -9.0‰. According to Lohmann and Walker (1989), Middle Ordovician marine calcite samples produce $\delta^{18}O$ values ranging from approximately -4.5 to -6.5‰. Land (1980; 1985) established that dolomite forming coeval to calcite would likely be enriched by approximately 3‰, allowing for estimations of low-temperature dolomite precipitated from Middle Ordovician seawater to be as depleted as -3.5‰. The $\delta^{18}O$ value in baroque dolomite is more negative than these values (by 6.5‰), eliminating a low-temperature seawater model.

The depleted $\delta^{18}O$ value in Simpson Group baroque dolomite correlates well with the previous interpretation of this cement resulting from hydrothermal activity. Though alternative models could be proposed that would account for depletion of $\delta^{18}O$ (meteoric or mixing-zone models), the elevated Th values, late-stage precipitation, and belief of a close association with Arbuckle Group baroque dolomite supports injection of fluids at temperatures higher than the formation temperature. High temperature fluids would allow for thermal fractionation to deplete $\delta^{18}O$ values. The most likely explanation for the presence of hydrothermal baroque dolomite in the Simpson Group is that the unit acted as a siliciclastic aquifer for advective fluids migrating from the nearby Anadarko basin. Homogenization temperatures and $\delta^{18}O_{dolomite}$ PDB data allow for an approximation of $\delta^{18}O_{water}$ PDB (Land, 1985 published equation):

*Equation 3.2:* $10^3 \ln \alpha = 2.78 * 10^6 / T^2 + 0.91$

where ($10^3$ ln α) is approximately equal to ($\delta^{18}O_{dolomite}$ - $\delta^{18}O_{water}$) and T is temperature in Kelvin (Land, 1985). The $\delta^{18}O_{water}$ PDB was then converted to $\delta^{18}O_{water}$ SMOW (Arthur et al., 1983). The highest and lowest recorded temperature values and the single $\delta^{18}O$ value were used in the equation above, producing $\delta^{18}O_{water}$ values of +2.0 and +3.2‰. The enrichment of $\delta^{18}O_{water}$ values is common in residual evaporite brines and could also be produced by long-term rock-water interaction at high temperatures (Epstein and Mayeda, 1953; Heimstra, 2003).

The $\delta^{13}C$ value of baroque dolomite is -2.4‰. The slight depletion of $\delta^{13}C$ values may be associated with thermochemical sulphate reduction (TSR). The Th values from fluid inclusions (119-132°C) fall within the range proposed by Machel (2001) (100-140°C) for this mechanism of carbon depletion to play an important role in the observed values.

### *7.2. Mississippian*

#### 7.2.1. Baroque dolomite

A total of two stratigraphic horizons containing baroque dolomite (MBD) were micro-sampled and processed for $\delta^{18}O$ and $\delta^{13}C$ isotopic values; all of the micro-samples were taken from the Wellington 1-32 core. Both horizons were microsampled multiple times, providing a total of five isotopic analyses (Appendix IV). The $\delta^{18}O$ values range from the most depleted value of -10.3‰ to the most enriched value of -8.3‰, with an average of -9.4‰ (Fig. 3.23) (Appendix IV). The $\delta^{13}C$ values range from the most depleted value of 1.6‰ to the most enriched value of 2.0‰, with an average of 1.9‰ (Fig. 3.23) (Appendix IV). $\delta^{18}O$ values are near the most depleted end of those in the Arbuckle Group (-6.6 to -10.2‰), whereas $\delta^{13}C$ values are more enriched than Arbuckle Group samples (-2.4 to -3.6‰) (Fig. 3.23).

Similar to the Arbuckle Group, $\delta^{18}O$ values become slightly more depleted with decreasing depth, with an overall decrease of -2.1‰ (-8.3‰ to -10.3‰) (Fig. 3.24), but the sample size only consists of two samples that are close to the base of the Mississippian strata. $\delta^{13}C$ values remain fairly constant from sample to sample. As with the Simpson Group, the MBD isotopic data is best used for comparison purposes with data gathered from other units, providing insight into the fluid migration history.

*Interpretation:* The $\delta^{18}O$ values range from the most negative value of -10.3‰ to the most positive value of -8.3‰, with an average of -9.4‰. According to Lohmann and Walker (1989), Mississippian marine calcite $\delta^{18}O$ values ranged from -2‰ in the early Mississippian and became more enriched toward the end of the Mississippian, to a value around -1‰. Land (1980; 1985) established that dolomite forming coeval to calcite would likely be enriched by approximately 3‰, allowing for estimations of low-temperature dolomite precipitated from Mississippian seawater to be as high as 1.0 to 2.0‰. Not surprisingly, both of the $\delta^{18}O$ values in baroque dolomite are more negative than these values (by at least 9.3‰), eliminating a low-temperature seawater model.

Though meteoric and mixing-zone models could account for further depletion of $\delta^{18}O$ values, it would be difficult to account for the observed range of Th values in Mississippian baroque dolomite (100.0-144.0°C). When combined with elevated Th values, especially values that have been found to be too high to be accounted for by burial conditions or an elevated geothermal gradient (see 6.3. Fluid Inclusion Discussion), depleted $\delta^{18}O$ values are most reasonably accounted for by injection of hydrothermal fluids into the formation, allowing for thermal fractionation to deplete $\delta^{18}O$.

Petrographic observations, fluid inclusion data, and $\delta^{18}O$ values all correlate well with values observed in the Arbuckle Group. Assuming that these correlations define a genetic link to fluids responsible for late-stage baroque dolomite in the Arbuckle Group, a similar basin-derived model can be applied to Mississippian strata. These fluids migrated via advective fluid flow into the study area, with the Mississippian acting as an aquifer for the high temperature-high salinity fluids. Using the equation and technique outlined in the Simpson Group baroque dolomite section (7.1.1.), $\delta^{18}O_{water}$ SMOW was calculated for the range of values recorded in Mississippian baroque dolomite. The $\delta^{18}O$ values of fluids responsible for precipitating baroque dolomite may have ranged from -1.2 to +4.9‰. Enriched $\delta^{18}O_{water}$ values are common in residual evaporite brines and could also be produced through long-term rock-water interaction during heating in the basin (Epstein and Mayeda, 1953). These values are similar to those interpreted for baroque dolomite in the Arbuckle Group (-1.9 to +5.6‰). If one assumes a consistent isotopic composition of the fluid during baroque dolomite precipitation (+2.0‰), the range in isotopic composition yields a temperature range of 22ºC, a range that is about half of that observed in fluid inclusion data (44ºC).

The $\delta^{13}C$ values range from the most depleted value of 1.6‰ to the most enriched value of 2.0‰. According to Lohmann and Walker (1989), $\delta^{13}C$ for Mississippian strata was around 4‰. Baroque dolomite is 2.0-2.4‰ more depleted than what would be expected from Mississippian seawater, requiring an alternative explanation for the depleted values. The most likely explanation for the depletion of carbon is that high temperatures (100.0-144.0C) allowed for TSR to be an active mechanism during the time of fluid migration.

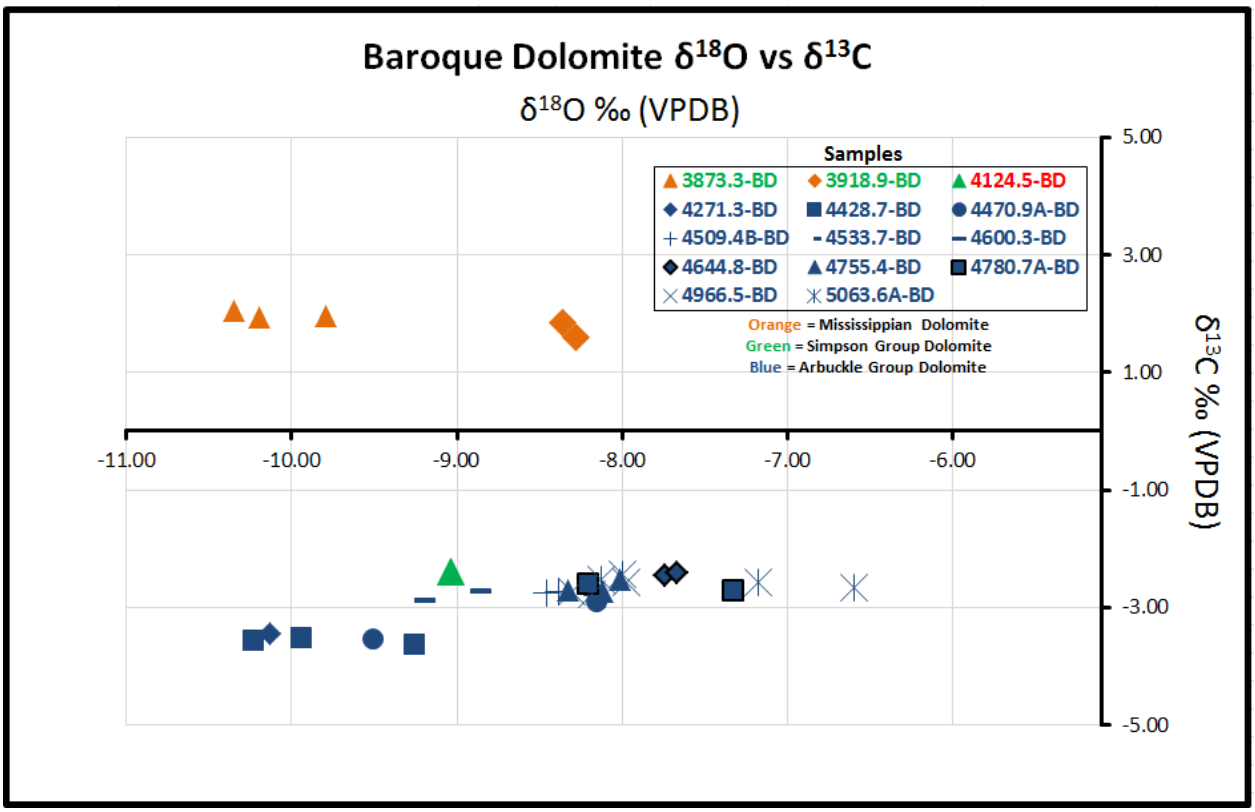


**Figure 3.23:** Cross-plot of baroque dolomite $\delta^{18}O$ and $\delta^{13}C$ from Arbuckle Group (blue data points), Simpson Group (green data point), and Mississippian (orange data points). Arbuckle Group and Simpson Group have similar $\delta^{18}O$ and $\delta^{13}O$ values, whereas Mississippian strata has similar $\delta^{18}O$ values but more enriched $\delta^{13}C$.

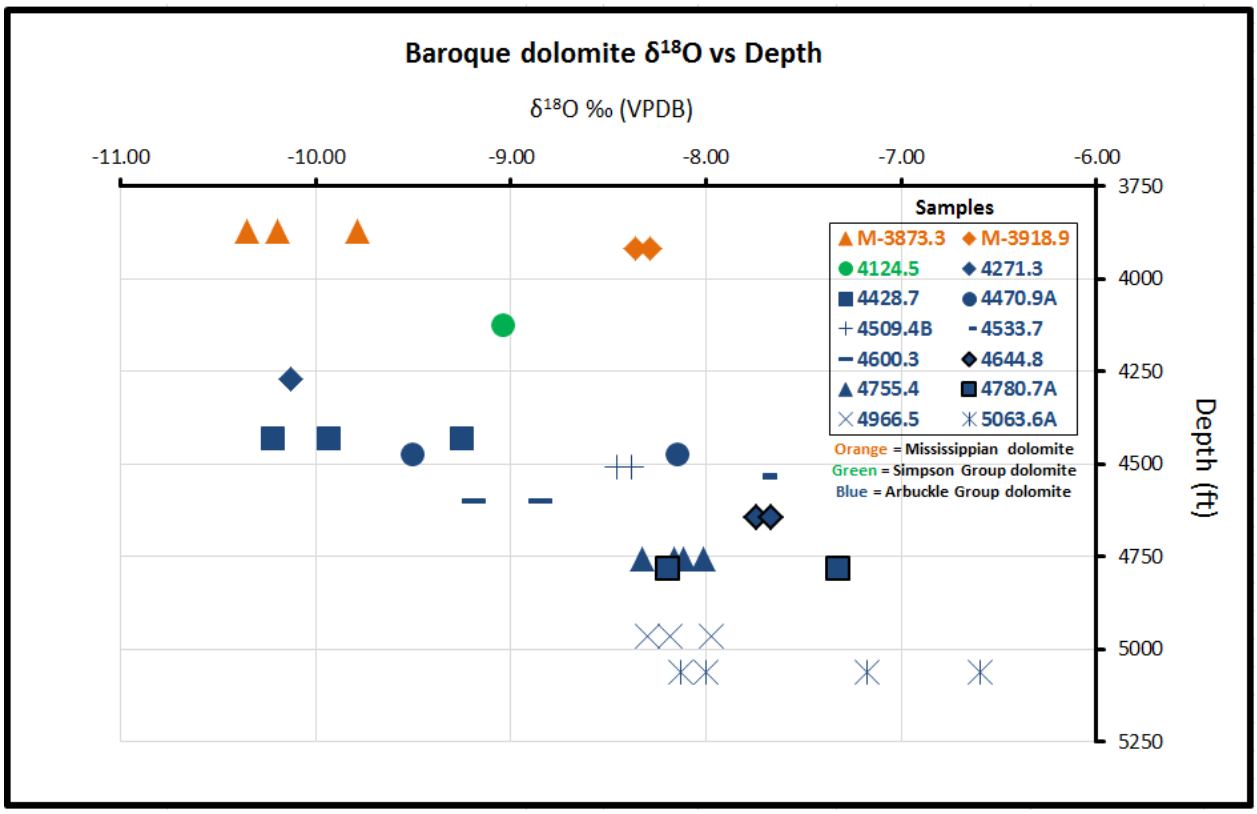


**Figure 3.24:** Cross-plot of baroque dolomite $\delta^{18}O$ and depth of Arbuckle Group (blue data points), Simpson Group (green data point), and Mississippian (orange data points). Arbuckle Group values become more depleted with decreasing depth and the most depleted range of values is present in Mississippian strata. The Simpson Group values falls between Arbuckle Group and Mississippian values.

### 7.2.2. Calcite cement

A total of five stratigraphic horizons containing calcite (MCC) were microsampled and processed for $\delta^{18}O$ and $\delta^{13}C$; all samples were taken from the Wellington 1-32 core. All of the horizons were microsampled multiple times, providing a total of fourteen isotopic analyses (Appendix IV). The $\delta^{18}O$ values range from the most negative value of -10.3‰ to the most positive value of -8.4‰, with an average of -8.9‰ (Fig. 3.25) (Appendix IV). The $\delta^{13}C$ values range from the most negative value of -0.4‰ to the most positive value of 1.7‰, with an average of 0.6‰ (Fig. 3.25) (Appendix IV). $\delta^{18}O$ values are slightly more depleted than values observed in Arbuckle Group calcite (-9.8 to -7.0‰), whereas $\delta^{13}C$ values are much more enriched than the

Arbuckle Group calcite (-18.5 to -3.7‰) (Fig. 3.25). There do not appear to be any recognizable trends with calcite data versus depth.

*Interpretation:* The $\delta^{18}O$ values range from the most negative value of -10.3‰ to the most positive value of -8.4‰. Marine calcite in the Mississippian has $\delta^{18}O$ values ranging from -2‰ in the early Mississippian to -1‰ later in the Mississippian (Lohmann and Walker, 1989). The $\delta^{18}O$ data are at least 6.4‰ more depleted than the most depleted value that could be expected from low-temperature Mississippian seawater. Similar to the isotope discussion for other late-stage cements in this study, a low-temperature seawater model cannot account for the presence of late-stage calcite cement in the Mississippian.

Meteoric and mixing-zone models could deplete $\delta^{18}O$ values, but neither can account for the temperatures and other geochemical characteristics produced by the samples. Again, injection of hydrothermal fluids is the best explanation for the high temperatures, which would allow for thermal fractionation to deplete $\delta^{18}O$ values. Similar to baroque dolomite, high temperatures, high salinities, and depleted $\delta^{18}O$ values could all be accounted for by migration of hydrothermal fluids that were sourced from the Anadarko basin. One can calculate the $\delta^{18}O_{water}$ of fluids responsible for calcite precipitation using the Th range. O'Neil et al. (1969) provide the equation:

$$\textit{Equation 3.3:}\quad 10^3 \ln \alpha = 2.78 * 10^6 / T^2 - 2.89$$

where ($10^3 \ln \alpha$) is approximately equal to ($\delta^{18}O_{calcite} - \delta^{18}O_{water}$) and T is temperature in Kelvin. The $\delta^{18}O_{water}$ PDB is then converted to $\delta^{18}O_{water}$ SMOW (Arthur et al., 1983). The $\delta^{18}O$ values of fluids responsible for precipitating calcite ranged from +5.0 to +1.8‰, a range that is consistent with evaporative brines or long-term rock-water interaction (Epstein and Mayeda, 1953). If one assumes a consistent isotopic composition of the fluid during calcite precipitation (+3.0‰), the

range in isotopic composition yields a temperature range of 17ºC, a range that is similar to that observed in fluid inclusion data (10.5ºC).

The $\delta^{13}C$ values range from the most negative value of -0.4‰ to the most positive value of 1.7‰. Similar to Mississippian baroque dolomite, the slight depletion of carbon in the calcite sample could be attributed to TSR. Primary fluid inclusions within calcite give temperatures ranging from 93.0-103.5ºC, with some values below and some values above Machel's (2001) estimated range for TSR (100-140°C).

An observation that should be noted is the significant difference between $\delta^{13}C$ values of Mississippian calcite (-0.4 to 1.7‰) and Arbuckle Group calcite (-18.5 to -3.7‰). The difference in $\delta^{13}C$ values may represent a differing degree of rock-water interaction in the two units, and that the fluids actually have the same origin; similar $\delta^{18}O$ values support the idea of similar fluids.

### *7.3. Pennsylvanian (Cherokee Group)*

#### 7.3.1. Calcite cement

One stratigraphic horizon containing Pennsylvanian calcite (PCC) was microsampled and processed for $\delta^{18}O$ and $\delta^{13}C$ isotopic values relative to VPDB; the sample was taken from the Wellington 1-32 core. The $\delta^{18}O$ value was -9.1‰ and the $\delta^{13}C$ value was -1.5‰ (Fig. 3.25) (Appendix IV). The $\delta^{18}O$ value falls within the range observed in calcite cements analyzed in underlying stratigraphic units, whereas the $\delta^{13}C$ value is slightly more depleted than Mississippian calcite (-0.4 to 1.7‰), but less depleted than Arbuckle Group calcite (-18.5 to -3.7‰) (Fig. 3.25).

As was noted in the Simpson Group section, one sample cannot provide a trend or any notable observations regarding spatial variability within the Cherokee Group. However, it does provide a data point that can be compared with values recorded from calcite in the Arbuckle Group and Mississippian strata.

*Interpretation:* The $\delta^{18}O$ value of calcite was -9.1‰. According to Lohmann and Walker (1989), Carboniferous low-temperature marine calcite samples produce $\delta^{18}O$ values that fall within a range from approximately -1.0 to -2.0‰. The $\delta^{18}O$ values in Pennsylvanian calcite are more negative than these values (by at least 7.1‰), eliminating a low-temperature seawater model.

The lack of microthermometric data and additional geochemical data severely limits the potential for interpretations regarding Pennsylvanian calcite. Meteoric, mixing-zone, and elevated temperature models could all provide depleted $\delta^{18}O$ values. Wojcik et al. (1992; 1994; 1997) conducted a diagenetic study on Pennsylvanian strata near the study area. They found evidence for early-, intermediate-, and late-stage calcite cementation events. In Wojcik et al.'s (1994; 1997) study, he stated that he observed a rare non-ferroan calcite cement as the latest event of precipitation, but no further analysis was provided. As is the case with previous cements discussed, depletion of $\delta^{18}O$ may result from thermal fractionation and depleted $\delta^{13}C$ may result from TSR.

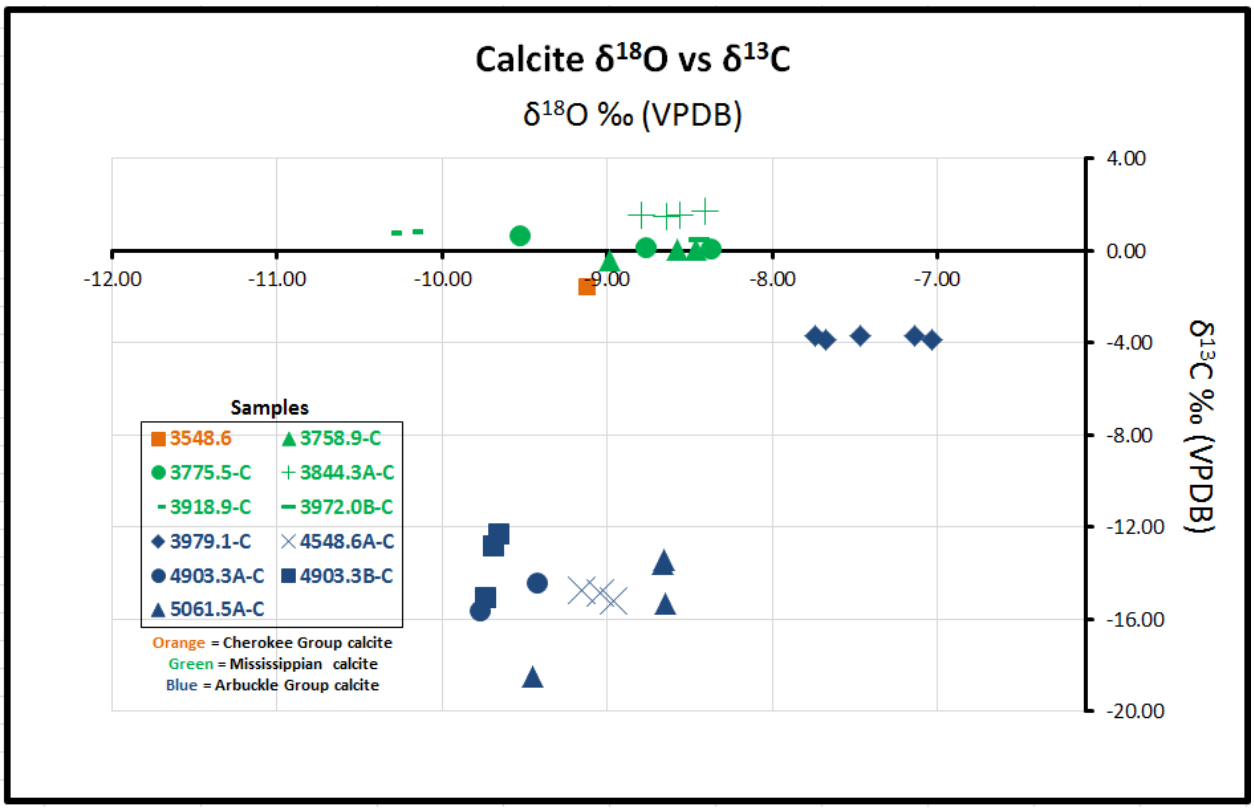


**Figure 3.25:** Cross-plot of calcite $\delta^{18}O$ and $\delta^{13}O$ of Arbuckle Group (blue data points), Mississippian (green data points), and Cherokee Group (orange data point). Arbuckle Group displays a wide range of data with the most enriched cluster of data points being recorded from calcite in the Vulcan core. Mississippian and Cherokee Group calcite displays significantly more enriched $\delta^{13}C$ values than those recorded from Arbuckle Group calcite.

## 8. Strontium Isotopic Data

The following section discusses strontium concentration and $^{87}Sr/^{86}Sr$ from the analysis of two baroque dolomite and five calcite samples obtained from Mississippian strata (Appendix IV). Baroque dolomite (MBD) is discussed first, followed by calcite cement (MCC). The range and average of data, as well as any observable trends, are presented first. Discussions of observed values and trends are offered at the end of each section. For comparison purposes, all values mentioned from previous authors' work have been normalized to NBS 987 at 0.710250.

### *8.1. Mississippian*

#### 8.1.1. Baroque dolomite

A total of two samples of baroque dolomite (MBD) were sampled from the Wellington 1-32 core; both samples were also paired with carbon and oxygen isotope analysis. Samples were at depths of 3873.3' and 3918.9', near the basal portion of Mississippian strata in the study area. Strontium concentrations range from 59 to 2590 ppm with an average of 1324 ppm, whereas $^{87}Sr/^{86}Sr$ values ranged from 0.70848 to 0.70976 with an average of 0.70912 (Fig. 3.26) (Appendix IV). The most radiogenic $^{87}Sr/^{86}Sr$ value falls within the range observed in Arbuckle Group baroque dolomite (0.70908 to 0.71019), whereas the other sample is slightly less radiogenic (0.70848) (Fig. 3.26).

Strontium concentration and $^{87}Sr/^{86}Sr$ cross-plots show that concentration decreases as ratio values become more radiogenic (Fig. 3.26). $^{87}Sr/^{86}Sr$ values were also cross-plotted with the $\delta^{13}C$ and $\delta^{18}O$ values derived from the same samples (Fig. 3.27, 3.28). The cross-plot with $\delta^{18}O$ data displays a trend of increasingly radiogenic values being associated with increasingly depleted $\delta^{18}O$, with the most radiogenic value (0.70976) being linked with the most depleted value (-10.11‰ VPDB) (Fig. 3.27). The cross-plot with $\delta^{13}C$ data displays the opposite trend, with the most radiogenic value being associated with the most enriched $\delta^{13}C$ value (Fig. 3.28). The fact that there are only two samples limits interpretations of what this may mean for Mississippian strata alone, but it does aid in comparison to other stratigraphic units.

*Interpretation:* Mississippian seawater yields $^{87}Sr/^{86}Sr$ values that fall within a range of approximately 0.70755-0.70812 (Denison et al., 1994). Both baroque dolomite samples produced values more radiogenic than unmodified Mississippian. The most depleted sample (0.70976) is more radiogenic than any seawater values from the Cambrian (0.70904) to the

modern (0.70896) (Denison et al., 1998). The radiogenic nature of the baroque dolomite samples suggests rock-water interaction with siliciclastic material or basement rock at some point during the fluid migration history (Banner, 1995). The $^{87}Sr/^{86}Sr$ values provide additional support to the earlier interpretation of oxygen isotopic data, supporting a basinal source for the fluids responsible for late-stage baroque dolomite precipitation (See Section 7.1.).

The limitation of two samples makes it difficult to decipher much from the spatial variability in the data (Section 8.1. and 8.2.). The most notable variability is that the most depleted $\delta^{18}O$ value (-10.3‰) is recorded from the same sample that has the most radiogenic $^{87}Sr/^{86}Sr$ value (0.70976) (Fig. 3.27), suggesting that the hottest fluids may have undergone the least amount of rock-water interaction, allowing for the geochemical signatures to be water-dominated. The cross-plot with $\delta^{13}C$ data displays a trend of increasingly radiogenic values being associated with increasingly enriched $\delta^{13}C$ values (Fig. 3.28), indicating there may be another controlling factor other than temperature behind depletion of carbon; this could possibly be linked with the location of organic matter in the Mississippian interval.

The observation that one of the $^{87}Sr/^{86}Sr$ values falls within the range observed in the Arbuckle Group, and that the other is still more radiogenic than Mississippian seawater, supports the idea of this cement being genetically related to Arbuckle Group baroque dolomite. As discussed in the oxygen and carbon isotope section, a fluid flow system consisting of advective fluid flow sourced from the Anadarko basin, subsequent to extensive rock-water interaction with siliciclastic material or basement rock, could account for the geochemical characteristics of Mississippian baroque dolomite.

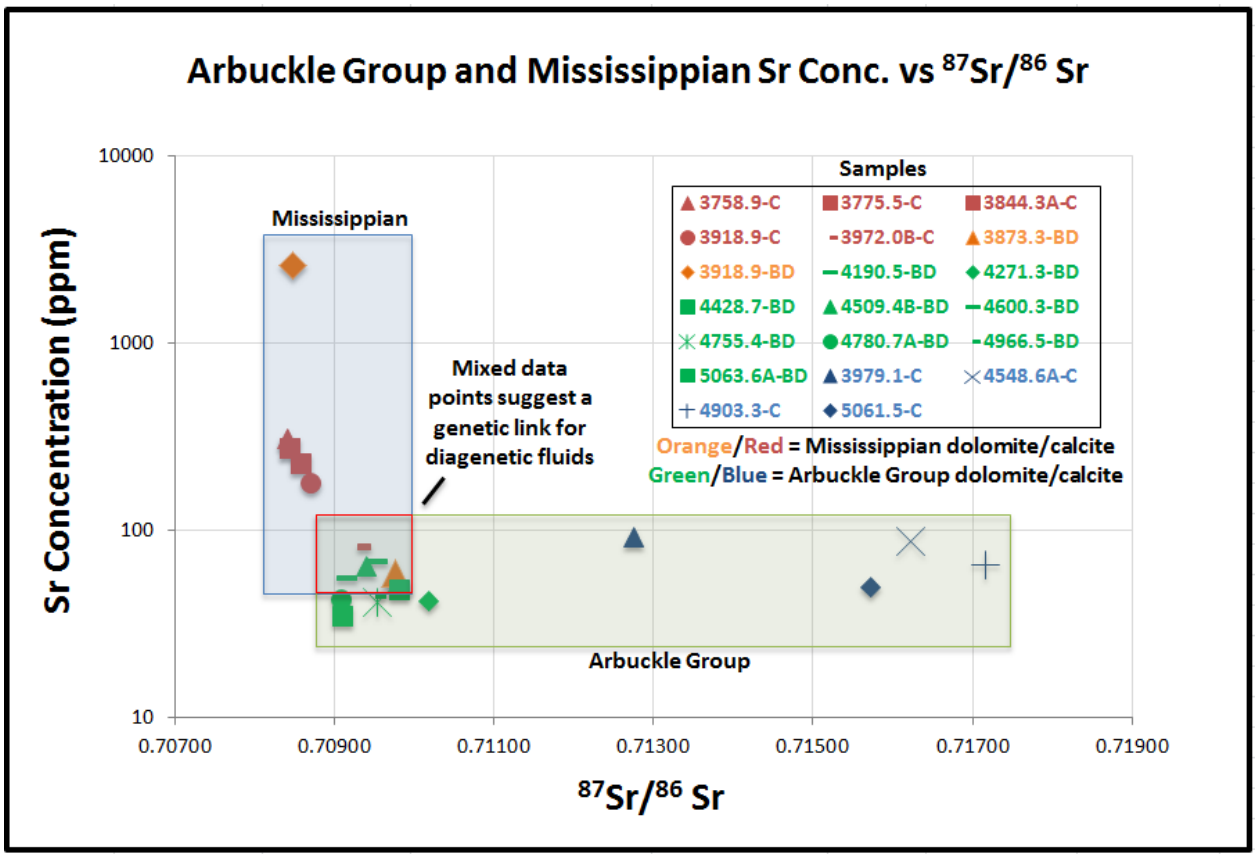


**Figure 3.26:** Cross-plot of strontium concentration and $^{87}Sr/^{86}Sr$ of Arbuckle Group baroque dolomite (green data points) and calcite (blue data points) and Mississippian baroque dolomite (orange data points) and calcite (red data points). Arbuckle Group baroque dolomite and Mississippian baroque dolomite and calcite fall within a similar range of $^{87}Sr/^{86}Sr$, suggesting a similar fluid source or migration pathway. Arbuckle Group calcite is notably more radiogenic than the other cements, supporting the hypothesis of this cement marking the influence of a different fluid flow system related to vertical migration of fluids sourced from fractures connecting the underlying Reagan sandstone or basement rock with overlying strata.

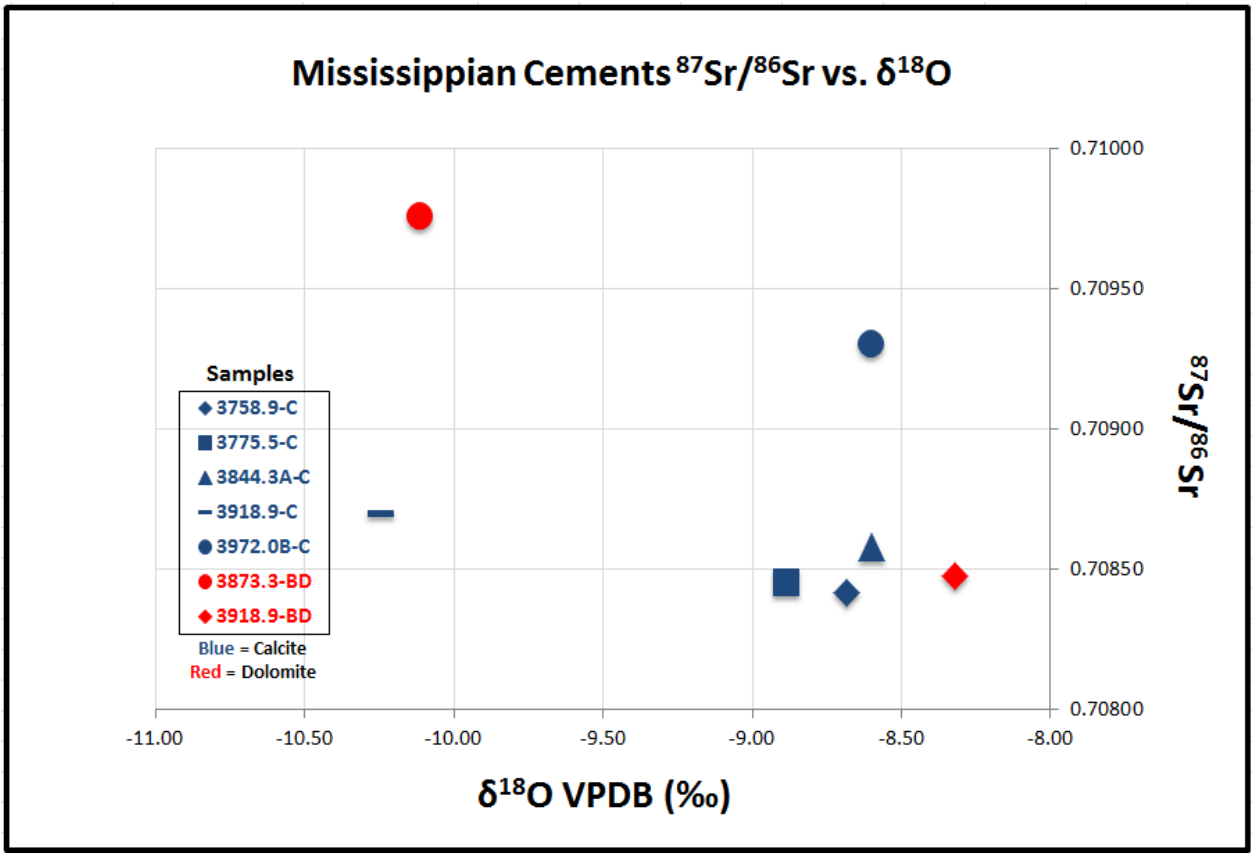


**Figure 3.27:** Cross-plot of $^{87}Sr/^{86}Sr$ and $\delta^{18}O$ of Mississippian baroque dolomite (red data points) and calcite (blue data points). Baroque dolomite displays a trend of the most radiogenic $^{87}Sr/^{86}Sr$ value being linked with the most depleted $\delta^{18}0$ value, though this is based on only two samples. There is no observable trend in calcite data.

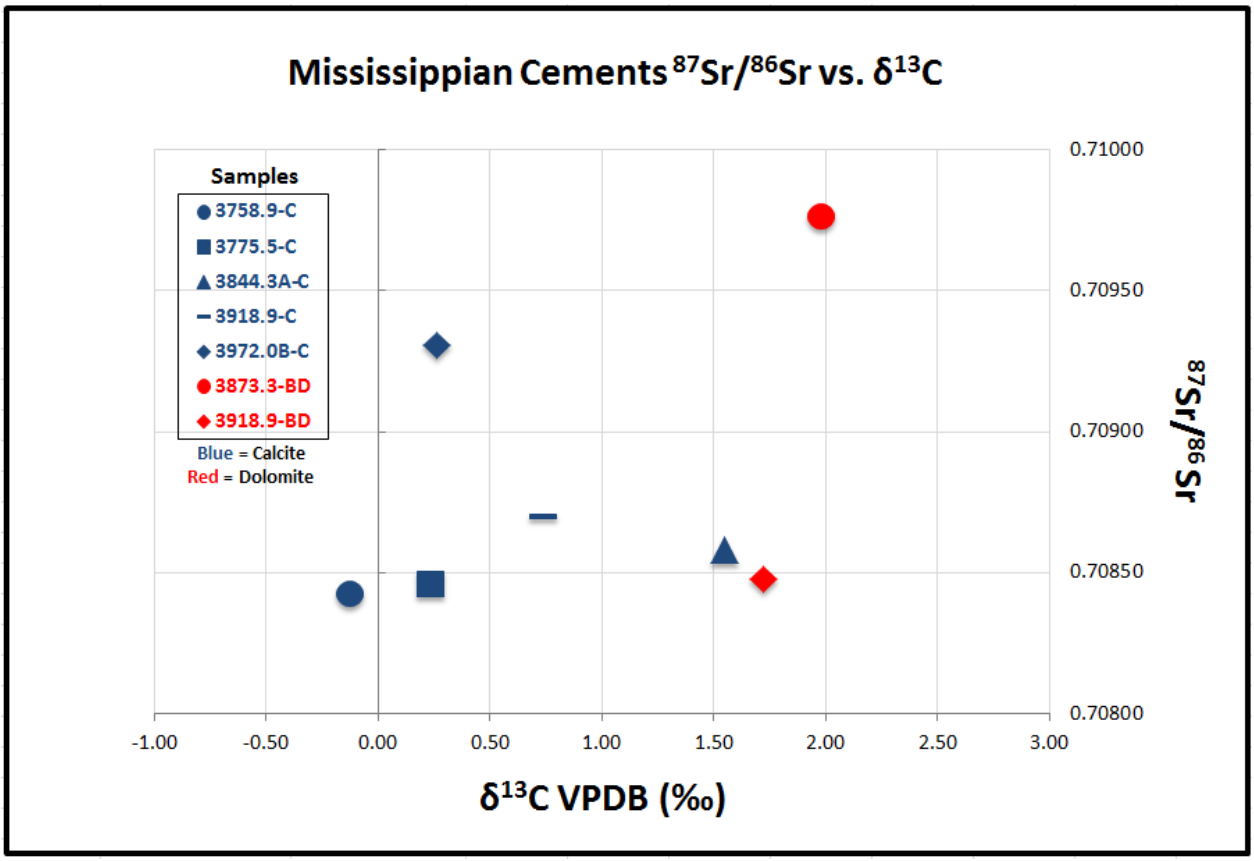


**Figure 3.28:** Cross-plot of $^{87}Sr/^{86}Sr$ and $\delta^{13}C$ of Mississippian baroque dolomite (red data points) and calcite (blue data points). Baroque dolomite sample display a trend that links the most enriched $\delta^{13}C$ values with the most radiogenic $^{87}Sr/^{86}Sr$ values; again, it is best to note that this is based on only samples. There are no observable trends in the plotted calcite data.

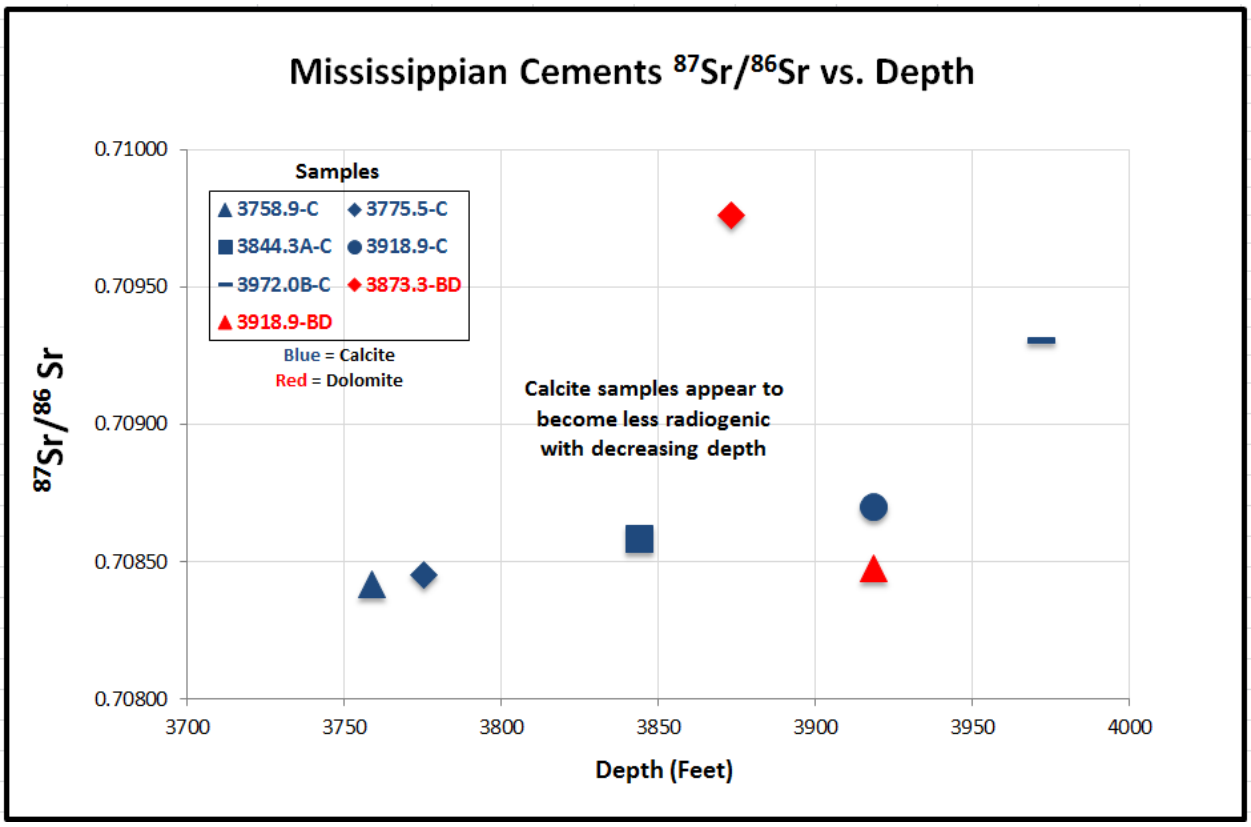


**Figure 3.29:** Cross-plot of $^{87}Sr/^{86}Sr$ and depth of Mississippian baroque dolomite (red data points) and calcite (blue data points). Calcite samples appear to become less radiogenic with decreasing depth, whereas baroque dolomite has the opposite trend but is still based on only two samples.

### 8.1.2. Calcite cement

A total of five sample locations with calcite (MCC) were sampled from the Wellington 1-32 core; all samples were also paired with carbon and oxygen isotope analysis. Sample depths ranged from 3758.9' to 3972.0', providing data points that span the middle portion of the Mississippian. Strontium concentrations varied from 80.80 to 309.31ppm with an average of 214.31ppm, whereas $^{87}Sr/^{86}Sr$ ranged from 0.70842 to 0.70930 with an average of 0.70869 (Fig. 3.26) (Appendix IV). The range of $^{87}Sr/^{86}Sr$ values is significantly less radiogenic than the range observed in Arbuckle Group calcite (0.71257 to 0.71716)

Strontium concentration and $^{87}Sr/^{86}Sr$ cross-plots show that concentration decreases as $^{87}Sr/^{86}Sr$ becomes more radiogenic (Fig. 3.26). When $^{87}Sr/^{86}Sr$ is cross-plotted with the depth of samples, values became more radiogenic with increasing depth (Fig. 3.29). $^{87}Sr/^{86}Sr$ values were also cross-plotted with the $\delta^{13}C$ and $\delta^{18}O$ values derived from the same samples, but no trends were readily observed (Fig. 3.27, 3.28).

*Interpretation:* Mississippian seawater yields $^{87}Sr/^{86}Sr$ values that fall within a range of approximately 0.70755-0.70812 (Denison et al., 1994). Every calcite sample yielded values more radiogenic than unmodified Mississippian seawater. The most depleted sample (0.70930) is more radiogenic than any seawater values from the Cambrian (0.70904) to the modern (0.70896) (Denison et al., 1998). The radiogenic nature of the calcite samples suggests rock-water interaction with siliciclastic material or basement rock at some point during the fluid migration history (Davies and Smith, 2006; Banner, 1995).

The cross-plotted calcite data differs from that observed in the baroque dolomite. There appears to be no direct correlation between $^{87}Sr/^{86}Sr$ values and oxygen and carbon isotopic data (Fig. 3.27, 3.28), though it is best to note that the trends observed in baroque dolomite samples are based on only two samples. The lack of a correlation between $\delta^{18}O$ data and $^{87}Sr/^{86}Sr$ values suggests there is more complexity to the system during calcite precipitation. It is possible that restricted fluid flow allowed temperatures of fluids to drop; the restricted fluid flow could also account for more rock-water interaction, resulting in rock-dominated values. Another possible explanation is that the calcite samples could reflect more than one cementation event. Previous authors have found evidence for multiple events of calcite precipitation in nearby systems believed to be related to regional hydrothermal fluid flow (Coveney et al., 2000).

Arbuckle Group $^{87}Sr/^{86}Sr$ values (0.71257 to 0.71716) are much more radiogenic than the range of values observed in Mississippian calcite (0.70842 to 0.70930) (Fig. 3.26, 3.30). The radiogenic nature of Arbuckle Group calcite could represent increased interaction with siliciclastic material during fluid migration, but as hypothesized in Chapter 2, it is more likely the values were obtained from a change in migration pathway or fluid source compared to the fluid system responsible for baroque dolomite precipitation. The difference between Arbuckle Group and Mississippian calcite could mean the two cements are unrelated. If this is the case, Mississippian calcite may have resulted from continued advective fluid flow sourced from the Anadarko basin. Alternatively, the decrease in $^{87}Sr/^{86}Sr$ values with decreasing depth may support rock-water interaction as fluids migrated vertically through the stratigraphic interval (Fig. 3.29, 3.30). If this is the case, then precipitation of Mississippian calcite may result from the same fracture-controlled fluid system that is suggested for Arbuckle Group calcite in Chapter 2.

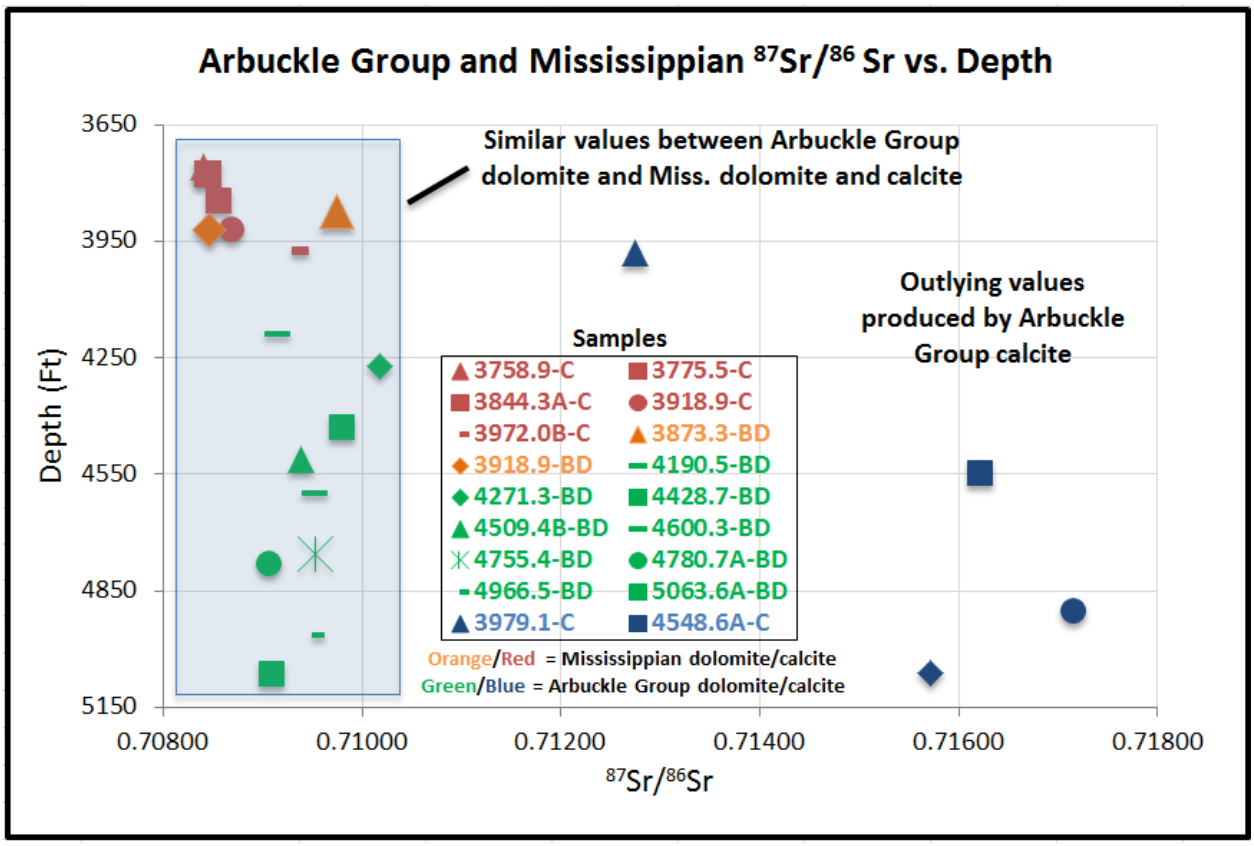


**Figure 3.30:** Cross-plot of $^{87}Sr/^{86}Sr$ and depth of Mississippian baroque dolomite (orange data points) and calcite (red data points), as well as Arbuckle Group baroque dolomite (green data points) and calcite (blue data points). Mississippian baroque dolomite, Mississippian calcite, and Arbuckle Group baroque dolomite produce values that fall within a similar range, supporting the idea of a genetic link between fluids responsible for precipitation. Arbuckle Group calcite is much more radiogenic than values observed in other late-stage cements, suggesting a change in fluid source or migration pathway.

## 9. Discussion

### *9.1. Hydrothermal activity*

The late-stage mineral assemblage, paragenesis, fluid inclusions, and mineral geochemistry of the Middle Ordovician Simpson Group through the Middle Pennsylvanian Cherokee Group is similar to that observed in the Arbuckle Group and regional MVT deposits, both of which are believed to be the result of migration of hydrothermal fluids (Chapter 2 of this study; Young, 2010; Leach and Sangster, 1995; Garven, 1993; Wojcik et al., 1992; Bethke and Marshak, 1990; Bethke, 1986; Garven and Freeze, 1984a; 1984b; Leach and Rowan, 1986;

Sverjensky, 1986; Oliver, 1986; Cathles and Smith, 1983). Previous authors have found evidence for multiple hydrothermal fluid migration events in the Mississippian and Pennsylvanian in the study area (Wojcik et al., 1992; 1994; 1997; Young, 2010). Petrographic observations, fluid inclusion analysis, and geochemical data derived from late-stage cements in overlying strata in this study provide further evidence that hydrothermal fluid flow extended from the Arbuckle Group through the Pennsylvanian (see Fluid inclusion discussion section 6.3. and Stable isotope interpretation sections 7.1. and 7.2.).

Fluid inclusion analysis produced elevated homogenization temperatures, higher than can be explained by burial conditions or geothermal gradient, in Simpson Group baroque dolomite (119.0-132.0ºC), Mississippian megaquartz cement (interpreted to be ≥86ºC), Mississippian baroque dolomite (100.0-144.0ºC), primary FIAs in Mississippian calcite cement (93.0-103.5ºC), and secondary FIAs in Mississippian calcite cement (67.0-83.0ºC)). Moreover, fluid inclusion crystal transects in Mississippian baroque dolomite resulted in fluctuations in homogenization temperatures, which would be difficult to produce via burial and unroofing. Depleted $\delta^{18}O$ values recorded in Simpson Group baroque dolomite, Mississippian baroque dolomite, Mississippian calcite, and Pennsylvanian calcite cement also suggest thermal fractionation that resulted from high temperatures commonly associated with heating of basin-derived brines. According to Newell (1997), a burial history model, using a reasonable geothermal gradient and Cretaceous thickness values, would produce a maximum formation temperature of around 74ºC for the bottom of the underlying Cambrian-Ordovician Arbuckle Group during Permian time in counties just outside the study area. As the Th values in units above the Arbuckle Group are much higher than that, an externally sourced influx of hydrothermal fluids is necessary to account for the elevated temperatures.

### *9.2. Genetic link between cements in Arbuckle Group and overlying units*

#### *9.2.1 Megaquartz and baroque dolomite*

Similarities in late-stage mineral assemblages between the Arbuckle Group and overlying units suggests there may be a genetic link between fluids migrating through the entire stratigraphic package, which ranges from Cambrian-Ordovician to Middle Pennsylvanian strata in this study. Petrographic observations show similarities in paragenetic relationships and appearances of late-stage megaquartz and baroque dolomite. Fluid inclusion microthermometric data provide evidence for low-salinity, high-temperature fluids (responsible for Arbuckle Group and Mississippian megaquartz precipitation) evolving to high-salinity, high-temperature fluids (responsible for Arbuckle Group baroque dolomite, Simpson Group baroque dolomite, and Mississippian baroque dolomite). Homogenization temperatures of megaquartz are ≥87°C from the Arbuckle Group and ≥86°C from the Mississippian, whereas salinities range from 3.1-6.0% for the Arbuckle Group and 3.2-3.9% for the Mississippian (Fig. 3.21). Homogenization temperatures of baroque dolomite in the Arbuckle Group, Simpson Group, and Mississippian fall within a range of 93.0-144.0°C, with the lowest temperature range recorded from the Arbuckle Group (93.0-131.0°C) and the highest temperature range recorded from Mississippian strata (100.0-144.0°C); salinities range from 16.3-20.4% for the Arbuckle Group and 15.0-23.0% for the Mississippian (Fig. 3.21). Similar temperature ranges and salinities of individual cements between stratigraphic units suggest late-stage cements were precipitated during the same events of high-temperature brines migrating through the entire stratigraphic interval. Isotopic analysis further supports that baroque dolomite for all units precipitated at approximately the same time from the same system of fluid flow, with depleted $\delta^{18}O$ and $\delta^{13}C$ values resulting from thermal

fractionation and thermochemical sulphate reduction associated with elevated temperatures. Radiogenic $^{87}Sr/^{86}Sr$ values of Arbuckle Group baroque dolomite (0.70908-0.71019) and Mississippian baroque dolomite (0.70848-0.70976) fall very close to the same range (Fig. 3.26, 30), suggesting that fluids responsible for cementation came from the same fluid source or followed the same fluid migration pathway.

Additionally, similar to Arbuckle Group cements, observations of late-stage cements in the Mississippian suggest pulses in fluid migration. Homogenization temperatures display fluctuations in temperature during baroque dolomite precipitation (Fig. 3.16), suggesting multiple pulses of hydrothermal fluids. The introduction of a single fluid migration event would likely result in an increase in temperature with time (Young, 2010), and though this is supported by an increase in temperature between precipitation of megaquartz and baroque dolomite, the observed fluctuations in homogenization temperatures recorded during crystal transects in baroque dolomite clearly conflict with what would be characteristic of a single migration event. Also, $Tm_{ice}$ values produce salinities that increase from precipitation of megaquartz (3.1-3.9 wt. % NaCl eq.) to precipitation of baroque dolomite (15.0-23.0 wt. % NaCl eq.). Multiple migration events of hydrothermal fluids most adequately explain the mineralogy, fluid inclusion data, and geochemical data produced by late-stage cements.

### *9.2.2. Calcite*

Arbuckle Group calcite displays more depleted $\delta^{13}C$ values (-18.5 to -3.7‰) and more radiogenic $^{87}Sr/^{86}Sr$ values (0.71257-0.71716) than Mississippian calcite, which has values (-0.4 to 1.7‰ and 0.70842-0.70930) that fall near the same range as baroque dolomite for both units. Arbuckle Group calcite is thought to mark the transition of the fluid-flow system to vertical fluid

flow sourced from fractures tapping fluids in underlying sandstone (possibly Cambrian Reagan sandstone) or basement rock. The same fluid-flow system could be applied to Mississippian calcite, with continued upward migration of fluids through the stratigraphic intervals overlying the Arbuckle Group, allowing for progressive rock-water interaction. The potential for the calcite in the Mississippian to be related to the continuation of advective fluid flow sourced from the Anadarko basin also remains. The fact that secondary FIAs in Arbuckle Group and Mississippian calcite display nearly the same temperatures and salinities suggests that the entire stratigraphic interval continued to be influenced by fluids from a similar source or fluid migration pathway after the hypothesized change to a fracture-controlled fluid flow system. The decrease in temperature after the time of calcite precipitation likely represents the transition of the system to reservoir conditions, after the cessation of hydrothermal fluid flow.

### *9.3. Hydrologic models*

#### *9.3.1. Advective fluid flow model*

Potential hypotheses regarding fluid flow mechanisms must account for multiple migration events of fluids sourced from areas that would produce high temperatures, variable salinities, and radiogenic $^{87}Sr/^{86}Sr$ values, as well as the known tectonic and stratigraphic history of the study area. A genetic link between fluids responsible for late-stage cement in the Arbuckle Group and overlying strata was established in section 9.2, indicating the entire stratigraphic interval experienced a similar history of fluid flow associated with late megaquartz and baroque dolomite. This indicates the entire stratigraphic interval should be viewed as a single system with hydrothermal fluids migrating into the study area, using carbonate and siliciclastic strata packages as aquifers. If this is the case, then the hydrologic interpretation

proposed for the Arbuckle Group may apply to overlying units as well. Similar to the Arbuckle Group, tectonic activity associated with the Ouachita orogeny may have generated advective migration of fluids out of the nearby Anadarko basin, using units in the stratigraphic interval as aquifers for hydrothermal fluids. Fluids sourced from the Anadarko basin would account for the high temperatures (burial heating), variable salinities (connate fluids, evaporative brines or dissolution of evaporites), and radiogenic values (rock-water interaction with siliciclastic material) (Johnson et al., 1988; Carter et al., 1998).

#### *9.3.1.1. Tectonically valved fluid flow*

Tectonically valved, episodic dewatering of multiple zones in basins is thought to be capable of expelling hot fluids (Kupecz and Land, 1991; Oliver, 1986; Cathles and Smith, 1983; Sharp, 1978), but it is also believed to produce too little fluid volume to account for high homogenization temperatures in regionally extensive hydrothermal deposits (Garven, 1993; Leach and Rowan, 1986). This limitation conflicts with the alleged regional extent of evidence for late-stage hydrothermal fluid flow. Even so, tectonic-valving by faulting and fracturing could help provide fluid pathways and improved permeability, even if episodic dewatering is not the primary drive for fluid flow. Young (2010) proposed that initial stages of orogenic activity associated with the Ouachita orogeny may have caused relatively shallow faulting of Arkoma basin strata, resulting in the earliest migration of hydrothermal fluids into Mississippian strata near the study area. If a similar process was invoked for the stratigraphic interval discussed in this study, the initial stage of hydrothermal activity (low-salinity megaquartz cement) could have been caused by shallow faulting in the Anadarko basin during the Ouachita orogeny, releasing connate fluids lower in salinity and potentially cooler by being sourced from shallower levels in

the basin. Young (2010) also proposed that deeper faulting occurred as tectonic activity progressed, tapping into deeper, and subsequently hotter, sections of the basin; this allowed discharge of refluxed Permian-age evaporitic fluids that are thought to be responsible for late-stage dolomite precipitation. Wojcik et al. (1994) found evidence for a high-salinity fluid in Pennsylvanian strata prior to injection of hydrothermal fluids, providing support for Permian-age reflux potentially recharging the Anadarko basin prior to regional hydrothermal fluid flow into the study area. Young's hypothesis is also a reasonable explanation for the data generated in this study. Although tectonic-valving could have been important for fluid migration responsible for late-stage cements, volume restrictions would still likely rule out episodic dewatering as the sole driver for hydrothermal fluids migrating through the entire stratigraphic interval. Additionally, the occurrence of slightly lower salinity fluid inclusions in calcite in the Mississippian, and a progression to lower salinity fluid inclusions in hydrothermal minerals from the Pennsylvanian section (Wojcik et al., 1992; 1994; 1997), may represent a freshwater influence as fluid flow out of the basin progressed. The stable isotopic data from calcite, however, show no unambiguous signal indicating meteoric influence. These observations, however, permit the consideration of the influence of gravity-driven fluid flow.

#### *9.3.1.2. Gravity-driven fluid flow*

Gravity-driven fluid flow likely resulted from topographic uplift of the land surface (Garven and Freeze, 1984a; 1984b; Garven, 1993; 1995). Tectonic uplift associated with the Ouachita orogeny caused deepening of the Anadarko basin while generating uplifts that border the basin (Burgess, 1976; Ye et al., 1996; Gallardo and Blackwell, 1999). In this scenario, the Anadarko basin (recharge site and source of heat) and the surrounding uplifts (hydraulic head

source) would have set the stage for regional hydrothermal fluid migration across the study area (e.g., Garven, 1995; 1993; 1985; Leach and Sangster, 1995; Leach and Rowan, 1986). This process could produce initial expulsion of relatively low salinity connate fluids from the basin during the precipitation of megaquartz. Ouachita deformation and uplift began before Permian reflux, and highly saline brines might not have been available until after the Permian. During the Permian, the hydrologic system of head in the mountains adjacent to a deep basin still existed (Johnson et al., 1988). This system could have continued driving hydrothermal fluids northward during and after the Permian reflux, which may have charged the basin with the more saline brines observed during baroque dolomite precipitation (e.g., Wojcik et al., 1994). Gravity-driven fluid flow requires freshwater fluids in the recharge area. In the Mississippian stratigraphic interval, the slight decrease in salinity in fluid inclusions from baroque dolomite to calcite might represent the necessary decrease in salinity. A gravity-driven hydrologic model combined with a period of Permian reflux would account for the initial low-salinity fluids (connate basin fluids) (Fig. 3.31A), subsequent high salinity fluids (acquired from Permian evaporative reflux or evaporite dissolution) (Fig. 3.31B, 3.31C), and latest slightly lower salinity fluids (acquired from progressive mixing with freshwater) (Fig. 3.31D). However, the calculation of the isotopic composition of fluid responsible for calcite precipitation produced an enriched ranged of $\delta^{18}O_{water}$ values (+5.0 to +1.8‰). Meteoric water produces more depleted $\delta^{18}O_{water}$ values, but extensive rock-water interaction may have allowed for enrichment of $\delta^{18}O_{water}$. This model does not account for evidence of pulsed fluid flow, which suggests some sort of tectonic valving.

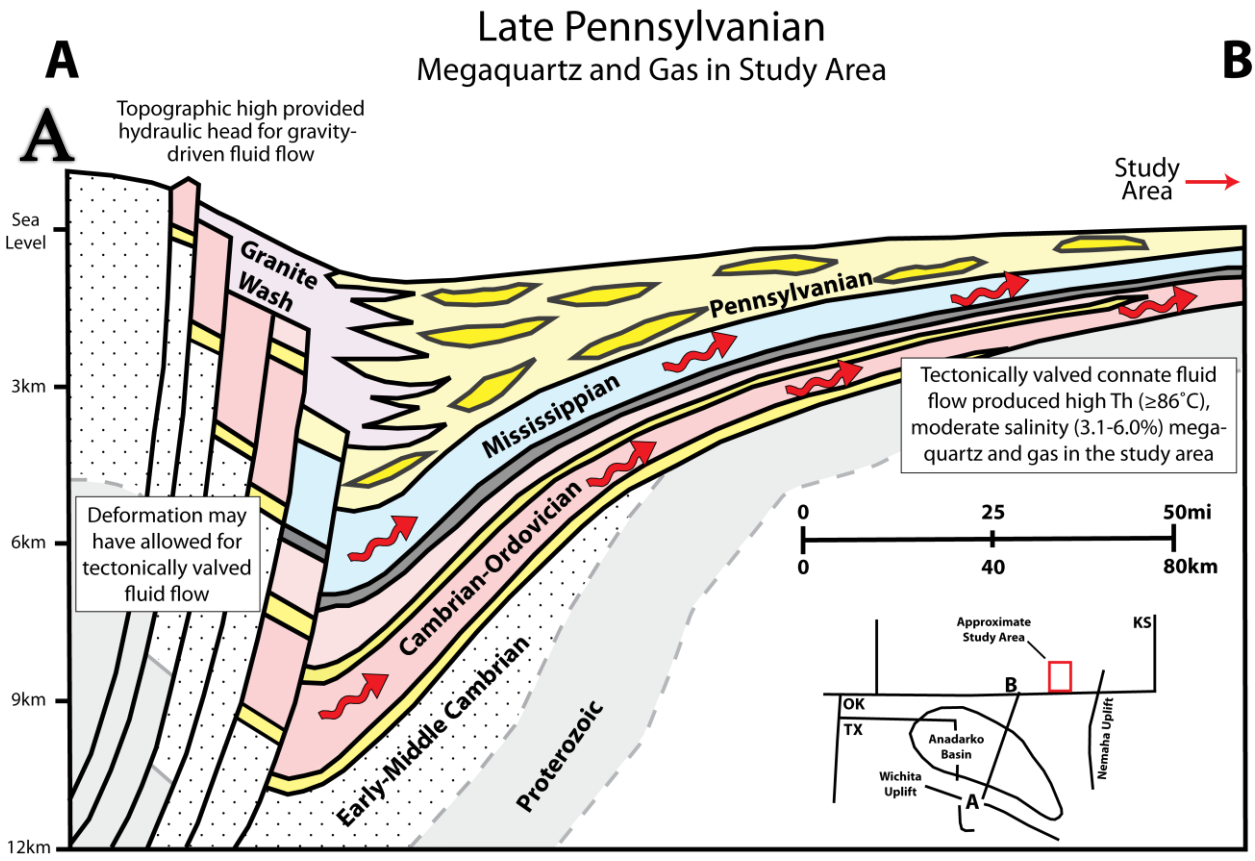
Late Pennsylvanian
Megaquartz and Gas in Study Area
A
B
A
Topographic high provided hydraulic head for gravity-driven fluid flow
Study Area
Sea Level
3km
6km
9km
12km
Granite Wash
Pennsylvanian
Mississippian
Cambrian-Ordovician
Early-Middle Cambrian
Proterozoic
Deformation may have allowed for tectonically valved fluid flow
Tectonically valved connate fluid flow produced high Th (≥86°C), moderate salinity (3.1-6.0%) mega-quartz and gas in the study area
0
25
50mi
0
40
80km
Approximate Study Area
KS
B
OK
TX
Anadarko Basin
Nemaha Uplift
Wichita Uplift
A

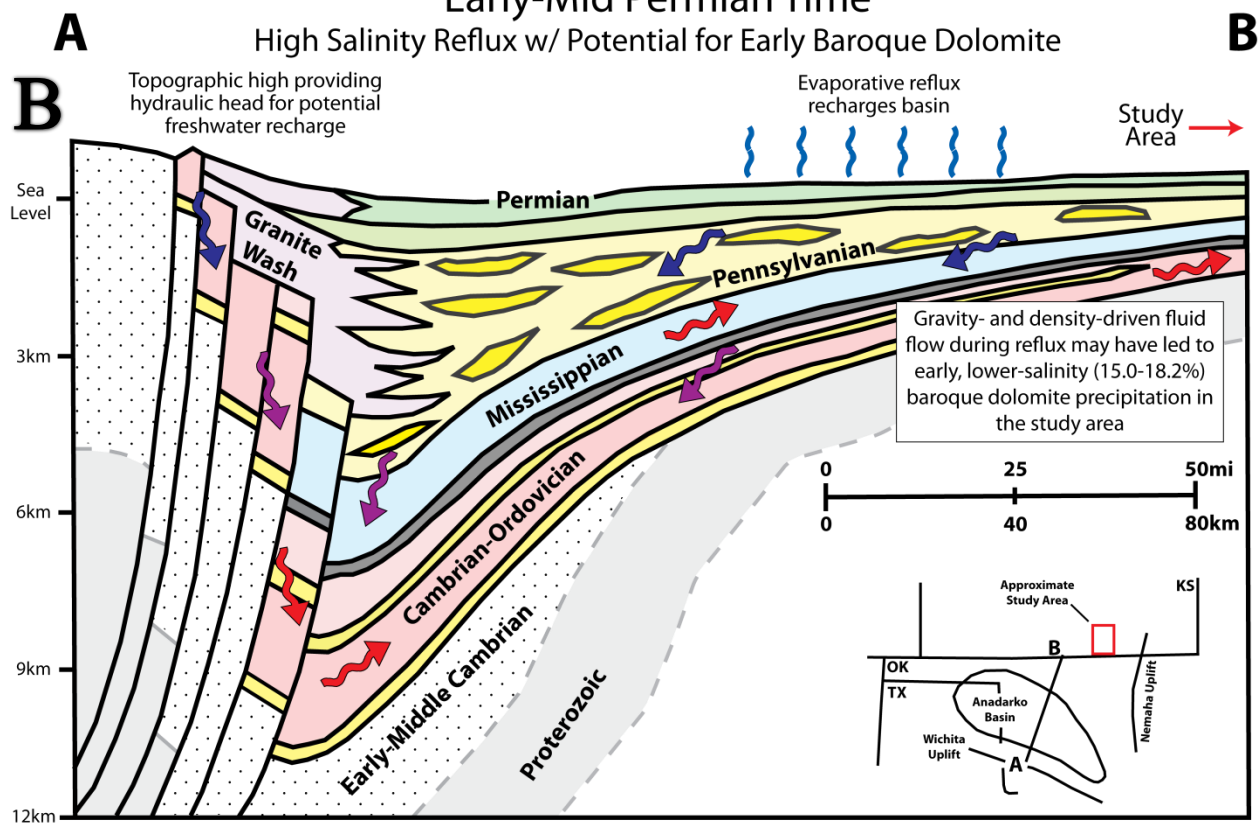
Early-Mid Permian Time
High Salinity Reflux w/ Potential for Early Baroque Dolomite
A
B
B
Topographic high providing hydraulic head for potential freshwater recharge
Evaporative reflux recharges basin
Study Area
Sea Level
3km
6km
9km
12km
Permian
Granite Wash
Pennsylvanian
Mississippian
Cambrian-Ordovician
Early-Middle Cambrian
Proterozoic
Gravity- and density-driven fluid flow during reflux may have led to early, lower-salinity (15.0-18.2%) baroque dolomite precipitation in the study area
0
25
50mi
0
40
80km
Approximate Study Area
KS
B
OK
TX
Anadarko Basin
Nemaha Uplift
Wichita Uplift
A

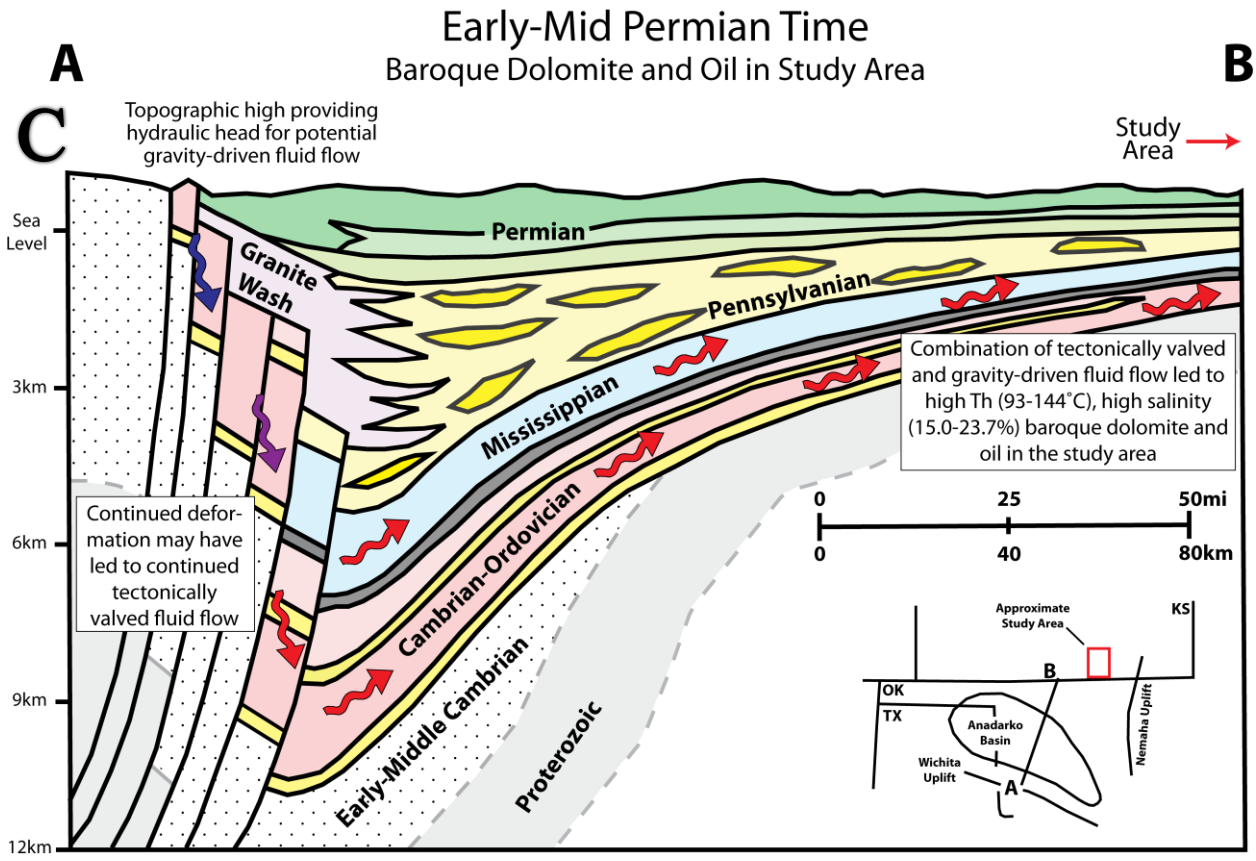
Early-Mid Permian Time
Baroque Dolomite and Oil in Study Area
A
B
C
Topographic high providing hydraulic head for potential gravity-driven fluid flow
Study Area
Sea Level
3km
6km
9km
12km
Granite Wash
Permian
Pennsylvanian
Mississippian
Cambrian-Ordovician
Early-Middle Cambrian
Proterozoic
Continued deformation may have led to continued tectonically valved fluid flow
Combination of tectonically valved and gravity-driven fluid flow led to high Th (93-144°C), high salinity (15.0-23.7%) baroque dolomite and oil in the study area
0
25
50mi
0
40
80km
Approximate Study Area
KS
B
OK
TX
Anadarko Basin
Nemaha Uplift
Wichita Uplift
A

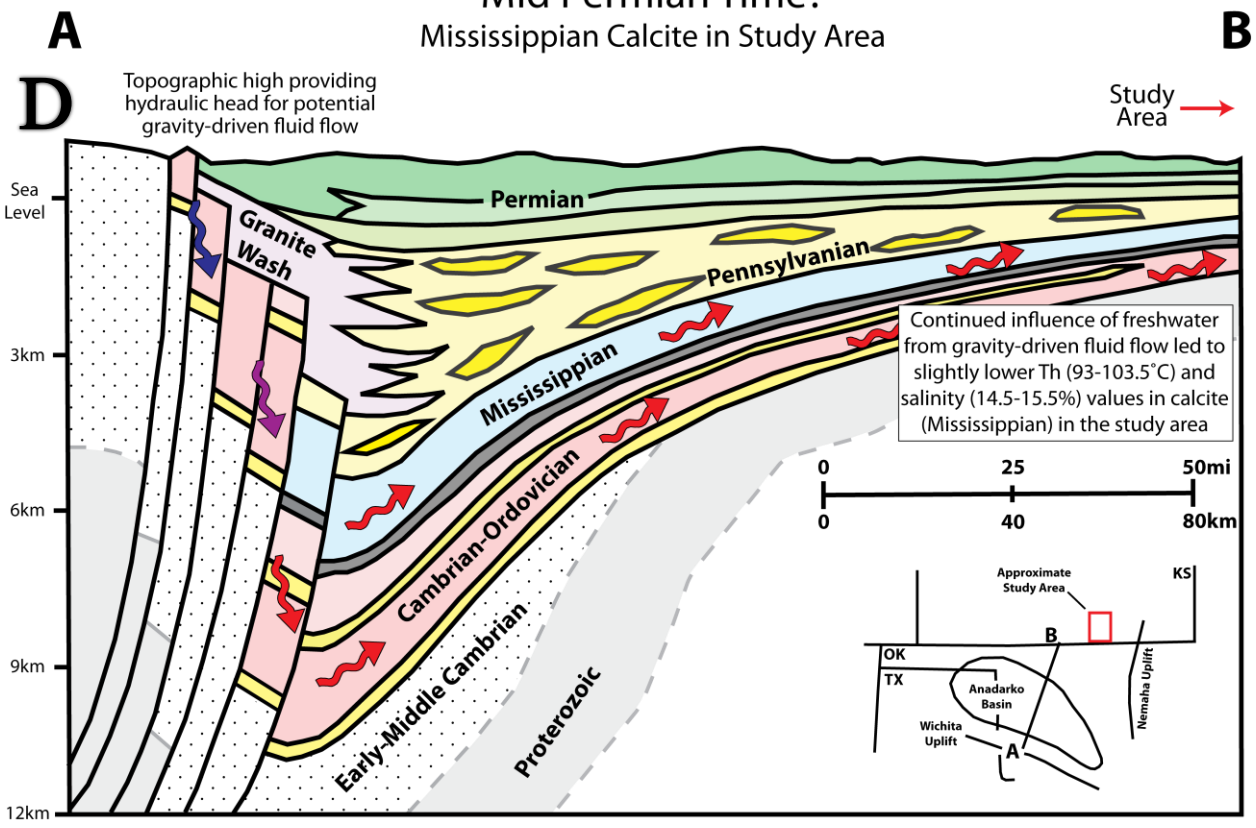
Mid Permian Time?
Mississippian Calcite in Study Area
A
B
D
Topographic high providing hydraulic head for potential gravity-driven fluid flow
Study Area
Sea Level
3km
6km
9km
12km
Granite Wash
Permian
Pennsylvanian
Mississippian
Cambrian-Ordovician
Early-Middle Cambrian
Proterozoic
Continued influence of freshwater from gravity-driven fluid flow led to slightly lower Th (93-103.5°C) and salinity (14.5-15.5%) values in calcite (Mississippian) in the study area
0
25
50mi
0
40
80km
Approximate Study Area
KS
B
OK
TX
Anadarko Basin
Nemaha Uplift
Wichita Uplift
A

**Figure 3.31:** (A) Initial expulsion of connate fluids from Anadarko basin strata may have occurred with the onset of orogenic activity related to the Ouachita orogeny during Late Pennsylvanian time. Tectonic activity could have tectonically valved fluids or provided a topographic high and set the stage for gravity-driven fluid flow out of the basin. This initial stage of fluid migration would have consisted of 3.1-6.0 wt. % NaCl equivalent connate fluids at temperatures ≥87°C, along with gas, migrating into the study area and precipitating megaquartz cement 2 (MQ2). (B) During Permian time, evaporitic conditions would have provided highly saline fluids refluxing through permeable strata and fractures associated with the earlier orogenic activity; this fluid could have actively recharged the basin with saline fluids. Besides tectonic-valving and gravity-driven fluid flow, density-driven fluid flow may have played an active role in fluid migration as well, with high density fluids migrating downward and pushing out lower density fluids. (C) After Permian reflux, continued tectonic activity, gravity-driven fluid flow, or even density-driven fluid flow could have been the driving forces behind continued fluid migration out of the basin and into the study area during Permian time. This stage of fluid migration would have consisted of the 16.3-20.4 wt. % NaCl eq. fluid, ranging from 93-131°C, which was responsible for baroque dolomite (BD) precipitation and petroleum migration in the study area. (D) Later in Permian time, tectonic activity associated with the Ouachita orogeny would have dissipated, while freshwater recharge associated with gravity-driven fluid flow would have continued to influence the fluid flow system. Fluids migrating into the study area from the Anadarko basin during this time may be represented by slightly lower temperatures (93.0-103.5°C) and salinities (14.5-15.5%) measured in Mississippian calcite. Images modified from Gallardo and Blackwell (1999).

### *9.3.2. Fracture-controlled fluid flow model*

Strike-slip faulting occurring after baroque dolomite precipitation in the study area may have pumped underlying fluids into overlying strata and allowed for vertical migration of high-temperature and highly radiogenic fluids responsible for late-stage calcite precipitation (Fig. 3.32) (Chapter 2, this study). In this scenario, high temperature, highly radiogenic fluids could have been sourced from underlying sandstone or the basement. If Mississippian calcite is genetically related to Arbuckle Group calcite, then the less radiogenic values observed in Mississippian calcite could be explained by progressive rock-water interaction as fluids migrated vertically through the stratigraphic interval. Overall, calcite $^{87}Sr/^{86}Sr$ values do become less radiogenic with decreasing depth (Fig. 3.29, 3.30). The similarities in secondary fluid inclusion

data in Arbuckle Group and Mississippian calcite may represent continued fluid connectivity between the two units via the same fracture-controlled system during the healing of fractures in calcite.

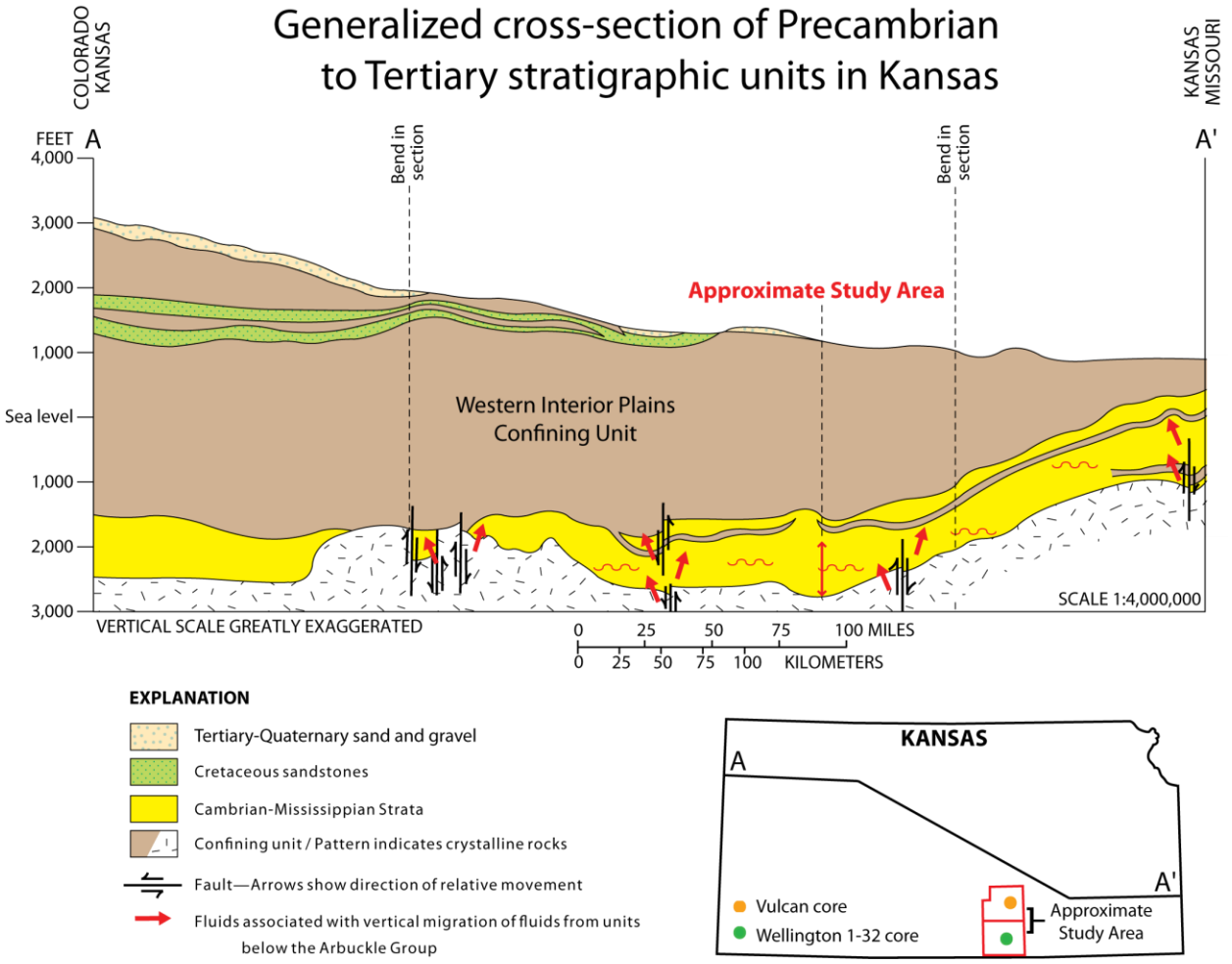


**Figure 3.32:** Following strike-slip faulting and extension of faults into overlying strata, high-temperature, highly radiogenic Reagan sandstone or basement fluids migrate along fractures into overlying strata (illustrated by red symbols). The proximity of specific areas to fractures may have resulted in enhanced fluid flow in areas directly affected by fracturing (Wellington 1-32 core in the case of this study), while areas located further from fractures would display lower temperatures and more rock-dominated isotopic values (Vulcan core in the case of this study). The injected fluids precipitated high-temperature, highly radiogenic calcite (CC) in the Arbuckle Group and continued upward migration of fluids may have been responsible for precipitation of calcite in the Mississippian section as well. Fluid flow associated with tectonic activity could mark the transition of an advective system with fluids sourced from the Anadarko basin, to a fracture-controlled fluid flow system with fluids sourced from underlying sandstone or basement rock. Image modified from Miller and Appel (1997).

### *9.3.3. Timing of driving forces*

Gravity-driven fluids (related to the Ouachita orogeny), varying in flux associated with deformation events, were likely the driving forces behind migration of fluids out of the Anadarko basin and into the study area, producing late-stage precipitation of megaquartz and baroque dolomite. The migration of connate fluids responsible for megaquartz precipitation occurred prior to Permian reflux, likely some time in the Pennsylvanian (Fig. 3.31A). The fact that fluids responsible for megaquartz precipitation recorded much lower salinities likely requires migration prior to the hypothesized reflux of evaporative Permian fluids (e.g., Wojcik et al., 1994). Either during or after Permian reflux (Fig. 3.31B), the migration of highly saline fluids responsible for baroque dolomite precipitation occurred (Fig. 3.31C). It is possible to speculate that lower salinity values in early baroque dolomite suggest fluid migration may have occurred during Early-Mid Permian time, with early reflux fluids potentially mixing with lower salinity connate fluids or fluids along the migration pathway. Precipitation of the highest salinity baroque dolomite could represent migration after the basin was completely flushed by refluxing fluids later in the Permian. Progressive mixing with freshwater sourced from topographic highs adjacent to the Anadarko basin may be represented by slightly lower salinities in Mississippian calcite (Fig. 3.31D).

Fluid flow for calcite appears significantly different than that of megaquartz and baroque dolomite. The change in geochemistry from calcite in the Arbuckle Group to calcite in the Mississippian calcite data may be related to progressive rock-water interaction during upward migration of fracture-controlled fluids sourced from underlying sandstone or basement. The fact that this calcite precipitates after baroque dolomite, and the fact that fluids responsible for baroque dolomite precipitation are hypothesized to be after Permian-age reflux, implies that the

Ouachita orogeny may be an unlikely timing for the strike-slip faulting because, for the most part, Ouachita deformation ended by Early Permian time (Marshak et al., 2003; Kluth and Coney, 1981; Frezon and Dixon, 1975; Flawn, 1961). Coveney et al. (2000) summarized radiometric dates of multiple calcite cements in the Tri-State area that included 251±11Ma, 137±3Ma, 66±2Ma, and 39±2Ma (Brannon et al., 1996a; 1996b; Blasch and Coveney, 1988). 251±11Ma and 137±3Ma both appear to fall between the Ouachita and Laramide orogenies. If the calcite is related to these timing, it is possible that it may be related to Mesozoic rifting in the Gulf of Mexico. The two youngest dates (66±2Ma and 39±2Ma) coincide with the estimated timing of the Laramide orogeny (Coveney et al., 2000; Tweto, 1980). If the calcite observed in the Mississippian and the Arbuckle Group is associated with the younger dates then strike-slip faulting during the Laramide orogeny could be a plausible mechanism for fluid-flow (Davies and Smith, 2006; Marshak et al., 2003). It is still possible that late-stage calcite, observed in the Mississippian and Arbuckle Groups, is unrelated to the calcites addressed in Coveney et al. (2000). Further research on the calcite cements is required to obtain a more complete understanding of the origin of the calcite.

The latest evidence of late-stage diagenetic fluids is observed in moderate-temperature, high-salinity fluids in secondary fluid inclusions in calcite in Mississippian strata and the Arbuckle Group. Similar salinities suggest the same fracture-controlled system may have been playing a role in connecting the Mississippian and Arbuckle Group. Temperatures are closer to the range estimated by Newell's (1997) burial history model, suggesting temperatures were transitioning to normal burial conditions when inclusions were entrapped, but the timing remains unknown.

*9.4. Temperature inversion – Baroque dolomite*

As discussed in sections 9.2. and 9.3., the potential genetic link between late-stage fluids during megaquartz and baroque dolomite precipitation suggests the entire stratigraphic interval should be viewed as a single vertically connected regional aquifer system.

Fluid inclusion microthermometric data and $\delta^{18}O$ data produced from baroque dolomite in this study reveal the thermal properties of such a system, which contrasts markedly from normal geothermal gradients typically seen in sedimentary basins. The influence of hydrothermal fluids appears to have created a temperature inversion with the highest temperatures highest in the section (Fig. 3.33, 3.34). Homogenization temperatures measured in Arbuckle Group baroque dolomite range from 93.0-131.0°C, whereas Mississippian baroque dolomite ranges from 100.0-144.0°C, evidence for higher temperatures in the Mississippian during the precipitation of baroque dolomite (Fig. 3.33). Additionally, Arbuckle Group baroque dolomite provides $\delta^{18}O$ data ranging from -10.2 to -6.6‰ and Mississippian baroque dolomite provides a range from -10.3 to -8.4‰ (Fig. 3.33). Higher mean values in the Mississippian during baroque dolomite precipitation indicate high temperatures were more consistently high in the Mississippian, supporting the idea of a temperature-controlled vertical density gradient. The Arbuckle Group displays evidence for a similar temperature-controlled density gradient at a smaller scale, with higher temperatures and more depleted $\delta^{18}O_{dolomite}$ values at the top of the unit. It appears that the temperature trends represent upward migration of the hottest fluids and preferential flow of those fluids higher in the aquifer. There is a simple physical explanation that is plausible, that higher temperatures lead to lower density, and lower density fluids move upward (Fig. 3.33, 3.34). During advective fluid migration, the lowest density fluids preferentially migrated vertically, encountering an apparently leaky baffle at the top of the

Arbuckle Group, leaving evidence for a smaller scale temperature-controlled density gradient (Fig. 3.34). The lowest density fluids continued to migrate vertically through the Mississippian until they encountered another baffle, preserving evidence for the larger scale temperature-controlled density gradient (Fig. 3.34). Warmer temperatures in shallower parts of the section cannot be ascribed to density controlled by differing salinity. In such a scenario, lower salinity fluids would float to the top of the section, but fluid inclusion data argue against such a relationship. Fluid migration associated with hydrothermal fluids in other study areas may produce the same type of temperature relationship with depth.

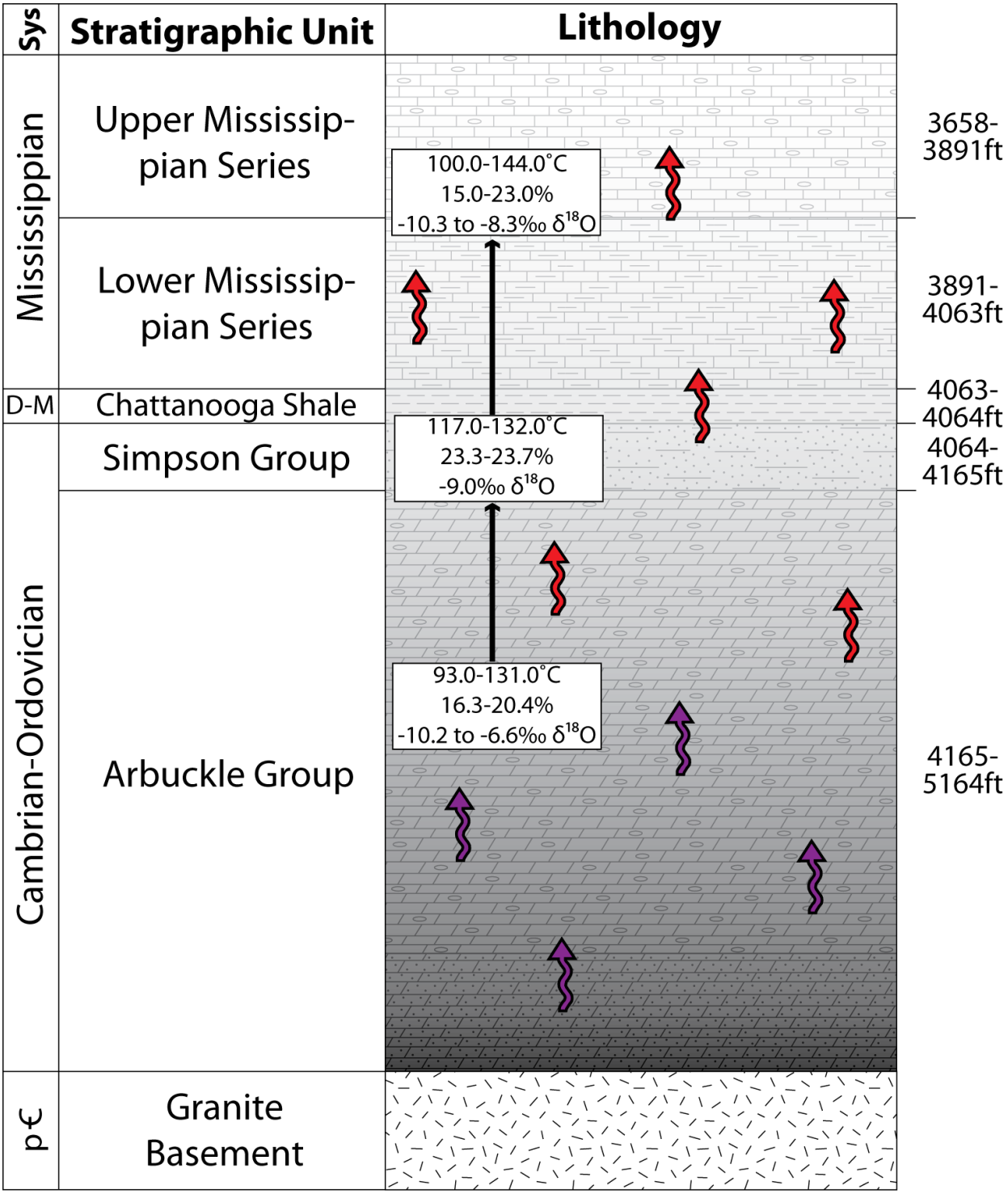


**Figure 3.33:** Stratigraphic column spanning from Precambrian basement to Upper Mississippian Series. Image illustrates influence of temperature-controlled density gradient on fluid flow throughout stratigraphic interval. Higher temperatures result in lower density fluids floating toward the top of the aquifer system, while lower temperatures result in higher density fluids sitting at the base of the system.

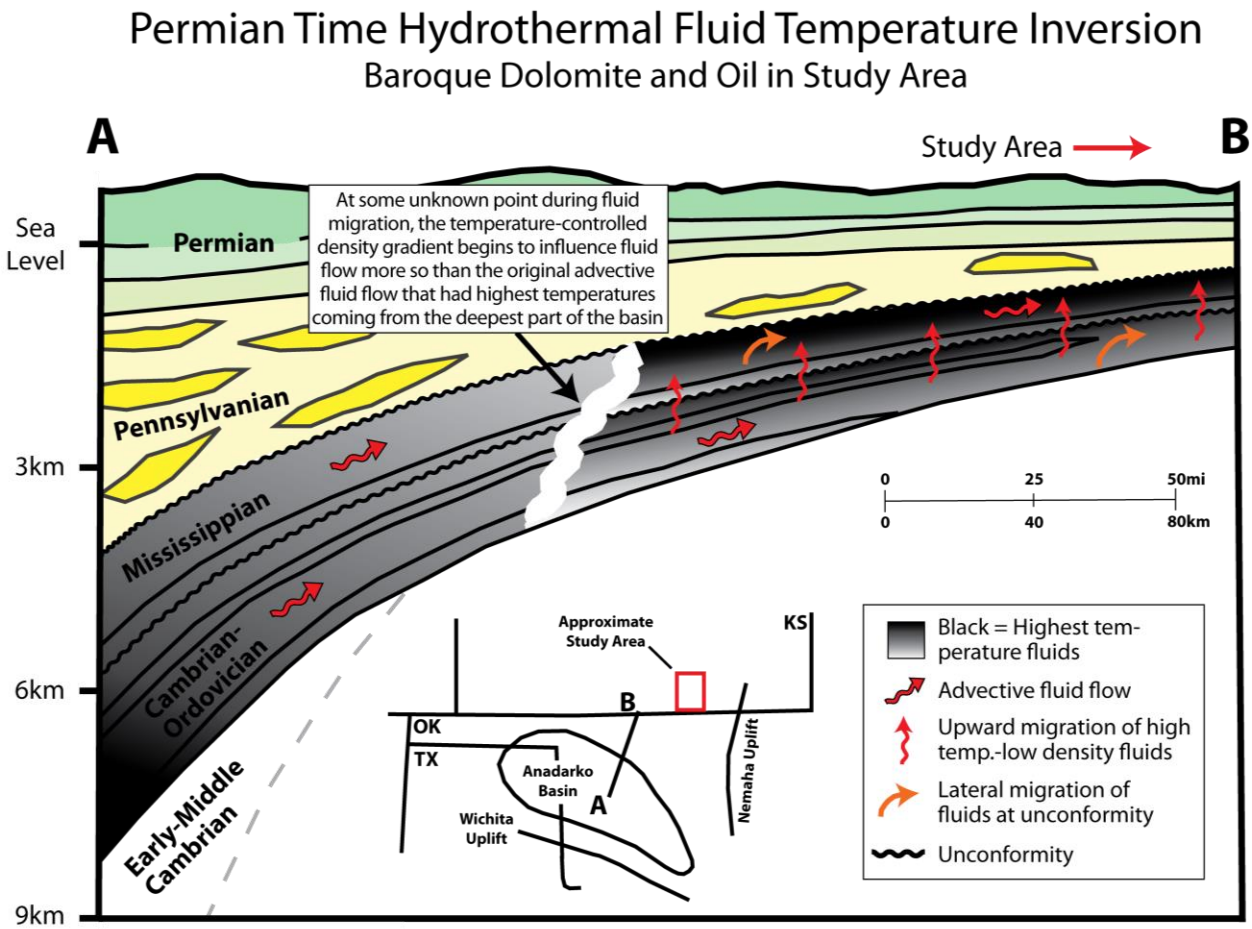


**Figure 3.34:** Figure illustrates fluid flow resulting from advective fluid flow (wide red arrows), temperature-controlled upward migration of lowest density fluids (thin red arrows), and lateral dispersion of fluids when they reach unconformities at the top of the Arbuckle Group and the top of the Mississippian (orange arrows). Advective fluid flow of hydrothermal brines sourced from the Anadarko basin migrates laterally through Arbuckle Group and Mississippian strata, using the interval as an aquifer system. The highest temperature fluids also have the lowest density, resulting in upward migration of the hottest fluids at some point during fluid migration and producing a temperature-controlled density gradient. The unconformity at the top of the Arbuckle Group lead to a smaller scale representation of this type of temperature inversion, whereas the sub-Pennsylvanian unconformity allowed for the larger scale representation of the temperature inversion in the entire stratigraphic interval ranging from the Arbuckle Group to the Mississippian. Image modified from Gallardo and Blackwell (1999).

### *9.5. Application to $CO_2$ sequestration*

Stratigraphic trapping, solubility trapping, capillary trapping, and mineral trapping enable $CO_2$ storage in underground geologic formations (Benson and Cole, 2008; Gunter et al., 1997).

Observations and interpretations related to the Arbuckle Group substantiate the unit as a reservoir for $CO_2$ sequestration (Chapter 2 of this study; Scheffer, 2012)). Overlying shale-rich units (Devonian-Mississippian Chattanooga Shale and Pennsylvanian Cherokee Group) appear to provide the stratigraphic trap necessary, and Scheffer (2012) demonstrated the modern effectiveness of these units as seals. Analysis of fluid connectivity in the past could expand on the dependability of the potential seals and elucidate mechanisms behind ancient leakage, which can be applied to future predictions.

The results of this study provide evidence for an ancient fluid-flow system that was dominated by advective fluid flow during Late Pennsylvanian and Permian time, and was possibly influenced by tectonic and gravity-driven processes associated with fracturing and uplift during the Ouachita orogeny. This system took advantage of carbonate (Arbuckle Group and Mississippian strata) and siliciclastic (Simpson Group) aquifers, precipitating late-stage megaquartz and baroque dolomite. Much more radiogenic $^{87}Sr/^{86}Sr$ values in Arbuckle Group calcite cement signifies a change in fluid source and migration pathway. It is hypothesized that fracturing allowed migration of high-temperature, highly radiogenic fluids to migrate into the unit and precipitate Arbuckle Group calcite (Chapter 2 of this study). Mississippian calcite may represent continued advective fluid flow from the Anadarko basin, or it could be the result of continued upward migration of fluids associated with the fracture-controlled system proposed for Arbuckle Group calcite. The latest evidence of late-stage diagenetic fluids is observed in moderate-temperature, high-salinity fluids in secondary fluid inclusions within Mississippian and Arbuckle Group calcite. This fluid likely represents a transition to normal burial conditions, with fractures allowing for continued fluid migration between Mississippian strata and the Arbuckle Group. Temperatures are closer to the range estimated by Newell's (1997) burial history model,

suggesting temperatures were transitioning to normal burial conditions when inclusions were entrapped. Modern day salinities are much higher in the Mississippian (~20.0%) than in the Arbuckle Group (~8%), suggesting the connection between the two units that appears to have existed in the ancient was sealed at some point in the geologic past.

Observations of late-stage cements indicate that Arbuckle Group and Mississippian strata were both affected by fluids responsible for precipitation of late-stage cements, suggesting the stratigraphic interval was connected. Significantly lower temperatures associated with modern reservoir conditions imply the system is drastically different than what was present at the time of late-stage cement precipitation. Fluid-flow systems responsible for late-stage cements appear to be dependent on tectonic activity associated with major orogenies and other tectonic activity, suggesting that these systems are not actively affecting present-day fluid composition in the Arbuckle Group or overlying units. The entire stratigraphic interval appears to have been connected from Late Pennsylvanian to as late as the timing of entrapment of secondary inclusions in calcite cement, of which the timing is unknown. Conversely, Scheffer (2012) provides evidence that supports the reliability of seals (Chattanooga and Cherokee Shale) in modern times, necessitating a change in seals since the time of hydrothermal fluid migration. This would imply that migration behavior of sequestered $CO_2$ in the Arbuckle would most adequately be modeled with the use of modern topographic groundwater flow. Modern fluids are sourced from the Front Ranges of the Rocky Mountains to the west, western flow from recharge in the topographic high of the Ozark Plateau, northern flow of basinal fluids from the south, and southern flow associated with the Nemaha uplift (Fig. 3.35) (Carr et al, 2005; Garven, 1993; Jorgensen et al., 1993; Miller and Appel, 1997; Macfarlane, 2000).

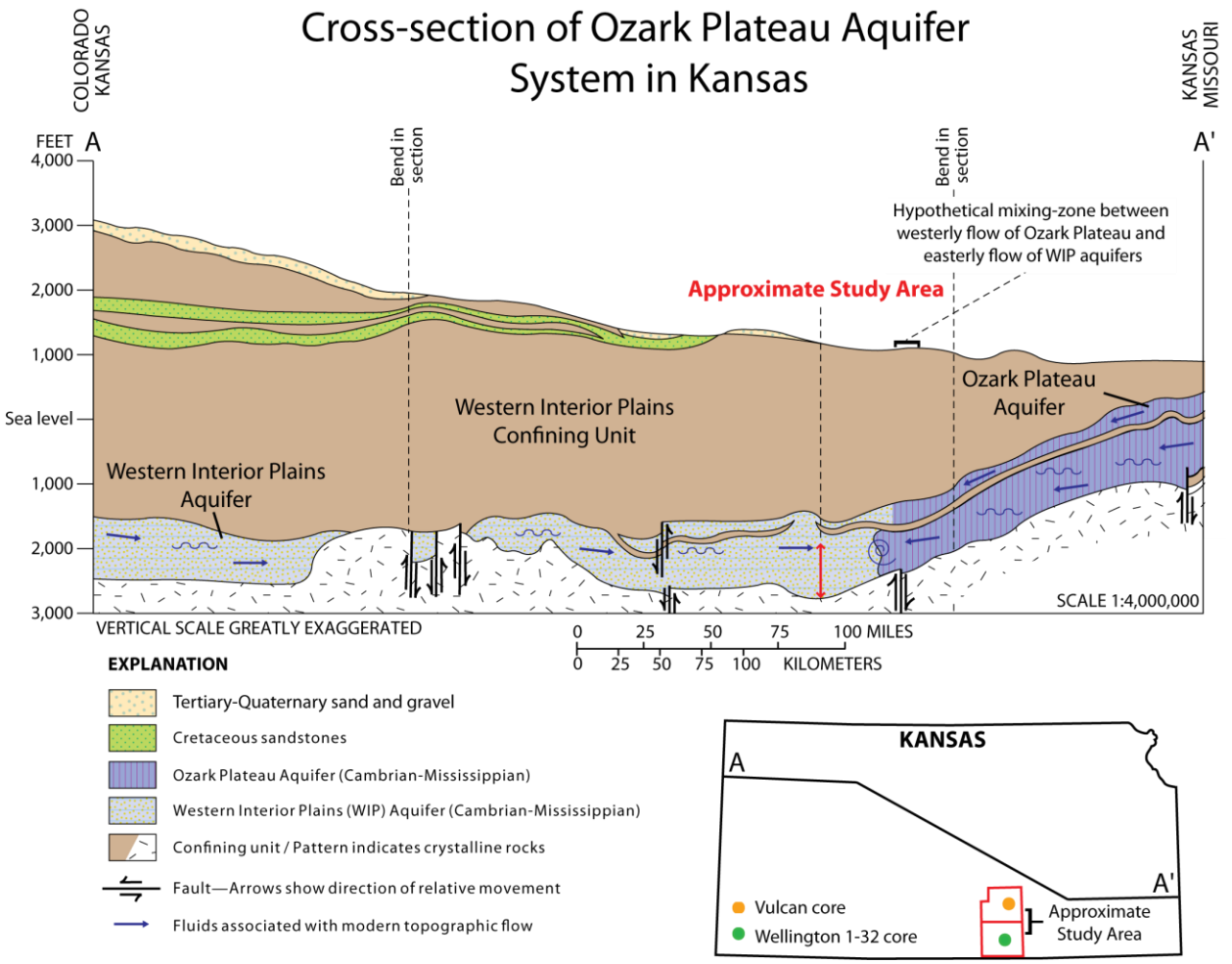


**Figure 3.35:** Cross-section of the Ozark Plateau aquifer system (OPAS), the Cambrian-Ordovician Arbuckle Group is the basal component of this system, with Mississippian strata making up the upper portion of the system (Carr et al., 2005). Illustration depicts easterly flow associated with the OPAS throughout the majority of Kansas, as well as the potential mixing-zone between the WIP aquifer and westerly flow from the Ozark Plateau aquifer in the eastern part of the state (Carr et al., 2005). Image modified from Miller and Appel (1997).

## 10. Conclusions

Fluid inclusion and geochemical analysis of late-stage cements in overlying units (Middle Ordovician Simpson Group to Middle Pennsylvanian Cherokee Group) produced data that support the migration of high-temperature, variable-salinity, and radiogenic fluids altering porosity in the units. Fracturing and dissolution events appear to have affected most units

initially, generating secondary porosity and permeability producing conduits for fluids that precipitated the late-stage cements and subsequently reduced the porosity. A late-stage mineral assemblage consisting of megaquartz, baroque dolomite, and calcite cement appears to be a common theme in units spanning the stratigraphic interval of this study, with cements either being directly observed in core used in this study or observed by others who have conducted diagenetic studies in the region (Young, 2010; Wojcik et al., 1992; 1994; 1997).

Similarities in mineral assemblage, fluid inclusion microthermometric data, and geochemical data support a genetic link between fluids precipitating megaquartz and baroque dolomite in the study area, supporting the concept that fluids were able to migrate across potential seals via connected pore systems. All late-stage cements produce homogenization temperatures higher than can be explained by normal burial conditions or geothermal gradients, and the geochemical data of the cements support an external source of fluids responsible for precipitation. The stratigraphic interval analyzed appears to have acted as a single aquifer system during advective fluid flow of hydrothermal fluids sourced from the nearby Anadarko basin, first expunging low-salinity connate fluids (megaquartz) and then high-salinity fluids after Permian reflux (baroque dolomite); this was followed by lower salinity fluids (Mississippian calcite) that might indicate influence of meteoric water. Late-stage calcite in the Arbuckle Group appears to represent the influence of a different fluid flow system that is characterized by fracture-controlled fluid flow that taps radiogenic fluids in the underlying Cambrian Reagan sandstone or basement rock. Continued upward migration of these fracture-controlled fluids could also be responsible for precipitation of calcite in the Mississippian section, or the calcite could form from a continuation of the earlier advective system. Secondary inclusions in calcite cement in both the Arbuckle Group and Mississippian strata record the latest evidence of late-

stage diagenetic fluids. These fluids are lower in temperature but slightly higher in salinity than original calcite precipitation, possibly reflecting the transition of the system to normal reservoir temperatures, but still supporting fluid connectivity across units.

Tectonic activity associated with the Ouachita orogeny seems to be the most likely driving force behind advective hydrothermal fluid migration out of the Anadarko basin along the various carbonate and siliciclastic aquifers in the stratigraphic interval. Uplifts and fractures generated by the tectonic activity resulted in a combination of tectonically valved and gravity-driven fluid flow out of the basin. Initial low salinity fluids that precipitated megaquartz were derived from connate basin fluids. High salinity fluids associated with the later precipitated baroque dolomite were derived after Permian reflux, with the range of salinities either due to mixing with earlier low salinity connate fluids or recharging by meteoric water. Slightly lower salinities in later calcite may represent the influence of recharging meteoric water associated with gravity-driven fluid flow. Later tectonism may have resulted in fractures that connected underlying sandstone or basement rock with overlying strata. Highly radiogenic fluids responsible for Arbuckle Group precipitation, and possibly Mississippian calcite, may have used these fractures as fluid-flow conduits.

Modern reservoir conditions suggest that stratigraphic units in this study have returned to normal burial temperatures, with low-temperature fluids recharging the study area from the Front Ranges to the West and from the Ozark Plateau to the East and slightly higher temperature, basinal fluids migrating into south Kansas due to thermal expansion. Though the results of this study suggest there was fluid connectivity between all units in this study area at the time of late-stage diagenesis, Scheffer (2012) provides evidence for the modern integrity of the Chattanooga and Cherokee Shales as seals for $CO_2$ sequestration in the Arbuckle Group. Moreover, a middle

baffle unit in the Arbuckle Group, the Middle Ordovician Simpson Group, the Lower Mississippian Kinderhookian Stage, and Permian evaporites also act as potential seals for injected $CO_2$. This likely means that deformation events are required for the breaching of seal integrity. The past history of fluid flow across seals is linked to tectonic events and similar deformation events are likely required for future leakage.

## References


Arne, D.C., 1992, Evidence from apatite fission-track analysis for regional Cretaceous cooling in the Ouachita mountain fold belt and Arkoma Basin of Arkansas: AAPG Bulletin, v. 76, p. 392-402.

Arne, D.C., Duddy, I.R., and Sangster, D.F., 1990, Thermochronologic constraints on ore formation at the Gays River Pb-Zn deposit Nova Scotia, Canada, from apatite fission track analysis: Canadian Journal of Earth Sciences, v. 27, p. 1013-1022.

Arthur, M.A., Anderson, T.F., Kaplan, I.R., Veizer, J., and Land, L.S., 1983, Stable isotopes in sedimentary geology: SEPM Short Course 10.

Bachtadse, V., Van der Voo, R., Haynes, F.M., and Kesler, S.E., 1987, Late Paleozoic magnetism of mineralized and unmineralized Ordovician carbonates from East Tennessee: evidence for post-ore chemical event: Journal of Geophysical Research, v. 92, p. 14165-14176.

Bakker, R.J., 2008, AqSoVir software package fluids: Fluid Inclusion Laboratory Leoben, http://fluids.unileoben.ac.at

Banner, J.L., 1995, Application of the trace element and isotope geochemistry of strontium to studies of carbonate diagenesis: Sedimentology, v. 42, p. 805-824.

Banner, J.L., Hanson, G.N., and Meyers, W.J., 1988, Water-rock interaction history of regionally

extensive dolomites of the Burlington-Keokuk Formation (Mississippian): Isotopic evidence: SEPM Special Publication, n. 43, p. 97-113.

Benson, S.M. and Cole, D.R., 2008, Carbon dioxide sequestration: $CO_2$ sequestration in deep sedimentary formations: Elements, v. 4, p. 325-331.

Bethke, C.M., 1986, Hydrologic constraints on the genesis of the upper Mississippi valley mineral district from Illinois Basin brines: Economic Geology, v. 81, n. 2, p. 233-249.

Bethke, C.M. and Marshak, S., 1990, Brine migrations across North America - The plate tectonics of groundwater: Annual Review of Earth and Planetary Sciences, v. 18, p. 287-315.

Bodnar, R.J., 1993, Revised equation and table for determining the freezing point depression of $H_20$-NaCl solutions: Geochimica et Cosmochimica Acta, v. 57, n. 3, p. 683-684.

Brannon, J.C., S.C. Cole, F.A. Podosek, V.M. Ragan, R.M. Jr. Coveney, M.W. Wallace, and A.J. Bradley, 1996a, Th-Pb and U-Pb dating of ore-stage calcite and Paleozoic fluid flow: Science, v. 271, p. 491-493.

Brannon, J.C., Podosek F.A., Cole, S.C., 1996b, Radiometric dating of Mississippi Valley-type ore deposits, in Sangster, E.D., ed., Carbonate-hosted lead-zinc deposit: SEG Special Publication, v. 4, p. 546-554.

Burgess, W.J., 1976, Geologic evolution of the mid-Continent and Gulf Coast areas – a plate tectonics view: Transactions-Gulf Coast Association of Geological Societies, v. 26, p. 132-143.

Carter, L.S., Kelley, S.A., Blackwell, D.D., and Naesar, N.D., 1998, Heat flow and thermal history of the Anadarko Basin, Oklahoma: AAPG Bulletin, v. 82, n. 2, p. 291-316.

Carr, T.R., Merriam D.C., and Bartley, J.D., 2005, Use of relational databases to evaluate regional

petroleum accumulation, groundwater flow, and $CO_2$ sequestration potential in Kansas: AAPG Bulletin, v. 89, n. 12, p. 1607-1627.

Cathles, L.M. and Smith, A.T., 1983, Thermal constraints on the formation of the Mississippi Valley-type lead-zinc deposits and their implications for episodic basin dewatering and deposit genesis: Economic Geology, v. 78, p. 983-1002.

Choquette, P.W. and Pray, L.C., 1970, Geologic nomenclature and classification of porosity in sedimentary carbonates: AAPG Bulletin, v. 54, n. 2, p. 207-250.

Coveney Jr., R.M., Ragan, V.M., and Brannon, J.C., 2000, Temporal benchmarks for modeling Phanerozoic flow of basinal brines and hydrocarbons in the southern Midcontinent based on radiometrically dated calcite: Geology, v. 28, n. 9, p. 795-798.

Davies, G. R., and Smith, T., 2006, Structurally controlled hydrothermal dolomite reservoir facies: An overview: American Association of Petroleum Geologists Bulletin, v. 90, p. 1641– 1690.

Denison, R.E., Koepnick, R.B., Burke, W.H., and Hetherington, E.A., 1998, Construction of the Cambrian and Ordovician seawater $^{87}Sr/^{86}Sr$ curve: Chemical Geology, v. 152, p. 325-340.

Denison, R.E., Koepnick, R.B., Burke, W.H., Hetherington, E.A., and Fletcher, A., 1994, Construction of the Mississippian, Pennsylvanian and Permian seawater $^{87}Sr/^{86}Sr$ curve: Chemical Geology, v. 112, p. 145-167.

Dickson, J.A.D., 1965, A modified staining technique for carbonates in thin section: Nature, v. 205, p. 587.

Epstein, S. and Mayeda, T., 1953, Variation of $^{18}O$ content of waters from natural sources: Geochimica et Cosmochimica Acta, v. 4, p. 213-224.

Folk, R.L., 1965, Some aspects of recrystallization in ancient limestones, in L.C. Pray and R.C. Murray, eds., Dolomitization and limestone diagenesis: a symposium: SEPM Special Publication 13, p. 14-48.

Gallardo, J. and Blackwell, D.D., 1999, Thermal structure of the Anadarko Basin: AAPG Bulletin, v. 83, n. 2, p. 333-361.

Garven, G., 1995, Continental-scale groundwater flow and geologic processes: Annual Review of Earth and Planetary Sciences, v. 23, p. 89-117.

Garven, G., 1993, Genesis of stratabound ore deposits in the Midcontinent basins of North America; 1, the role of regional groundwater flow: The American Journal of Science, v.293, n. 6, p. 497-568.

Garven, G. and Freeze R.A., 1984a, Theoretical analysis of the role of groundwater flow in the genesis of stratabound ore deposit: 1 . Mathematical and numerical model: The American Journal of Science, v. 284, n. 10, p. 1085-1124.

Garven, G. and Freeze, R.A., 1984b, Theoretical analysis of the role of groundwater flow in the genesis of stratabound ore deposits: 2. Quantitative results: The American Journal of Science, v. 284, n. 10, p. 1125-1174.

Goldstein, R.H. and Reynolds, T.J., 1994, Systematics of fluid inclusions in diagenetic minerals: SEPM Short Course 31.

Goldstein, R.H., 2003, Ch. 2: Petrographic analysis of fluid inclusions, in I. Samson, A. Anderson, and D. Marshall, eds., Fluid Inclusions: Analysis and Interpretation, Mineralogical Association of Canada Short Course 32, p. 9-53.

Gregg, J.M, 1985, Regional epigenetic dolomitization in the Bonneterre Dolomite (Cambrian), southeastern Missouri: Geology, vol. 13, p. 503-506.

Gregg, J.M. and Sibley, D.F., 1984, Epigenetic dolomitization and the origin of xenotopic dolomite texture: Journal of Sedimentary Petrology, v. 54, n. 3, p. 908-931.

Gunter, W.D., Wiwchar, B., and Perkins, E.H., 1997, Aquifer storage of CO2-rich greenhouse gases: extension of the time scale of experiment for CO2-sequestering reactions by geochemical modeling: Mineralogy and Petrology, v. 59, p. 121-140.

Hanor, J.S., 1979, The sedimentary genesis of hydrothermal fluids: Geochemistry of Hydrothermal Ore Deposits, 2nd edition, 137-172.

Heimstra, E.J., 2003, The diagenesis and fluid migration history of the Indian Basin field, Eddy County, New Mexico: University of Kansas Master's Thesis, p. 1-359.

Johnson, K.S., Amsden, T.W., Denison, R.E., Dutton, S.P., Goldstein, A.G., Rascoe, B., Sutherland, B.K., and Thompson, D.M., 1988, Southern Midcontinent region, in Sloss, L.L., ed., Sedimentary Cover – North American craton; U.S.: Boulder, Coloroda, Geological Society of America, The Geology of North America, v. D-2, p. 307-359.

Jorgensen, D.G., Helgesen, J.O., and Imes, J.L., 1993, Regional aquifers in Kansas, Nebraska, and parts of Arkansas, Colorado, Missouri, New Mexico, Oklahoma, South Dakota, Texas, and Wyoming – Geohydrologic framework: U.S. Geological Survey Professional Paper, v. 1414-B, p. 1-68.

Kansas Geological Survey (KGS), 2012, South-Central Kansas $CO_2$ Project, http://www.kgs.ku.edu/PRS/Ozark/Reports/Activities/2012_04_09.html.

Kansas Geological Survey (KGS), 2010, Brine Analyses in Kansas, http://www.kgs.ku.edu/Magellan/Brine/index.html.

Kupecz, J.A. and Land, L.S., 1991, Late-stage dolomitization of the Lower Ordovician

Ellenburger Group, West Texas: Journal of Sedimentary Petrology, v. 61, n. 4, p. 551-574.

Land, L.S., 1985, The origin of massive dolomite: Journal of Geological Education, v. 33, n. 2, p. 112-125.

Land, L.S., 1980, The isotopic and trace element geochemistry of dolomite: The state of the art: SEPM Special Publication, n. 28, p. 87-110.

Land, L.S., Macpherson, G.L., and Mack, L.E., 1988, The geochemistry of saline formation waters, Miocene, offshore Louisiana: Transactions-Gulf Coast Association of Geological Societies, v. 38, p. 503-511.

Lange, S., Chaudhuri, S., and Clauer, N., 1983, Strontium isotopic evidence for the origin of barites and sulfides from the Mississippi Valley-type ore deposits in southeast Missouri: Economic Geology, v. 78, p. 1255-1261.

Leach, D.L. and Rowan, E.L., 1986, Genetic link between Ouachita foldbelt tectonism and the Mississippi valley-type lead-zinc deposits of the Ozarks: Geology, v. 14, no. 11, p. 931-935.

Leach, D.L. and Sangster, D.F., 1995, Mississippi Valley-type lead-zinc deposits, in Kirkham, R.V., Sinclair, W.D.,Thorp, R.I., and Duke, J.M., eds., Mineral Deposit Modeling: Geological Association of Canada Special Paper 40, p. 289-314.

Leach D.L., Bradley, D., Lewchuk, M.T., Symons, D.T.A., Marsily, G., and Brannon, J., 2001, Mississippi Valey-type lead-zinc deposits through geological time: implications from recent age-dating research: Mineralium Deposita, v. 36, p. 711-740.

Lewchuk, M.T., and Symons, D.T.A., 1996, Paleomagnetism and Mississippi Valley-type ore

genesis in the Ordovician Knox Supergroup of Central Tennessee, in Sangster, D.F., ed., Carbonate-hosted lead-zinc deposits: SEG Special Publication, v. 4, p. 567-576.

Lohmann, K.C. and Walker, C.G., 1989, The $\delta^{18}O$ record of Phanerozoic abiotic marine calcite cements: Geophysical Research Letters, v. 16, n. 4, p. 319-322.

Macfarlane, P.A., 2000, Revisions to the nomenclature for Kansas aquifers: Current Research in Earth Sciences, Kansas Geological Survey Bulletin 244, part 2. <http://www.kgs.ku.edu/Current/2000/macfarlane1.html>

Machel, H.G., 2001, Bacterial and thermochemical sulfate reduction in diagenetic settings - old and new insights: Sedimentary Geology, v. 140, p. 143-175.

Marshak, S., Nelson, W.J., and McBride, J.H., 2003, Phanerozoic strike-slip faulting in the continental interior platform of the United States: Examples from the Laramide Orogen, midcontinent, and Ancestral Rocky Mountains: Geological Society Special Publication, v. 210, p. 159-184.

Merriam, D.F., 1963, The geologic history of Kansas: Kansas Geological Survey Bulletin, v. 162, http://www.kgs.ku.edu/Publications/Bulletins/162/10_app_g.html

Miller, J.A. and Appel, C.L., 1997, Groundwater atlas of the United States: Kansas, Missouri, Nebraska: United States Geological Survey, Hydrologic Atlas 730-D, http://pubs.usgs.gov/ha/ha730/ch_d/D-text.html.

Musgrove, M. and Banner, J.L., 1993, Regional ground-water mixing and the origin of saline fluids: Midcontinent, United States: Science, v. 259, p. 1877-1882.

Nakai, S., Halliday, A.N., Kesler, S.F., and Jones, H.D., 1990, Rb-Sr dating of sphalerites from Tennessee and the genesis of Mississippi Valley-type ore deposits: Nature, v. 346, p. 354-357.

Nakai, S., Halliday, A.N., Kesler, S.F., Jones, H.D., Kyle, J.R., and Lane, T.E., 1993, Rb-Sr

dating of sphalerites from Mississippi Valley-type (MVT) ore deposits: Geochimica Cosmochimica Acta, v. 57, p. 417-427.

Newell, K.D., 1997, Comparison of maturation data and fluid inclusion homogenization temperatures to simple thermal models: Implications for thermal history and fluid flow in the Midcontinent: Current Research in Earth Sciences, Kansas Geological Survey Bulletin 240, part 2, p. 13-27, http://www.kgs.ku.edu/Current/1997/newell/newell1.html.

Oliver, J., 1986, Fluids expelled tectonically from orogenic belts: Their role in hydrocarbon migration and other geologic phenomena: Geology, v. 14, p. 99-102.

O'Neil, J.R., Clayton, R.N., and Mayeda, T.K., 1969, Oxygen isotope fractionation in divalent metal carbonates: Journal of Chemical Physics, v. 51, n. 12, p. 5547-5558.

Pan, H., Symons, D.T.A., and Sangster, D.F., 1990, Paleomagnetism of Mississippi Valley-type ore and host rocks in the northern Arkansas and Tri-State districts: Canadian Journal of Earth Sciences, v. 27, p. 923-931.

Radke, B.M. and Mathis, R.L., 1980, On the formation and occurrence of saddle dolomite: Journal of Sedimentary Petrology, v. 50, n. 4, p. 1149-1168.

Scheffer, A., 2012, Geochemical and microbiological characterization of the Arbuckle saline aquifer, a potential CO2 storage reservoir; Implications for hydraulic separation and caprock integrity: University of Kansas Master's Thesis, p. 1-88.

Sharp, J.M., 1978, Energy and momentum transport model of the Ouachita basin and its possible impact on formation of economic mineral deposits: Economic Geology, v. 73, p. 1057-1068.

Smith Jr., L. B. and Davies, G. D., 2006, Structurally controlled hydrothermal alteration of

carbonate reservoirs: Introduction: American Association of Petroleum Geologists Bulletin, v. 90, p. 1635-1640.

Sverjensky, D.A., 1986, Genesis of Mississippi valley-type lead-zinc deposits: Annual Review of Earth and Planetary Sciences, vol. 14, p. 177-199.

Symons, D.T.A., Lewchuk, M., and Leach, D.L., 1998a, Age and duration of the Mississippi Valley-type mineralizing fluid flow events in the Viburnum Trend, southeast Missouri, USA, from paleomagnetism: Geological Society Special Publications, v. 144, p. 27-39.

Symons, D.T.A. and Sangster D.F., 1991, Paleomagnetic age of the Central Missouri barite deposits and its genetic implications: Economic Geology, v. 86, p. 1-12.

Symons, D.T.A. and Stratakos, 2000, Palaeomagnetic dating of dolomitization and Mississippi Valley-type zinc mineralization in the Mascot-Jefferson City district of eastern Tennessee: a preliminary analysis, in Pueyo, J.J., Cardellach, E., Bitzer, K., and Taberner, C., eds., Proceedings of geofluids III; third international conference on fluid evolution, migration, and interaction in sedimentary basins and orogenic belts: Journal of Geochemical Exploration, v. 69-70, p. 373-376.

Tweto, Ogden, 1980, Summary of Laramide orogeny in Colorado, in Kent, H.C., and Porter, K.W., eds., Colorado geology: Rocky Mountain Association of Geologists Symposium on Colorado, p. 129-134.

Watney, W.L. and Bhattacharya, S., 2009, Modeling $CO_2$ sequestration in saline aquifer and depleted oil reservoir to evaluate regional $CO_2$ sequestration potential of Ozark Plateau Aquifer System, South-Central Kansas: DOE Grant Proposal 076248616.

Wisniowiecki, M.J., Van der Voo, R., McCabe, C., and Kelly, W.C., 1983, A Pennsylvanian

paleomagnetic pole from the mineralized Late Cambrian Bonneterre Formation, southeast Missouri: Journal of Geophysical Research, v. 88, p. 6540-6548.

Walton, A.W., Wojcik, K.M., Goldstein, R.H., and Barker, C.E., 1995, Diagenesis of Upper Carboniferous rocks in the Ouachita foreland shelf in mid-continent U.S.A.: an overview of widespread effects of a Variscan-equivalent orogeny: Geologische Rundschau, v. 84, n. 3, p. 535-551.

Wojcik, K.M., M.E. McKibben, R.H. Goldstein, and A.W. Walton, 1992, Diagenesis, thermal history, and fluid migration, Middle and Upper Pennsylvanian rocks, southeastern Kansas: Oklahoma Geological Survey Circular, v. 93, p. 144-159.

Wojcik, K.M., Goldstein, R.H., and Walton, A.W., 1994, History of diagenetic fluids in a distant foreland area, Middle and Upper Pennsylvanian, Cherokee Basin, Kansas, USA: Fluid inclusion evidence: Geochimica et Cosmochimica Acta, v. 58, n. 3, p. 1175-1191.

Wojcik, K.M., R.H. Goldstein, and A.W. Walton, 1997, Regional and local controls of diagenesis driven by basin-wide flow system: Pennsylvanian sandstones and limestones, Cherokee basin, southeastern Kansas, in I.P. Montaneez, J.M. Gregg, and K.L. Shelton, eds., Basin-wide diagenetic patterns; integrated petrologic, geochemical, and hydrologic considerations: SEPM Special Publication No. 57, p. 235-252.

Ye, H., Royden, L., Burchfiel, C., and Schuepbach, M., 1996, Late Paleozoic deformation of interior North America: The Greater Ancestral Rocky Mountains: AAPG Bulletin, v. 80, n. 9, p. 1397-1492.

Young, E.M., 2010, Controls on reservoir character in carbonate-chert strata, Mississippian (Osagean-Meramecian), southeast Kansas: University of Kansas Master's Thesis, p. 1-207.

Zeller, D., 1968, The stratigraphic succession in Kansas: Kansas Geological Survey, Bulletin 189, p. 1-81.

# Chapter 4

## 1. Conclusions

The Arbuckle Group was originally deposited as shallow shelf carbonate strata with primary fenestral and interparticle porosity. A total of 22 diagenetic events altered the porosity and mineralogy of the unit, reducing and generating porosity in a series of dissolution and cementation events. Transmitted light, UV-epifluorescence, and cathodoluminescence display distinctive features within the Arbuckle Group mineral assemblage, enabling the generation of a paragenesis that can be separated into early- and late- stage diagenetic events, based on timing relative to compaction. Early diagenetic events primarily enhanced porosity, mainly due to pervasive karsting and brecciation associated with the regionally extensive post-Sauk subaerial exposure event at the end of Early Ordovician Arbuckle Group deposition. The Middle Ordovician post-Sauk subaerial exposure event created a porous, highly permeable interval in the upper Arbuckle Group. Porosity was reduced with middle- to late-stage cements, but then enhanced again by fracturing likely associated with late Paleozoic tectonic activity. At some point after the commencement of fracturing, hydrothermal brines were injected into the unit, initially resulting in silica and carbonate dissolution, and then precipitation of late-stage cements. Though pore space throughout the Arbuckle Group appears to be lined with either early- or late-stage cements in every example, substantial primary and secondary porosity persists in the unit today.

Fluid inclusion analysis supplemented petrographic observations, displaying distinct differences between early and late stage cements. All-liquid aqueous fluid inclusions present in early dolomite cements, middle dolomite cements, and early megaquartz cement strongly suggest formation of inclusions at low-temperatures (<50ºC), and possibly from high salinities (20.6-25.6

wt. % NaCl eq.) suggesting interaction with evaporites. These characteristics coincide with occurrence early in the diagenetic history, either during Arbuckle Group deposition or during sea-level fluctuations post-dating marine inundation of the Sauk unconformity, when low-temperature and evaporative fluids would have been most likely to exist. Homogenization temperatures measured in late stage megaquartz cement (≥87ºC), baroque dolomite (93.0-131.0ºC), and calcite cement (70.5-89.8ºC) reveal entrapment temperatures higher than expected from elevated geothermal gradients or normal burial conditions, necessitating a hydrothermal influence during late-stage cementation. Lower salinities measured in late megaquartz cement (3.1-6.0 wt. % NaCl eq.) also mark the transition from early- to late-stage cementation, whereas an increase in salinity of subsequent baroque dolomite (16.3-20.4 wt. % NaCl eq.) and secondary inclusions in calcite cements (18.2-19.6 wt. % NaCl eq.) imply interaction with Permian-age evaporated fluids or evaporite dissolution within the Anadarko basin during the fluid migration history. Both high temperature and high salinities support a basinal or basement source for hydrothermal brines.

Geochemical data further support the migration of basin-derived hydrothermal fluids within Arbuckle Group strata. Depleted $\delta^{18}O_{\text{baroque dolomite and calcite}}$ values observed in baroque dolomite and calcite cement can be attributed to thermal fractionation produced from elevated fluid temperatures, whereas enrichment of $\delta^{18}O_{\text{water}}$ supports an origin as evaporative brines. $\delta^{18}O_{\text{dolomite}}$ values become more depleted with decreasing depth, supporting higher temperatures with decreasing depth in the Arbuckle Group, temperature-controlled density stratification, and possibly some preferential fluid flow in the upper Arbuckle Group. Slightly more depleted $\delta^{13}C$ values in the upper Arbuckle Group may record thermochemical sulfate reduction that could have persisted along with higher temperatures produced in the upper portion of the unit.

Radiogenic $^{87}Sr/^{86}Sr$ values imply rock-water interaction with siliciclastics or basement, likely during migration through various stratigraphic sections of a sedimentary basin before migration into the study area or, in the case that fluids were basement derived, interaction with basement rock before vertical migration into overlying strata.

The most likely source for hydrothermal basinal brines responsible for late-stage megaquartz and baroque dolomite precipitation appears to be the Anadarko basin. The believed association of hydrocarbon production in the basin with hydrocarbons present in the Arbuckle Group of Kansas supports migration of fluids from the basin into the study area. The immense depth of the basin, especially Cambrian-Ordovician strata (approx. 9km (~29,500ft) in the deepest portions of the basin), would easily provide the heat necessary for the most elevated homogenization temperatures (131ºC) and prevalent siliciclastic material within the basin could have caused the radiogenic $^{87}Sr/^{86}Sr$ values. Initial discharge of lower salinity (3.1-6.0 wt. % NaCl eq.) connate fluids would account for late megaquartz cement. Reflux of evaporative fluids generated during Permian time could have recharged the basin, accounting for discharge of high salinity (16.3-20.4 wt. % NaCl eq.) fluids responsible for later precipitation of baroque dolomite and calcite cements.

A combination of tectonically valved and gravity-driven fluid flow most adequately accounts for the petrographic observations, fluid inclusion analysis, and geochemical data derived from megaquartz and baroque dolomite, especially when linked to the stratigraphic and tectonic history of the Anadarko basin and the study area. Though compaction due to overburden and tectonic activity may have played a role in the initial expulsion of low-salinity connate fluids, these forces would not have been able to produce the volume of fluid necessary for the regionally extensive nature of high temperature-high salinity baroque dolomite.

Fracturing during the Ouachita orogeny would have allowed for tectonic valving of basin fluids, and uplifts would have provided a topographic high adjacent to the deep Anadarko basin, setting the stage for gravity-driven fluid flow. Migration likely began with fracturing of basinal strata, discharging connate fluids first, and then continued following reflux and recharge of evaporative fluids during Permian time.

The precipitation of calcite cement appears to mark a transition from an advective fluid-flow system, with fluids being sourced from the Anadarko basin, to a vertical fluid-flow system with fluids being sourced from the underlying Cambrian Reagan sandstone or the basement. $^{87}Sr/^{86}Sr$ values recorded in late calcite cement are much more radiogenic than the values observed in baroque dolomite, necessitating an alternative source or fluid migration pathway, and $\delta^{18}O$ values in calcite do not appear to be dependent on depth or the enhanced porosity zone at the top of the Arbuckle Group. Fracturing related to the Laramide orogeny may have reactivated fractures present in basement rock and extended those fractures into overlying strata, providing the needed conduits for high temperature, highly radiogenic fluids to migrate into the Arbuckle Group.

Observations of the Arbuckle Group support long-term sequestration of $CO_2$, especially through mineral formation and reaction with formation brines. Substantial porosity and permeability would allow for extensive migration of the $CO_2$ through the aquifer, providing widespread interaction and storage. Evidence for a baffle separating that upper and lower Arbuckle Group may benefit sequestration by acting as another potential seal or hurt sequestration by reducing storage capacity. Past hydrothermal migration of fluids appears to be related to tectonic events in the distant geologic past, and bear little relation to the current system of fluid flow.

Fluid inclusion and geochemical analysis of late-stage cements in overlying units (Middle Ordovician Simpson Group to Middle Pennsylvanian Cherokee Group) produced data that support the migration of high-temperature, variable-salinity, and radiogenic fluids altering porosity in the overlying units as well. Fracturing and dissolution events appear to have affected most units initially, generating secondary porosity and permeability producing conduits for fluids that precipitated the late-stage cements and subsequently reduced the porosity. A late-stage mineral assemblage consisting of megaquartz, baroque dolomite, and calcite cement appears to be a common theme in units spanning the stratigraphic interval of this study, with cements either being directly observed in core used in this study or observed by others who have conducted diagenetic studies in the region (Young, 2010; Wojcik et al., 1992; 1994; 1997).

Similarities in mineral assemblage, fluid inclusion microthermometric data, and geochemical data support a genetic link between fluids precipitating megaquartz and baroque dolomite in the study area, supporting the concept that fluids were able to migrate across potential modern-day seals via connected pore systems. All late-stage cements produce homogenization temperatures higher than can be explained by normal burial conditions or geothermal gradients, and the geochemical data of the cements support an external source of fluids responsible for precipitation. The stratigraphic interval analyzed appears to have acted as a single aquifer system during advective fluid flow of hydrothermal fluids sourced from the nearby Anadarko basin, first expunging low-salinity connate fluids (megaquartz) and then high-salinity fluids after Permian reflux (baroque dolomite); this was followed by lower salinity fluids (Mississippian calcite) that might indicate influence of meteoric water. Late-stage calcite in the Arbuckle Group appears to represent the influence of a different fluid flow system that is characterized by fracture-controlled fluid flow that taps radiogenic fluids in underlying sandstone

or basement rock. Continued upward migration of these fracture-controlled fluids could also be responsible for precipitation of calcite in the Mississippian section, or the calcite could form from a continuation of the earlier advective system. Secondary inclusions in calcite cement in both the Arbuckle Group and Mississippian strata record the latest evidence of late-stage diagenetic fluids. These fluids are lower in temperature but slightly higher in salinity than original calcite precipitation, possibly reflecting the transition of the system to normal reservoir temperatures, but still supporting fluid connectivity across units.

Tectonic activity associated with the Ouachita orogeny seems to be the most likely driving force behind advective hydrothermal fluid migration out of the Anadarko basin along the various carbonate and siliciclastic aquifers in the stratigraphic interval. Uplift and fractures generated by the tectonic activity resulted in a combination of tectonically valved and gravity-driven fluid flow out of the basin. Similar to findings in the Arbuckle Group, initial low salinity fluids that precipitated megaquartz were derived from connate basin fluids, and high salinity fluids associated with baroque dolomite were after Permian reflux, with the range of salinities either due to mixing with earlier low salinity connate fluids or recharging by meteoric water. Slightly lower salinities in later calcite may represent the influence of recharging meteoric water associated with gravity-driven fluid flow. Alternatively, later tectonism may have resulted in fractures that connected underlying sandstone or basement rock with overlying strata, enabling highly radiogenic fluids responsible for Arbuckle Group calcite, and possibly Mississippian calcite, to have used these fractures as fluid-flow conduits.

Modern reservoir conditions suggest that stratigraphic units in this study have returned to normal burial temperatures, with low-temperature fluids recharging the study area from the Front Ranges to the West and from the Ozark Plateau to the East. Though the results of this study

suggest there was fluid connectivity between all units in this study area at the time of late-stage diagenesis, Scheffer (2012) provides evidence for the modern integrity of the Chattanooga and Cherokee shales as seals for $CO_2$ sequestration in the Arbuckle Group. Moreover, a middle baffle unit in the Arbuckle Group, the Middle Ordovician Simpson Group, the Lower Mississippian Kinderhookian Stage, and Permian evaporites also act as potential seals for injected $CO_2$. This likely means that deformation events are required for the breaching of seal integrity. The past history of fluid flow across seals is linked to tectonic events and similar deformation events are likely required for future leakage.

# Appendix I

## *Arbuckle Group Thick Sections*

Vulcan Core

| Sample (Depth in feet) | Description |
|---|---|
| 3-1 (4012.5) | replacement dolomite with early dolomite cements; detrital quartz and sulfides present as a minor component; stylolites cut across sample and incorporate detrital quartz grains; fractures emanating from stylolites are reduced with baroque dolomite |
| 3-2 (4008.5) | replacement dolomite with early dolomite cements; silicified evaporite nodule; multiple open fractures cutting across sample, may have been produced during sample preparation |
| 3-3 (4004.3) | replacement dolomite with early and middle dolomite cements reducing interparticle porosity; detrital quartz grains present as a minor component; baroque dolomite reduces interparticle porosity last |
| 3-4 (4005.5) | replacement dolomite with early dolomite cements reducing interparticle porosity |
| 3-5AB (4005.5) | replacement dolomite with early dolomite cements; cherty matrix; large vugs are line with late-stage megaquartz cement |
| 3-6 (4002.2) | replacement dolomite with early dolomite cements is fractured and fractures are subsequently reduced with baroque dolomite |
| 3-7 (3992.8) | replacement dolomite with early dolomite cements; vug porosity is reduced with baroque dolomite; stylolite cuts across sample and emanating fractures are reduced with baroque dolomite |
| 3-8 (3990.3) | replacement dolomite with early dolomite cements; dissolved ooids formed geopetals with carbonate debris at the bottom of dissolved ooid; baroque dolomite reduces pore space left by dissolved ooids |
| 3-9 (3987.3) | replacement dolomite with early and middle dolomite cements; micritic envelops are incorporated into replacement dolomite; baroque dolomite is last cement reducing interparticle pore space |
| 3-10 (3983.9) | replacement dolomite with early and middle dolomite cements; detrital quartz grains present as a lesser component; precipitation of euhedral quartz grains likely related to late-stage megaquartz cement |
| 3-11 (3983.2) | replacement dolomite with early dolomite cements; stylolite cuts across sample and appears to cut across early fractures that are lined with middle dolomite cements and then further reduced with baroque dolomite and calcite |

| | |
|---|---|
| 3-12 (3980.4) | replacement dolomite with successive precipitation of early dolomite cement, middle dolomite cement, and baroque dolomite reducing porosity |
| 3-13 (3980.1) | replacement dolomite with early dolomite cements; stylolites cut across sample and have emanating fractures reduced with baroque dolomite; later fractures appear to cut across stylolite fractures but may have been produced during preparation |
| 3-14 (3979.1) | replacement dolomite with early dolomite cements is extensively brecciated; chert and chalcedony replaced earlier dolomite and chert is tripolitic in places; baroque dolomite reduces porosity and is followed by calcite precipitation |
| 3-15 (3971.8) | replacement dolomite with early dolomite cements; chalcedony is replacing earlier dolomite; multiple stylolites cutting across sample; fracture cutting across sample but appear to be caused by sample preparation |
| 3-16 (3969.5) | replacement dolomite with early dolomite cements; earlier dolomite is replaced by chert and then chalcedony; chert appears tripolitic in places; middle dolomite cements and baroque dolomite precipitate later, with late-stage megaquartz filling some porosity with euhedral crystals; galena reduces porosity last |
| 3-17 (3967.3) | replacement dolomite with early dolomite cements is replaced by chert; chert is tripolitic in places |
| 3-18 (3965.6) | replacement dolomite with early dolomite cements is replaced by chert that is tripolitic in places; baroque dolomite reduced pore space last |
| 3-19 (3963.5) | replacement dolomite with early dolomite cements is replaced by chert; chert is tripolitic in places; early megaquartz replaced evaporite nodule and baroque dolomite reduced pore space last |

Wellington 1-32 Core

| **Sample (Depth in feet)** | **Description** |
|---|---|
| 5154.6 | replacement dolomite with early dolomite cement followed by dissolution; baroque dolomite reduces vug porosity; pyrite scattered throughout sample, likely before baroque dolomite because it is not present in baroque dolomite |
| 5145.7AB | replacement dolomite and early dolomite cements were fractured; dissolving fluids sourced from fracture produced large horizontal vug that was subsequently reduced with baroque dolomite |

| | |
|---|---|
| 5137.7 | replacement dolomite with detrital quartz grains present; stylolites cut across sample and appear to enlarged with baroque dolomite as last precipitate |
| 5130.4 | replacement dolomite with detrital quartz common; baroque dolomite is last cement reducing pore space |
| 5125.9 | replacement dolomite; fracture and horizontal vug cut across early dolomite and are reduced with baroque dolomite |
| 5116.8 | replacement dolomite; brecciated fabric and horizontal vug, both are reduced with baroque dolomite |
| 5101.4AB | replacement dolomite with early dolomite cements; detrital quartz grains common; solution enlarged fracture cuts across earlier dolomite and is reduced with baroque dolomite |
| 5093.0ABC | replacement dolomite with early dolomite cements; solution enlarged fracture cuts across earlier dolomite and is reduced with baroque dolomite |
| 5083.7 | replacement dolomite and early dolomite cement has been silicified; vertical fractures intersect horizontal vug and both pore types are reduced with late-stage megaquartz cement |
| 5081.9 | replacement dolomite with early dolomite cement; fracture cuts across sample and intersects vug, both pore types are reduced with baroque dolomite |
| 5070.6 | replacement dolomite with early dolomite cements and minor amount of detrital quartz grains; stylolite cuts across sample and has emanating fractures; emanating fracture cuts across chalcedony and chalcedony is dissolved along fracture |
| 5063.6ABCD | replacement dolomite with early dolomite cements; early dolomite was dissolved, leaving horizontal vug pore; internal sediment deposited on top of early dolomite; baroque dolomite is last cement to reduce vug pore space |
| 5061.5AB | replacement dolomite with early dolomite cements; dissolution produced large horizontal vug that may be lined with middle dolomite cements; baroque dolomite reduces vug pore space and is followed by precipitation of calcite |
| 4984.4ABC | replacement dolomite with early dolomite cements and silicified patches; brecciated fabric with related fractures; pyrite precipitates after early dolomite cements and is followed my early megaquartz; baroque dolomite is last cement to reduce pore space |
| 4981.5 | chert has replaced original fabric; chert is commonly tripolitic; baroque dolomite is last cement to reduce pore space |
| 4977.7 | silicified material with early megaquartz; brecciated fabric with |

| | |
|---|---|
| | associated fractures cutting across early megaquartz; pyrite appears to have precipitated after early megaquartz and was followed by baroque dolomite precipitation |
| 4968.5 | replacement dolomite with early dolomite cements; late-stage megaquartz cement and baroque dolomite are present but scarce; large open vug pore present |
| 4966.5 | chert has replaced original fabric; dissolution lead to large vug or mold that was first lined with late-stage megaquartz cement and then reduced further by baroque dolomite |
| 4903.3 | replacement dolomite with early dolomite cements; baroque dolomite reduces pore space and is followed by calcite precipitation |
| 4828.8 | replacement dolomite with early dolomite cements; sample is cut across by fracture that is reduced with internal sediment and late-stage megaquartz cement last |
| 4818.0 | replacement dolomite with early dolomite cements; sample consists of brecciated clasts; early megaquartz reduces porosity last |
| 4814.5 | replacement dolomite with early dolomite cements; sample consists of brecciated clasts that were later lined with late-stage megaquartz |
| 4806.0 | replacement dolomite that was dissolved, leaving vug pore; vug pore is lined with late-stage megaquartz cement that appears to be cut across by fracture; fracture is lined with pyrite |
| 4790.5 | replacement dolomite with early dolomite cements; baroque dolomite reduces interparticle porosity and vug pore space |
| 4780.7AB | base of sample is detrital quartz grains with replacement dolomite overlying; fractures cut across sample and are lined with middle dolomite cements and then reduced with baroque dolomite |
| 4763.2 | replacement dolomite with early dolomite cements; baroque dolomite is last cement to reduce primary and secondary porosity |
| 4755.4 | replacement dolomite with early dolomite cements was subjected to brecciation and related fractures; fracture appear to be reduced with middle dolomite cements; later fracturing cuts across earlier events; baroque dolomite is last cement to reduce remaining fracture porosity |
| 4750.2 | replacement dolomite; dissolution event produced vug pore space that was later reduced with baroque dolomite |
| 4728.7 | replacement dolomite with early dolomite cements; evaporite nodule replaced by early megaquartz; dissolution led to vug pore space that is reduced with baroque dolomite |
| 4680.3 | replacement dolomite; dissolution led to vug pore space that was lined with chalcedony; chalcedony was subsequently replaced by early megaquartz; internal sediment rests on top of megaquartz |

| | |
|---|---|
| 4653.9 | replacement dolomite with early dolomite cements; early anhydrite was replaced by early dolomite cements and early megaquartz; internal sediment reduces vug pore space last |
| 4644.8 | replacement dolomite; horizontal vug lined with early dolomite cements; internal sediment rests on top of early dolomite cement; baroque dolomite is last cement to reduce vug pore space |
| 4600.3 | replacement dolomite with early dolomite cements and patches of replacement chert; dissolution led to vug pore that is reduced with internal sediment and then reduced late-stage megaquartz cement and baroque dolomite |
| 4595.7 | brecciated fabric with clasts of replacement dolomite and early and middle dolomite cements and large clast of fractured replacement chert |
| 4587.2 | replacement dolomite with early dolomite cement; anhydrite nodule is almost completely replaced by early megaquartz; part of sample appears to have been plucked during sample preparation |
| 4577.0 | clast of chert that is cut across by fractures; internal sediment reduces fractures and appears to be partially dissolved; middle dolomite cements appear to line part of fracture; baroque dolomite is last cement reducing fracture pore space |
| 4574.4 | replacement dolomite with early dolomite cements; dissolution allowed for precipitation of middle dolomite cements into vug porosity |
| 4566.2 | replacement dolomite; dissolution produced vug porosity that was reduced with middle dolomite cements; internal sediment rests on top of middle dolomite cements; minor amount of chalcedony present and appears to have replaced early dolomite in some instances |
| 4556.5 | replacement dolomite with solution-enhanced fractures cutting across sample; fractures are reduced with late-stage megaquartz cement |
| 4548.6AB | replacement dolomite with early and middle dolomite cements reducing vug porosity; calcite reduces large vug and displays deformation twins |
| 4536.4 | replacement dolomite; dissolution produced vug porosity that is lined with middle dolomite cements; internal sediment rests on top of dolomite cements; remaining porosity if fully occluded with baroque dolomite |
| 4533.7 | replacement dolomite; dissolution produced vug pore that is lined by middle dolomite cements and internal sediment later; fracture intersects reduced vug and led to partial dissolution of internal sediment; fracture porosity is reduced by baroque dolomite |
| 4529.8 | replacement dolomite with vug porosity lined with middle dolomite |

| | |
|---|---|
| | cements; stylolite cuts across sample and displays emanating fractures; baroque dolomite is last cement to reduce vug and fracture pore space |
| 4524.8 | replacement dolomite lined with early and middle dolomite cements; fracture cuts across earlier dolomite and is reduced by internal sediment first and then baroque dolomite last |
| 4522.4 | replacement dolomite; dissolution produced vug porosity that was first lined with middle dolomite cements and then further reduced by precipitation of baroque dolomite |
| 4520.0 | replacement dolomite and replacement chert; sample was fractured, leading to dissolution of chert (tripolitic); baroque dolomite reduces fracture pore space |
| 4515.8 | replacement dolomite; dissolution led to vug pore that was subsequently reduced with baroque dolomite |
| 4509.4ABCD | replacement dolomite and replacement chert; fractures cut across sample and appear to have led to dissolution of chert (tripolitic); late-stage megaquartz cement lines fractures; baroque dolomite reduces remaining pore space |
| 4506.7 | almost completely composed of ooids that have been completely replaced by replacement chert |
| 4493.7 | replacement dolomite; early and middle dolomite cements line vug pore space following dissolution event; vertical fractures cut across sample are art reduced with internal sediment |
| 4492.5 | replacement dolomite; samples is cut across by fractures that preceded chalcedony and middle dolomite cements |
| 4483.4 | replacement dolomite with early and middle dolomite cements present as a minor component; internal sediment infiltrates pore space and is followed by baroque dolomite precipitation; pyrite can be observed throughout sample |
| 4474.8 | replacement dolomite; dissolution event allowed for middle dolomite cement precipitation into pore space; vug pore is first reduced by pyrite and then further reduced by baroque dolomite |
| 4470.9AB | replacement dolomite; sample is cut across by multiple fractures; fractures are reduced with internal sediment lined with late-stage megaquartz cement, and then further reduced with baroque dolomite; baroque dolomite also reduces vug pore space |
| 4467.8 | replacement dolomite; dissolution event produced vug porosity that was lined with middle dolomite cements which were then capped by internal sediment; fracture cuts across vug and both fracture and vug pore space is reduced with baroque dolomite |
| 4460.7 | replacement dolomite is cut across by stylolites displaying emanating fractures; emanating fractures are reduced with baroque dolomite |

| | |
|---|---|
| 4448.3 | replacement dolomite with minor amounts of middle dolomite cement; internal sediment reduces pore space and was subsequently partially dissolved; minor amounts of late-stage megaquartz cement reducing pore space; baroque dolomite is last precipitate reducing pore space |
| 4440.7 | replacement dolomite; dissolution produced vug porosity that was first lined with middle dolomite cements and then reduced by internal sediment; fractures cut across sample; both fracture and vug pore space is reduced by baroque dolomite |
| 4435.6 | replacement dolomite with early dolomite cements; stylolites cut across sample and display emanating fractures; emanating fractures are reduced with baroque dolomite |
| 4428.7 | replacement dolomite; dissolution produced vug porosity; later fracturing cut across sample; both fracture and vug porosity are lined with middle dolomite cements; baroque dolomite is last precipitate reducing vug and fracture porosity |
| 4427.2 | replacement dolomite of shelly lag material; chalcedony present in minor amounts; vertical fractures cut across sample |
| 4421.1AB | brecciated with clasts of replacement dolomite and early and middle dolomite cement clasts and replacement chert and chalcedony clasts; silica dissolution has occurred, apparently after brecciation; breccia porosity reduced with sphalerite |
| 4401.7 | replacement dolomite and replacement chert; dissolution produced vug porosity that is lined with late-stage megaquartz cement; fracture cuts across sample and is reduced with baroque dolomite |
| 4394.1 | replacement dolomite with early and middle dolomite cements; early and middle dolomite cements line vug porosity produced by early dissolution; baroque dolomite further reduces vug pore space |
| 4388.3 | replacement dolomite and early dolomite cements; anhydrite nodule is almost completely replaced by early megaquartz; baroque dolomite is the last cement that reduces primary and secondary porosity |
| 4382.9 | replacement dolomite and early dolomite cements; sample is cut across by stylolites and fractures; stylolite incorporates large clast of early megaquartz and fractures are reduced with baroque dolomite; fractures are stained with petroleum and hydrocarbon fluid inclusion can be observed in baroque dolomite |
| 4379.5 | skeletal fragments and ooids replaced with dolomite and early dolomite cements; chert appears to replace remaining material and some early dolomite; middle dolomite cements present in minor amounts; following major dissolution event, baroque dolomite lines pore space as small rhombohedral crystals in some instances |

| | |
|---|---|
| 4348.2 | replacement dolomite with early dolomite cements; stylolites cut across sample and incorporate fragments of early dolomite |
| 4342.9 | replacement dolomite; dissolution led to vug porosity; early megaquartz replaces anhydrite nodule; internal sediment infiltrates vug porosity with late-stage megaquartz cement precipitating after; baroque dolomite is last precipitate to reduce vug porosity |
| 4340.3 | replacement dolomite with early dolomite cements; dissolution produced vug porosity that was first reduced by baroque dolomite and then by precipitation of sphalerite |
| 4325.3 | replacement dolomite; dissolution produced vug porosity that is lined with middle dolomite cements; stylolites cut across sample and display emanating fractures; baroque dolomite reduces vug pore space and emanating fractures, with sphalerite precipitating after |
| 4325.2 | replacement dolomite; dissolution produced horizontal vug that is lined with middle dolomite cements which are then capped by internal sediment; fractures cut across sample and appear to be stained by petroleum; baroque dolomite is last precipitate to reduce vug and fracture pore space |
| 4324.9 | replacement dolomite; dissolution produced vug porosity that is lined with middle dolomite cements which are then capped by internal sediment; fracture intersects vug and appears to have initially led to dissolution of internal sediment; baroque dolomite then reduces vug and fracture pore space; galena is last precipitate that reduces fracture pore space |
| 4314.8 | replacement dolomite and replacement chert; ooids were partially replaced by early dolomite and then completely silicified by replacement chert; anhydrite nodule is almost completely replaced by early megaquartz |
| 4280.0 | replacement dolomite preserved excellent interparticle porosity; interparticle porosity is reduced by early and middle dolomite cements; very minor amounts of late-stage euhedral megaquartz cement crystals in pore space |
| 4276.5 | anhydrite nodule with replacement chert overlying nodule, which is then then overlain by replacement dolomite layer; anhydrite was replaced by early megaquartz; sample is cut across by multiple fractures that produced tripolitic chert along boundaries; late-stage megaquartz cement reduces vug porosity |
| 4271.3 | replacement dolomite with large clast of replacement chert; dissolution produced vug porosity that is lined with middle dolomite cements and then further reduced by baroque dolomite |

| | |
|---|---|
| 4268.4 | replacement dolomite with early dolomite cements; early dolomite is partially replaced with replacement chert in some instances |
| 4257.8 | replacement dolomite; dissolution produced vug porosity that was subsequently lined with middle dolomite cements and then further reduced by baroque dolomite |
| 4241.7 | replacement dolomite with replacement chert; chalcedony present in minor amounts; dissolution led to vug porosity; baroque dolomite is last precipitate to reduce vug and fracture pore space |
| 4239.7 | replacement dolomite with early dolomite cements; ooids are partially dissolved in some instances and replaced by dolomite and chert in other instances; baroque dolomite is last precipitate to reduce porosity |
| 4221.6 | replacement dolomite with minor amounts of replacement chert; dissolution produced horizontal vug porosity; middle dolomite cements line vug pore, followed by further reduction in pore space by baroque dolomite |
| 4211.3 | replacement dolomite is separated from anhydrite nodule by horizontal stylolite; anhydrite is almost completely replaced by early megaquartz |
| 4190.5 | replacement dolomite overlain by detrital quartz grains; sample is cut across by multiple fractures; late-stage megaquartz cement can be observed precipitating off of detrital quartz grains into open fractures; baroque dolomite is last precipitate that reduces pore space |
| 4185.6 | replacement dolomite and early dolomite cements separated from replacement chert by horizontal stylolite; fractures cut across sample; fractures are first reduced by late-stage megaquartz cement and then further reduced by baroque dolomite |
| 4182.0 | replacement dolomite; dissolution produced vug porosity that was then lined with middle dolomite cements; internal sediments rests on top of middle dolomite cements; baroque dolomite is last cement to reduce pore space |
| 4169.9 | replacement dolomite with early dolomite cements; fracture cuts across sample and earlier dolomite; fracture is reduced by precipitation of baroque dolomite |

### ***Simpson Group Thick Sections***

Wellington 1-32 Core

| **Sample (Depth in feet)** | **Description** |
|---|---|
| 4154.6 | detrital quartz grains with minor amounts of small shaley clasts; late- |

| | |
|---|---|
| | stage megaquartz cement precipitates as cement overgrowths on detrital quartz grains |
| 4126.8 | detrital quartz grains with minor amounts of small shaley clasts; late-stage megaquartz cement precipitates as cement overgrowths on detrital quartz grains |
| 4126.0 | detrital quartz grains with minor amounts of small shaley clasts; late-stage megaquartz cement precipitates as cement overgrowths on detrital quartz grains; dissolution produced moldic pores in some instances; fracture cuts across sample, appearing to trace around detrital grains, suggesting fracturing occurred prior to late-stage megaquartz; fracture and moldic pore space was subsequently reduced with baroque dolomite |
| 4124.5 | detrital quartz grains with minor amounts of small shaley clasts; late-stage megaquartz cement precipitates as cement overgrowths on detrital quartz grains; fracture cuts across sample, appearing to trace around detrital grains, suggesting fracturing occurred prior to late-stage megaquartz; baroque dolomite reduces fracture pore space |
| 4101.0 | finer grained detrital quartz grains with muddy matrix; late-stage megaquartz occurs as overgrowth cements on detrital grains |
| 4082.4AB | replacement dolomite and replacement chert; fracture splits chert and appears to have allowed dissolution of chert (tripolitic); fractures are subsequently reduced with late-stage megaquartz cement |
| 4078.3 | replacement dolomite with detrital quartz grains abundant; cherty material was dissolved at some point, producing a tripolitic texture |
| 4075.8 | replacement dolomite with abundant detrital quartz grains; stylolite cuts across sample and incorporates both replacement dolomite and detrital quartz grains |
| 4066.3AB | detrital quartz grains with minor amounts of small shaley clasts; late-stage megaquartz cement precipitates as cement overgrowths on detrital quartz grains; fracture cuts across sample, appearing to splinter detrital grains and overgrowths, suggesting fracturing occurred after late-stage megaquartz precipitation |

### *Mississippian Thick Sections*

Wellington 1-32 Core

| **Sample (Depth in feet)** | **Description** |
|---|---|
| 4007.3 | muddy material partially replaced by dolomite; replacement chert nodules can be observed |

| | |
|---|---|
| 4003.0 | muddy material with minor amount of detrital quartz grains; ptygmatic fractures can be observed cutting across sample, with shape suggesting an early origin; chalcedony reduces early fractures and was then dissolved at a later time |
| 3972.0AB | silicified muddy material that was affected by earlier fractures that are ptygmatic in appearance; early fractures are reduced by chalcedony that was then dissolved at a later time; late-stage megaquartz reduces open pore space and is followed by a reduction in porosity by calcite |
| 3943.1AB | muddy material with chalcedony reducing primary porosity; early anhydrite nodule is almost completely replaced by early megaquartz; late-stage megaquartz cement precipitates on early megaquartz; calcite and later anhydrite are the last cements to reduce pore space |
| 3918.9 | muddy material was dolomitized and silicified in some instances; later dissolution produced vug porosity that was first reduced by baroque dolomite and then further reduced by calcite cement |
| 3913.0 | muddy material was dolomitized and silicified in some instances; later dissolution produced vug porosity that was first reduced with baroque dolomite and then completely occluded with sphalerite |
| 3900.6 | silicified and dolomitized material; early anhydrite nodule was almost completely replaced by early megaquartz; later dissolution led to brecciated fabric; late anhydrite is the last precipitate to reduce pores |
| 3893.9 | silicified and dolomitized material; dissolution produced secondary porosity that was first reduced with early chalcedony; early anhydrite nodule was almost completely replaced by early megaquartz; later dissolution produced tripolitic chert texture; late-stage megaquartz is the last cement to reduce remaining pore space |
| 3883.0 | chert nodule is splintered by fractures; dissolution emanating from fractures produced a tripolitic chert texture; baroque dolomite reduces fracture pore space last |
| 3876.0 | chert nodule is splintered by fractures; dissolution emanating from fractures produced a tripolitic chert texture; baroque dolomite reduces fracture pore space last |
| 3873.3 | dolomitized and silicified material; early chalcedony reduces pore space; early anhydrite is almost completely replaced by early megaquartz; silica dissolution produced tripolitic chert texture; late-stage megaquartz then reduces pore space and is followed by a reduction in pore space with baroque dolomite |
| 3844.3AB | silicified and dolomitized material; early dissolution produced secondary porosity that was first reduced with early chalcedony; early anhydrite nodule was almost completely replaced by early |

| | |
|---|---|
| | megaquartz; late-stage megaquartz cement precipitated on early megaquartz; late chalcedony precipitated on late-stage megaquartz cements and then calcite cement reduced pore space last |
| 3840.4 | silicified and dolomitized material; dissolution produced secondary porosity that was first lined with early chalcedony; extensive brecciation ensued, this was followed by late chalcedony precipitation and then calcite cement |
| 3836.5 | silicified and dolomitized material; dissolution produced secondary porosity that was first lined with early chalcedony; extensive brecciation ensued, this was followed by late chalcedony precipitation and then calcite cement |
| 3835.8 | silicified and dolomitized material; dissolution produced secondary porosity that was first lined with early chalcedony; extensive brecciation ensued, this was followed by late chalcedony precipitation and then calcite cement |
| 3796.6 | skeletal fragments dissolved; early chalcedony lines primary and secondary porosity; early anhydrite nodule almost completely replaced with early megaquartz; late-stage megaquartz cement reduces remaining pore space as cement overgrowth on early megaquartz |
| 3787.2 | replacement dolomite; dissolution produced vug porosity that was first lined with early chalcedony; early megaquartz then reduces porosity and is fractured and then dissolved along fractures; calcite and anhydrite are the last cements to reduce pore space |
| 3781.0 | silicified and dolomitized material was affected by early fracturing as evidenced by ptygmatic appearance; early fractures are reduced with early chalcedony and chalcedony is then dissolved at a later time; vug pore space is lined with early chalcedony and then brecciated at a later time; calcite is last cement to reduce both fracture and vug pore space |
| 3775.5 | dolomitized material is affected by dissolution that resulted in brecciation and collapse features; brecciated fabric is then almost completely occluded with calcite cement |
| 3774.0AB | dolomitized material is affected by dissolution that resulted in brecciation and collapse features; brecciated fabric is then almost completely occluded with late-stage megaquartz cement |
| 3771.0 | silicified and dolomitized material and is cut across by nearly vertical fractures that were subsequently occluded with calcite |
| 3758.9 | silicified and dolomitized material was subjected to early dissolution that was first lined with early chalcedony; material was then brecciated and breccia fabric was reduced with calcite; pyrite present throughout sample |
| 3683.2 | sample appears to have been mechanically altered during sample preparation; chalcedony lines dolomitized material and is followed by late anhydrite precipitation |
| 3663.7 | silicified material was subjected to dissolution at some point, producing a tripolitic texture; late-stage megaquartz was last to cement to reduce pore space |

***Cherokee Group Thick Sections***

Wellington 1-32 Core

| **Sample (Depth in feet)** | **Description** |
|---|---|
| 3548.6 | shaley material originally deposited; shale then fractured at an unknown orientation because sample was loose fragment in core box; fracture was subsequently occluded with late-stage calcite cement |

# Appendix II

### *Arbuckle Group BSE Samples*

Wellington 1-32 Core

| Sample (Depth in feet) | Description |
|---|---|
| 5063.6C | banding of early light-grey zone, middle light-grey zone, middle medium-grey zone, and late dark-grey zone; microfractures shatter samples and late dark-grey zone recrystallizes earlier dolomite phase along fractures |
| 4522.4 | middle light-grey zone with microfractures and late dark-grey zone recrystallizing earlier dolomite phase along fractures |
| 4182.0 | middle light-grey zone with microfractures and late dark-grey zone recrystallizing earlier dolomite phase along fractures |

### *Mississippian BSE Samples*

Wellington 1-32 Core

| Sample (Depth in feet) | Description |
|---|---|
| 3873.3 | early light-grey zone with microfractures and late dark-grey zone recrystallizing earlier dolomite phase along fractures |

# Appendix III

## *Arbuckle Group Fluid Inclusion Data*

Vulcan Core

| Sample (Depth in feet) | Cement | FIA number and designation | Th (°C) | $Tm_{ice}$ (°C) |
|---|---|---|---|---|
| 3-16 (3969.5) | Dolomite Cement 1 | Primary FIA #1 | --- | -22.5, -23.0, -21.3 |
| 3-16 (3969.5) | Dolomite Cement 2 | Primary FIA #1 | --- | -22.0, -22.3, -21.9, -18.5, -19.0 |
| 3-16 (3969.5) | Dolomite Cement 2 | Primary FIA #2 | --- | -21.9, -18.5, -17.5 |
| 3-5 (4005.5) | Megaquartz Cement 2 | Primary FIA #1 | 124.0, 124.0, 90.0 | -3.2, -3.0, -3.7 |
| 3-5 (4005.5) | Megaquartz Cement 2 | Primary FIA #2 | 145.0, 122.0 | -1.8, -1.9, -2.0, -1.9 |
| 3-5 (4005.5) | Megaquartz Cement 2 | Primary FIA #5 | 97.0, 94.0, 125.0 | --- |
| 3-5 (4005.5) | Megaquartz Cement 2 | Primary FIA #6 | 104.0, 101.0 | --- |
| 3-5 (4005.5) | Megaquartz Cement 2 | Primary FIA #7 | 131.0, 145.0 | --- |
| 3-5 (4005.5) | Megaquartz Cement 2 | Primary FIA #8 | 149.0, 152.0, 150.0, 155.0, 157.0 | --- |
| 3-3 (4004.3) | Baroque Dolomite | Secondary FIA #1 | 113.0, 113.0, 117.0, 115.0, 133.0 | -15.1, -14.0 |
| 3-3 (4004.3) | Baroque Dolomite | Secondary FIA #2 | 107.0, 110.0, 113.0, 117.0, 119.0 | -16.5, -16.5, -15.8, -16.7 |
| 3-3 (4004.3) | Baroque Dolomite | Secondary FIA #3 | 122.0, 120.0, 118.0, 115.0, 128.0, 131.0 | -16.0, -16.3, -16.5 |
| 3-16 (3969.5) | Baroque Dolomite | Primary FIA #1 | 117.0, 117.0, 117.5, 120.0, 113.0 | -17.0, -17.3, -15.3, -15.9 |
| 3-16 (3969.5) | Baroque Dolomite | Primary FIA #2 | 97.5, 97.0, 102.5 | -15.7, -13.2 |
| 3-16 (3969.5) | Baroque Dolomite | Primary FIA #3 | 116.0, 122.0, 124.0, 119.0 | -14.2, -14.5 |
| 3-14 (3979.1) | Calcite | Secondary FIA #1 | 70.5, 71.0, 70.8, | -15.1, -15.0, - |

| | | | | |
|---|---|---|---|---|
| | Cement | | 71.3 | 14.9 |
| 3-14 (3979.1) | Calcite Cement | Secondary FIA #2 | 76.8, 77.1, 89.8, 88.3, 87.0 | -16.0, -15.8, -16.2 |
| 3-14 (3979.1) | Calcite Cement | Secondary FIA #3 | 70.8, 72.7, 72.1 | -15.2, -14.6, -14.6, -14.9 |
| 3-14 (3979.1) | Calcite Cement | Secondary FIA #4 | 77.1, 77.6, 80.0, 89.2, 89.7 | --- |
| 3-14 (3979.1) | Calcite Cement | Secondary FIA #5 | 75.3, 75.2, 74.9, 82.0, 82.1, 81.4 | --- |

Wellington 1-32 Core

| **Sample (Depth in feet)** | **Mineral** | **FIA number and designation** | **Th (ºC)** | **$Tm_{ice}$ (ºC)** |
|---|---|---|---|---|
| 4467.8 | Dolomite Cement 3 | Primary FIA #1 | --- | -19.9, -20.8, -21.2 |
| 4467.8 | Dolomite Cement 3 | Primary FIA #2 | --- | -19.0, -22.9, -19.5, -23.0 |
| 4276.5 | Megaquartz 1 | Primary FIA #1 | --- | -24.9, -23.0, -24.0, -23.5 |
| 4276.5 | Megaquartz 1 | Primary FIA #2 | --- | -23.1, -23.7, -22.8, -22.4, -23.1 |
| 4314.8 | Megaquartz 1 | Primary FIA #3 | --- | -22.3, -22.3, -22.7 |
| 4314.8 | Megaquartz Cement 2 | Primary FIA #3 | 105.0, 105.0, 100.0 | -1.8, -1.9 |
| 4814.5 | Megaquartz Cement 2 | Primary FIA #4 | 135.0, 133.0, 111.0 | -2.1, -1.8, -1.8 |
| 5085.7 | Megaquartz Cement 2 | Primary FIA #9 | 91.0, 93.0, 97.0, 103.0, 87.0, 106.0, 109.0 | -2.2, -2.4, -2.1, -2.0, -2.1 |
| 4122.0 | Early Baroque Dolomite | Primary FIA #1 | 98.0, 101.0, 101.0, 107.0 | -14.5, -14.5, -14.3, -13.8 |
| 4388.3 | Early Baroque Dolomite | Primary FIA #2 | 103.0 | -14.2 |
| 4522.4 | Early Baroque Dolomite | Primary FIA #3 | 111.0, 113.0 | -12.4, -13.0 |
| 5063.6C | Early Baroque Dolomite | Primary FIA #4 | 97.0, 102.0 | -13.7, -13.5 |
| 4122.0 | Baroque | Primary FIA #4 | 106.0, 110.0, 115.0, 105.0, | --- |

| | | | | |
|---|---|---|---|---|
| | Dolomite | | 107.5 | |
| 4122.0 | Baroque Dolomite | Primary FIA #5 | 109.5, 112.0, 113.0, 108.0 | --- |
| 4122.0 | Baroque Dolomite | Primary FIA #6 | 114.0, 124.0, 120.0, 114.0, 123.5 | --- |
| 4522.4 | Baroque Dolomite | Primary FIA #7 | 112.5, 113.0, 100.0 | --- |
| 4522.4 | Baroque Dolomite | Primary FIA #8 | 105.0, 109.0, 108.5, 105.0 | --- |
| 4522.4 | Baroque Dolomite | Primary FIA #9 | 93.0, 94.5, 102.5, 105.0, 104.5 | --- |
| 4522.4 | Baroque Dolomite | Primary FIA #10 | 121.0, 129.0, 130.6, 124.0 | --- |
| 4388.3 | Baroque Dolomite | Primary FIA #11 | 105.0, 106.0, 104.0, 105.0, 107.0 | --- |
| 4388.3 | Baroque Dolomite | Primary FIA #12 | 114.0, 114.0, 119.0, 123.0, 122.0, 115.0 | --- |
| 5063.6C | Baroque Dolomite | Primary FIA #13 | 107.0, 115.0, 120.0, 122.0, 122.0 | --- |

***Simpson Group Fluid Inclusion Data***

Wellington 1-32 Core

| **Sample (Depth in feet)** | **Cement** | **FIA number and designation** | **Th (ºC)** | **$Tm_{ice}$ (ºC)** |
|---|---|---|---|---|
| 4126.0 | Baroque Dolomite | Primary FIA #1 | 132.0, 132.0, 128.0, 128.0 | -21.8 |
| 4126.0 | Baroque Dolomite | Primary FIA #2 | 119.0, 127.0, 127.0 | -21.5, -21.3 |
| 4126.0 | Baroque Dolomite | Secondary FIA #1 | 117.0, 117.0, 125.0 | --- |

***Mississippian Fluid Inclusion Data***

Wellington 1-32 Core

| Sample (Depth in feet) | Mineral | FIA number and designation | Th (ºC) | $Tm_{ice}$ (ºC) |
|---|---|---|---|---|
| 3770.4B | Megaquartz Cement 2 | Primary FIA #1 | 111.0, 133.0, 120.0, 115.0 | -2.3, -2.3, -2.2 |
| 3770.4B | Megaquartz Cement 2 | Primary FIA #2 | 96.0, 96.0, 105.0, 120.0, 107.0, 116.0, 117.0, 116.0, 132.0 | -1.9, -2.1 |
| 3770.4B | Megaquartz Cement 2 | Primary FIA #3 | 88.0, 87.0, 102.5, 103.0, 104.0, 120.0 | -2.0, -2.1, -2.3 |
| 3770.4B | Megaquartz Cement 2 | Primary FIA #4 | 106.0, 110.0, 161.0, 123.0, 122.0, 120.0 | -1.9, -2.0, -2.0, -2.0 |
| 3770.4B | Megaquartz Cement 2 | Primary FIA #5 | 98.0, 97.5, 114.0, 114.0, 120.0, 122.0, 125.0, 120.0 | --- |
| 3770.4B | Megaquartz Cement 2 | Primary FIA #6 | 88.0, 86.0, 87.0, 88.0, 89.0, 93.0, 94.0, 91.0 | --- |
| 3770.4B | Megaquartz Cement 2 | Primary FIA #7 | 97.0, 99.0, 110.0, 106.5, 100.0, 100.0 | --- |
| 3770.4B | Megaquartz Cement 2 | Primary FIA #8 | 95.0, 95.0, 105.0, 104.5, 93.0, 101.0, 105.0 | --- |
| 3918.9 | Baroque Dolomite | Primary FIA #1 | 115.0, 115.0, 110.0 | -19.0, -19.0, -18.0 |
| 3918.9 | Baroque Dolomite | Primary FIA #2 | 105.0, 105.0 | -18.0, -18.0, -19.0 |
| 3918.9 | Baroque Dolomite | Primary FIA #3 | 118.0, 118.0, 116.0, 115.0 | -17.5 |
| 3918.9 | Baroque Dolomite | Primary FIA #4 | 131.0, 133.0, 144.0, 143.0 | -20.0, -19.0, -21.0 |
| 3918.9 | Baroque Dolomite | Primary FIA #5 | 103.0, 105.0, 104.0 | -21.0, -21.0, -20.0 |
| 3918.9 | Baroque Dolomite | Primary FIA #6 | 124.0, 135.0, 138.0, 139.0 | --- |
| 3873.3 | Baroque Dolomite | Primary FIA #7 | 128.0, 128.0 | --- |

| | | | | |
|---|---|---|---|---|
| 3873.3 | Baroque Dolomite | Primary FIA #8 | 119.0, 119.0, 127.0, 127.0, 124.0, 124.0, 119.0 | -11.0, -11.0, -12.0, -11.5, -11.0, -12.0 |
| 3873.3 | Baroque Dolomite | Primary FIA #9 | 112.0, 112.0, 112.0, 118.0, 118.0 | -12.0, -11.0, -11.0, -11.0, -11.5, -11.5 |
| 3873.3 | Baroque Dolomite | Primary FIA #10 | 115.0, 115.0, 114.0, 122.0 | -12.0, -12.0, -12.5, -12.5, -12.5, -12.1 |
| 3873.3 | Baroque Dolomite | Primary FIA #11 | 112.0, 120.5, 120.5, 107.0, 115.5, 120.0 | --- |
| 3873.3 | Baroque Dolomite | Primary FIA #12 | 105.0, 105.0, 107.0 | --- |
| 3873.3 | Baroque Dolomite | Primary FIA #13 | 106.0, 106.0, 115.0 | --- |
| 3873.3 | Baroque Dolomite | Primary FIA #14 | 100.0, 100.0, 106.0 | --- |
| 3873.3 | Baroque Dolomite | Primary FIA #15 | 115.0, 118.0, 120.0, 119.0, 115.0, 118.0 | --- |
| 3775.5 | Calcite Cement | Primary FIA #1 | 94.0, 94.0, 98.0, 97.0, 97.5, 98.5 | -10.5, -10.9 |
| 3775.5 | Calcite Cement | Primary FIA #2 | 98.0, 98.5, 102.0, 103.0, 103.0, 102.5, 102.0 | -11.0, -11.5, -11.5 |
| 3775.5 | Calcite Cement | Primary FIA #3 | 100.0, 103.0, 100.5, 91.0, 92.5, 94.0, 94.0, 96.0 | -11.0, -11.2, -11.2 |
| 3775.5 | Calcite Cement | Primary FIA #4 | 93.0, 100.0, 103.5, 96.0, 97.0 | --- |
| 3775.5 | Calcite Cement | Secondary FIA #1 | 77.0, 77.0, 82.0 | -16.6, -16.3, -16.6 |
| 3775.5 | Calcite Cement | Secondary FIA #2 | 83.0, 71.0, 71.5, 76.0 | -16.4, -16.4, -16.2, -16.3 |
| 3775.5 | Calcite Cement | Secondary FIA #3 | 76.5, 70.5, 70.0, 67.0, 68.0 | --- |

# Appendix IV

## *Arbuckle Group Isotopic Data*

Vulcan Core

| Sample (Mineralogy) | $\delta^{13}C$ ‰ VPDB | $\delta^{18}O$ ‰ VPDB | Strontium Concentration (ppm) | $^{87}Sr/^{86}Sr$ |
|---|---|---|---|---|
| 3-14 (3979.1)-1 (Calcite) | -3.67 | -7.74 | 92.47 | 0.71275 |
| 3-14 (3979.1)-2 (Calcite) | -3.72 | -7.46 | --- | --- |
| 3-14 (3979.1)-3 (Calcite) | -3.89 | -7.03 | --- | --- |
| 3-14 (3979.1)-4 (Calcite) | -3.71 | -7.13 | --- | --- |
| 3-14 (3979.1)-5 (Calcite) | -3.87 | -7.68 | --- | --- |

Wellington 1-32 Core

| Sample (Mineralogy) | $\delta^{13}C$ ‰ VPDB | $\delta^{18}O$ ‰ VPDB | Strontium Concentration (ppm) | $^{87}Sr/^{86}Sr$ |
|---|---|---|---|---|
| 5063.6A-1 (Dolomite) | -2.66 | -6.60 | 34.68 | 0.70911 |
| 5063.6A-2 (Dolomite) | -2.58 | -7.18 | --- | --- |
| 5063.6A-3 (Dolomite) | -2.45 | -8.00 | --- | --- |
| 5063.6A-4 (Dolomite) | -2.54 | -8.13 | --- | --- |
| 4966.5-1 (Dolomite) | -2.56 | -7.97 | 44.82 | 0.70951 |
| 4966.5-2 (Dolomite) | -2.72 | -8.30 | --- | --- |
| 4966.5-3 (Dolomite) | -2.78 | -8.18 | --- | --- |
| 4780.7A-1 (Dolomite) | -2.61 | -8.20 | 42.99 | 0.70908 |

| | | | | |
|---|---|---|---|---|
| 4780.7A-2 (Dolomite | -2.74 | -7.32 | --- | --- |
| 4755.4-1 (Dolomite) | -2.72 | -8.12 | 41.22 | 0.70954 |
| 4755.4-2 (Dolomite) | -2.62 | -8.17 | --- | --- |
| 4755.4-3 (Dolomite) | -2.71 | -8.33 | --- | --- |
| 4755.4-4 (Dolomite) | -2.54 | -8.02 | --- | --- |
| 4644.8-1 (Dolomite) | -2.45 | -7.74 | N/A | N/A |
| 4644.8-2 (Dolomite) | -2.41 | -7.67 | --- | --- |
| 4600.3-1 (Dolomite) | -2.74 | -8.85 | 68.33 | 0.70953 |
| 4600.3-2 (Dolomite) | -2.88 | -9.19 | --- | --- |
| 4533.7 (Dolomite) | -2.51 | -7.71 | N/A | N/A |
| 4509.4B-1 (Dolomite) | -2.73 | -8.38 | 63.79 | 0.70939 |
| 4509.4B-2 (Dolomite) | -2.76 | -8.46 | --- | --- |
| 4470.9A-1 (Dolomite) | -3.55 | -9.51 | N/A | N/A |
| 4470.9A-2 (Dolomite) | -2.91 | -8.15 | --- | --- |
| 4428.7-1 (Dolomite) | -3.64 | -9.26 | 47.83 | 0.70981 |
| 4428.7-2 (Dolomite) | -3.56 | -10.22 | --- | --- |
| 4428.7-3 (Dolomite) | -3.52 | -9.94 | --- | --- |
| 4271.3-1 (Dolomite) | -3.45 | -10.13 | 42.24 | 0.71019 |
| 4271.3-2 (Dolomite) | -3.44 | -10.13 | --- | --- |
| 4190.5 (Dolomite) | N/A | N/A | 56.09 | 0.70916 |

| | | | | |
|---|---|---|---|---|
| 5061.5A-1 (Calcite) | -13.57 | -8.67 | 50.09 | 0.71572 |
| 5061.5A-2 (Calcite) | -13.41 | -8.65 | --- | --- |
| 5061.5A-3 (Calcite) | -15.30 | -8.64 | --- | --- |
| 5061.5A-4 (Calcite) | -18.48 | -9.45 | --- | --- |
| 4903.3A-1 (Calcite) | -14.43 | -9.42 | 65.30 | 0.71716 |
| 4903.3A-2 (Calcite) | -15.69 | -9.76 | --- | --- |
| 4903.3B-1 (Calcite) | -12.31 | -9.65 | N/A | N/A |
| 4903.3B-2 (Calcite) | -12.85 | -9.68 | --- | --- |
| 4903.3B-3 (Calcite) | -15.09 | -9.73 | --- | --- |
| 4548.6A-1 (Calcite) | -15.21 | -8.97 | 87.34 | 0.71622 |
| 4548.6A-2 (Calcite) | -14.86 | -9.04 | --- | --- |
| 4548.6A-3 (Calcite) | -14.75 | -9.16 | --- | --- |

***Overlying Units Isotopic Data***

Wellington 1-32 Core

| **Sample (Mineralogy)** | **Unit** | **$\delta^{13}C$ ‰ VPDB** | **$\delta^{18}O$ ‰ VPDB** | **Strontium Concentration (ppm)** | **$^{87}Sr/^{86}Sr$** |
|---|---|---|---|---|---|
| 4124.5 (Dolomite) | Mid. Ordovician Simpson Group | -2.40 | -9.04 | N/A | N/A |
| 3918.9-1 (Dolomite) | Mississippian | 1.84 | -8.36 | 2589.79 | 0.70847 |
| 3918.9-2 (Dolomite) | Mississippian | 1.60 | -8.28 | --- | --- |
| 3873.3-1 (Dolomite) | Mississippian | 1.96 | -9.79 | 59.15 | 0.70976 |

| | | | | | |
|---|---|---|---|---|---|
| 3873.3-2 (Dolomite) | Mississippian | 2.05 | -10.35 | --- | --- |
| 3873.3-3 (Dolomite) | Mississippian | 1.94 | -10.20 | --- | --- |
| 3972.0B-1 (Calcite) | Mississippian | 0.08 | -8.76 | 80.80 | 0.70930 |
| 3972.0B-2 (Calcite) | Mississippian | 0.45 | -8.44 | --- | --- |
| 3918.9-1 (Calcite) | Mississippian | 0.77 | -10.17 | 179.61 | 0.70870 |
| 3918.9-2 (Calcite) | Mississippian | 0.72 | -10.30 | --- | --- |
| 3944.3A-1 (Calcite) | Mississippian | 1.48 | -8.64 | 228.15 | 0.70858 |
| 3944.3A-2 (Calcite) | Mississippian | 1.53 | -8.56 | --- | --- |
| 3944.3A-3 (Calcite) | Mississippian | 1.69 | -8.41 | --- | --- |
| 3944.3A-4 (Calcite) | Mississippian | 1.51 | -8.79 | --- | --- |
| 3775.5-1 (Calcite) | Mississippian | 0.09 | -8.76 | 273.70 | 0.70845 |
| 3775.5-2 (Calcite) | Mississippian | 0.04 | -8.36 | --- | --- |
| 3775.5-3 (Calcite) | Mississippian | 0.60 | -9.52 | --- | --- |
| 3758.9-1 (Calcite) | Mississippian | -0.41 | -8.99 | 309.31 | 0.70842 |
| 3758.9-2 (Calcite) | Mississippian | 0.04 | -8.46 | --- | --- |
| 3758.9-3 (Calcite) | Mississippian | 0.02 | -8.58 | --- | --- |
| 3548.6 (Calcite) | Pennsylvanian Cherokee Group | -1.55 | -9.12 | --- | --- |